Multivalent nanoparticles for the treatment of ocular diseases

Dissertation to obtain the Degree of Doctor of Natural Sciences

(Dr. rer. nat.)

from the Faculty of Chemistry and Pharmacy

University of Regensburg

Presented by

Robert Hennig

from Thalheim (Erzgebirge)

February 2016

This work was carried out from April 2011 until July 2015 at the Department of Pharmaceutical Technology of the University of Regensburg.

The thesis was prepared under supervision of Prof. Dr. Achim Göpferich.

Submission of the PhD application:	February 19, 2016
Date of examination:	March 30, 2016

Examination board:	Chairman:	Prof. Dr. Sigurd Elz
	1st Expert:	Prof. Dr. Achim Göpferich
	2nd Expert:	PD Dr. Andreas Ohlmann
	3rd Examiner:	Prof. Dr. Joachim Wegener

To my family

The truth is, most of us discover

where we are headed when we arrive.

Bill Watterson

Table of Contents

Nanoparticles for the treatment of ocular neovascularizations

Published in European Journal of Pharmaceutics and Biopharmaceutics 2015, 95b, 294–306

This chapter was published as: R. Hennig and A. Goepferich, Europ. J. Pharm. Biopharm. 2015, 95b, 294-306, doi: 10.1016/j.ejpb.2015.02.027.

Abstract

Neovascular diseases of the posterior eye like age-related macular degeneration, proliferative diabetic retinopathy or retinopathy of prematurity carry a tremendous burden for patient and health care system alike. Although intravitreal injections of anti-VEGF based therapeutics have significantly improved the visual outcome for many patients, current therapeutic options still show significant drawbacks such as the injection-related risk of contracting an infection. Due to their ability to encapsulate drugs with otherwise poor bioavailability, accumulate in areas of increased vascular permeability and control the release of active ingredients over time, nanoparticle systems have been widely researched to enhance current therapeutic strategies and expand the therapeutic arsenal. In this review, emphasis is placed both on the possibilities and drawbacks that a systemic nanoparticle-based therapy could have in the context of neovascular posterior eye diseases. Recent investigations into intravenous and intravitreal administration of nanomaterials and their potential to deliver potent drugs and genes to pathologic lesions will also be presented. Furthermore, we will focus on the exceptional anti-oxidative and anti-angiogenic properties of selected nanoscale systems that carve out new paths for the treatment of these severe posterior eye diseases.

1 Introduction

Proliferative diseases of blood vessels in the posterior eye are responsible for many cases of vision loss every year [1]. The three most common ophthalmologic neovascular diseases - exudative age-related macular degeneration (wet AMD), proliferative diabetic retinopathy (PDR) and retinopathy of prematurity (ROP) - are among the main causes of blindness and severe impairment of visual acuity in children (ROP), working-age adults (PDR) and elderly patients (wet AMD) [2–4]. They share pathophysiological mechanisms of neovascularization, leading first to fluid accumulation and hemorrhage in the retina and finally to retinal detachment and photoreceptor death/degeneration (Fig. 1) [5–7].

In the healthy eye, a sophisticated balance between pro-angiogenic and anti-angiogenic factors tightly controls the formation of new blood vessels [8]. Usually, because anti-angiogenic factors such as pigment epithelium-derived factor (PEDF) prevail, this complex balance is biased to an anti-angiogenic state. Thus, excessive and pathologic neovascularizations are normally suppressed. PEDF has potent anti-vascular endothelial growth factor (VEGF) activity and is expressed by the retinal pigment epithelium (RPE) [9], a cell layer located between the outer segments of the photoreceptors and the major underlying blood vessels, the choriocapillaris.

One strong factor that can push this delicate equilibrium towards pro-angiogenesis is hypoxia. Over a prolonged period of time, retinal ischemia leads to hypoxia. Concomitantly, expression of hypoxia-inducible factor 1α (HIF-1α) initiates a complex signaling cascade that ultimately results in the upregulation of several pro-angiogenic factors [10], with VEGF being the most prominent and crucial one (Fig. 1). VEGF, which exists in several isoforms, has been shown to be one of the key regulator for pathological angiogenesis [11].

The development of intravitreal therapies targeting VEGF like ranibizumab (Lucentis®), bevacizumab (Avastin®), pegaptanib (Macugen®) and aflibercept (Eylea®) were a major breakthrough in the treatment of neovascular eye diseases. However, these therapies also have drawbacks. Besides the risk related intravitreal injection of the formulation into the eye, there are also relevant systemic risks that stem from antibodies which exit the eye and enter into systemic circulation [12]. The small but prolonged suppression of the plasma VEGF level which may result is postulated to lead to an increased risk of cardiovascular diseases like stroke and thromboembolic events [12,13].

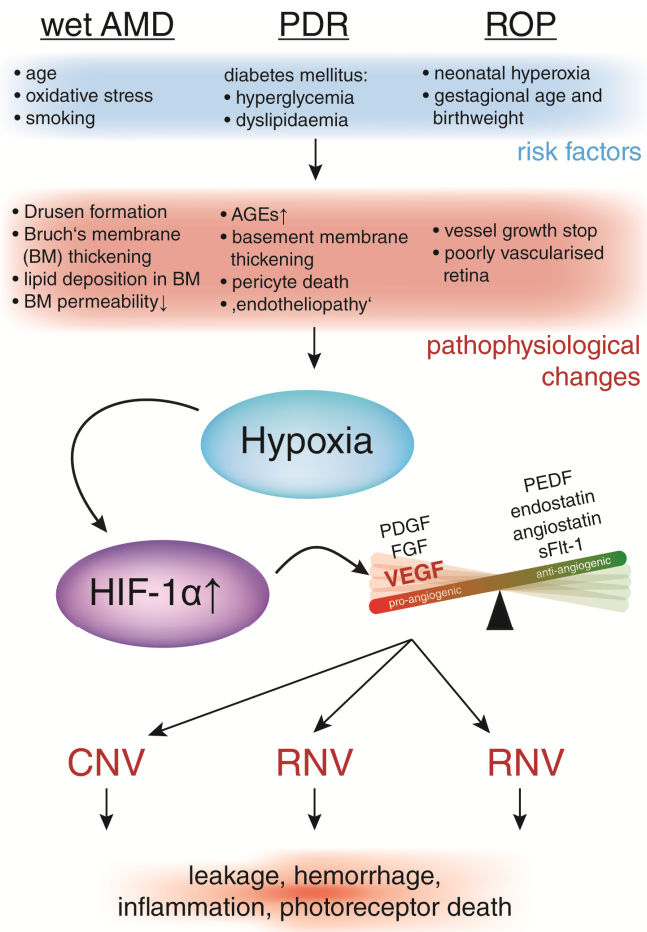

Figure 1: Simplified schematic representation of hypoxia as one key event in the formation of neovascular lesions. Hypoxic conditions lead to the upregulation of HIF-1α, which in turn increases expression of VEGF tilting the angiogenic balance towards pro-angiogenesis. This results in pathological neovascularizations. AGEs - Advanced glycosylation end products, FGF – Fibroblast growth factor, HIF-1α - Hypoxia-inducible factor 1α, PEDF – pigment epithelium-derived factor, PDGF – Platelet-derived growth factor, VEGF - Vascular endothelial growth factor, CNV - choroidal neovascularization; RNV - retinal neovascularization.

Furthermore, because VEGF also plays an important protective role in the retinal tissue itself [14], broad and rigorous VEGF knockout in the retina can lead to severe side effects: defects in the RPE-choroid complex or the loss of interaction between the RPE and photoreceptors' outer segments [15]. Additionally, VEGF deprivation results in a reduction of endothelial cell fenestrations in the choriocapillaris [16], which can in turn induce endothelial wall thickening and lead to decreased nutritional support for the photoreceptors and RPE [15]. This is also the reason why the therapy with anti-VEGF antibodies increased the development of foveal and non-foveal geographic atrophy in a number of patients with neovascular AMD [17].

Therefore, alternative therapeutic concepts would be highly desirable. Unfortunately, the eye as a target organ possesses several important superficial and internal barriers that

impede both direct and systemic drug access [18]. The outer and inner blood-retinal barriers (BRB), which consist of tight junctions between neighboring RPE cells and retinal endothelial cells, respectively, strictly limit the transport of unwanted molecules from the blood stream to the retina. On the other hand, the blood-aqueous barrier (BAB), located in the anterior eye segment and formed by the ciliary epithelium and the uveal capillaries, prevents drugs from diffusing into the anterior eye from the systemic circulation. In the pathogenesis of neovascular diseases of the posterior eye, newly formed vessels sprout into the retina or vitreous, infiltrate the ocular tissue and break down the BRBs. In this case, the drug's target tissue is directly accessible from the circulation, circumventing the need to cross challenging biological barriers. However, compared to intravitreal injection, a substantially higher dose is needed to maintain therapeutic concentrations in the pathologic lesions [19]. For instance, just 2.5 mg of bevacizumab are required to achieve therapeutic drug levels in the eye with an intravitreal injection, whereas 5 mg/kg bevacizumab are needed to achieve the same therapeutic effect after intravenous injection [20]. The systemic side effects and elevated cost that result mean that systemic therapies with free drug are often unfavorable in comparison.

In cancer therapy, we find an instructive case study for how encapsulation of therapeutics in nanoparticles (NPs) may significantly advance the therapy of neovascular posterior eye disease. In both cases, systemic administration of free drug leads to dose-limiting toxicities. The physiology is also quite similar; abnormal tumor vasculature and pathologic neovascular eye lesions both exhibit enhanced permeability to and retention of macromolecules and NPs. In other words, both sets of disease experience the same limitations on conventional systemic treatments and are characterized by highly similar physiological architectures, where drug delivery is concerned. Thus, we believe that the therapeutic index of intravenously injected drugs could be vastly improved by encapsulation within NPs.

Nanoparticle formulations are also of great interest for intravitreally administered drugs, with intravitreal injections of drug containing solutions remaining the gold standard for therapy of the posterior eye. In this regard, intravitreal delivery is also highly interesting for nanomedical applications: The eye's highly compartmentalised anatomy leads to slow elimination of colloidal systems, which may be found in the eye several months after application [21]. In addition, since the eye is an immune-privileged organ, some severe drawbacks of systemic NP application, such as clearance by the mononuclear phagocyte system, can be avoided.

This review is a comprehensive systematic overview of nanoparticle systems that were investigated for the treatment of retinal and choroidal neovascularization for the therapy of AMD, PDR and ROP. Along with drug and gene delivery applications, use of the inherent anti-angiogenic and anti-oxidative properties of nanomaterials in the context of neovascular ocular diseases is highlighted. Furthermore, this review focuses on the opportunities, pitfalls and challenges related to developing systemic nanoscale therapies of the previously mentioned neovascular eye diseases.

2 Ocular diseases related to neovascularizations

Neovascularizations are a hallmark of a small number of severe eye diseases. Due to its enormous metabolic activity, the eye (and particularly, the retina) has the highest oxygen consumption of any tissue in the human body [22]. When small capillaries are damaged, e.g. through hyperglycemia in diabetes, the retina can rapidly suffer from hypoxic conditions; neovascularization sets in to compensate for the lack of oxygen. Unfortunately, the newly built blood vessels are often leaky and cause more problems than they solve. Below, the epidemiology and current treatment options for the three most common neovascular posterior eye diseases will briefly be presented.

2.1 Age-related macular degeneration

AMD is the most common cause of vision loss in the elderly [23]. In 2011, it was estimated that 6.5 % of the population of the United States over the age of 40 years had signs of AMD [24]. Furthermore, it is predicted that the total number of people with AMD worldwide will rise to 196 million in 2020 and further to 288 million in 2040 [25]. The disease occurs via two processes, either through exudative neovascularizations (called “wet” AMD) or by a non-exudative geographic atrophy (often referred to as “dry” AMD) [12]. Wet AMD is characterized by pathological neovascularizations that originate in the choriocapillaris and break through Bruch’s membrane as well as the RPE. These neovascular vessels leak into the subretinal space and often lead to sudden vision loss [26]. Although just 10 to 15 % of all patients with AMD suffer from the wet form, this exudation and hemorrhage into the retina is primarily responsible for the occurrence of rapid vision loss in the entire AMD population. In contrast to wet AMD, dry AMD progresses more slowly and is characterized by the appearance of drusen: small, yellowish deposits that ultimately lead to atrophy and thinning of the RPE, the choriocapillaris and the photoreceptors in the macula. Although vision loss is less aggressive for dry AMD

patients, a certain percentage of patients with dry AMD can develop wet AMD [27]. Before anti-VEGF therapy was introduced into clinical practice, the neovascular form of AMD was mainly treated by laser photocoagulation and photodynamic therapy (PDT) of the pathologic lesions, both of which have mediocre therapeutic outcomes [12]. Consequently, the development of anti-VEGF treatments represented an enormous breakthrough in the standard of care for wet AMD. Besides anti-VEGF antibodies, the current palette of anti-VEGF molecules additionally consists of pegaptanib, a VEGF binding aptamer and aflibercept, which is a soluble decoy receptor fusion protein [28].

2.2 Diabetic retinopathy

DR is the most prevalent microvascular complication of diabetes mellitus [29], a disease currently affecting more than 285 million worldwide [30]. Nearly all patients that suffer from diabetes for more than 20 years will have at least some symptoms of diabetic retinopathy [29]. In 2010, it was estimated that 93 milion people worldwide are affected by diabetic retinopathy [31] and that in the United States alone 10,000 people are going blind due to diabetic retinopathy every year. Similar to AMD, DR can also be divided into proliferating and non-proliferating disease forms. Proliferative diabetic retinopathy (PDR) is characterized by pathological neovascularizations that originate in the venous side of the retinal circulation and subsequently penetrate through the inner limiting membrane into the vitreous cavity [29]. This can result in vitreous hemorrhage, the proliferation of fibrous tissue and ultimately, retinal detachment. By comparison, non-proliferative diabetic retinopathy (NPDR) often occurs in early stages of diabetic retinopathy and is characterized by microaneurysms and retinal hemorrhages that are a consequence of sustained hyperglycemia in diabetic patients. Until recently, the standard of care treatment for PDR has been pan-retinal photocoagulation (PRP) [32], in which peripheral VEGF-releasing retinal cells are destroyed. Moreover, because the overall retinal oxygen demand by the outer retina is reduced, more oxygen is available for the macula, preserving the important central vision. Based on the results of the RISE and RIDE phase 3 trials [33], the US Food and Drug Administration (FDA) approved Lucentis® Breakthrough Therapy for the treatment of diabetic macular edema. Both trials impressively showed that patients under anti-VEGF therapy were less likely to develop the proliferative form of DR. However, for therapy of PDR, all anti-VEGF therapies were beneficial and effective but only in the short-term. Compared to the gold standard PRP, whose therapeutic effects are remarkably long-lasting [32], the anti-VEGF substances did

not have a similarly sustained impact. Furthermore, in a few patients with severe PDR, bevacizumab caused tractional retinal detachment [34].

2.3 Retinopathy of Prematurity

Around 10 % of all births worldwide occur preterm [35]. Of these preterm births, 73 % of infants with a gestational age of 27 weeks or less are prone to develop ROP [36], a condition which blinds around 50,000 children worldwide every year [37]. The most important risk factor for the development of ROP is the supplemental oxygen found in neonatal incubators. On one hand, supplemental oxygen significantly improves the survival of preterm infants, but on the other hand, it contributes heavily to the pathogenesis of ROP [5]. In the first phase, hyperoxia leads to suppression of angiogenic growth factors like erythropoietin and VEGF [5]. This halts physiological vessel growth. After the neonatal oxygen therapy is finished, the matured retina, which has an increased metabolic activity, experiences hypoxic conditions. The local hypoxia upregulates pro-angiogenic growth factors stimulating neovascularization. However, the newly formed blood vessels are leaky and insufficiently perfuse the retina [5]. This results in fibrous scarring, which can cause retinal detachment and subsequently lead to blindness [38]. To date, the standard therapy for ROP has been laser or cryoablation of the peripheral avascular retina with the goal of controlling pathologic neovascularizations [5]. However, due to the limited efficiency and high morbidity, anti-VEGF treatments have recently been investigated as an alternative [2]. Although successful for many children, treatment with bevacizumab did not show significant results for neovascularizations in all retinal areas. Moreover, because a rigorous VEGF knockdown is highly detrimental for the developing retina, the right dose of antibody must be carefully titrated to inhibit pathologic neovascularizations but allow normal vascular development [39]. For this reason, alternative VEGF-independent strategies would be incredibly beneficial in the treatment of ROP.

3 Systemic nanoparticle therapy – Opportunities and Challenges

3.1 Is there a need for a systemic therapy?

Discovery of the anti-VEGF antibodies ranibizumab (Lucentis®) and bevacizumab (Avastin®) as well as the anti-VEGF aptamer pegaptanib (Macugen®) were a major breakthrough in the therapy of eye diseases that are characterized by neovascularization and exudation. Lucentis®, Macugen® and Eylea® have the FDA approval for the treatment

of AMD, whereas Avastin® is approved for treatment of several forms of cancer and is used on an off-label basis for AMD therapy, mainly due to its significantly lower cost per dose [40]. Especially for AMD, antibody-based therapeutics were the first to not only prevent vision loss but also significantly improve visual acuity. Compared with intravenous administration, intravitreal dosing reduces systemic exposure and requires a 500-fold reduced dose of antibody [19]. As such, the therapeutics are usually administered intravitreally once every four weeks. Although highly beneficial, ocular injections are associated with patient discomfort and carry attendant risks. These include infection, bleeding, inflammation and more severe side-effects like elevated intraocular pressure, endophthalmitis and detachment of the retina [41,42]. Besides injection-related risks, the patient and the patient's caretaker must visit the ophthalmologist's office on a monthly basis. Furthermore, the economic burden that is connected to the frequent intravitreal injections should not be underestimated [43].

With less invasive therapeutic options, the current treatment burden for anti-VEGF therapy could be enormously reduced. Here, a safe systemic therapy using nanoparticles to deliver potent drugs and genes to the ocular tissue could be highly beneficial.

3.2 Importance of choroidal blood flow in systemic delivery

The retina has by far the highest oxygen consumption of any tissue in the human body, as a direct consequence of the photoreceptor's tremendous metabolic activity [22]. This activity leads to the generation of an enormous amount of heat, which can severely damage the photoreceptors if it is not dissipated [44]. The choroid, which acts as the predominant of the two retinal blood supplies supports the immense oxygen and nutrients needs of the retina, removes waste products like lactic acid and actively controls retinal temperature via cooling or heating [45]. This is accomplished by an incredibly high blood flow through the choroid, which far exceeds the perfusion of all other vascular beds within the human body (Fig. 2). Compared to the brain, the blood flow which transits the choroid is 10 times higher per unit tissue weight [46], reaching values up to 2000 mL/min/100 g tissue [47].

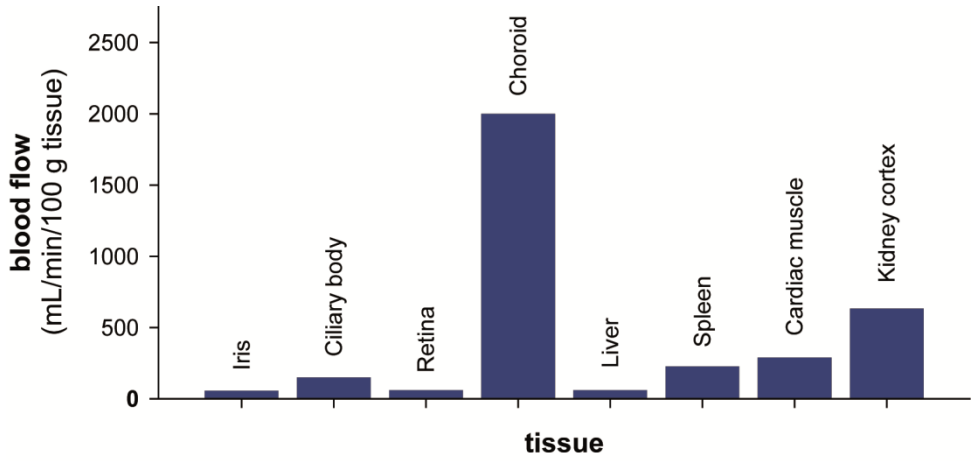

Figure 2: Rate of blood flow normalized to weight in several tissues as measured in cynomolgus monkeys . (Adapted from [46,47])

For a nanoparticle formulation to successfully accumulate within a specific tissue after systemic administration the colloids need to have long circulation time and the site must be well-perfused and readily accessible. Here, the enormous blood flow through the choroid is very useful for delivering nanoparticles to ocular tissue. Although AMD and PDR can lead to a decrease in choroidal blood flow [48,49], the perfusion is still immense and thus very favorable for the deposition of nanomaterials in ocular tissue.

3.3 Passive accumulation via an EPR-like effect

The enhanced permeability and retention (EPR) effect of tumors was originally observed by Maeda and Matsumura nearly 30 years ago [50]. When tumors reach a certain size, tumor cells far away from existing vessels become hypoxic due to limited diffusion of oxygen into the neoplastic tissue [8]. As a result of hypoxia, the expression of pro-angiogenic molecules such as VEGF and angiostatin are highly upregulated [51]. This leads to rapidly growing, pathological neovascularizations that show a multitude of structural aberrations. The trademarks of this ill-formed vasculature are wide intercellular clefts between endothelial cells and a disrupted or absent basement membrane [52]. Additionally, high intratumoral VEGF concentration causes the endothelial lining to be packed with wide fenestrations [53]. These abnormalities lead to extravasation and thus passive accumulation of macromolecules and nanoparticles into the tumor tissue. Furthermore, the absence of lymphatic vessels in the tumor architecture results in retention of accumulated macromolecules and NPs. Discovery of the EPR effect was the starting point for the development of a plethora of polymeric drugs and nanoparticles for cancer therapy.

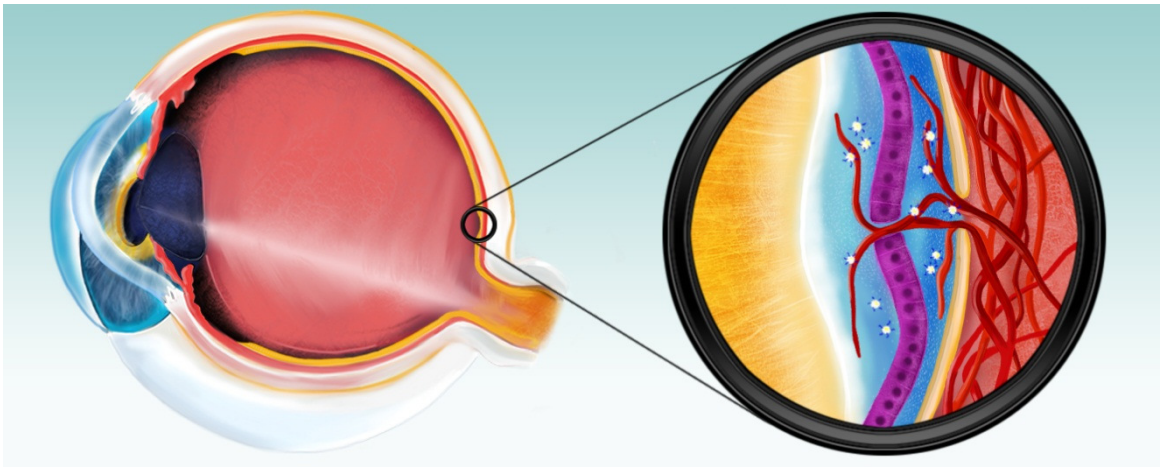

Figure 3: Schematic depiction of passive nanoparticle accumulation in the subretinal space as a result of choroidal neovascularizations that breach the RPE.

A similar but not identical situation can be found in neovascular pathological lesions in the eye. As originally observed for high molecular weight polymers and polymer-drug conjugates at the beginning of the century [54–56], intravenously administered macromolecules showed increased accumulation in the CNV areas and were retained for a prolonged time in the eye. The cause of this passive accumulation may be found in the morphology of the CNV lesions themselves: Similar to the conditions in tumor vasculature, ocular neovascular membranes have fenestrations [57,58] that allow NPs to extravasate. Moreover, before maturing, the vessels of the leaky lesions exhibit open interendothelial clefts [59], through which leakage can occur. Upon maturation, the interendothelial junctions close, but the fenestrations remain [59]. Because the eye lacks a functional lymphatic system – it is characterized instead by the presence of prelymphatics [60] - accumulated nanoparticles are retained around the neovascularized areas where they may then release drugs and exert their effects. In the context of tumor therapy, the EPR effect is often overestimated [61,62]. Although artificial tumor xenografts in mice exhibit a strong EPR effect, several “naturally grown” human tumors do not [63]. This is one of the main reasons many nanoparticle systems fail in human trials, even though they demonstrated potency in animal studies [62]. Two important reasons for this discrepancy are high tumor cell density and high interstitial fluid pressure (IFP), hypothesized to be the main barriers for macromolecules and NPs to deeply penetrate tumor tissue [64]. The high IFP is a consequence of the EPR effect itself, namely the increased permeation of fluid into the tissue and the lack of lymphatic drainage, but it is also a result of the dense collagen network in the tumor extracellular matrix [65]. This situation is slightly different in ocular tissue. In the eye, when the outer BRB breaks down due to subretinal

neovascularizations, intense exudation creates a fluid pressure gradient for proteins [66], other macromolecules and NPs. In addition, blood vessel defects, especially in advanced disease, can be more pronounced, resulting in not only fluid leakage but also bleeding into the surrounding tissue. This hemorrhage into the retina can be one of the first signs of wet AMD [27] and one of the main reasons for the loss of visual acuity [67]. Overall, compared to the tumor EPR effects, the EPR effect exerted by neovascularities in ocular tissue is potentially even greater. Thus, especially in advanced and end-stage neovascularizations, the capability of macromolecules and nanoparticles to passively accumulate in ocular lesions strongly suggests a path toward effective systemic administration.

3.4 Initial use of the ocular EPR effect with the photosensitizer Visudyne®

Visudyne® is a liposomal formulation of the photosensitizer verteporfin that was approved by the FDA in 2000 for the therapy of occult subfoveal choroidal neovascularizations in AMD [12,68]. Its application is a two-step process which involves intravenous application of Visudyne® followed by activation by shining infrared light directly into the eye. After injection, the liposomes encapsulating verteporfin preferentially accumulate in the abnormal and leaky blood vessels in the eye. Thus, Visudyne® was the first commercially available and systemically administered pharmaceutical product that exploited the unique neovascular environment in the eye. Because of the large amount of unsaturated phosphatidylglycerols and the absence of cholesterol in the formulation, Visudyne® liposomes are characterized by a high level of membrane disorder and are easily destabilized [69]. Therefore, in the presence of serum, the hydrophobic photosensitizer is rapidly transferred from the liposomal formulation to lipoproteins such as low density lipoprotein (LDL) [70]. By virtue of the EPR effect, these also accumulate at neovascular sites and are taken up by endothelial cells, which usually have increased expression of LDL receptors [71]. Upon activation with infrared light, the photosensitizer generates reactive oxygen species (ROS) like singlet oxygen and free radicals. The cytotoxic radicals damage the pathologic neovascularizations and “close” the abnormal blood vessels.

However, the clinical efficacy of Visudyne® was not overwhelming [72], which prompted researchers to evaluate new photosensitizers as well as new nanoparticle formulations for the photodynamic therapy of CNV. Ideta and coworkers designed a dendrimer-based photosensitizer, where a porphyrin molecule is surrounded by poly(benzyl ether)

dendrons [73]. This architecture inhibits photosensitizer aggregation, thus preventing self-quenching effects [74]. In a model of CNV initiated by laser-induced photocoagulation, a micellar formulation of the dendrimer-based photosensitizers accumulated in the neovascular lesions and resulted in a 280-fold increase in phototoxicity, which led to significantly reduced fluid leakage from the neovascularizations [73]. Since a distinct upregulation of VEGF after PDT can lead to CNV regrowth [75], another approach combined PDT with an anti-VEGF therapy in targeted liposomes [76]. Sorafenib, an active multi-kinase inhibitor that targets VEGF receptor tyrosine kinase signaling, and photocyanine as photosensitizer were encapsulated in liposomes which were toxic to human umbilical vein endothelial cells (HUVECs) but showed no toxicity to RPE cells *in vitro*. In a mouse model of laser-induced CNV the targeted liposomes loaded with both substances exhibited the lowest CNV area and leakage [76]. When verteporfin was incorporated into cationic liposomes, photodynamic therapy of the neovascular lesions was as effective as Visudyne® but induced less damage in the surrounding tissue, showing a more specific accumulation [77]. Cationic nanoparticles preferentially bind to angiogenic endothelial cells due to an increased exposure of anionic molecules on the proliferating blood vessel surface [78], a phenomenon that has also been thoroughly investigated for targeting of tumor vasculature [79]. Likewise, compared to cationic liposomes, neutral liposomes showed no specific accumulation at the angiogenic sites in the eye [80].

3.5 Active targeting of nanoparticles to the posterior eye

In the early stages of neovascular diseases, where an effective treatment would be highly desirable, the capillaries are less leaky and dislocated, preventing extensive passive accumulation of nanoscale carriers. In this case, to successfully target the endothelial lining in the choriocapillaris and the intraretinal capillaries, where cells proliferate under increased VEGF concentrations, high affinity targeting strategies have to be applied. By far the most widely used approach to actively target NPs to neovascular lesions is attachment of the arginine-glycine-aspartate (RGD) peptide sequence to the nanoparticle corona. The RGD sequence is capable of binding several integrins, including $\alpha_v\beta_3$ and $\alpha_v\beta_5$: two common integrins that are pivotal for the formation of new blood vessels and are upregulated in the angiogenic state [81]. The reason for this sharp upregulation is the function of the $\alpha_v\beta_3$ integrin: during angiogenesis, it provides endothelial cells with the capability of migrating and attaching to extracellular matrix in the process of

remodeling [82]. Conversely, in the healthy, non-proliferative choroid, the expression of both integrins is only minimal [83]. Interestingly, in the normal healthy eye, nanoparticles coupled to linear RGD sequences were unable to bind to intact vasculature and did not significantly accumulate [84,85]. However, when a cyclic RGD peptide was coupled to the colloidal surface, NPs were able to target and bind healthy capillaries (Fig. 4) [86]. Due to the conformational restriction imposed by cyclization, cyclic RGD peptides exhibit approximately 100-fold higher integrin affinity than their linear counterparts [87], which is reflected in the increased NP binding in the choroid, despite only low-level integrin expression. During the pathogenesis of neovascularities, integrin expression tremendously increases [88]. We hypothesize that this enables binding of nanoparticles coupled to low-affinity ligands like linear RGDs to the endothelium due to increased avidity of multivalent binding to the vasculature (Fig. 4). Because NPs display multiple identical ligands on their surface, they have the capability to bind several receptors simultaneously [89]. Although the affinity of one ligand to the receptor does not change, the higher expression of integrin receptors leads to multiple nanoparticle-receptor interactions, higher avidity of interaction and subsequently stronger association.

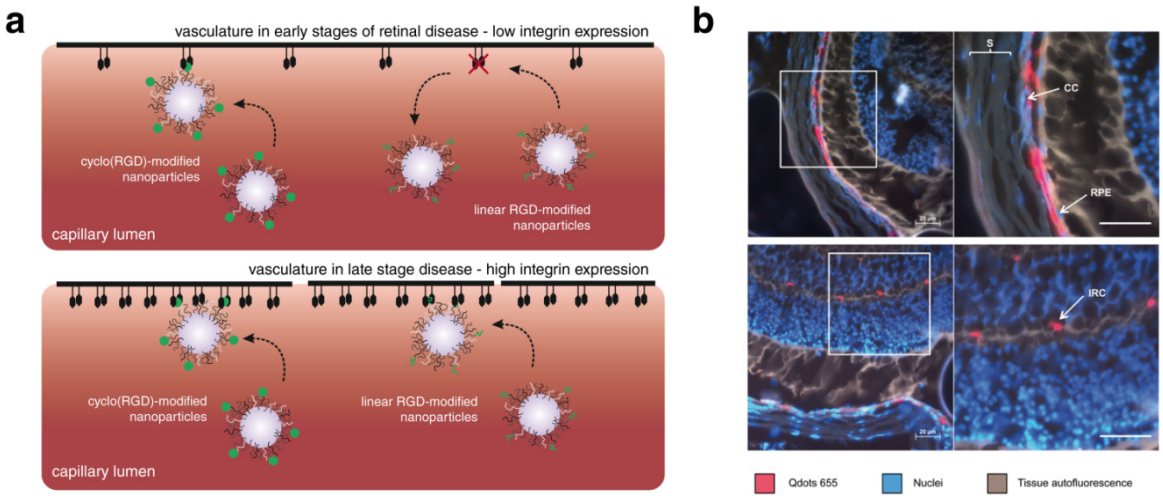

Figure 4: Association of RGD-modified nanoparticles with the ocular vasculature. Cyclo(RGD)-NPs bind the retinal vasculature in early and late stages of disease, whereas linear RGD-NPs only bind the pathological vessels (a). The cyclo(RGDfC)-modified NPs accumulate in the choriocapillaris (b, top) and intraretinal capillaries (b, bottom) of healthy retinae after systemic administration [86].

However, besides the targeting function for which the RGD peptides are primarily used, they also have intrinsic anti-angiogenic activity. Because of their ability to antagonize integrins after binding [90], the cyclic peptides showed a potent inhibitory effect on choroidal [54] and retinal neovascularizations [91]. Furthermore, RGD peptides also seem to have a positive effect on fibrovascular remodeling during the progression of

neovascular diseases in the eye [92]. This inherent anti-fibrotic activity [93] is also a consequence of the antagonistic effects of small RGD peptides on α_v integrins.

One of the first examples to show the feasibility of RGD peptide-mediated targeting to neovascular lesions was conducted by Singh et al. [84]. They encapsulated a plasmid encoding a VEGF intraceptor within poly(lactide-*co*-glycolide) (PLGA) nanoparticles [84]. The intraceptor is a recombinant construct of the VEGF receptor 1 and is coupled to an endoplasmic reticulum (ER) retention signaling sequence, which prevents secretion of endogenous ER proteins. With the help of this VEGF intraceptor, VEGF is intracellularly bound and degraded without exerting its effects [94]. Interestingly, NPs that were not surface-functionalized showed only minute accumulation in the laser-treated eyes. It is possible that their large size of ~400 nm [94] prevented them from extravasating and accumulating passively. However, by introducing linear RGD peptide and transferrin targeting moieties onto the surface of the PLGA nanoparticles, NP accumulation within the laser-treated eye could be significantly increased. Concomitantly, delivery of the intraceptor plasmid and thus CNV lesion therapy could be markedly enhanced [84]. In a follow-up study this effect could be translated to primates. Here, the systemic administration of RGD-functionalized PLGA nanoparticles encapsulating the VEGF intraceptor plasmid was more efficient than the standard therapy of intravitreal anti-VEGF antibodies [92].

3.6 Size does matter: the eye as systemic nanoparticle target

Despite the excellent specific perfusion rates of the posterior eye segment, the eye is one of the smaller organs in the body. The accumulation of nanomaterials follows a perfusion-driven distribution into the organs, where bigger organs have a natural advantage. In one of our own studies we analyzed the deposition of cyclo(RGD)-modified NPs in the choroid; we were able to deposit 3.3 ± 0.7 % of the injected dose per g organ weight (% ID/g) into the choroid [86]. Compared to the kidney (1.6 % ID/g) and the heart (1.5 % ID/g) the nanoparticle content in the choroid was significantly higher, whereas it was comparable to the nanoparticle content in the lung (4.4 % ID/g). Although this might seem like a high deposited dose into the healthy, non-leaky vascular tissue, it is easy to overestimate the amount of accumulated nanoparticles. When not adjusted to the weight of the choroid only 0.14 ‰ ± 0.016 ‰ of the total injected dose was deposited after 1 hour of nanoparticle circulation [86]. In our experiments, the eye and the choroid had masses of 0.19 % and 0.013 % body weight, respectively, which are minuscule compared to the

weights of tumor xenografts that easily reach up to 10 % body weight, especially in fast-growing implanted tumors. Although the percent dose per gram of tissue may be lower here, the actual deposited dose is of course much higher. Nevertheless, during the progression of neovascular diseases in the eye and with the leakiness of abnormal vessels, nanoparticle accumulation greatly increases (see EPR-like effect). Taken together, this means that in the early stages of retinal disease in which capillaries are not yet leaky and dislocated, highly effective targeting strategies are needed to deliver a sufficient dose for a successful therapy. That being said, unless the circulation time of NPs greatly increase from what is presently possible, the majority of colloids will not end up in ocular tissue.

3.7 Bruch's membrane as the main barrier after systemic administration

Although potent targeting strategies are able to bind NPs to the vasculature in early stages of retinal disease [86], the actual cause for CNV may occur elsewhere. The retinal pigment epithelium (RPE), the key component of the outer blood-retinal-barrier (oBRB), has a central role in the pathogenesis of AMD. Impairment of RPE cell functions can be an initial and deciding event leading to the clinical signs of AMD [95]. Furthermore, VEGF secretion by the RPE, which is pivotal for maintenance of the choriocapillaris, is also speculated to itself induce CNV [1]. Therefore, a nanoparticle therapy targeted to the RPE to tackle the early stages of AMD could be incredibly beneficial. Although several reports show the feasibility of RPE targeting with NPs *in vitro* [96–99] and *in vivo* after intravitreal [21,100] and subretinal injection [101–103], *in vivo* data describing systemic administration of NPs targeted to RPE cells before neovascularizations take place is scarce.

Like the photoreceptors, the RPE is supplied by the choroid and especially the choriocapillaris. Between the choriocapillaris and the RPE lies Bruch's membrane (BM), a 2-4 µm acellular, five-layered extracellular matrix (Fig. 5). Interestingly, the endothelial lining of the choriocapillaris that faces Bruch's membrane is highly fenestrated, potentially allowing NP extravasation towards Bruch's membrane in the extravascular space (Fig. 5). However, the capillaries' fenestrations are limited to a diameter of approximately 80 nm and feature a fenestral diaphragm [104]. Additionally, an endothelial glycocalyx surrounds the fenestrations and further reduces the pore size. These ultrastructural properties already heavily limit the passage of macromolecules and nanoparticles through the fenestrae [105]. However, the most effective barrier to nanoparticle passage to the RPE is the five-layered Bruch's membrane.

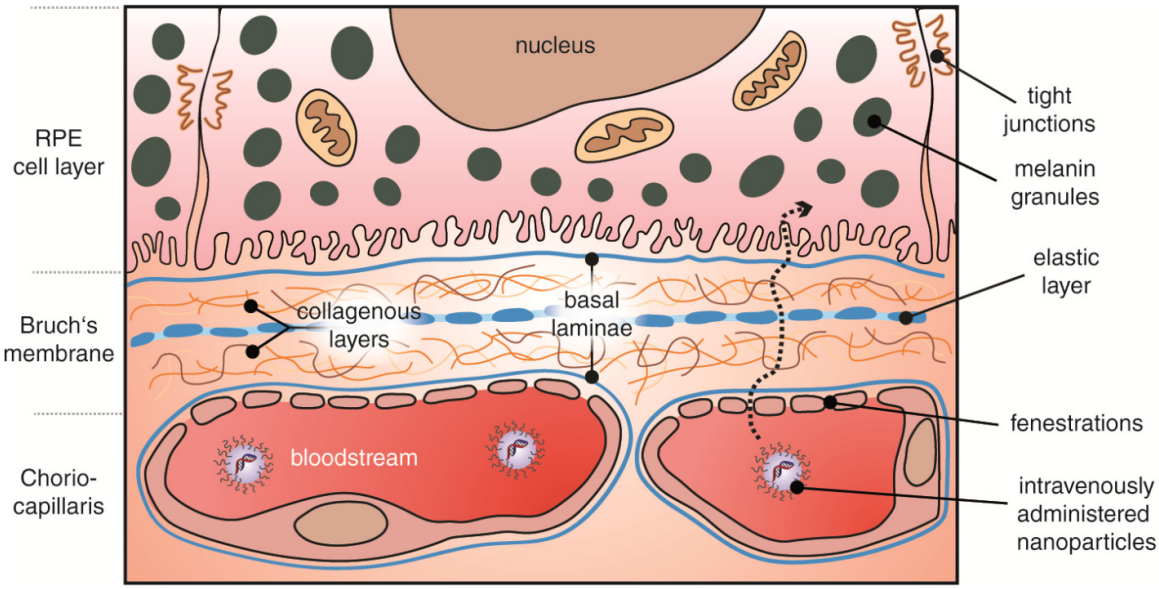

Figure 5: Schematic overview of nanoparticle transport to the RPE. After leaving the fenestrated choriocapillaris the NP has to cross the five-layered Bruch's membrane, consisting of a central elastic layer, two collagenous layers and the RPE and choriocapillaris basal laminae (adapted from [27]).

Although earlier studies suggested a molecular exclusion limit of 100- 200 kDa for crossing Bruch's membrane, depending on patient age [106], more recent studies show that LDL with a size of 19 – 23 nm and a mass up to 3900 kDa are able to pass through. Even though LDL, which has a size comparable to small NPs and micelles, cannot pass completely freely, its transport is only modestly inhibited [107]. Similarly, 20 nm gold NPs were also found to pass the BRB and distributed throughout the retina [108]. However, it is unclear if the gold NPs also passed through Bruchs' membrane or if they exclusively reached the retina by transiting the inner blood-retinal barrier. Similar to all basement membranes throughout the body, Bruch's membrane consists of proteoglycans and several other proteins [106]. Its glycosaminoglycan moieties are highly negatively charged and decrease the mobility of negative charged NPs by electrostatic repulsion [109]. Therefore, for NPs to effectively cross through the Bruchs' membrane, they have to be relatively small (probably <25 nm) and most likely possess a neutral or positive surface charge [110,111]. Negatively charged PLGA NPs with a size of ~400 nm were only able to transfect the RPE after CNV was induced and the BRB was damaged [84]. Interestingly, the amount of glycosaminoglycans in Bruch's membrane and their degree of sulfation decreases with age [112], which possibly weakens the charge-selective barrier for NPs in elderly patients. With respect to the passage of NPs, the structure of the choriocapillaris, Bruch's membrane and the RPE are similar to that of the renal filter. As such, NPs that are able to deliver a payload to the RPE have to be very

precisely tailored regarding their size, charge and plasticity, making them similar to nanomaterials designed to be filterable by the kidneys [113].

However, the permeability of Bruch's membrane is drastically decreased in an aged eye and further still in AMD [114]. Thickening of Bruch's membrane, drusen formation [115], the accumulation of cholesterol [116] and basal linear and laminar deposits [117], further complicate the passing of NPs through Bruch's membrane. Nevertheless, once a NP encounters the RPE, sophisticated active targeting strategies are not necessarily required, since the RPE is among the most phagocytically active tissues in the body [118]. Potentially, that could lead to natural endocytosis of the NPs once within reach of the cells, and further to therapeutic activity at the RPE.

4 Intravitreal nanoparticle therapy

4.1 Nanoparticle systems for ocular gene therapy

Gene therapy, which can be defined as the transfer of nucleic acids into a cell, tissue or organ [119], ultimately aims to treat the cause rather than the symptoms of a disease. This can either happen by the introduction of corrective genes into cells or by blocking malfunctioning genes using RNA interference mechanisms. However, the lack of efficient and safe viral and non-viral delivery systems has posed substantial problems for gene therapy applications in the past. Here, non-viral nanoparticles can tremendously help not only to compact the DNA but also to protect it and effectively deliver it to the target tissue. The eye is an ideal candidate for gene therapy especially in the context of intravitreal injections because of several outstanding features. First, its highly compartmentalized anatomy allows precise delivery of nanoparticle vectors into specific tissues in the eye, which concomitantly minimizes systemic dissemination [120]. Second, since the ocular tissue consists of a stable population of cells, highly efficient transduction with adequate longevity can be expected [120]. And last, due to the eye's immune privilege, an immunogenic response can be mostly avoided [121]. For ocular applications, several different modalities of gene therapy and gene delivery have been investigated for the nanoparticle-based treatment of choroidal and retinal neovascularizations (Table 1). In recent approaches, gene therapy has been mainly used to modulate the expression of VEGF, the key regulator of angiogenesis and vascular permeability. The two most prominent strategies used were (1) increasing the expression of VEGF-capturing

molecules or anti-angiogenic factors or (2) directly decreasing the VEGF expression or manipulating VEGF-signaling cascades.

Table 1
Gene delivery approaches for treatment of experimental CNV using NPs

Incorporated gene	Type of NP	NP size	Targeting ligand	Injection route	CNV model	Outcome	Refs.
Anti-VEGF sense oligonucleotide	Lipid-lysine dendrimer	n/a	none	IVT	Laser photocoagulation	FA leakage↓	[122] [123]
Plasminogen kringle 5 pDNA	PLGA-chitosan NPs	260 nm[1]	none	IVT	OIR, streptozotocin-induced DR	VEGF expression↓ FA leakage↓	[126]
Hypoxia-inducible factor 1α shRNA pDNA	PLGA NPs	303 nm	none	IVT	Laser photocoagulation	FA leakage↓	[127]
VEGF receptor 1 siRNA	PEGylated liposome-protamine-hyaluronic acid NPs	132 nm[1]	none	IVT	Laser photocoagulation	CNV Area↓	[98]
Soluble VEGF receptor 1 pDNA	PEG-*b*-PASp(DET) micelles	n/a	none	IV	Laser photocoagulation	CNV Area↓	[167]
ATPμ-Raf pDNA	cationic polymerized lipid-based NPs	45 nm[1]	linear RGD	IV	Laser photocoagulation	CNV Area↓	[85]
Anti-VEGF intraceptor pDNA	PLGA NPs	375-420 nm[1]	linear RGD, transferrin	IV	Laser photocoagulation	VEGF Expression↓ CNV Area↓	[84]
Anti-VEGF intraceptor pDNA	PLGA NPs	570 nm[1]	linear RGD	IV	Laser photocoagulation, soluble VEGF receptor knockdown	CNV Area↓ Fibrosis↓ Vision function↑	[92]

CNV, choroidal neovascularization; DR, diabetic retinopathy; FA, fluorescein angiography; IV, intravenous; IVT, intravitreal; OIR, oxygen-induced retinopathy; nanoparticle; PEG-*b*-PASp(DET), poly(ethylene glycol)-*b*-poly{N-[N-(2-aminoethyl)-2-aminoethyl]aspartamide}, pDNA, plasmid DNA; PLGA, poly(lactide-*co*-glycolide); shRNA, small hairpin RNA; siRNA, small interfering RNA; VEGF, vascular endothelial growth factor

[1] as measured by dynamic light scattering

One of the first examples of nanomaterial-based intraocular gene therapy to decrease the VEGF expression was demonstrated by Marano and coworkers nearly 10 years ago. By synthesizing a lipid-lysine dendrimer they were able to deliver a sense oligonucleotide with anti-VEGF activity into the choroidal lesions. Interestingly, eyes that were subject to photocoagulation two months after intravitreal injection of the dendrimer-

oligonucleotide complex still showed smaller CNV areas, illustrating the longevity of the anti-CNV activity [122]. The complexes not only inhibited CNV development for several months, but were also found throughout the whole retina up to the RPE and showed no apparent toxicity [123]. Similarly, PEGylated cationic liposomes loaded with small interfering RNA (siRNA) targeted to VEGF receptor 1 mRNA lowered the CNV area after intravitreal injection [98]. For delivery of plasmids encoding anti-angiogenic proteins, nanoparticles made of FDA-approved PLGA have been most extensively investigated for ocular applications. As polyesters, PLGA nanoparticles are biodegradable. After injection, they undergo hydrolysis and release their payload in a sustained fashion [124]. Furthermore, by incorporating the plasmid into the PLGA matrix it can be effectively protected against degradation by nucleases [125]. Using a plasmid encoding the plasminogen kringle 5, a potent anti-angiogenic polypeptide consisting of 80 amino acids, expression of VEGF and intracellular adhesion molecule-1 (ICAM-1) could be lowered [126]. In a diabetes model, intravitreal injection of plasminogen kringle 5 plasmid-loaded PLGA nanomaterials ameliorated retinal damage [126]. PLGA nanoparticles encapsulating a plasmid encoding hypoxia-inducible factor 1α (HIF-1α) small hairpin RNA (shRNA) resulted in significantly reduced leakage from neovascular lesions after intravitreal administration [127]. HIF-1α regulates the transcription of pro-angiogenic factors like VEGF (Fig. 1); this is why therapeutic interference with shRNA leads to decreased VEGF expression [127].

4.2 Nanoparticle systems for improved drug delivery

Incorporating a drug into a nanomaterial can offer several advantages over the administration of the free drug. Nanoparticle-mediated drug delivery allows for prolonged release from the nanocarriers resulting in improved drug bioavailability [128]. In addition, when loaded into a nanoparticle system the effective aqueous solubility of the drug can be greatly increased and its degradation prevented [128]. A summary of intravitreal and intravenous drug delivery approaches can be found in Table 2. The controlled release of active substances from nanoparticles holds great potential for ocular applications by increasing the dosing interval between intravitreal injections. However, release of the drug from the nanoparticles has to be precisely tuned and controlled. For example, intravitreal injections of bevacizumab encapsulated in PLGA NPs were unable to prolong decreases in the area of CNV lesions compared with bevacizumab injections alone [129]. Excluding antibodies and other macromolecules, which already have an

acceptable vitreal half-life of 6 to 10 days [130], sustained release from NPs significantly favors small drugs with very low vitreal half-lives like triamcinolone acetonide or dexamethasone acetate.

Table 2
Drug delivery approaches for treatment of experimental CNV using NPs

Incorporated drug	Type of NP	NP size	Targeting ligand	Injection route	CNV model	Outcome	Refs.
Combrestatin A4	PEGylated liposomes	116 nm[1]	linear RGD	IV	Laser photocoagulation	FA leakage↓ CNV Area↓	[168]
C16Y	PLA/PLA-PEG NPs	302 nm[1]	none	Sub-retinal	Laser photocoagulation	CNV Area↓	[138]
Bevacizumab	PLGA NPs	819 nm	none	IVT	Laser photocoagulation	CNV Area↓	[129]
Antagonistic peptide for VEGF receptor 1	Selfassembled hyaluronate-peptide micelles	234 nm[2]	none	IVT	Laser photocoagulation, Streptozotocin-induced DR	FA leakage↓	[135]
Genistein	Selfassembled hyaluronate-peptide micelles	172 nm[1]	none	IVT	Streptozotocin-induced DR	Vascular hyperper-meability↓	[137]
Doxorubicin	PEG-PSA NPs	650 nm[1]	none	IVT	Laser photocoagulation, OIR, VEGF-overexpressing mice	CNV Area↓	[140]
Paclitaxel, Paclitaxel succinate	Cationic liposomes	n/a	none	IV	Laser photocoagulation	CNV Area↓	[77]
Triamcinolone acetonide	PLA NPs	551 nm[2]	none	Subcon-junctival	Laser photocoagulation	Higher release due to CNV	[132]
Dexamethasone acetate	PLGA NPs	253 nm[1]	none	IVT	Laser photocoagulation	CNV Area↓ Fibrosis↓	[131]
TNP-470 (Fumagilin analog)	mPEG-PLA micelles[169]	8 nm [169]	none	IVT, PO	Laser photocoagulation	CNV Area↓ Fibrosis↓ Pro-inflammatory cytokines↓	[170]

CNV, choroidal neovascularization; DR, diabetic retinopathy; FA, fluorescein angiography; IV, intravenous; IVT, intravitreal; NP, nanoparticle; OIR, oxygen-induced retinopathy; PEG, poly(ethylene glycol); PLA, poly(lactic acid); PLGA, poly(lactide-*co*-glycolide); PO, peroral; PSA, poly(sebacic acid); VEGF, vascular endothelial growth factor

[1] as measured by dynamic light scattering

[2] as measured by electron microscopy

An intravitreal injection of dexamethasone-loaded PLGA NPs prevented leaking from CNV lesions [131]. Conversely, triamcinolone-encapsulated poly(lactic acid) (PLA) NPs could not successfully deliver the drug over a prolonged period of time into the ocular tissue after a periocular injection [132]. Because of the high surface area to volume ratio of NPs, a large amount of glucocorticoid was rapidly released from the colloidal system and a sustained release could not be maintained [132]. A similar effect was observed for budesonide-loaded PLA NPs after subconjunctival application [133]. While the great therapeutic success of intravitreal antibody-based VEGF therapeutics has pushed the intravitreal use of corticosteroids into the background [134], a sustained release formulation of corticosteroid-loaded NPs that is co-injected together with the antibody and shows a similar half-life could have synergistic effects on disease progression without further burden for the patient. Oh and coworkers synthesized a micellar system consisting of hyaluronate and a water-insoluble VEGF receptor 1-antagonist peptide [135]. In a model of streptozotocin-induced diabetic retinopathy, the micelle-like NPs inhibited CNV more than the anti-VEGF receptor 1 peptide alone [135]. By loading the micelles with genistein, an isoflavonoid that interferes with expression of VEGF and suppresses cell proliferation [136], vascular leakage could be further suppressed – similar to treatment with the gold standard bevacizumab [137]. Likewise, C16Y, an integrin-antagonist peptide encapsulated in poly(lactic acid)/poly(lactic acid-*b*-ethylene oxide) (PLA/PLA-PEO) NPs reduced the area of CNV more than the peptide solution itself due to controlled release from the nanocarriers [138].

Another advantageous aspect of controlled release systems is that by releasing active agents in a sustained fashion from NPs, toxicity issues stemming from high drug concentrations can be avoided. Doxorubicin (DXR), an anthracycline that acts as an inhibitor of HIF-1α, has strong anti-angiogenic potential but is also known and used for its antineoplastic properties [139]. Though DXR effectively suppresses neovascularization in the eye it also has a deleterious effect on retinal function [140]. However, when prepared in poly(ethylene glycol)-poly(sebacic acid) (PEG-PSA) NPs its strong anti-angiogenic effect remained, whereas the accompanying retinal toxicity was diminished [140].

Unfortunately, one shortcoming that can be seen in several investigations is the lack of comparison against the anti-VEGF therapy gold standard. Although the use of bevacizumab and ranibizumab is widely established and used on a daily basis in ophthalmology, a direct comparison is often avoided. Thus, assessment of neovascular

inhibition is difficult, especially when drug-free NPs themselves appear to have a positive effect on the neovascular outcomes [77]. In laser-induced CNV, which is the most common model for wet AMD, a head-to-head comparison should be a necessity.

4.3 Anti-oxidative nanoceria for treating ocular neovascularization

For several years it has been known that oxidative damage plays a fundamental role in the pathogenesis of age-regulated macular degeneration (AMD) [141]. Cigarette smoking, being over 65 years old, and obesity – all of which are environmental and demographic characteristics linked to oxidative stress – are known to be major risk factors for developing AMD [142,143]. Another indication that oxidative stress has a prominent role in the development of AMD is that supplementation with anti-oxidants like vitamin C/E, zinc or beta carotene has a delaying effect on the pathogenesis of AMD and reduces the risk of vision loss [144]. Furthermore, many of the proteins found in drusen of patients with dry AMD were found to be modified with degradation products of docosahexaenoic acid (DHA), which are generated by oxidative damage [145]. Increased levels of reactive oxygen species (ROS) in the retina are a consequence of high oxygen levels in the tissue, delivered by the well-perfused choriocapillaris, in combination with the intensively focused light that reaches the retina every day throughout the lifespan of each individual [145,146].

Nanoceria, a nanoscale formulation of cerium oxide ranging from 3-5 nm, represent a promising nanoparticle platform to treat ocular diseases related to oxidative stress. The nanoceria's capacity to scavenge ROS involves their ability to switch between dual oxidation states, making them comparable to biologic antioxidants [147,148]. In an AMD model they inhibited the rise of ROS and decreased the formation of intraretinal and subretinal neovascularizations after a single intravitreal injection [149]. This is possible due to the high redox capacity of cerium oxide and its ability to regenerate its activity when formulated as a nanoparticle system [150]. Notably, by catalytically scavenging ROS, nanoceria also prevented increase in VEGF and inhibited pro-inflammatory cytokines and other pro-angiogenic growth factors besides VEGF [149,151]. In toxicology studies, nanoceria were rapidly taken up by the retina but showed neither acute nor long-term negative effects on retinal function or architecture [152]. Furthermore, the nanoceria had a remarkable half-life of 414 days in the retina [152]. Nanoceria sustained their antioxidant function for up to 6 weeks and not only reduced vascular leakage from

neovascular lesions, but also led to the regression of existing abnormal blood vessels by about 50 % (Fig. 6b) [153].

4.4 Inherent anti-angiogenic properties of nanoparticles

Ocular diseases like wet AMD, proliferative DR and ROP share pathological neovascularization of retina or choroid as a common hallmark. Pioneering work to investigate the anti-angiogenic effects of gold nanoparticles (AuNPs) was conducted by Bhattacharya and coworkers based on the known positive effects of gold salts in the therapy of rheumatoid arthritis [154]. Via *in vitro* studies they concluded that AuNPs derive their intrinsic anti-angiogenic properties by specifically inhibiting heparin-binding glycoproteins like VEGF165 and basic fibroblast growth factor (bFGF) [155,156]. Interestingly, the proliferation induced by VEGF121 and epidermal growth factor (EGF), two non-heparin-binding growth factors, were not inhibited. Interaction between AuNPs and VEGF165 was proposed to occur through bindings between thiol and amine groups in the heparin binding domain and the gold surface [155]. When VEGF165 was preincubated with AuNPs, its proliferative effect was significantly reduced compared to the untreated VEGF [156]. Conversely, in the absence of VEGF165, AuNPs showed no inhibition of cellular proliferation. Further *in vitro* investigations on bovine retinal pigment epithelium cells revealed that AuNPs additionally inhibited VEGF-induced proliferation via blockade of the Src pathway [157], a family of kinases that is pivotal for VEGF-induced proliferation *in vivo* [158]. Besides AuNPs, inhibition of angiogenesis was also observed for silver [159], silicate [160] and cuprous oxide nanoparticles [161]. In an *in vivo* study using a mouse model of ROP, the intravitreal injection of 1 µM 20 nm AuNPs in 1 µL phosphate-buffered saline greatly inhibited retinal neovascularizations and nearly eliminated neovascular lumens (Fig. 6a) [162]. AuNPs showed intraocular biocompatibility and did not alter the electrical activity of the retina for at least 6 weeks [163,164]. Recently, titanium dioxide (TiO2) nanoparticles were evaluated for their anti-angiogenic potential [165]; a non-toxic intravitreal injection of 20 nm TiO_2 nanoparticles reduced the number of vascular tufts. Interestingly, gold, silver and silicate nanoparticles exerted their anti-proliferative effects through the phosphatidyl inositol 3-kinase/Akt and ERK1/2 pathways, which are downstream signaling pathway of VEGF-VEGFR2. In contrast, TiO_2 nanoparticles inhibited the VEGFR-2/MAPK pathway and did not affect the PI3K/Akt pathway [165].

However, because they are non-biodegradable and not easily eliminated after intravitreal injection, repeated injections of inorganic nanoparticles could lead to toxicity problems. Although one injection may be tolerable, accumulation and decomposition over time may pose problems to the sensitive neural retina. For instance, in an *ex vivo* tissue culture model of the retina, gold and silver NPs of 20 and 80 nm exhibited significant neurotoxic effects on the photoreceptors, despite being administered in a single dose at a low concentration [166]. Therefore, to fully evaluate the potential harm that metallic nanoparticles could have on the neural retina, extensive long-term toxicology studies are desperately needed.

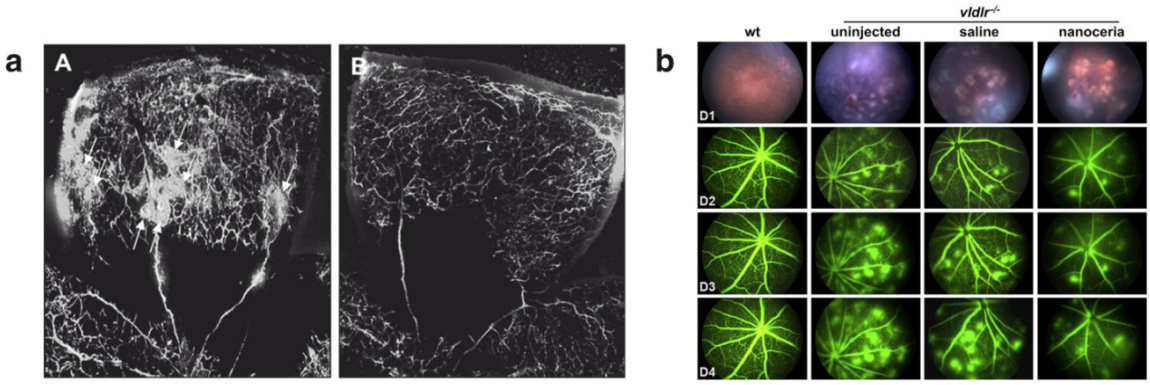

Figure 6: Anti-angiogenic properties of AuNPs (a) and nanoceria (b). Fluorescein angiography shows leakage in retinae after oxygen-induced retinopathy (a, left). Intravitreal injection of 20 nm AuNPs greatly inhibited retinal neovascularizations and showed fewer neovascular lumens (a, right). Reprinted from Biomaterials 2011; 32(7); 1865-71 [162] with permission from Elsevier. Capital A and B refer to the images in the original publication.
In vldlr knockout mice, a mouse model that features pathological retinal neovascularizations, injections of anti-oxidative nanoceria greatly reduced the number of neovascular lesions compared to the control injections (b). Reprinted from Biomaterials 2014; 35(1); 249-58 [153] with permission from Elsevier.

5 Concluding remarks and future perspectives

Nanoscale materials have great potential to resolve the shortcomings of established anti-neovascular therapies and open new therapeutic avenues. With nanoparticulate systems, an effective therapy is within reach that can increase intravitreal drug dosing intervals, introduce corrective genes into the ocular tissue or completely circumvent the need to inject directly into the eye. Together with powerful NP targeting strategies, an effective, safe and intravenously administered treatment can be achieved. In the coming years, we will presumably know whether or not the promising preclinical data can be translated to yield the first successful clinical studies which demonstrate safety and efficacy in humans. Furthermore, the novel anti-oxidative and anti-angiogenic features of selected

nanomaterials may potentially allow for interesting compound materials that exert synergistic effects in the treatment of neovascular eye diseases. Taken together, NPs hold great potential to shape the future of ocular anti-angiogenic therapy.

References

[1] A.N. Witmer, G.F.J.M. Vrensen, C.J.F. Van Noorden, R.O. Schlingemann, Vascular endothelial growth factors and angiogenesis in eye disease, Prog. Retin. Eye Res. 22 (2003) 1–29.

[2] H.A. Mintz-Hittner, K.A. Kennedy, A.Z. Chuang, Efficacy of intravitreal bevacizumab for stage 3+ retinopathy of prematurity, N. Engl. J. Med. 364 (2011) 603–615.

[3] C. Bunce, W. Xing, R. Wormald, Causes of blind and partial sight certifications in England and Wales: April 2007-March 2008, Eye (Lond) 24 (2010) 1692–1699.

[4] R.D. Jager, W.F. Mieler, J.W. Miller, Age-related macular degeneration, N. Engl. J. Med. 358 (2008) 2606–2617.

[5] A. Hellström, L.E.H. Smith, O. Dammann, Retinopathy of prematurity, Lancet 382 (2013) 1445–1457.

[6] R.P. Danis, M.D. Davis, Proliferative Diabetic Retinopathy, in: E.J. Duh (Ed.), Diabetic Retinopathy, Humana Press, Totowa, NJ, 2008.

[7] I. Bhutto, G. Lutty, Understanding age-related macular degeneration (AMD): relationships between the photoreceptor/retinal pigment epithelium/Bruch's membrane/choriocapillaris complex, Mol. Aspects Med. 33 (2012) 295–317.

[8] G. Gao, Y. Li, D. Zhang, S. Gee, C. Crosson, J. Ma, Unbalanced expression of VEGF and PEDF in ischemia-induced retinal neovascularization, FEBS Lett. 489 (2001) 270–276.

[9] J. Tombran-Tink, C.J. Barnstable, PEDF: a multifaceted neurotrophic factor, Nat. Rev. Neurosci. 4 (2003) 628–636.

[10] C.W. Pugh, P.J. Ratcliffe, Regulation of angiogenesis by hypoxia: role of the HIF system, Nat. Med. 9 (2003) 677–684.

[11] M. Shibuya, Vascular endothelial growth factor and its receptor system: physiological functions in angiogenesis and pathological roles in various diseases, J. Biochem. 153 (2013) 13–19.

[12] L.S. Lim, P. Mitchell, J.M. Seddon, F.G. Holz, T.Y. Wong, Age-related macular degeneration, Lancet 379 (2012) 1728–1738.

[13] M. Tolentino, Systemic and ocular safety of intravitreal anti-VEGF therapies for ocular neovascular disease, Surv. Ophthalmol. 56 (2011) 95–113.

[14] M. Saint-Geniez, A.S.R. Maharaj, T.E. Walshe, B.A. Tucker, E. Sekiyama, T. Kurihara, D.C. Darland, M.J. Young, P.A. D'Amore, Endogenous VEGF is required for visual function: evidence for a survival role on müller cells and photoreceptors, PLoS ONE 3 (2008) e3554.

[15] K.M. Ford, M. Saint-Geniez, T. Walshe, A. Zahr, P.A. D'Amore, Expression and role of VEGF in the adult retinal pigment epithelium, Invest. Ophthalmol. Vis. Sci. 52 (2011) 9478–9487.

[16] S. Peters, P. Heiduschka, S. Julien, F. Ziemssen, H. Fietz, K.U. Bartz-Schmidt, U. Schraermeyer, Ultrastructural findings in the primate eye after intravitreal injection of bevacizumab, Am. J. Ophthalmol. 143 (2007) 995–1002.

[17] D.F. Martin, M.G. Maguire, S.L. Fine, G.-s. Ying, G.J. Jaffe, J.E. Grunwald, C. Toth, M. Redford, F.L. Ferris, Ranibizumab and bevacizumab for treatment of neovascular age-related macular degeneration: two-year results, Ophthalmology 119 (2012) 1388–1398.

[18] Y. Diebold, M. Calonge, Applications of nanoparticles in ophthalmology, Prog. Retin. Eye Res. 29 (2010) 596–609.

[19] F.M. Penha, P.J. Rosenfeld, Management of Neovascular AMD, in: A.C. Ho, C.D. Regillo (Eds.), Age-related Macular Degeneration Diagnosis and Treatment, Springer New York, New York, NY, 2011.

[20] Z.F. Bashshur, A. Bazarbachi, A. Schakal, Z.A. Haddad, C.P. El Haibi, B.N. Noureddin, Intravitreal bevacizumab for the management of choroidal neovascularization in age-related macular degeneration, Am. J. Ophthalmol. 142 (2006) 1–9.

[21] J.-L. Bourges, S.E. Gautier, F. Delie, R.A. Bejjani, J.-C. Jeanny, R. Gurny, D. BenEzra, F.F. Behar-Cohen, Ocular drug delivery targeting the retina and retinal pigment epithelium using polylactide nanoparticles, Invest. Ophthalmol. Vis. Sci. 44 (2003) 3562–3569.

[22] G.B. Arden, S. Sivaprasad, The pathogenesis of early retinal changes of diabetic retinopathy, Doc. Ophthalmol. 124 (2012) 15–26.

[23] B.S. Hawkins, A. Bird, R. Klein, S.K. West, Epidemiology of age-related macular degeneration, Mol. Vis. 5 (1999) 26.

[24] R. Klein, C.-F. Chou, B.E.K. Klein, X. Zhang, S.M. Meuer, J.B. Saaddine, Prevalence of age-related macular degeneration in the US population, Arch. Ophthalmol. 129 (2011) 75–80.

[25] W.L. Wong, X. Su, X. Li, C.M.G. Cheung, R. Klein, C.-Y. Cheng, T.Y. Wong, Global prevalence of age-related macular degeneration and disease burden projection for 2020 and 2040: a systematic review and meta-analysis, Lancet Glob. Health 2 (2014) e106.

[26] T.H. Tezel, N.S. Bora, H.J. Kaplan, Pathogenesis of age-related macular degeneration, Trends Mol. Med. 10 (2004) 417–420.

[27] P.T.V.M. de Jong, Age-related macular degeneration, N. Engl. J. Med. 355 (2006) 1474–1485.

[28] J. Holash, S. Davis, N. Papadopoulos, S.D. Croll, L. Ho, M. Russell, P. Boland, R. Leidich, D. Hylton, E. Burova, E. Ioffe, T. Huang, C. Radziejewski, K. Bailey, J.P. Fandl, T. Daly, S.J. Wiegand, G.D. Yancopoulos, J.S. Rudge, VEGF-Trap: a VEGF blocker with potent antitumor effects, Proc. Natl. Acad. Sci. U.S.A. 99 (2002) 11393–11398.

[29] A.W. Stitt, N. Lois, R.J. Medina, P. Adamson, T.M. Curtis, Advances in our understanding of diabetic retinopathy, Clin. Sci. 125 (2013) 1–17.

[30] J.E. Shaw, R.A. Sicree, P.Z. Zimmet, Global estimates of the prevalence of diabetes for 2010 and 2030, Diabetes Res. Clin. Pract. 87 (2010) 4–14.

[31] J.W.Y. Yau, S.L. Rogers, R. Kawasaki, E.L. Lamoureux, J.W. Kowalski, T. Bek, S.-J. Chen, J.M. Dekker, A. Fletcher, J. Grauslund, S. Haffner, R.F. Hamman, M.K. Ikram, T. Kayama, B.E.K. Klein, R. Klein, S. Krishnaiah, K. Mayurasakorn, J.P. O'Hare, T.J. Orchard, M. Porta, M. Rema, M.S. Roy, T. Sharma, J. Shaw, H. Taylor, J.M. Tielsch, R. Varma, J.J. Wang, N. Wang, S. West, L. Xu, M. Yasuda, X. Zhang, P. Mitchell, T.Y. Wong, Global prevalence and major risk factors of diabetic retinopathy, Diabetes Care 35 (2012) 556–564.

[32] P. Osaadon, X.J. Fagan, T. Lifshitz, J. Levy, A review of anti-VEGF agents for proliferative diabetic retinopathy, Eye (Lond) 28 (2014) 510–520.

[33] D.M. Brown, Q.D. Nguyen, D.M. Marcus, D.S. Boyer, S. Patel, L. Feiner, P.G. Schlottmann, A.C. Rundle, J. Zhang, R.G. Rubio, A.P. Adamis, J.S. Ehrlich, J.J. Hopkins, Long-term outcomes of ranibizumab therapy for diabetic macular edema: the 36-month results from two phase III trials: RISE and RIDE, Ophthalmology 120 (2013) 2013–2022.

[34] M.E. Torres-Soriano, E. Reyna-Castelán, M. Hernández-Rojas, G. García-Aguirre, V. Kon-Jara, J.L. Diaz-Rubio, J.L. Guerrero-Naranjo, J.M. Jiménez-Sierra, H. Quiroz-Mercado, Tractional retinal detachment after intravitreal injection of bevacizumab in proliferative diabetic retinopathy, Retin. Cases Brief Rep. 3 (2009) 70–73.

[35] R.L. Goldenberg, J.F. Culhane, J.D. Iams, R. Romero, Epidemiology and causes of preterm birth, Lancet 371 (2008) 75–84.

[36] D. Austeng, Källen, Karin B M, U.W. Ewald, P.G. Jakobsson, G.E. Holmström, Incidence of retinopathy of prematurity in infants born before 27 weeks' gestation in Sweden, Arch. Ophthalmol. 127 (2009) 1315–1319.

[37] O.D. Saugstad, Oxygen and retinopathy of prematurity, J. Perinatol. 26 Suppl 1 (2006) S46-50; discussion S63-4.

[38] J. Chen, L.E.H. Smith, Retinopathy of prematurity, Angiogenesis 10 (2007) 133–140.

[39] D.G. Vavvas, Anti-VEGF in retinopathy of prematurity, need to titrate, Invest. Ophthalmol. Vis. Sci. 54 (2013).

[40] R.L. Avery, D.J. Pieramici, M.D. Rabena, A.A. Castellarin, M.A. Nasir, M.J. Giust, Intravitreal bevacizumab (Avastin) for neovascular age-related macular degeneration, Ophthalmology 113 (2006) 363-372.e5.

[41] L. Wu, M.A. Martínez-Castellanos, H. Quiroz-Mercado, J.F. Arevalo, M.H. Berrocal, M.E. Farah, M. Maia, J.A. Roca, F.J. Rodriguez, Twelve-month safety of intravitreal injections of bevacizumab (Avastin): results of the Pan-American Collaborative Retina Study Group (PACORES), Graefes Arch. Clin. Exp. Ophthalmol. 246 (2008) 81–87.

[42] E.S. Gragoudas, A.P. Adamis, E.T. Cunningham, M. Feinsod, D.R. Guyer, Pegaptanib for neovascular age-related macular degeneration, N. Engl. J. Med. 351 (2004) 2805–2816.

[43] A. Cruess, G. Zlateva, X. Xu, S. Rochon, Burden of illness of neovascular age-related macular degeneration in Canada, Can. J. Ophthalmol. 42 (2007) 836–843.

[44] L.M. Parver, Temperature modulating action of choroidal blood flow, Eye (Lond) 5 (Pt 2) (1991) 181–185.

[45] D.L. Nickla, J. Wallman, The multifunctional choroid, Prog. Retin. Eye Res. 29 (2010) 144–168.

[46] A. Alm, A. Bill, Ocular and optic nerve blood flow at normal and increased intraocular pressures in monkeys (Macaca irus): a study with radioactively labelled microspheres including flow determinations in brain and some other tissues, Exp. Eye Res. 15 (1973) 15–29.

[47] L. lSchmetterer, G. Garhöfer, Retinal Blood Flow, in: A.M. Joussen (Ed.), Retinal vascular disease, Springer, Berlin, New York, ©2007.

[48] E. Friedman, S. Krupsky, A.M. Lane, S.S. Oak, E.S. Friedman, K. Egan, E.S. Gragoudas, Ocular blood flow velocity in age-related macular degeneration, Ophthalmology 102 (1995) 640–646.

[49] M.E. Langham, R. Grebe, S. Hopkins, S. Marcus, M. Sebag, Choroidal blood flow in diabetic retinopathy, Exp. Eye Res. 52 (1991) 167–173.

[50] Y. Matsumura, H. Maeda, A new concept for macromolecular therapeutics in cancer chemotherapy: mechanism of tumoritropic accumulation of proteins and the antitumor agent smancs, Cancer Res. 46 (1986) 6387–6392.

[51] P. Carmeliet, R.K. Jain, Angiogenesis in cancer and other diseases, Nature 407 (2000) 249–257.

[52] H. Kobayashi, R. Watanabe, P.L. Choyke, Improving conventional enhanced permeability and retention (EPR) effects; what is the appropriate target?, Theranostics 4 (2013) 81–89.

[53] J. Fang, H. Nakamura, H. Maeda, The EPR effect: Unique features of tumor blood vessels for drug delivery, factors involved, and limitations and augmentation of the effect, Adv. Drug Deliv. Rev. 63 (2011) 136–151.

[54] T. Yasukawa, H. Kimura, Y. Tabata, H. Miyamoto, Y. Honda, Y. Ikada, Y. Ogura, Targeted delivery of anti-angiogenic agent TNP-470 using water-soluble polymer in the treatment of choroidal neovascularization, Invest. Ophthalmol. Vis. Sci. 40 (1999) 2690–2696.

[55] M.J. Tolentino, D. Husain, P. Theodosiadis, E.S. Gragoudas, E. Connolly, J. Kahn, J. Cleland, A.P. Adamis, A. Cuthbertson, J.W. Miller, Angiography of fluoresceinated anti-vascular endothelial growth factor antibody and dextrans in experimental choroidal neovascularization, Arch. Ophthalmol. 118 (2000) 78–84.

[56] H. Kamizuru, H. Kimura, T. Yasukawa, Y. Tabata, Y. Honda, Y. Ogura, Monoclonal antibody-mediated drug targeting to choroidal neovascularization in the rat, Invest. Ophthalmol. Vis. Sci. 42 (2001) 2664–2672.

[57] T. Tobe, S. Ortega, J.D. Luna, H. Ozaki, N. Okamoto, N.L. Derevjanik, S.A. Vinores, C. Basilico, P.A. Campochiaro, Targeted disruption of the FGF2 gene does not prevent choroidal neovascularization in a murine model, Am. J. Pathol. 153 (1998) 1641–1646.

[58] R.-i. Kohno, Y. Hata, Y. Mochizuki, R. Arita, S. Kawahara, T. Kita, M. Miyazaki, T. Hisatomi, Y. Ikeda, L.P. Aiello, T. Ishibashi, Histopathology of neovascular tissue from eyes with proliferative diabetic retinopathy after intravitreal bevacizumab injection, Am. J. Ophthalmol. 150 (2010) 223-229.e1.

[59] H. Miller, B. Miller, S.J. Ryan, Newly-formed subretinal vessels. Fine structure and fluorescein leakage, Invest. Ophthalmol. Vis. Sci. 27 (1986) 204–213.

[60] J.R. Casley-Smith, L. Clodius, E. Földi-Börcsök, J. Grüntzig, M. Földi, The effects of chronic cervical lymphostasis on regions drained by lymphatics and by prelymphatics, J. Pathol. 124 (1978) 13–17.

[61] Y.H. Bae, K. Park, Targeted drug delivery to tumors: myths, reality and possibility, J. Control. Release 153 (2011) 198–205.

[62] T. Lammers, F. Kiessling, W.E. Hennink, G. Storm, Drug targeting to tumors: principles, pitfalls and (pre-) clinical progress, J. Control. Release 161 (2012) 175–187.

[63] V.P. Chauhan, R.K. Jain, Strategies for advancing cancer nanomedicine, Nat. Mater. 12 (2013) 958–962.

[64] S. Torosean, B. Flynn, J. Axelsson, J. Gunn, K.S. Samkoe, T. Hasan, M.M. Doyley, B.W. Pogue, Nanoparticle uptake in tumors is mediated by the interplay of vascular and collagen density with interstitial pressure, Nanomed. Nanotechnol. 9 (2013) 151–158.

[65] C.-H. Heldin, K. Rubin, K. Pietras, A. Ostman, High interstitial fluid pressure - an obstacle in cancer therapy, Nat. Rev. Cancer 4 (2004) 806–813.

[66] M.F. Marmor, Mechanisms of fluid accumulation in retinal edema, Doc. Ophthalmol. 97 (1999) 239–249.

[67] P.J. Rosenfeld, H. Shapiro, L. Tuomi, M. Webster, J. Elledge, B. Blodi, Characteristics of patients losing vision after 2 years of monthly dosing in the phase III ranibizumab clinical trials, Ophthalmology 118 (2011) 523–530.

[68] L. Berger, U. Wolf-Schnurrbusch, C. Brinkmann, S. Wolf, Current indications for ocular photodynamic therapy – A review of the literature and two case reports, Med. Laser Appl. 25 (2010) 235–241.

[69] P. Skupin-Mrugalska, J. Piskorz, T. Goslinski, J. Mielcarek, K. Konopka, N. Düzgüneş, Current status of liposomal porphyrinoid photosensitizers, Drug Discov. Today 18 (2013) 776–784.

[70] R.K. Chowdhary, I. Shariff, D. Dolphin, Drug release characteristics of lipid based benzoporphyrin derivative, J. Pharm. Pharm. Sci. 6 (2003) 13–19.

[71] U. Schmidt-Erfurth, T. Hasan, Mechanisms of action of photodynamic therapy with verteporfin for the treatment of age-related macular degeneration, Surv. Ophthalmol. 45 (2000) 195–214.

[72] R. Wormald, J. Evans, L. Smeeth, K. Henshaw, Photodynamic therapy for neovascular age-related macular degeneration, Cochrane Database Syst. Rev. (2007) CD002030.

[73] R. Ideta, F. Tasaka, W.-D. Jang, N. Nishiyama, G.-D. Zhang, A. Harada, Y. Yanagi, Y. Tamaki, T. Aida, K. Kataoka, Nanotechnology-based photodynamic therapy for neovascular disease using a supramolecular nanocarrier loaded with a dendritic photosensitizer, Nano Lett. 5 (2005) 2426–2431.

[74] W.-D. Jang, N. Nishiyama, G.-D. Zhang, A. Harada, D.-L. Jiang, S. Kawauchi, Y. Morimoto, M. Kikuchi, H. Koyama, T. Aida, K. Kataoka, Supramolecular nanocarrier of anionic dendrimer porphyrins with cationic block copolymers modified with polyethylene glycol to enhance intracellular photodynamic efficacy, Angew. Chem. Int. Ed. 44 (2005) 419–423.

[75] U. Schmidt-Erfurth, U. Schlötzer-Schrehard, C. Cursiefen, S. Michels, A. Beckendorf, Naumann, Gottfried O H, Influence of photodynamic therapy on expression of vascular endothelial growth factor (VEGF), VEGF receptor 3, and pigment epithelium-derived factor, Invest. Ophthalmol. Vis. Sci. 44 (2003) 4473–4480.

[76] J.-l. Wang, Y. Xi, Y.-l. Liu, Z.-h. Wang, Q. Zhang, Combination of targeted PDT and anti-VEGF therapy for rat CNV by RGD-modified liposomal photocyanine and sorafenib, Invest. Ophthalmol. Vis. Sci. 54 (2013) 7983–7989.

[77] N. Gross, M. Ranjbar, C. Evers, J. Hua, G. Martin, B. Schulze, U. Michaelis, L.L. Hansen, H.T. Agostini, Choroidal neovascularization reduced by targeted drug delivery with cationic liposome-encapsulated paclitaxel or targeted photodynamic therapy with verteporfin encapsulated in cationic liposomes, Mol. Vis. 19 (2013) 54–61.

[78] S. Ran, A. Downes, P.E. Thorpe, Increased exposure of anionic phospholipids on the surface of tumor blood vessels, Cancer research 62 (2002) 6132–6140.

[79] G. Thurston, J.W. McLean, M. Rizen, P. Baluk, A. Haskell, T.J. Murphy, D. Hanahan, D.M. McDonald, Cationic liposomes target angiogenic endothelial cells in tumors and chronic inflammation in mice, J. Clin. Invest. 101 (1998) 1401–1413.

[80] J. Hua, N. Gross, B. Schulze, U. Michaelis, H. Bohnenkamp, E. Guenzi, L.L. Hansen, G. Martin, H.T. Agostini, In vivo imaging of choroidal angiogenesis using fluorescence-labeled cationic liposomes, Mol. Vis. 18 (2012) 1045–1054.

[81] M. Millard, S. Odde, N. Neamati, Integrin targeted therapeutics, Theranostics 1 (2011) 154–188.

[82] D.G. Stupack, D.A. Cheresh, Integrins and angiogenesis, Curr. Top. Dev. Biol. 64 (2004) 207–238.

[83] R.B. Brem, S.G. Robbins, D.J. Wilson, L.M. O'Rourke, R.N. Mixon, J.E. Robertson, S.R. Planck, J.T. Rosenbaum, Immunolocalization of integrins in the human retina, Invest. Ophthalmol. Vis. Sci. 35 (1994) 3466–3474.

[84] S.R. Singh, H.E. Grossniklaus, S.J. Kang, H.F. Edelhauser, B.K. Ambati, U.B. Kompella, Intravenous transferrin, RGD peptide and dual-targeted nanoparticles enhance anti-VEGF intraceptor gene delivery to laser-induced CNV, Gene Ther. 16 (2009) 645–659.

[85] H. Salehi-Had, M.I. Roh, A. Giani, T. Hisatomi, S. Nakao, I.K. Kim, E.S. Gragoudas, D. Vavvas, S. Guccione, J.W. Miller, Utilizing targeted gene therapy with nanoparticles binding alpha v beta 3 for imaging and treating choroidal neovascularization, PLoS ONE 6 (2011) e18864.

[86] K. Pollinger, R. Hennig, A. Ohlmann, R. Fuchshofer, R. Wenzel, M. Breunig, J. Tessmar, E.R. Tamm, A. Goepferich, Ligand-functionalized nanoparticles target endothelial cells in retinal capillaries after systemic application, Proc. Natl. Acad. Sci. U.S.A. 110 (2013) 6115–6120.

[87] C. Mas-Moruno, F. Rechenmacher, H. Kessler, Cilengitide: the first anti-angiogenic small molecule drug candidate design, synthesis and clinical evaluation, Anticancer Agents Med. Chem. 10 (2010) 753–768.

[88] M. Friedlander, C.L. Theesfeld, M. Sugita, M. Fruttiger, M.A. Thomas, S. Chang, D.A. Cheresh, Involvement of integrins alpha v beta 3 and alpha v beta 5 in ocular neovascular diseases, Proc. Natl. Acad. Sci. U.S.A. 93 (1996) 9764–9769.

[89] R. Hennig, K. Pollinger, A. Veser, M. Breunig, A. Goepferich, Nanoparticle multivalency counterbalances the ligand affinity loss upon PEGylation, J. Control. Release 194C (2014) 20–27.

[90] S.M. Weis, D.A. Cheresh, αV integrins in angiogenesis and cancer, Cold Spring Harb. Perspect. Med. 1 (2011) a006478.

[91] H.P. Hammes, M. Brownlee, A. Jonczyk, A. Sutter, K.T. Preissner, Subcutaneous injection of a cyclic peptide antagonist of vitronectin receptor-type integrins inhibits retinal neovascularization, Nat. Med. 2 (1996) 529–533.

[92] L. Luo, X. Zhang, Y. Hirano, P. Tyagi, P. Barabás, H. Uehara, T.R. Miya, N. Singh, B. Archer, Y. Qazi, K. Jackman, S.K. Das, T. Olsen, S.R. Chennamaneni, B.C. Stagg, F. Ahmed, L. Emerson, K. Zygmunt, R. Whitaker, C. Mamalis, W. Huang, G. Gao, S.P. Srinivas, D. Krizaj, J. Baffi, J. Ambati, U.B. Kompella, B.K. Ambati, Targeted intraceptor nanoparticle therapy reduces angiogenesis and fibrosis in primate and murine macular degeneration, ACS Nano 7 (2013) 3264–3275.

[93] K. Kotoh, M. Nakamuta, M. Kohjima, M. Fukushima, S. Morizono, N. Kobayashi, M. Enjoji, H. Nawata, Arg-Gly-Asp (RGD) peptide ameliorates carbon tetrachloride-induced liver fibrosis via inhibition of collagen production and acceleration of collagenase activity, Int. J. Mol. Med. 14 (2004) 1049–1053.

[94] N. Singh, S. Amin, E. Richter, S. Rashid, V. Scoglietti, P.D. Jani, J. Wang, R. Kaur, J. Ambati, Z. Dong, B.K. Ambati, Flt-1 intraceptors inhibit hypoxia-induced VEGF expression in vitro and corneal neovascularization in vivo, Invest. Ophthalmol. Vis. Sci. 46 (2005) 1647–1652.

[95] J.Z. Nowak, Age-related macular degeneration (AMD): pathogenesis and therapy, Pharmacol. Rep. 58 (2006) 353–363.

[96] R.A. Bejjani, D. BenEzra, H. Cohen, J. Rieger, C. Andrieu, J.-C. Jeanny, G. Gollomb, F.F. Behar-Cohen, Nanoparticles for gene delivery to retinal pigment epithelial cells, Mol. Vis. 11 (2005) 124–132.

[97] A. del Pozo-Rodríguez, D. Delgado, M.A. Solinís, A.R. Gascón, J.L. Pedraz, Solid lipid nanoparticles for retinal gene therapy: transfection and intracellular trafficking in RPE cells, Int. J. Pharm. 360 (2008) 177–183.

[98] H.-a. Liu, Y.-l. Liu, Z.-z. Ma, J.-c. Wang, Q. Zhang, A lipid nanoparticle system improves siRNA efficacy in RPE cells and a laser-induced murine CNV model, Invest. Ophthalmol. Vis. Sci. 52 (2011) 4789–4794.

[99] P. Mastorakos, S.P. Kambhampati, M.K. Mishra, T. Wu, E. Song, J. Hanes, R.M. Kannan, Hydroxyl PAMAM dendrimer-based gene vectors for transgene delivery to human retinal pigment epithelial cells, Nanoscale (2014).

[100] T.W. Prow, I. Bhutto, S.Y. Kim, R. Grebe, C. Merges, D.S. McLeod, K. Uno, M. Mennon, L. Rodriguez, K. Leong, G.A. Lutty, Ocular nanoparticle toxicity and

transfection of the retina and retinal pigment epithelium, Nanomed. Nanotechnol. 4 (2008) 340–349.

[101] R. Farjo, J. Skaggs, A.B. Quiambao, M.J. Cooper, M.I. Naash, Efficient non-viral ocular gene transfer with compacted DNA nanoparticles, PLoS ONE 1 (2006) e38.

[102] A. Koirala, R.S. Makkia, M.J. Cooper, M.I. Naash, Nanoparticle-mediated gene transfer specific to retinal pigment epithelial cells, Biomaterials 32 (2011) 9483–9493.

[103] R.N. Mitra, Z. Han, M. Merwin, M. Al Taai, S.M. Conley, M.I. Naash, Synthesis and characterization of glycol chitosan DNA nanoparticles for retinal gene delivery, ChemMedChem 9 (2014) 189–196.

[104] S. Melamed, I. Ben-Sira, Y. Ben-Shaul, Ultrastructure of fenestrations in endothelial choriocapillaries of the rabbit--a freeze-fracturing study, Br. J. Ophthalmol. 64 (1980) 537–543.

[105] V.-P. Ranta, E. Mannermaa, K. Lummepuro, A. Subrizi, A. Laukkanen, M. Antopolsky, L. Murtomäki, M. Hornof, A. Urtti, Barrier analysis of periocular drug delivery to the posterior segment, J. Control. Release 148 (2010) 42–48.

[106] D.J. Moore, G.M. Clover, The effect of age on the macromolecular permeability of human Bruch's membrane, Invest. Ophthalmol. Vis. Sci. 42 (2001) 2970–2975.

[107] Z. Cankova, J.-D. Huang, H.S. Kruth, M. Johnson, Passage of low-density lipoproteins through Bruch's membrane and choroid, Exp. Eye Res. 93 (2011) 947–955.

[108] J.H. Kim, J.H. Kim, K.-W. Kim, M.H. Kim, Y.S. Yu, Intravenously administered gold nanoparticles pass through the blood-retinal barrier depending on the particle size, and induce no retinal toxicity, Nanotechnology 20 (2009) 505101.

[109] Y.S. Kanwar, A. Linker, M.G. Farquhar, Increased permeability of the glomerular basement membrane to ferritin after removal of glycosaminoglycans (heparan sulfate) by enzyme digestion, J. Cell Biol. 86 (1980) 688–693.

[110] W.D. Comper, E.F. Glasgow, Charge selectivity in kidney ultrafiltration, Kidney Int. 47 (1995) 1242–1251.

[111] H.G. Rennke, R.S. Cotran, M.A. Venkatachalam, Role of molecular charge in glomerular permeability. Tracer studies with cationized ferritins, J. Cell Biol. 67 (1975) 638–646.

[112] T.D.L. Keenan, C.E. Pickford, R.J. Holley, S.J. Clark, W. Lin, A.W. Dowsey, C.L. Merry, A.J. Day, P.N. Bishop, Age-dependent changes in heparan sulfate in human Bruch's membrane: implications for age-related macular degeneration, Invest. Ophthalmol. Vis. Sci. 55 (2014) 5370–5379.

[113] H.S. Choi, W. Liu, P. Misra, E. Tanaka, J.P. Zimmer, B. Itty Ipe, M.G. Bawendi, J.V. Frangioni, Renal clearance of quantum dots, Nat. Biotechnol. 25 (2007) 1165–1170.

[114] R.F. Fisher, The influence of age on some ocular basement membranes, Eye (Lond) 1 (Pt 2) (1987) 184–189.

[115] J. Ambati, B.K. Ambati, S.H. Yoo, S. Ianchulev, A.P. Adamis, Age-related macular degeneration: etiology, pathogenesis, and therapeutic strategies, Surv. Ophthalmol. 48 (2003) 257–293.

[116] C.A. Curcio, C.L. Millican, T. Bailey, H.S. Kruth, Accumulation of cholesterol with age in human Bruch's membrane, Invest. Ophthalmol. Vis. Sci. 42 (2001) 265–274.

[117] R.W. Young, Pathophysiology of age-related macular degeneration, Surv. Ophthalmol. 31 (1987) 291–306.

[118] Y. Chang, S.C. Finnemann, Tetraspanin CD81 is required for the alpha v beta5-integrin-dependent particle-binding step of RPE phagocytosis, J. Cell. Sci. 120 (2007) 3053–3063.

[119] I.M. Verma, M.D. Weitzman, Gene therapy: twenty-first century medicine, Annu. Rev. Biochem. 74 (2005) 711–738.

[120] J.W.B. Bainbridge, M.H. Tan, R.R. Ali, Gene therapy progress and prospects: the eye, Gene Ther. 13 (2006) 1191–1197.

[121] J. Bennett, Immune response following intraocular delivery of recombinant viral vectors, Gene Ther. 10 (2003) 977–982.

[122] R.J. Marano, N. Wimmer, P.S. Kearns, B.G. Thomas, I. Toth, M. Brankov, P.E. Rakoczy, Inhibition of in vitro VEGF expression and choroidal neovascularization by synthetic dendrimer peptide mediated delivery of a sense oligonucleotide, Exp. Eye Res. 79 (2004) 525–535.

[123] R.J. Marano, I. Toth, N. Wimmer, M. Brankov, P.E. Rakoczy, Dendrimer delivery of an anti-VEGF oligonucleotide into the eye: a long-term study into inhibition of laser-induced CNV, distribution, uptake and toxicity, Gene Ther. 12 (2005) 1544–1550.

[124] J. Panyam, V. Labhasetwar, Biodegradable nanoparticles for drug and gene delivery to cells and tissue, Adv. Drug Deliv. Rev. 55 (2003) 329–347.

[125] M.L. Hedley, J. Curley, R. Urban, Microspheres containing plasmid-encoded antigens elicit cytotoxic T-cell responses, Nat. Med. 4 (1998) 365–368.

[126] K. Park, Y. Chen, Y. Hu, A.S. Mayo, U.B. Kompella, R. Longeras, J.-x. Ma, Nanoparticle-mediated expression of an angiogenic inhibitor ameliorates ischemia-induced retinal neovascularization and diabetes-induced retinal vascular leakage, Diabetes 58 (2009) 1902–1913.

[127] C. Zhang, Y.-S. Wang, H. Wu, Z.-X. Zhang, Y. Cai, H.-Y. Hou, W. Zhao, X.-M. Yang, J.-X. Ma, Inhibitory efficacy of hypoxia-inducible factor 1alpha short hairpin RNA plasmid DNA-loaded poly (D, L-lactide-co-glycolide) nanoparticles on choroidal neovascularization in a laser-induced rat model, Gene Ther. 17 (2010) 338–351.

[128] S. Parveen, R. Misra, S.K. Sahoo, Nanoparticles: a boon to drug delivery, therapeutics, diagnostics and imaging, Nanomed. Nanotechnol. 8 (2012) 147–166.

[129] C.K. Pan, C. Durairaj, U.B. Kompella, O. Agwu, Oliver, Scott C N, H. Quiroz-Mercado, N. Mandava, J.L. Olson, Comparison of long-acting bevacizumab formulations in the treatment of choroidal neovascularization in a rat model, J. Ocul. Pharmacol. Ther. 27 (2011) 219–224.

[130] T.U. Krohne, Z. Liu, F.G. Holz, C.H. Meyer, Intraocular pharmacokinetics of ranibizumab following a single intravitreal injection in humans, Am. J. Ophthalmol. 154 (2012) 682-686.e2.

[131] J. Xu, Y. Wang, Y. Li, X. Yang, P. Zhang, H. Hou, Y. Shi, C. Song, Inhibitory efficacy of intravitreal dexamethasone acetate-loaded PLGA nanoparticles on choroidal neovascularization in a laser-induced rat model, J. Ocul. Pharmacol. Ther. 23 (2007) 527–540.

[132] R.S. Kadam, P. Tyagi, H.F. Edelhauser, U.B. Kompella, Influence of choroidal neovascularization and biodegradable polymeric particle size on transscleral sustained delivery of triamcinolone acetonide, Int. J. Pharm. 434 (2012) 140–147.

[133] U.B. Kompella, N. Bandi, S.P. Ayalasomayajula, Subconjunctival nano- and microparticles sustain retinal delivery of budesonide, a corticosteroid capable of inhibiting VEGF expression, Invest. Ophthalmol. Vis. Sci. 44 (2003) 1192–1201.

[134] E.M. Becerra, F. Morescalchi, F. Gandolfo, P. Danzi, G. Nascimbeni, B. Arcidiacono, F. Semeraro, Clinical evidence of intravitreal triamcinolone acetonide in the management of age-related macular degeneration, Curr. Drug. Targets 12 (2011) 149–172.

[135] E.J. Oh, J.-S. Choi, H. Kim, C.-K. Joo, S.K. Hahn, Anti-Flt1 peptide - hyaluronate conjugate for the treatment of retinal neovascularization and diabetic retinopathy, Biomaterials 32 (2011) 3115–3123.

[136] B.B. Aggarwal, S. Shishodia, Molecular targets of dietary agents for prevention and therapy of cancer, Biochem. Pharmacol. 71 (2006) 1397–1421.

[137] H. Kim, J.-S. Choi, K.S. Kim, J.-A. Yang, C.-K. Joo, S.K. Hahn, Flt1 peptide-hyaluronate conjugate micelle-like nanoparticles encapsulating genistein for the treatment of ocular neovascularization, Acta Biomater. 8 (2012) 3932–3940.

[138] H. Kim, K.G. Csaky, Nanoparticle-integrin antagonist C16Y peptide treatment of choroidal neovascularization in rats, J. Control. Release 142 (2010) 286–293.

[139] K. Lee, D.Z. Qian, S. Rey, H. Wei, J.O. Liu, G.L. Semenza, Anthracycline chemotherapy inhibits HIF-1 transcriptional activity and tumor-induced mobilization of circulating angiogenic cells, Proc. Natl. Acad. Sci. U.S.A. 106 (2009) 2353–2358.

[140] T. Iwase, J. Fu, T. Yoshida, D. Muramatsu, A. Miki, N. Hashida, L. Lu, B. Oveson, Lima e Silva, Raquel, C. Seidel, M. Yang, S. Connelly, J. Shen, B. Han, M. Wu, G.L. Semenza, J. Hanes, P.A. Campochiaro, Sustained delivery of a HIF-1 antagonist for ocular neovascularization, J. Control. Release 172 (2013) 625–633.

[141] B.S. Winkler, M.E. Boulton, J.D. Gottsch, P. Sternberg, Oxidative damage and age-related macular degeneration, Mol. Vis. 5 (1999) 32.

[142] J.M. Seddon, R. Reynolds, Y. Yu, M.J. Daly, B. Rosner, Risk models for progression to advanced age-related macular degeneration using demographic, environmental, genetic, and ocular factors, Ophthalmology 118 (2011) 2203–2211.

[143] J.M. Seddon, W.C. Willett, F.E. Speizer, S.E. Hankinson, A prospective study of cigarette smoking and age-related macular degeneration in women, JAMA 276 (1996) 1141–1146.

[144] Age-Related Eye Disease Study Research Group, A randomized, placebo-controlled, clinical trial of high-dose supplementation with vitamins C and E, beta carotene, and zinc for age-related macular degeneration and vision loss: AREDS report no. 8, Arch. Ophthalmol. 119 (2001) 1417–1436.

[145] J.G. Hollyfield, Age-related macular degeneration: the molecular link between oxidative damage, tissue-specific inflammation and outer retinal disease: the Proctor lecture, Invest. Ophthalmol. Vis. Sci. 51 (2010) 1275–1281.

[146] A. King, E. Gottlieb, D.G. Brooks, M.P. Murphy, J.L. Dunaief, Mitochondria-derived reactive oxygen species mediate blue light-induced death of retinal pigment epithelial cells, Photochem. Photobiol. 79 (2004) 470–475.

[147] S. Patil, S. Seal, Y. Guo, A. Schulte, J. Norwood, Role of trivalent La and Nd dopants in lattice distortion and oxygen vacancy generation in cerium oxide nanoparticles, Appl. Phys. Lett. 88 (2006) 243110.

[148] A.S. Karakoti, N.A. Monteiro-Riviere, R. Aggarwal, J.P. Davis, R.J. Narayan, W.T. Self, J. McGinnis, S. Seal, Nanoceria as Antioxidant: Synthesis and Biomedical Applications, JOM (1989) 60 (2008) 33–37.

[149] X. Zhou, L.L. Wong, A.S. Karakoti, S. Seal, J.F. McGinnis, Nanoceria inhibit the development and promote the regression of pathologic retinal neovascularization in the Vldlr knockout mouse, PLoS ONE 6 (2011) e16733.

[150] J. Chen, S. Patil, S. Seal, J.F. McGinnis, Rare earth nanoparticles prevent retinal degeneration induced by intracellular peroxides, Nat. Nanotech. 1 (2006) 142–150.

[151] S.V. Kyosseva, L. Chen, S. Seal, J.F. McGinnis, Nanoceria inhibit expression of genes associated with inflammation and angiogenesis in the retina of Vldlr null mice, Exp. Eye Res. 116 (2013) 63–74.

[152] L.L. Wong, S.M. Hirst, Q.N. Pye, C.M. Reilly, S. Seal, J.F. McGinnis, Catalytic nanoceria are preferentially retained in the rat retina and are not cytotoxic after intravitreal injection, PLoS ONE 8 (2013) e58431.

[153] X. Cai, S. Seal, J.F. McGinnis, Sustained inhibition of neovascularization in vldlr-/- mice following intravitreal injection of cerium oxide nanoparticles and the role of the ASK1-P38/JNK-NF-κB pathway, Biomaterials 35 (2014) 249–258.

[154] T. Pincus, G. Ferraccioli, T. Sokka, A. Larsen, R. Rau, I. Kushner, F. Wolfe, Evidence from clinical trials and long-term observational studies that disease-modifying anti-rheumatic drugs slow radiographic progression in rheumatoid arthritis: updating a 1983 review, Rheumatology (Oxford) 41 (2002) 1346–1356.

[155] R. Bhattacharya, P. Mukherjee, Z. Xiong, A. Atala, S. Soker, D. Mukhopadhyay, Gold Nanoparticles Inhibit VEGF165-Induced Proliferation of HUVEC Cells, Nano Lett. 4 (2004) 2479–2481.

[156] P. Mukherjee, R. Bhattacharya, P. Wang, L. Wang, S. Basu, J.A. Nagy, A. Atala, D. Mukhopadhyay, S. Soker, Antiangiogenic properties of gold nanoparticles, Clin. Cancer Res. 11 (2005) 3530–3534.

[157] B. Karthikeyan, K. Kalishwaralal, S. Sheikpranbabu, V. Deepak, R. Haribalaganesh, S. Gurunathan, Gold nanoparticles downregulate VEGF-and IL-1β-induced cell proliferation through Src kinase in retinal pigment epithelial cells, Exp. Eye Res. 91 (2010) 769–778.

[158] B.P. Eliceiri, R. Paul, P.L. Schwartzberg, J.D. Hood, J. Leng, D.A. Cheresh, Selective requirement for Src kinases during VEGF-induced angiogenesis and vascular permeability, Mol. Cell 4 (1999) 915–924.

[159] K. Kalishwaralal, E. Banumathi, Ram Kumar Pandian, SureshBabu, V. Deepak, J. Muniyandi, S.H. Eom, S. Gurunathan, Silver nanoparticles inhibit VEGF induced cell proliferation and migration in bovine retinal endothelial cells, Colloids Surf., B 73 (2009) 51–57.

[160] D.H. Jo, J.H. Kim, Y.S. Yu, T.G. Lee, J.H. Kim, Antiangiogenic effect of silicate nanoparticle on retinal neovascularization induced by vascular endothelial growth factor, Nanomed. Nanotechnol. 8 (2012) 784–791.

[161] H. Song, W. Wang, P. Zhao, Z. Qi, S. Zhao, Cuprous oxide nanoparticles inhibit angiogenesis via down regulation of VEGFR2 expression, Nanoscale 6 (2014) 3206–3216.

[162] J.H. Kim, M.H. Kim, D.H. Jo, Y.S. Yu, T.G. Lee, J.H. Kim, The inhibition of retinal neovascularization by gold nanoparticles via suppression of VEGFR-2 activation, Biomaterials 32 (2011) 1865–1871.

[163] D.A. babAmmar, N. Nghiem, J.L. Olson, C.R. Stoldt, R. Velez-Montoya, Intraocular Biocompatibility of Gold-Nanoparticles, J. Nanomater. Mol. Nanotechnol. 02 (2013).

[164] S.J. Bakri, J.S. Pulido, P. Mukherjee, R.J. Marler, D. Mukhopadhyay, Absence of histologic retinal toxicity of intravitreal nanogold in a rabbit model, Retina (Philadelphia, Pa.) 28 (2008) 147–149.

[165] D.H. Jo, J.H. Kim, J.G. Son, N.W. Song, Y.-I. Kim, Y.S. Yu, T.G. Lee, J.H. Kim, Anti-angiogenic effect of bare titanium dioxide nanoparticles on pathologic neovascularization without unbearable toxicity, Nanomed. Nanotechnol. 10 (2014) 1109–1117.

[166] E. Söderstjerna, P. Bauer, T. Cedervall, H. Abdshill, F. Johansson, U.E. Johansson, Silver and gold nanoparticles exposure to in vitro cultured retina--studies on nanoparticle internalization, apoptosis, oxidative stress, glial- and microglial activity, PLoS ONE 9 (2014) e105359.

[167] A. Iriyama, M. Oba, T. Ishii, N. Nishiyama, K. Kataoka, Y. Tamaki, Y. Yanagi, Gene transfer using micellar nanovectors inhibits choroidal neovascularization in vivo, PLoS ONE 6 (2011) e28560.

[168] L. Ma, Y.-l. Liu, Z.-z. Ma, H.-L. Dou, J.-H. Xu, J.-c. Wang, X. Zhang, Q. Zhang, Targeted treatment of choroidal neovascularization using integrin-mediated sterically stabilized liposomes loaded with combretastatin A4, J. Ocul. Pharmacol. Ther. 25 (2009) 195–200.

[169] S.P. Massia, S.S. Rao, J.A. Hubbell, Covalently immobilized laminin peptide Tyr-Ile-Gly-Ser-Arg (YIGSR) supports cell spreading and co-localization of the 67-kilodalton laminin receptor with alpha-actinin and vinculin, J. Biol. Chem. 268 (1993) 8053–8059.

[170] O. Benny, K. Nakai, T. Yoshimura, L. Bazinet, J.D. Akula, S. Nakao, A. Hafezi-Moghadam, D. Panigrahy, P. Pakneshan, R.J. D'Amato, Broad spectrum antiangiogenic treatment for ocular neovascular diseases, PLoS ONE 5 (2010).

Chapter 2

Goals of the Thesis

Over the last two decades, nanoparticles have emerged as powerful tools for drug delivery and biomedical imaging. Due to their incredible versatility in respect to size, composition and surface characteristics they can be chemically engineered to suit a wide range of applications. As such, the conjugation of receptor ligands to a colloid's polymer corona is a commonly seen strategy to precisely tailor nanoparticle-cell interactions. This way, it is thought that nanoparticles can be efficiently addressed towards specific tissues which express the targeted receptors.

However, the story is much more complex. Cell surface receptors are usually not only expressed in diseased tissue but also show significant physiological expression in off-target tissue. This demands for new strategies that allow distinct discrimination between pathological and healthy tissue. One possible way of achieving this is to take advantage of the inherent capability of nanoparticles to bind several receptors simultaneously and thus differentially target tissues with differences in receptor expression. The angiotensin II receptor type 1 (AT_1R) is a prominent example of a receptor that is physiologically expressed in several organs but shows a distinct up-regulation and overexpression in many pathologic conditions. Furthermore, because of its immense pharmacological significance it is highly suitable for nanoparticle targeting.

Although conjugation of ligands to shielding polymer such as poly(ethylene glycol) (PEG) is a common technique to increase nanoparticle-cell interactions it is often overlooked that the attachment of ligand molecules to the polymer corona can drastically alter their receptor binding affinity. Using EXP3174, a small molecule antagonist for the AT_1R, the price of PEGylation on the ligand affinity was investigated. Furthermore, it was elucidated to what extent nanoparticle multivalency can compensate for the ligand affinity loss (**Chapter 3**).

AT_1 receptors play a significant role in proliferative diseases of the vasculature in the posterior eye such as proliferative age-related macular degeneration and proliferative diabetic retinopathy. In an in vivo study with healthy mice, the accumulation of EXP3174-targeted Qdots in the retinal and choroidal blood vessels was investigated. The unique Qdot fluorescence was identified by multispectral imaging and pinpointed by

immunohistochemistry. Complete biodistribution studies were performed with the help of inductively-coupled plasma mass spectrometry (**Chapter 4**).

Since Qdots were mainly used as reporter particles and are not well suited for therapeutic interventions, the multivalent targeting principle was transferred to polymer structures. For that reason ligands were attached to branched PEG molecules and poly(amido amine) dendrimers. Besides affinity and cytotoxicity, emphasis was also placed on polymer-drug interactions (**Chapter 5**).

In contrast to antagonist-modified nanoparticles that rest at the cell membrane, agonist-coupled colloids are rapidly endocytosed by inducing a distinct receptor response. Consequentially, the contact time of the colloids on the cell surface is greatly limited, which could impede formation of a multivalent nanoparticle-cell binding. A thiolated angiotensin II molecule was used to coat nanoparticles to yield agonistic particles. Flow cytometry, confocal microscopy and intracellular calcium measurements were employed to characterize cellular association, ligand affinity and thus the extent of multivalency (**Chapter 6**).

Integrins, a class of cell surface receptors responsible for cell-matrix interactions and growth factor signaling, have a high significance in the pathogenesis of glaucoma in the trabecular meshwork, a sponge-like tissue responsible for aqueous humor drainage. The anti-fibrotic effects of the integrin-specific antagonist cyclo(Arg-Gly-Asp-D-Phe-Cys) (RGDfC) were investigated by western blotting and real-time polymerase chain reaction. Finally, to explore if cyclo(RGDfC) peptides can be used as nanoparticle targeting moieties for the trabecular meshwork, the interaction of cyclo(RGDfC)-coated nanoparticles with primary and immortalized trabecular meshwork cells was investigated (**Chapter 7**).

Chapter 3

Nanoparticle multivalency counter-balances the ligand affinity loss upon PEGylation

Published in Journal of Controlled Release
2014, 194, 20-27

This chapter was published as: R. Hennig, K. Pollinger, A. Veser, M. Breunig and A. Goepferich, J. Control Release 2014, 194, 20-27, doi:10.1016/j.jconrel.2014.07.062. Data that was not obtained or analyzed by R. Hennig is highlighted.

Abstract

The conjugation of receptor ligands to shielded nanoparticles is a widely used strategy to precisely control nanoparticle-cell interactions. However, it is often overlooked that a ligand's affinity can be severely impaired by its attachment to the polyethylene glycol (PEG) chains that are frequently used to protect colloids from serum protein adsorption. Using the model ligand EXP3174, a small-molecule antagonist for the angiotensin II receptor type 1 (AT_1R), we investigated the ligand's affinity before and after its PEGylation and when attached to PEGylated nanoparticles. The PEGylated ligand displayed a 580-fold decreased receptor affinity compared to the native ligand. Due to their multivalency, the nanoparticles regained a low nanomolar receptor affinity, which is in the range of native ligand's affinity. Moreover, a four orders of magnitude higher concentration of free ligand was required to displace PEGylated nanoparticles carrying EXP3174 from the receptor. On average, one nanoparticle was decorated with 11.2 ligand molecules, which led to a multivalent enhancement factor of 22.5 compared to the monovalent PEGylated ligand. The targeted nanoparticles specifically bound the AT_1R and showed no interaction to receptor negative cells. Our study shows that the attachment of a small-molecule ligand to a PEG chain can severely affect its receptor affinity. Concomitantly, when the ligand is tethered to nanoparticles, the immense avidity greatly increases the ligand-receptor interaction. Based on our results, we highly recommend the affinity testing of receptor ligands before and after PEGylation to identify potent molecules for active nanoparticle targeting.

1 Introduction

Camouflaging the surface by PEGylation or other measures is essential to avoid the uptake of nanoparticles by the mononuclear phagocyte system (MPS) [1]. Concomitantly, it prevents aggregation by sterically stabilizing the colloidal particles [2]. However, with the introduction of polyethylene glycol (PEG) strands on its surface, the interaction between a nanoparticle and its target cell can be severely hampered. To overcome this severe drawback, which is often referred to as the "PEGylation dilemma" [3], the nanoparticle surface can be decorated with ligands. These ligands then bind to their respective receptors on the cell surface and contribute to greatly controlled nanoparticle-cell interactions [4]. This includes processes such as nanoparticle endocytosis via receptor-mediated pathways [5] or an increased accumulation into a defined target tissue [6]. When choosing such targeting moieties for conjugation to a nanoparticle, small-molecule ligands (MW < 1000 Da) are preferred over antibodies because they are non-immunogenic, do not alter the physicochemical properties of the nanoparticles, and do not hinder their extravasation [7–9].

Unfortunately, the attachment of small molecules to PEG strands can severely affect their receptor binding capabilities. This phenomenon, which is well-known for macromolecules including proteins, polysaccharides and nucleic acids [10–13], is caused by the steric interference of the PEG tether with the active site of the respective binding partners [14,15]. Due to the size of small-molecule ligands and their frequently small binding pockets, the PEGylation of these molecules can massively damage their receptor affinity. Although there are numerous nanoparticle systems that make use of small-molecule ligands like folic acid [16], RGD peptides [17] or glutathione [18] as targeting moieties, few reports address the effect of PEGylation on ligand receptor affinity. Another important aspect of such systems is that nanoparticles are able to reach out to several receptors simultaneously [19]. This is possible due to the multiple presentation of ligand molecules on the nanoparticle surface and can drastically improve the affinity of receptor-targeted ligands compared to the monovalent units [4,20].

Despite the continually growing amount of publications in the field of active nanoparticle targeting, the affinity of nanoparticle-bound ligands is rarely evaluated. Although multivalent nanoparticle-receptor interactions are well documented in the literature, the change in affinity that is a result of the ligand's attachment to the nanoparticle is often neglected. Therefore, we investigated in detail how PEGylation influences a small ligand's

affinity with a simultaneous look at how nanoparticles are able to compensate for this loss of affinity.

For this purpose we made use of the well-investigated G protein-coupled receptor angiotensin II receptor type 1 (AT_1R), a receptor that recently came into focus for targeted drug delivery [21] and offers a multitude of high affinity non-peptide ligands [22]. Here, we used the active metabolite of the prominent AT_1R antagonist losartan, known as EXP3174, and attached it to PEG and PEGylated nanoparticles. Quantum dots (Qdots) were chosen as a suitable nanoparticle platform because of their high intrinsic fluorescence and their remarkably uniform size [23,24]. We compared the receptor affinity of both the native ligand and the PEGylated ligand to the ligand's affinity when conjugated to multivalent nanoparticles. By determining the amount of deposited ligand per nanoparticle, we investigated the extent of multivalent interactions. In addition, flow cytometry and confocal microscopy studies were conducted to gain further insight into the multi-ligand binding nature of the nanoparticles.

2 Material and methods

2.1 Material

Qdots® 655 ITK™ amino PEG (Life Technologies, Carlsbad, CA, USA) were used as nanoparticle starting material. EXP3174, also known as losartan carboxylic acid, was purchased from Santa Cruz (Heidelberg, Germany). All chemicals were obtained from Sigma Aldrich (Taufkirchen, Germany) in analytical grade unless stated otherwise. Buffers used for PEGylation, nanoparticle labeling and purification were 10 mM 2-(N-morpholino)ethanesulfonic acid (MES) buffer pH 4.8, 50 mM borate buffer pH 8.5 and Dulbecco's phosphate buffered saline (DPBS) pH 7.4 consisting of 1.5 mM KH_2PO_4, 8 mM Na_2HPO_4, 2.7 mM KCl and 138 mM NaCl.

2.2 Cell culture

Human adrenal gland carcinoma cells NCI-H295R and rat mesangial cells were cultured in RPMI1640 medium containing 10 % fetal bovine serum (Sigma Aldrich, Taufkirchen, Germany) and supplemented with insulin-transferrin-selenine (PAA, Pasching, Austria), penicillin-streptomycin (Life Technologies, Carlsbad, CA, USA) and 100 nM hydrocortisone. Rat mesangial cells were a gift from Armin Kurtz (Department of Physiology, University of Regensburg, Germany). HeLa cells (ATCC No. CCL-2) were

maintained in Eagle's Minimum Essential Medium (EMEM) containing 10 % fetal bovine serum and 1 mM sodium pyruvate. All cells were cultured in T-75 cell culture flasks (Corning, Corning, NY, USA).

2.3 EXP3174 PEGylation

mPEG5k-amine was synthesized from its mPEG5k-OH precursor using the Mitsonubu reaction as previously described [25]. EXP3174 (2 µmol) was activated using N-(3-dimethylaminopropyl)-N'-ethylcarbodiimide hydrochloride (EDC, 25 mM) and N-hydroxysulfosuccinimide (sulfo-NHS, 10 mM) for 1 h in MES buffer pH 4.8. After activation of the carboxylic group of EXP3174, the pH was increased by the addition of borate buffer pH 8.5. Amino-mPEG5k (3.3 µmol) was added and the solution was vortexed for 16 h at room temperature. Subsequently, the reaction mixture was purified by size exclusion chromatography using a Sephadex G-25 resin in a PD-10 column (GE Healthcare, Munich, Germany) with DPBS as the eluent. Fractions containing mPEG-EXP3174 were pooled and further purified by ultrafiltration using a 3 KDa molecular weight cut-off Amicon Ultra-15 filter unit (Millipore, Billerica, MA, USA). Final mPEG-EXP3174 concentration was measured using a LS-55 fluorescence plate reader (Perkin Elmer, Waltham, MA, USA) against an EXP3174 calibration using an excitation wavelength of 250 nm and an emission wavelength of 370 nm., since the fluorescence properties of EXP3174 did not change upon PEGylation (Supplementary information, Fig. S2).

2.4 Nanoparticle labeling

Similarly to the PEGylation procedure, EXP3174 (16 nmol) was activated using EDC and sulfo-NHS in MES-buffered solution. After activation of EXP3174 for 1 h the pH was raised by addition of 50 mM borate buffer pH 8.5. Qdots® 655 ITK™ amino PEG (160 pmol) were added to the reaction mixture for the actual labeling reaction. After 16 hours of gentle shaking, EXP3174-modified Qdots were purified by size exclusion chromatography using a Sephadex G-25 resin in a PD-10 column with DPBS as the eluent. Further purification and concentration of the modified Qdots was achieved by ultrafiltration using a 100 KDa molecular weight cut-off Amicon Ultra-4 filter unit (Millipore, Billerica, MA, USA). Finally, Qdot concentration was determined by fluorescence measurement using a FluoStar Omega fluorescence microplate reader (BMG Labtech, Ortenberg, Germany) with an excitation and emission wavelength of 450 nm and 650 nm, respectively.

2.5 Size-exclusion chromatography

The purity of ligand-modified Qdots was analyzed by size exclusion chromatography (SEC) consisting of a Shimadzu LC-10ATVP pump (Shimadzu, Duisburg, Germany), a Shimadzu SIL-10ADVP autosampler connected to a Shimadzu RF-10AXL fluorescence detector. As a separation column, a TSKgel G3000 SW_{XL} column, 7.8 mm x 30 mm, 5 µm particle size (Tosoh Bioscience, Stuttgart, Germany) was used. The isocratic mobile phase consisted of citrate buffer (pH 3; 50 mM)-acetonitrile (80:20 v/v) and the column was operated at room temperature. Eluted EXP3174 was detected by fluorescence analysis with an excitation wavelength of 250 nm and an emission wavelength of 370 nm. For analysis of the Qdot fluorescence a mobile phase consisting of DPBS (pH 7.2)-acetonitrile (80:20 v/v) was used. The Qdot fluorescence was detected with an excitation and emission wavelength of 350 nm and 655 nm, respectively.

2.6 Intracellular calcium mobilization assay

The antagonistic affinity of the conjugated ligands was investigated using the fluorescent fura-2 Ca^{2+} chelator method established by Grynkiewicz *et al.* [26]. Suspensions of rat mesangial cells were incubated with 5 µM fura-2AM (Life Technologies, Carlsbad, CA, USA) and 0.05 % Pluronics F-127 in Leibovitz's L-15 medium (Life Technologies, Carlsbad, CA, USA) for 1 h at room temperature in the dark. After loading, cells were repeatedly washed by centrifugation (3 x, 5 min, 200 g, RT) and resuspension in Leibovitz's medium. A range of concentrations of EXP3174, mPEG-EXP3174 and EXP3174-Qdots were pipetted into 96-well plates (Greiner Bio One, Frickenhausen, Germany) at 20 µL per sample and 90 µL of loaded cells ($2*10^6$ cells/mL) were then injected into the wells. After 10 minutes of antagonist incubation, 90 µL of the EC_{80} (the concentration that leads to 80 % of the maximum signal) of the agonist angiotensin II (Bachem, Bubendorf, Switzerland) was injected into each well. The fluorescence signal was immediately recorded with a FluoStar Omega fluorescence microplate reader (BMG Labtech, Ortenberg, Germany) for 30 s. The EC_{80} was graphically determined from the agonist calcium curve produced with angiotensin II and rat mesangial cells. Excitation filters for the ratiometric measurement were 340/20 nm and 380/20 nm and the emission was recorded in a 510/20 nm bandpass filter. Analogously, the fluorescence signal was calibrated by incubating loaded cells with 0.1 % Triton-X 100 for measuring the maximal ratio (Rmax) and 0.1 % Triton-X 100 with 45 mM ethylene glycol-bis(2-aminoethylether)-N,N,N′,N′-tetraacetic acid (EGTA) to determine the minimal ratio

(Rmin). The intracellular calcium concentrations were calculated from the maximal fluorescence ratios based on the equation of Grynkiewicz *et al.* assuming a K_d value of 225 nM for the fura-2-calcium complex [26]. The IC_{50} values (the half maximal inhibitory concentration) were calculated using SigmaPlot 12.2 (Systat Software, San Jose, CA, USA) with the help of the sigmoidal dose-response (variable slope) equation. The multivalent enhancement (MVE) was calculated as initially proposed by Montet *et al.* MVE = IC_{50}(ligand) / IC_{50}(ligand when displayed by nanoparticle) but with minor changes as shown in equation 1 [19].

2.7 Flow cytometry

AT_1R expressing NCI-H295R cells were seeded into 24-well plates (Corning, Corning, NY, USA) at a density of 150,000 cells/well. Receptor-negative HeLa cells were seeded at a density of 100,000 cells/well. For nanoparticle binding studies, Qdot solutions of non-modified and EXP3174-modified Qdots with a concentration of 10 nM were prepared in Leibovitz's medium supplemented with 0.1 % bovine serum albumin. After the cells adhered overnight, they were washed with DPBS and the pre-warmed nanoparticle test solutions were pipetted onto the cell monolayer. After 1 h incubation at 37 °C, the cells were vigorously washed with DPBS and trypsinized. After suspension, the cells were centrifuged (5 min, 200 g), resuspended in DPBS, centrifuged again and finally resuspended in 200 µL DPBS and analyzed for their cellular fluorescence with a FACSCalibur flow cytometer (Becton Dickinson, Franklin Lakes, NJ, USA). Qdot fluorescence was excited at 488 nm and the fluorescence was analyzed using a 661/16 nm bandpass filter. For Qdot displacement studies, NCI-H295R cells were incubated with 5 nM EXP3174-modified Qdots and a concentration series of free EXP3174. After 1 h incubation at 37 °C the cells were processed analog to the nanoparticle binding studies.

Flow cytometry data was analyzed using WinMDI 2.9 (The Scripps Research Institute, San Diego, CA, USA). Only the population of viable cells was gated and used for the analysis of the cellular fluorescence. The geometrical mean was determined from the fluorescence histogram. The curve fitting for the displacement study was carried out with SigmaPlot 12.2 using the one site competition model, whereas maximal Qdot binding was set as cellular fluorescence when incubated with 5 nM EXP3174-modified Qdots and minimal binding was set as the cellular autofluorescence, which was determined in the absence of Qdots.

2.8 Confocal laser scanning microscopy

To analyze the nanoparticle binding pattern on the cells confocal microscopy was conducted. NCI-H295R cells were seeded into 8-well µ-slides (Ibidi, Martinsried, Germany) at a density of 15,000 cells/well. After adherence of the cells overnight, they were washed with DPBS. The pre-warmed nanoparticle test solution in Leibovitz's medium supplemented with 0.1 % bovine serum albumin were pipetted onto the cells and incubated for 1 hour at 37 °C. Then, cells were washed with DPBS, fixed with paraformaldehyde 2 % in DPBS for 10 min at room temperature, washed extensively with DPBS and analyzed with a Zeiss Axiovert 200 microscope combined with a LSM 510 laser-scanning device using a 63x Plan-Apochromat (NA 1.4) objective (Zeiss, Jena, Germany). Qdot fluorescence was excited with an argon laser at 488 nm. Qdot emission was recorded in a 650 nm longpass filter. The focal plane was adjusted to 1.8 µm. For image acquisition and processing AIM 4.2 (Zeiss, Jena, Germany) was used. Qdot fluorescence was displayed in false color green for better visibility.

2.9 Indirect ligand quantification

The amount of covalently bound EXP3174 on the nanoparticle surface was analyzed indirectly. One reaction identical to the nanoparticle labeling but without Qdots was conducted parallel to the standard nanoparticle labeling procedure (Fig. 5a). In place of the nanoparticles, the same volume of borate buffer pH 8.5 was added to the activated EXP3174. After 16 h of gentle shaking 50 µL of each mixture were diluted 20-fold with 50 mM borate buffer pH 9.0 and stirred for 6 h at 60 °C to hydrolyze the unreacted sulfo-NHS-activated ester of EXP3174. Non-nanoparticle bound EXP3174 concentration was analyzed by reversed phase high performance liquid chromatography (RP18-HPLC) consisting of a Shimadzu LC-10ATVP pump (Shimadzu, Duisburg, Germany), a Shimadzu SIL-10ADVP autosampler connected to a Shimadzu CTO-10ASVP column oven and a Shimadzu RF-10AXL fluorescence detector. As the separation column, a Luna® 5 µm C18(2) 100 Å 250 x 4.60 mm LC column (Phenomenex, Aschaffenburg, Germany) was used. The isocratic mobile phase consisted of citrate buffer (pH 3.0; 50 mM)-acetonitrile (50:50 v/v) and the column temperature was maintained at 30 °C. Eluted EXP3174 was detected by fluorescence analysis with an excitation wavelength of 250 nm and an emission wavelength of 370 nm. The difference in the amount of soluble EXP3174 from the reaction with and without Qdots was related to the Qdot concentration of 160 pmol from the initial labeling reaction to calculate the amount of

EXP3174 per nanoparticle. The affinity of one EXP3174 molecule when displayed by the PEGylated nanoparticle was calculated by multiplying the affinity of the EXP3174-Qdots by the number of EXP3174 molecules per nanoparticles using Gauss' law of error propagation.

2.10 Statistics

To assess statistical significance two-way analysis of variances (ANOVA) was carried out with a multiple comparisons test (Tukey's test) by using SigmaPlot 12.2. Levels of statistical significance were set as indicated.

3 Results and discussion

3.1 Ligand PEGylation and affinity comparison

First, by utilizing intracellular calcium measurements we characterized the angiotensin receptor expression on rat mesangial cells, adrenal gland carcinoma cells (NCI-H295R) and HeLa cells. Since the AT_1R is a Gq-coupled membrane receptor [27], cytosolic calcium measurements can be used to investigate receptor response rates and, therefore, to estimate receptor expression levels. Although the calcium signal is not linearly related to the ligand binding activity, we chose the calcium mobilization assay to determine binding strengths since our main focus is the pharmacological receptor blockade that results from a successful ligand-receptor interaction. Rat mesangial cells and the adrenal gland carcinoma cell line NCI-H295R both showed a positive calcium signal upon binding of the physiological agonist angiotensin II with an EC_{50} of 70.1 ± 1.8 nM and 21.6 ± 5.6 nM, respectively. HeLa cells, in contrast, showed no calcium signal after angiotensin II stimulation (Fig. 1a). For this reason, rat mesangial cells and NCI-H295R cells were used as receptor-positive cells and HeLa cells as receptor-negative control cells for ligand and nanoparticle binding experiments. The small non-peptide antagonist EXP3174, which is the active metabolite of losartan, blocked the angiotensin II signaling on rat mesangial cells with low nanomolar affinity and an IC_{50} of 1.1 ± 0.2 nM, which is in agreement with literature data [28] (Fig. 1b). To determine the affinity of EXP3174 after the attachment to a PEG tether, its carboxylic group was conjugated to methoxy-PEG5000-NH2 with EDC and sulfo-NHS. We chose a PEG with a molecular weight of 5000 g/mol and a most narrow size distribution (polydispersity index of 1.04). This chain length is often considered the minimum PEG chain length to effectively reduce serum protein adsorption [29]. Furthermore, the narrow size distribution of the used PEG species allows the measuring of discrete PEG-ligand affinities without the added variance of the polydisperse polymer tether.

After purification by size exclusion chromatography and ultrafiltration the purity of the synthesized PEGylated ligand and the absence of free EXP3174 were ensured by size-exclusion chromatography (Supplementary information, Fig. S1). Compared to the native EXP3174, the affinity of the PEGylated ligand heavily dropped by a factor of 580 to 630 ± 130 nM (Fig. 1b). The substantial decrease in receptor affinity can be attributed to the location of the receptor binding pocket for non-peptide ligands, which is formed by amino acids in the membrane-spanning regions of the AT_1R and is buried deep in the

seven transmembrane regions [27]. Though the receptor affinity of the mPEG-EXP3174 ligand was greatly decreased, it was not eliminated. Amides and esters of EXP3174's carboxylic functional group retain a high receptor binding affinity [30], therefore, the affinity loss in this system is a consequence of the PEG's distortion within the binding pocket rather than functional group changes. Recently, Vlashi and coworkers reported the extent to which the receptor affinity of folic acid, a very prominent small ligand used for nanoparticle targeting, is reduced by the attachment of differently sized PEG molecules [31]. In their study, the conjugation of linear PEG chains to folic acid and rhodamine decreased its binding affinity by a factor of approx. 70 to 187, depending on the PEG chain length. Although folic acid is known to retain a high affinity when grafted to PEG via its favorable γ-carboxyl group [32], the apparent affinity loss after attachment to a PEG chain is still substantial and should not be underestimated. Few cases are known where conjugated PEG enhanced the receptor binding of low-affinity ligands, which could be attributed to the entropy gain after the PEG-bound water is released upon receptor binding [33].

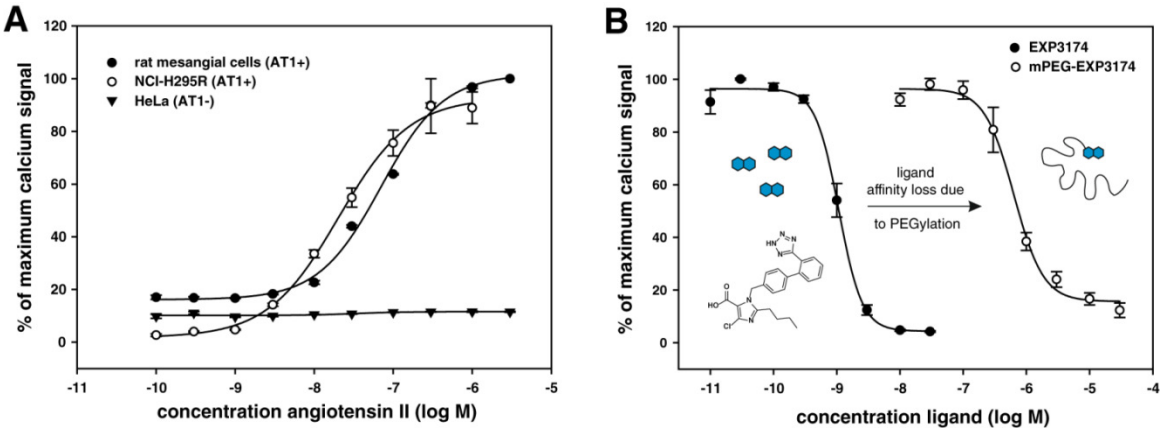

Figure 1: Affinity comparison of EXP3174 and its PEGylated counterpart. **(A)** Rat mesangial cells and adrenal gland carcinoma cells NCI-H295R express a functional AT_1 receptor, as shown through intracellular calcium measurements. HeLa cells without a functional AT_1R were used as receptor-negative control cells. **(B)** The native ligand EXP3174 blocks the AT_1R with nanomolar affinity of 1.1 ± 0.2 nM. Upon PEGylation, the affinity of the small non-peptide ligand is substantially decreased to 630 ± 130 nM.

3.2 Nanoparticle binding and localization

To analyze the affinity of EXP3174 when conjugated to nanoparticles, PEGylated and amine-terminated Qdots were covalently labeled with EXP3174 with the help of EDC and sulfo-NHS linker chemistry (Fig. 2a). Transmission electron microscopy (TEM) images revealed that the ligand conjugation process did not alter the particle uniformity as the

Qdots were evenly distributed and showed no sign of aggregation (Supplementary information, Fig. S3).

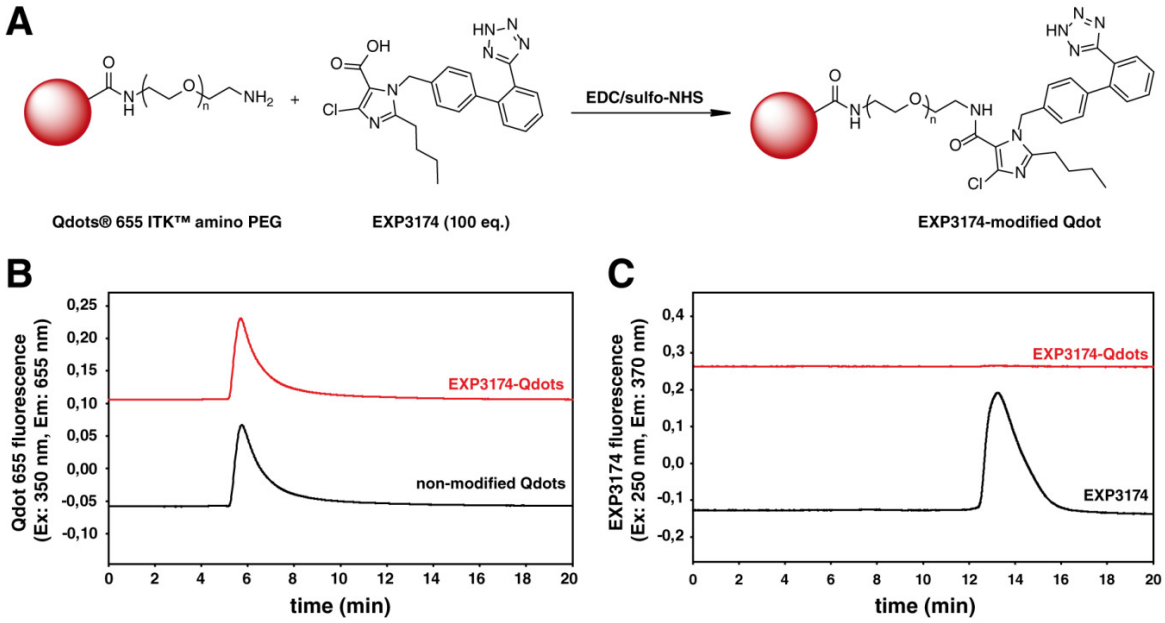

Figure 2. Conjugation reaction of EXP3174 to PEGylated Qdots and purification analysis by size-exclusion chromatography (SEC). **(A)** Illustrated for one PEG chain, EXP1374 was covalently coupled to PEGylated Qdots 655 by EDC and sulfo-NHS chemistry. The resulting EXP3174-decorated nanoparticles were extensively purified in a three-step procedure to remove unbound ligand. **(B)** The purified EXP3174-Qdots were analyzed by size-exclusion chromatography and showed no alteration of the fluorescence signal or the retention time. **(C)** Unreacted EXP3174 was successfully removed by the purification procedure. Since the high absorbance of the quantum dot core quenches the EXP3174 fluorescence at 370 nm, an indirect EXP3174 quantification method was conducted (see fig. 5a).

Zeta-potential measurements indicated that the conjugation procedure was successful (Supplementary information, Fig. S4). After the coupling of the ligand to the nanoparticles, the colloids were purified from unreacted ligand by ultrafiltration and preparative size-exclusion chromatography (SEC). With the help of an analytical SEC we ensured that the conjugation procedure did not alter the fluorescence properties of the Qdots (Fig. 2b) and that the unreacted EXP3174 had successfully been removed (Fig. 2c). Confocal laser scanning microscopy (CLSM) and flow cytometry experiments were conducted to analyze the association of nanoparticles to receptor-expressing NCI-H295R and receptor-negative HeLa cells. Confocal microscopy revealed a strong binding of EXP3174-modified Qdots to the cell membrane of the receptor-expressing NCI-H295R cells, while the unspecific binding of the non-modified Qdots was substantially weaker (Fig. 3a). Since EXP3174 as an AT_1R antagonist does not induce receptor internalization [34] it is not expected that the nanoparticles are immediately taken up by

the cells, but instead rest at the cell membrane where they bind multiple receptors at once [4].

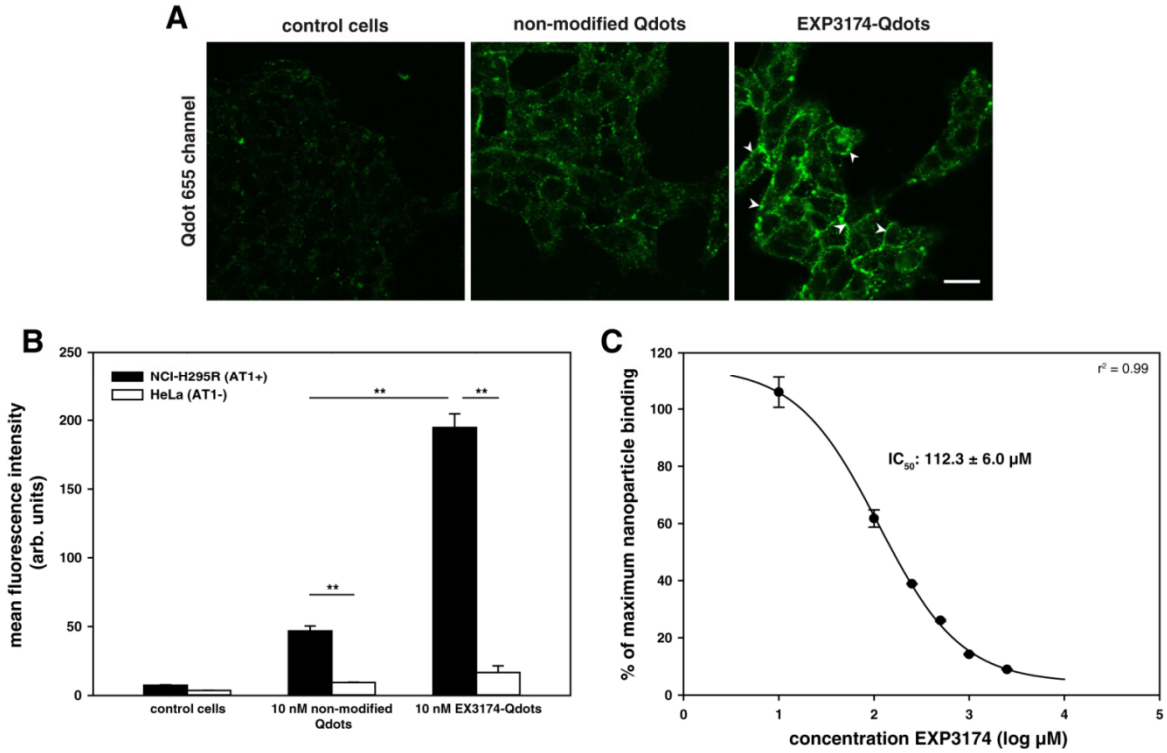

Figure 3. Nanoparticle binding to cells as observed by confocal microscopy and flow cytometry. **(A)** By confocal laser scanning microscopy, a strong binding of ligand-conjugated nanoparticles to the cell membrane of receptor expressing NCI-H295R cells could be observed (arrowheads). Non-modified Qdots only showed sparse unspecific binding to the cells. The autofluorescence of the cells was negligible. Qdot fluorescence is depicted in false color green. Scale bar: 20 µm **(B)** When quantified by flow cytometry, the ligand-modified Qdots showed a strong binding to receptor-positive cells and virtually no binding to receptor-negative HeLa cells. Although non-modified Qdots showed some increased unspecific binding to the NCI-H295R cells, the binding of EXP1374-Qdots was significantly higher. **(C)** In a displacement experiment, a tremendous amount of free ligand was needed to displace 5 nM of EXP3174-Qdots from the receptor. Levels of statistical significance are indicated as: (**) $p < 0.01$.

Flow cytometry experiments with receptor-negative and receptor-positive cells further demonstrated the strong binding of the EXP3174-modified Qdots to the receptor-expressing cells (Fig. 3b). Cells were incubated with nanoparticles with different surface functionalities, thoroughly washed and analyzed for their Qdot fluorescence. Although the non-modified nanoparticles showed weak, unspecific binding, the association of the ligand-conjugated Qdots to the receptor-positive cells was significantly higher.

In contrast, the AT_1R-targeted EXP3174-Qdots showed no association to receptor-negative cells, which confirmed the successful receptor binding to the target cells. To displace a concentration of 5 nM EXP3174-Qdots from the cells, extraordinarily high amounts of free ligand were needed (Fig. 3c). The inhibitory constant (IC_{50}, the

concentration of EXP3174 that displaces 50 % of the nanoparticles) was 112.3 ± 6.0 µM, which is about four orders of magnitude higher than the applied concentration of nanoparticles. This phenomenon, in which exceptionally high concentrations of free ligand are needed to displace the nanoparticles from the receptor, is often observed and is typical for multivalent ligand-receptor interactions [4,19,35].

3.3 Affinity of ligand-conjugated nanoparticles

Once we verified that EXP3174-modified Qdots bind the angiotensin II receptor type 1 and show no association to receptor-negative cells, we analyzed the affinity of both ligand-modified and non-modified Qdots by intracellular calcium quantifications with AT_1R-expressing rat mesangial cells. The high and broad absorbance of Qdots can interfere with many fluorescent calcium chelators, which is the reason we chose fura-2AM as the calcium indicator due to its ratiometric measurement.

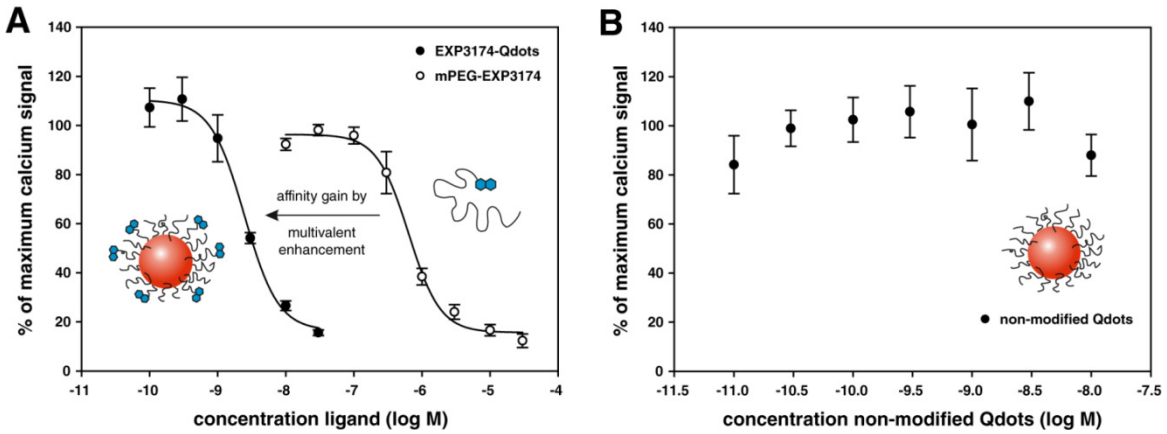

Figure 4: Ligand-conjugated nanoparticles regain high affinity by exhibiting multivalent interactions. **(A)** By binding several receptors at once, EXP3174-modified Qdots have an enhanced affinity of 2.5 ± 0.02 nM compared to the monovalent PEGylated unit. **(B)** Non-modified Qdots showed no receptor blocking and therefore no influence on the receptor binding of angiotensin II and the subsequent calcium influx into the cytosol.

In this intracellular calcium measurement, the antagonist-modified Qdots regained a nanomolar IC_{50} of 2.5 ± 0.02 nM, which is an affinity increase of a factor of 252 compared to the monovalent PEGylated ligand (Fig. 4a). The enhanced affinity of the EXP3174-Qdots compared to the mPEG-EXP3174 can be explained by multivalent ligand-receptor interactions, where one nanoparticle binds several receptors simultaneously. This multivalent enhancement is described for several nanoparticle platforms including Qdots [36–38], dendrimers [39,40], polymeric [41] or gold nanoparticles [42,43]. Another mechanism that could lead to measuring an increased affinity is the steric blockade of receptors by nanoparticles that bind neighboring receptors. However, we think this effect

is not predominant in our calcium assay since the signal-inducing angiotensin II, a small octapeptide, is able to diffuse rather freely and the nanoparticle is not able to shield the receptor from this small molecule. In addition, the high affinity loss upon PEGylation seen for mPEG-EXP3174 could be a consequence of the soluble PEG chain wrapping around the ligand molecule. When the PEG chain is covalently linked to the nanoparticle core, in contrast, its spatial flexibility could be decreased and the ligand molecule could be more accessible.

Compared to ligand-targeted nanoparticles, non-modified Qdots showed no influence on the cytosolic calcium concentrations, proving that the receptor blockage was indeed triggered by the surface-immobilized ligand and not the nanoparticle species itself (Fig. 4b). Since it is not the absolute fura-2 emission, but rather its ratio that is important, the broadband absorbance of Qdots only resulted in problems with higher nanoparticle concentrations than tested here.

3.4 Ligand quantification

To know if a nanoparticle exhibits a multivalent enhancement compared to the monovalent ligand or if the increased affinity is just the sum of ligand-receptor bindings, the exact amount of surface-bound EXP3174 had to be evaluated. However, because of the broad absorbance of Qdots [44], direct ligand quantification based on spectroscopic methods is not feasible. For this reason, the amount of surface-conjugated ligand is often only estimated based on the coupling efficiency but rarely quantified [45–47]. Additionally, fluorescence or isotopic labeling of the small-molecule ligand can drastically alter the receptor binding and the coupling efficacy to the nanoparticle.

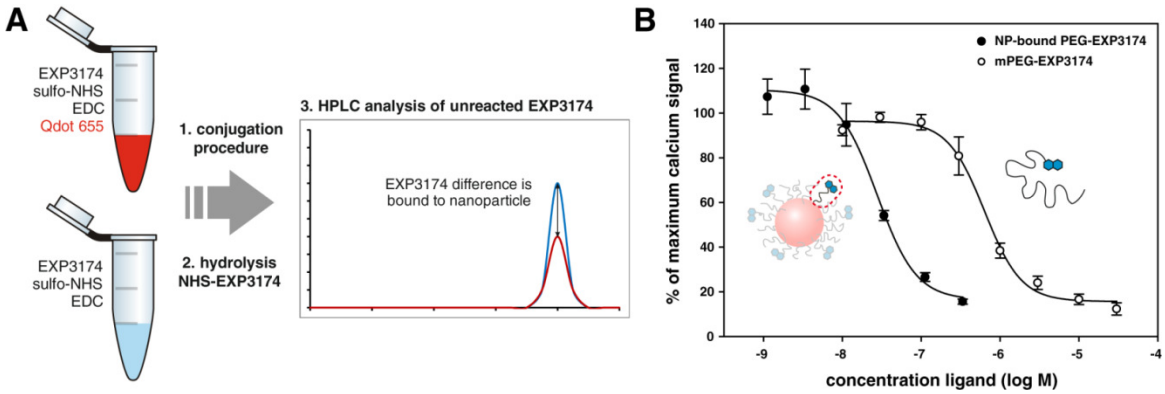

Figure 5: The analysis of ligand deposition on the nanoparticle surface allows for calculation of the nanoparticle-bound ligand affinity. **(A)** Scheme for the indirect quantification of ligand conjugated to the Qdots. As illustrated, two separate labeling reactions were conducted, in which one was free of Qdots. This allowed for the amount of deposited ligand to be determined as 11.2 ± 3.1 molecules EXP3174 per nanoparticle by. **(B)** When the monovalent PEGylated EXP3174 is compared to the nanoparticle-bound PEGylated EXP3174, the multi-ligand binding influence on the ligand affinity is obvious.

To circumvent these problems we made use of an indirect ligand quantification strategy to measure the nanoparticle-conjugated ligand. We evaluated the amount of non-reacted soluble ligand with reversed-phase high performance liquid chromatography (RP-18 HPLC) and compared it to an identical reaction that was free of Qdots (Fig. 5a).This way, ligand adsorption phenomena to glass and plastic could be quantified and the exact amount of nanoparticle-associated ligand was readily available. Using this method, we determined that 11.2 ± 3.1 molecules EXP3174 were bound to each Qdot. This is consistent with literature data, where 1 to 15 small ligands were covalently coupled to 20 nm Qdots with similar EDC/sulfo-NHS chemistry [48]. The calculated affinity of a single nanoparticle-bound PEG-EXP3174 is 28 ± 7.8 nM (Fig. 5b). Compared to the monovalent mPEG-EXP3174, the multivalent enhancement factor (MVE) was 22.5, which is in range of other multivalent systems described in the literature [19,49]. It must be noted that the MVE is highly dependent on the analyzed receptor and the applied assay. MVE estimations with living cells usually yield lower values [19] than calculations based on experimental conditions where nanoparticles interact with artificially immobilized binding partners such as receptors on a surface plasmon resonance (SPR) sensor chip [49–51]. The multivalent formation is mainly influenced by the nanoparticle size [52] and shape [53], the ligand density [54] and the receptor response after ligand binding. However, for a complete insight into multivalent interactions between ligands and receptors, the nanoparticle-bound ligand should not be compared to the native ligand, but rather to the PEGylated counterpart (Eq. 1). This way, the affinity decrease

that arises from the PEG tether would be included and the real nanoparticle multivalent enhancement would be accessible.

$$\mathrm{MVE} = \frac{\mathrm{IC_{50}\ (PEGylated\ ligand)}}{\mathrm{IC_{50}\ (ligand\ when\ displayed\ by\ PEGylated\ nanoparticle)}}$$

Equation 1. Adaption to the calculation of the multivalent enhancement factor (MVE) that was originally proposed by Montet *et al. [19]* for the assessment of the real multivalency.

The present example shows the necessity of this approach: When the free EXP3174 is compared to the EXP3174-decorated nanoparticle it appears there are no multivalent effects since the affinity is marginally decreased. However, when compared to the PEGylated counterpart, the multivalent enhancement of the nanoparticles can be clearly seen and measured.

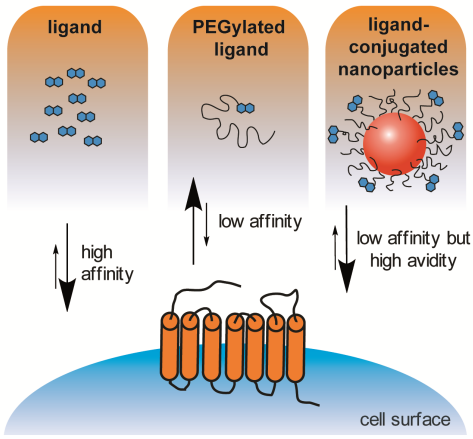

Figure 6: Summary of monovalent and multivalent ligand receptor interaction between EXP3174 and AT_1R

4 Conclusion

We demonstrated that the affinity of a small non-peptide ligand can severely suffer from its attachment to a PEG chain. By binding to their target receptors in a multivalent fashion, nanoparticles have the ability to compensate for this profound affinity loss. These avidity-driven interactions lead to strong particle-receptor bindings that surpass that of monovalent ligands. The present work is the first study that addresses both effects in a common context, which is pivotal for understanding the targeting efficacy of nanoparticles (Fig. 6).

Based on our findings, we strongly recommend affinity testing of small-molecule ligands after PEGylation and before attaching them to the PEG corona of nanoparticles. This way, many results in which the active-targeted nanoparticles are not more effective than their passive-targeted counterpart could eventually be attributed to a strong ligand affinity

decline after the conjugation to nanoparticles. If PEGylation nullifies the binding capacity of the ligand, a different ligand or even another targeting strategy should be applied.

References

[1] T.M. Allen, Long-circulating (sterically stabilized) liposomes for targeted drug delivery, Trends Pharmacol. Sci. 15 (1994) 215–220.

[2] W.P. Wuelfing, S.M. Gross, D.T. Miles, R.W. Murray, Nanometer Gold Clusters Protected by Surface-Bound Monolayers of Thiolated Poly(ethylene glycol) Polymer Electrolyte, J. Am. Chem. Soc. 120 (1998) 12696–12697.

[3] H. Hatakeyama, H. Akita, H. Harashima, A multifunctional envelope type nano device (MEND) for gene delivery to tumours based on the EPR effect: a strategy for overcoming the PEG dilemma, Adv. Drug Deliv. Rev. 63 (2011) 152–160.

[4] W. Hild, K. Pollinger, A. Caporale, C. Cabrele, M. Keller, N. Pluym, A. Buschauer, R. Rachel, J. Tessmar, M. Breunig, A. Goepferich, G protein-coupled receptors function as logic gates for nanoparticle binding and cell uptake, Proc. Natl. Acad. Sci. U.S.A. 107 (2010) 10667–10672.

[5] K. Pollinger, R. Hennig, M. Breunig, J. Tessmar, A. Ohlmann, E.R. Tamm, R. Witzgall, A. Goepferich, Kidney podocytes as specific targets for cyclo(RGDfC)-modified nanoparticles, Small 8 (2012) 3368–3375.

[6] K. Pollinger, R. Hennig, A. Ohlmann, R. Fuchshofer, R. Wenzel, M. Breunig, J. Tessmar, E.R. Tamm, A. Goepferich, Ligand-functionalized nanoparticles target endothelial cells in retinal capillaries after systemic application, Proc. Natl. Acad. Sci. U.S.A. 110 (2013) 6115–6120.

[7] X.-H. Peng, X. Qian, H. Mao, A.Y. Wang, Z.G. Chen, S. Nie, D.M. Shin, Targeted magnetic iron oxide nanoparticles for tumor imaging and therapy, Int J Nanomedicine 3 (2008) 311–321.

[8] S.D. Steichen, M. Caldorera-Moore, N.A. Peppas, A review of current nanoparticle and targeting moieties for the delivery of cancer therapeutics, Eur J Pharm Sci 48 (2012) 416–427.

[9] W. Cai, T. Gao, H. Hong, J. Sun, Applications of gold nanoparticles in cancer nanotechnology, Nanotechnol Sci Appl 2008 (2008).

[10] F.M. Veronese, O. Schiavon, G. Pasut, R. Mendichi, L. Andersson, A. Tsirk, J. Ford, G. Wu, S. Kneller, J. Davies, R. Duncan, PEG-doxorubicin conjugates: influence of polymer structure on drug release, in vitro cytotoxicity, biodistribution, and antitumor activity, Bioconjug. Chem. 16 (2005) 775–784.

[11] R. Das, E. Baird, S. Allen, B. Baird, D. Holowka, B. Goldstein, Binding mechanisms of PEGylated ligands reveal multiple effects of the PEG scaffold, Biochemistry 47 (2008) 1017–1030.

[12] S.H. Kim, J.H. Jeong, S.H. Lee, S.W. Kim, T.G. Park, PEG conjugated VEGF siRNA for anti-angiogenic gene therapy, J Control Release 116 (2006) 123–129.

[13] X. Lin, S. Wang, Y. Jiang, Z.-J. Wang, G.-L. Sun, D.-S. Xu, Y. Feng, L. Shen, Poly(ethylene glycol)-radix Ophiopogonis polysaccharide conjugates: preparation, characterization, pharmacokinetics and in vitro bioactivity, Eur J Pharm Biopharm 76 (2010) 230–237.

[14] A.P. Chapman, PEGylated antibodies and antibody fragments for improved therapy: a review, Adv. Drug Deliv. Rev. 54 (2002) 531–545.

[15] C.S. Fishburn, The pharmacology of PEGylation: balancing PD with PK to generate novel therapeutics, J Pharm Sci 97 (2008) 4167–4183.

[16] A. Garcia-Bennett, M. Nees, B. Fadeel, In search of the Holy Grail: Folate-targeted nanoparticles for cancer therapy, Biochem. Pharmacol. 81 (2011) 976–984.

[17] F. Danhier, A. Le Breton, V. Préat, RGD-based strategies to target alpha(v) beta(3) integrin in cancer therapy and diagnosis, Mol. Pharm. 9 (2012) 2961–2973.

[18] J. Kreuter, Drug delivery to the central nervous system by polymeric nanoparticles: What do we know?, Advanced Drug Delivery Reviews 71 (2014) 2–14.

[19] X. Montet, M. Funovics, K. Montet-Abou, R. Weissleder, L. Josephson, Multivalent effects of RGD peptides obtained by nanoparticle display, J. Med. Chem. 49 (2006) 6087–6093.

[20] R. Weissleder, K. Kelly, E.Y. Sun, T. Shtatland, L. Josephson, Cell-specific targeting of nanoparticles by multivalent attachment of small molecules, Nat. Biotechnol. 23 (2005) 1418–1423.

[21] T. Dvir, M. Bauer, A. Schroeder, J.H. Tsui, D.G. Anderson, R. Langer, R. Liao, D.S. Kohane, Nanoparticles targeting the infarcted heart, Nano Lett. 11 (2011) 4411–4414.

[22] S.-I. Miura, S.S. Karnik, K. Saku, Review: angiotensin II type 1 receptor blockers: class effects versus molecular effects, J Renin Angiotensin Aldosterone Syst 12 (2011) 1–7.

[23] W.A. Hild, M. Breunig, A. Goepferich, Quantum dots - nano-sized probes for the exploration of cellular and intracellular targeting, Eur J Pharm Biopharm 68 (2008) 153–168.

[24] C.B. Murray, D.J. Norris, M.G. Bawendi, Synthesis and characterization of nearly monodisperse CdE (E = sulfur, selenium, tellurium) semiconductor nanocrystallites, J. Am. Chem. Soc. 115 (1993) 8706–8715.

[25] S. Kirchhof, F.P. Brandl, N. Hammer, A.M. Goepferich, Investigation of the Diels–Alder reaction as a cross-linking mechanism for degradable poly(ethylene glycol) based hydrogels, J. Mater. Chem. B 1 (2013) 4855.

[26] G. Grynkiewicz, M. Poenie, R.Y. Tsien, A new generation of Ca2+ indicators with greatly improved fluorescence properties, J. Biol. Chem. 260 (1985) 3440–3450.

[27] M. de Gasparo, K.J. Catt, T. Inagami, J.W. Wright, T. Unger, International union of pharmacology. XXIII. The angiotensin II receptors, Pharmacol. Rev. 52 (2000) 415–472.

[28] A. Sachinidis, Y. Ko, P. Weisser, M.K. Meyer zu Brickwedde, R. Düsing, R. Christian, A.J. Wieczorek, H. Vetter, EXP3174, a metabolite of losartan (MK 954, DuP 753) is more potent than losartan in blocking the angiotensin II-induced responses in vascular smooth muscle cells, J. Hypertens. 11 (1993) 155–162.

[29] Gref, Lück, Quellec, Marchand, Dellacherie, Harnisch, Blunk, Müller, 'Stealth' corona-core nanoparticles surface modified by polyethylene glycol (PEG): influences of the corona (PEG chain length and surface density) and of the core composition on phagocytic uptake and plasma protein adsorption, Colloids Surf B Biointerfaces 18 (2000) 301–313.

[30] J.B. Santella, J.V. Duncia, C.L. Ensinger, M.K. VanAtten, D.J. Carini, R.R. Wexler, A.T. Chiu, P.C. Wong, P.B. Timmermans, Balanced angiotensin II receptor antagonists. III. The effects of substitution at the imidazole 5-position, Bioorganic & Medicinal Chemistry Letters 4 (1994) 2235–2240.

[31] E. Vlashi, L.E. Kelderhouse, J.E. Sturgis, P.S. Low, Effect of folate-targeted nanoparticle size on their rates of penetration into solid tumors, ACS Nano 7 (2013) 8573–8582.

[32] J. Sudimack, R.J. Lee, Targeted drug delivery via the folate receptor, Adv. Drug Deliv. Rev. 41 (2000) 147–162.

[33] D. Ponader, F. Wojcik, F. Beceren-Braun, J. Dernedde, L. Hartmann, Sequence-defined glycopolymer segments presenting mannose: synthesis and lectin binding affinity, Biomacromolecules 13 (2012) 1845–1852.

[34] S. Miserey-Lenkei, Z. Lenkei, C. Parnot, P. Corvol, E. Clauser, A functional enhanced green fluorescent protein (EGFP)-tagged angiotensin II at(1a) receptor recruits the endogenous Galphaq/11 protein to the membrane and induces its specific internalization independently of receptor-g protein coupling in HEK-293 cells, Mol. Endocrinol. 15 (2001) 294–307.

[35] A. Gabizon, A.T. Horowitz, D. Goren, D. Tzemach, F. Mandelbaum-Shavit, M.M. Qazen, S. Zalipsky, Targeting folate receptor with folate linked to extremities of poly(ethylene glycol)-grafted liposomes: in vitro studies, Bioconjug. Chem. 10 (1999) 289–298.

[36] Y. Yang, X.-C. Xue, X.-F. Jin, L.-J. Wang, Y.-L. Sha, Z.-J. Li, Synthesis of multivalent N-acetyl lactosamine modified quantum dots for the study of carbohydrate and galectin-3 interactions, Tetrahedron 68 (2012) 7148–7154.

[37] H.A. Gussin, I.D. Tomlinson, D. Cao, H. Qian, S.J. Rosenthal, D.R. Pepperberg, Quantum dot conjugates of GABA and muscimol: binding to α1β2γ2 and ρ1 GABA(A) receptors, ACS Chem Neurosci 4 (2013) 435–443.

[38] Y. Lu, Y. Zhong, J. Wang, Y. Su, F. Peng, Y. Zhou, X. Jiang, Y. He, Aqueous synthesized near-infrared-emitting quantum dots for RGD-based in vivo active tumour targeting, Nanotechnology 24 (2013) 135101.

[39] S. Hong, P.R. Leroueil, I.J. Majoros, B.G. Orr, J.R. Baker, M.M. Banaszak Holl, The binding avidity of a nanoparticle-based multivalent targeted drug delivery platform, Chem. Biol. 14 (2007) 107–115.

[40] J.H. Myung, K.A. Gajjar, J. Saric, D.T. Eddington, S. Hong, Dendrimer-mediated multivalent binding for the enhanced capture of tumor cells, Angew. Chem. Int. Ed. Engl. 50 (2011) 11769–11772.

[41] L. de Miguel, M. Noiray, G. Surpateanu, B.I. Iorga, G. Ponchel, Poly(γ-benzyl-l-glutamate)-PEG-alendronate multivalent nanoparticles for bone targeting, Int J Pharm 460 (2014) 73–82.

[42] E.C. Dreaden, B.E. Gryder, L.A. Austin, B.A. Tene Defo, S.C. Hayden, M. Pi, L.D. Quarles, A.K. Oyelere, M.A. El-Sayed, Antiandrogen gold nanoparticles dual-target and overcome treatment resistance in hormone-insensitive prostate cancer cells, Bioconjug. Chem. 23 (2012) 1507–1512.

[43] P. Valentini, P.P. Pompa, Gold nanoparticles for naked-eye DNA detection: smart designs for sensitive assays, RSC Adv. 3 (2013) 19181.

[44] I.L. Medintz, H.T. Uyeda, E.R. Goldman, H. Mattoussi, Quantum dot bioconjugates for imaging, labelling and sensing, Nat Mater 4 (2005) 435–446.

[45] W. Cai, D.-W. Shin, K. Chen, O. Gheysens, Q. Cao, S.X. Wang, S.S. Gambhir, X. Chen, Peptide-labeled near-infrared quantum dots for imaging tumor vasculature in living subjects, Nano Lett. 6 (2006) 669–676.

[46] X. Gao, Y. Cui, R.M. Levenson, Chung, Leland W K, S. Nie, In vivo cancer targeting and imaging with semiconductor quantum dots, Nat. Biotechnol. 22 (2004) 969–976.

[47] S.J. Rosenthal, I. Tomlinson, E.M. Adkins, S. Schroeter, S. Adams, L. Swafford, J. McBride, Y. Wang, L.J. DeFelice, R.D. Blakely, Targeting cell surface receptors with ligand-conjugated nanocrystals, J. Am. Chem. Soc. 124 (2002) 4586–4594.

[48] M. Amela-Cortes, V. Roullier, C. Wolpert, S. Neubauer, H. Kessler, O. Bedel, S. Mignani, V. Marchi-Artzner, Stable functionalized PEGylated quantum dots micelles with a controlled stoichiometry, Chem. Commun. 47 (2011) 1246.

[49] C. Tassa, J.L. Duffner, T.A. Lewis, R. Weissleder, S.L. Schreiber, A.N. Koehler, S.Y. Shaw, Binding affinity and kinetic analysis of targeted small molecule-modified nanoparticles, Bioconjug. Chem. 21 (2010) 14–19.

[50] J.E. Silpe, M. Sumit, T.P. Thomas, B. Huang, A. Kotlyar, M.A. van Dongen, M.M. Banaszak Holl, B.G. Orr, S.K. Choi, Avidity modulation of folate-targeted

multivalent dendrimers for evaluating biophysical models of cancer targeting nanoparticles, ACS Chem. Biol. 8 (2013) 2063–2071.

[51] M.-H. Li, S.K. Choi, T.P. Thomas, A. Desai, K.-H. Lee, A. Kotlyar, M.M. Banaszak Holl, J.R. Baker, Dendrimer-based multivalent methotrexates as dual acting nanoconjugates for cancer cell targeting, Eur J Med Chem 47 (2012) 560–572.

[52] W. Jiang, Kim, Betty Y. S., J.T. Rutka, Chan, Warren C. W., Nanoparticle-mediated cellular response is size-dependent, Nature Nanotech 3 (2008) 145–150.

[53] P. Kolhar, A.C. Anselmo, V. Gupta, K. Pant, B. Prabhakarpandian, E. Ruoslahti, S. Mitragotri, Using shape effects to target antibody-coated nanoparticles to lung and brain endothelium, Proceedings of the National Academy of Sciences 110 (2013) 10753–10758.

[54] J. Wang, S. Tian, R.A. Petros, M.E. Napier, J.M. DeSimone, The Complex Role of Multivalency in Nanoparticles Targeting the Transferrin Receptor for Cancer Therapies, J. Am. Chem. Soc. 132 (2010) 11306–11313.

Nanoparticle multivalency counterbalances the ligand affinity loss upon PEGylation

1 Size exclusion chromatography

The purity of mPEG-EXP3174 was analyzed by size exclusion chromatography (SEC) consisting of a Shimadzu LC-10ATVP pump (Shimadzu, Duisburg, Germany), a Shimadzu SIL-10ADVP autosampler connected to a Shimadzu RF-10AXL fluorescence detector. As a separation column, a TSKgel G3000 SW_{XL} column, 7.8 mm x 30 mm, 5 µm particle size (Tosoh Bioscience, Stuttgart, Germany) was used. The isocratic mobile phase consisted of citrate buffer (pH 3; 50 mM)-acetonitrile (80:20 v/v) and the column was operated at room temperature. Eluted EXP3174 and mPEG-EXP3174 were detected by fluorescence analysis with an excitation wavelength of 250 nm and an emission wavelength of 370 nm.

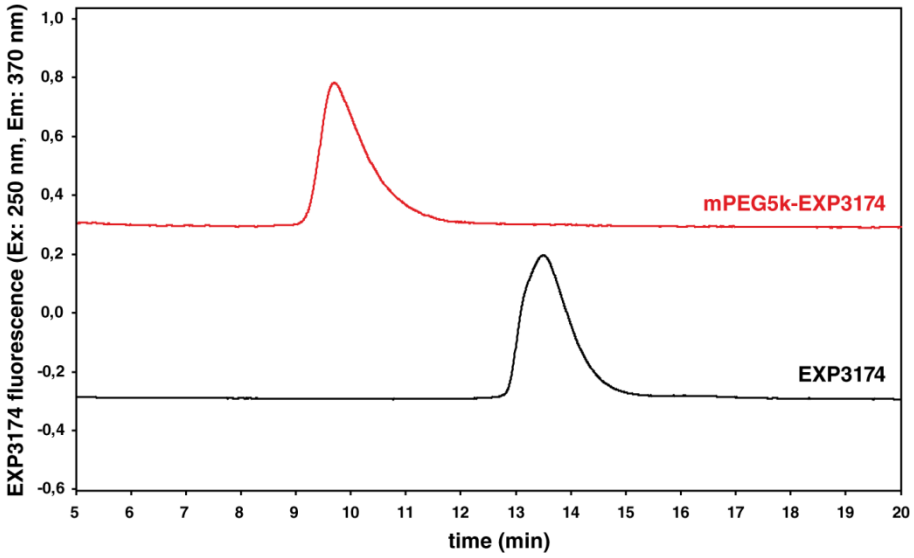

Figure S1. Size exclusion chromatogram of EXP3174 and mPEG-EXP3174. The absence of unreacted EXP3174 can be clearly seen for the mPEG5K-EXP3174 derivative.

2 Fluorescence Spectra of EXP3174 and mPEG5k-EXP3174

The fluorescence spectra of EXP3174 and EXP3174 upon PEGylation were investigated with a LS-55 fluorescence plate reader (Perkin Elmer, Waltham, MA, USA) at a concentration of 100 µM in citrate buffer pH 2.5 (100 mM).

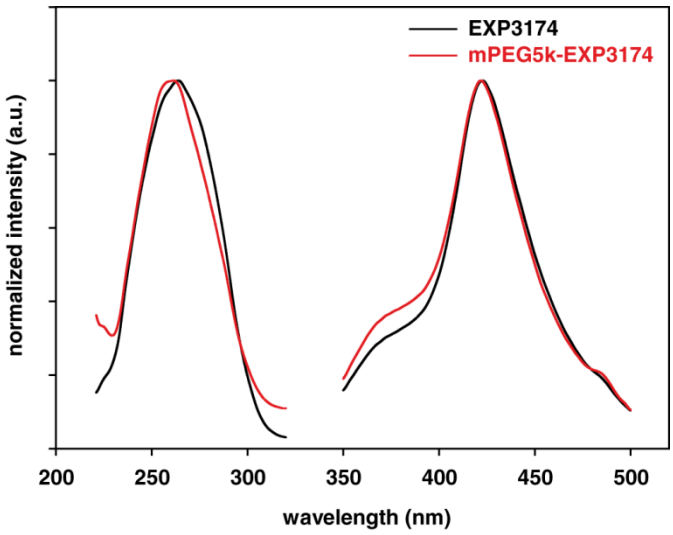

Figure S2. Excitation and emission spectra of EXP3174 and PEGylated EXP3174 show no significant change in fluorescence properties upon PEGylation

3 Transmission electron microscopy

4 µL of a 60 nM aqueous solution Qdots was pipetted on a carbon-coated copper grid (Plano, Wetzlar, Germany) and air dried. The sample was analyzed using a Zeiss Libra 120 electron microscope (Zeiss, Oberkochen, Germany). Electron micrographs were acquired and analyzed with Image SP (Zeiss, Oberkochen, Germany).

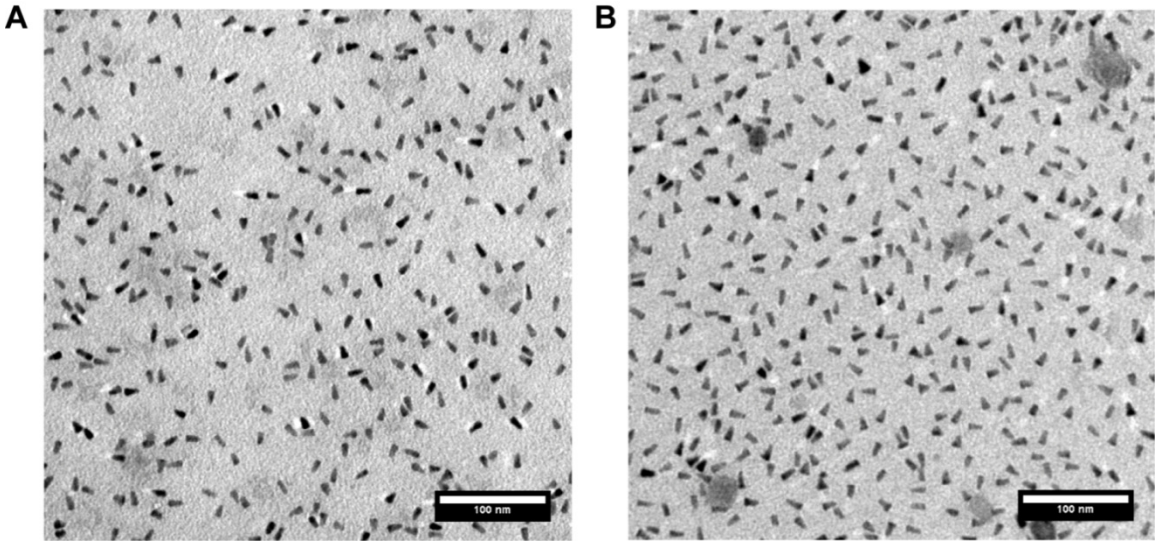

Figure S3. Transmission electron micrograph displaying non-modified (a) and EXP3174-modified Qdots 655 (b). Both nanoparticles have a rod-like shape. EXP3174-modified Qdots are monodisperse and show no sign of aggregation after the conjugation and purification procedure. The inorganic core of the non-modified Qdots has a length of 16.0 ± 1.6 nm with a width of 7.9 ± 0.9 nm. Similarly, the inorganic core of EXP3174-modified Qdots has a length of 17.8 ± 2.1 nm and a width of 7.7 ± 1.1 nm (each value was analyzed for 50 nanoparticles).

4 Zeta-potential

The electrophoretic mobility was measured at 25 °C using a Malvern ZetaSizer Nano ZS (Malvern Instruments GmbH, Herrenberg, Germany). Purified Qdot samples were diluted to a concentration of 10 nM with DPBS 0.1X and analyzed using a standard capillary electrophoresis cell (Malvern Instruments). For comparison purposes glycolic acid was similarly conjugated to the terminal amine-groups of the Qdots as EXP3174 using EDC and sulfo-NHS chemistry as stated in the Materials and Methods.

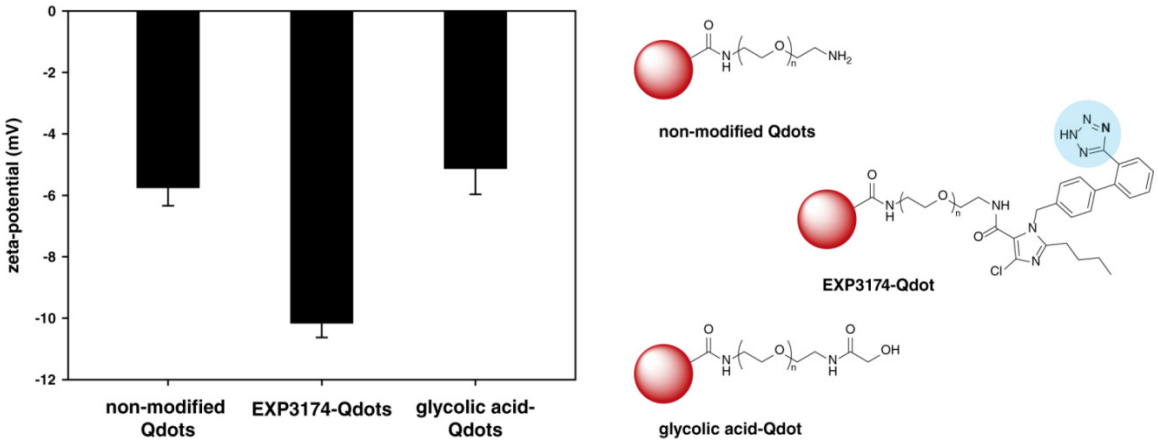

Figure S4. Zeta-potential measurements of non-modified, EXP3174- and glycolic-acid conjugated Qdots. By coupling of EXP3174 to the Qdot amine groups, the zeta potential is substantially lowered. The reason is the tetrazole group of EXP3174 (circled), which is deprotonated at physiologic pH values. To exclude that the more negative zeta-potential is not due to the depletion of the terminal amine groups a comparable coupling with glycolic acid was conducted. Here, the zeta-potential is comparable to the non-modified Qdots, proving the more negative zeta-potential of EXP3174-Qdots is a consequence of the EXP3174 coupling.

Chapter 4

Multivalent nanoparticles bind the retinal and choroidal vasculature

Published in Journal of Controlled Release
2015, 220A, 265-274

This chapter was published as: R. Hennig, A. Ohlmann, J. Staffel, K. Pollinger, A. Haunberger, M. Breunig, F. Schweda, E. Tamm and A. Goepferich, Journal of Controlled Release 2015, 220A, 265-274, doi:10.1016/j.jconrel.2015.10.033. Data that was not obtained or analyzed by R. Hennig is highlighted.

Abstract

The angiotensin II receptor type 1 (AT_1R), which is expressed in blood vessels of the posterior eye, is of paramount significance in the pathogenesis of severe ocular diseases such as diabetic retinopathy and age-related macular degeneration. However, small molecule angiotensin receptor blockers (ARBs) have not proven to be a significant therapeutic success. We report here on a nanoparticle system consisting of ARB molecules presented in a multivalent fashion on the surface of quantum dots (Qdots). As a result of the multivalent receptor binding, nanoparticles targeted cells with high AT_1R expression and inhibited their angiotensin receptor signaling with an IC_{50} of 3.8 nM while showing only minor association to cells with low AT_1R expression. After intravenous injection into the tail vein of mice, multivalent nanoparticles accumulated in retinal and choroidal blood vessels of the posterior eye. At the same time, multivalent ligand display doubled the Qdot concentration in the blood vessels compared to non-targeted Qdots. Remarkably, ARB-targeted Qdots showed no pronounced accumulation in AT_1R-expressing off-target tissues such as the kidney. Following systemic application, this multivalent targeting approach has the potential to amplify AT_1R blockade in the eye and concomitantly deliver a therapeutic payload into ocular lesions.

1 Introduction

The angiotensin II receptor type 1 (AT_1R) is a G protein-coupled receptor (GPCR) that is known for its role in regulating physiologic fluid and salt homeostasis and blood pressure [1]. However, it also serves as a key mediator of inflammation [2] and potent growth factor [3]. As such, AT_1R and its ligand angiotensin II are critically important in pathological angiogenesis [4]. Two prominent examples of pathologies in which the receptor plays a pivotal role are exudative age-related macular degeneration (wet AMD) and proliferative diabetic retinopathy, diseases of the posterior eye that lead to blindness and severe visual impairment in a large number of patients each year [5,6]. In both of these neovascular diseases, inflammation mediated by AT_1R appears to be crucial for pathogenesis and disease progression [7,8]. This is not surprising, since angiotensin II stimulates formation of retinal blood vessels and concomitantly increases their leakiness [9]. Despite this clear link between AT_1R and ocular disease, the effect of angiotensin receptor blockers (ARBs) on therapeutic outcomes has only been modest [10–12]. Since ARBs display enormous plasma protein binding of more than 95 % [13,14] and may be taken up by several other tissues such as kidneys, adrenal glands, vascular smooth muscle cells and heart, all of which abundantly express the receptor [15], it is possible that therapeutic ARB levels cannot be maintained in the eye.

To improve AT_1R antagonism in the ocular vasculature we developed a nanoparticle system that displays multiple receptor antagonists at the surface of a colloid, thus allowing the formation of multivalent ligand-receptor interactions towards AT_1 receptors [16]. The nanoparticles retain overall binding affinity while each individual ligand receptor-interaction is reduced. This gives these colloids the capability to differentially target tissues with higher AT_1R expression. We envision a scenario in which the enhanced receptor binding – resulting in prolonged contact times on the cell surface – and the nanoparticles' diminished off-target tissue accumulation could enhance the ocular bioavailability of ARBs and thus amplify their therapeutic benefit.

Although *in vitro* data have convincingly proven that multivalent nanoparticles bind AT_1R-expressing cells [16], the capability of these nanomaterials to interact with the choroidal and retinal blood vessels has not been assessed so far. Since the choroidal blood vessels, the major underlying blood vessels of the retina, have the highest perfusion of all vascular beds within the human body [17], only a limited timeframe is available for the colloids to establish strong nanoparticle-cell interaction and thus bind endothelial cells.

Therefore, this study aims to explore the *in vivo* potential of nanomaterials that use ARBs as multivalent targeting ligands and not as the nanoparticles themselves [18] or as a nanoparticle payload [19,20]. EXP3174, the active metabolite of the prominent ARB losartan, was covalently immobilized on the surface of highly fluorescent PEGylated quantum dots (Qdots), which were used as model colloids due to their intense fluorescence and highly monodisperse size [21]. *In vitro* binding and receptor affinity of nanoparticles to cell lines with different levels of AT_1R expression was investigated with confocal microscopy and intracellular calcium measurements. Multi-spectral imaging, immunohistochemistry and inductively coupled plasma mass spectrometry (ICP-MS) were utilized to follow the nanoparticles' fate *in vivo* and gain insight into their biodistribution and tissue accumulation.

2 Materials and methods

2.1 Materials

EXP3174, also known as losartan carboxylic acid, was purchased from Santa Cruz (Heidelberg, Germany). Qdots® 655 ITK™ amino PEG (Life Technologies, Carlsbad, CA, USA) were used as nanoparticle starting material. All chemicals were obtained from Sigma Aldrich (Taufkirchen, Germany) in analytical grade unless stated otherwise. All buffers and solutions were prepared using ultrapure water, which was obtained from a Milli-Q water purification system (Millipore, Billerica, MA, USA). Buffers used for nanoparticle labeling and purification were 10 mM 2-(N-morpholino)ethanesulfonic acid (MES) buffer pH 4.8, 50 mM borate buffer pH 8.5 and Dulbecco's phosphate buffered saline (DPBS) pH 7.4 consisting of 1.5 mM KH_2PO_4, 8 mM Na_2HPO_4, 2.7 mM KCl and 138 mM NaCl.

Mowiol mounting medium was prepared by mixing 6.9 g glycerol 87 % (AppliChem GmbH, Darmstadt, Germany) with 2.4 g Mowiol 4-88, 5.1 mL H_2O and 12.0 mL Tris buffered solution (0.2 M, pH 8.50). Mowiol mounting medium was prepared without the antifading agent 1,4-diazabicyclo[2.2.2]octane (DABCO) since it potentially quenches the Qdot fluorescence [22].

2.2 Cell culture

Human adrenal gland carcinoma cells NCI-H295R (ATCC No. CRL-2128) were cultured in RPMI1640 medium containing 10 % fetal bovine serum (Sigma Aldrich, Taufkirchen,

Germany) and supplemented with insulin-transferrin-selenium (Life Technologies, Carlsbad, CA, USA), penicillin-streptomycin (Life Technologies, Carlsbad, CA, USA) and 100 nM hydrocortisone. HeLa cells (ATCC No. CCL-2) were maintained in Eagle's Minimum Essential Medium (EMEM) containing 10 % fetal bovine serum and 1 mM sodium pyruvate. All cells were cultured in T-75 cell culture flasks (Corning, Corning, NY, USA).

2.3 Real-time PCR

To quantify the AT_1 receptor expression on NCI-H295R and HeLa cells, real-time reverse-transcriptase polymerase chain reaction (qRT-PCR) was conducted. For that reason, cells were cultured in T-25 cell culture flasks (Corning, Corning, NY, USA). After the cells had reached subconfluency, RNA was isolated using the peqGOLD total RNA kit (Peqlab, Erlangen, Germany) including an on-column DNAse digestion step (peqGOLD DNase I Digest Kit, Peqlab, Erlangen, Germany). The purity and concentration of RNA was determined with the help of a Nanodrop ND-1000 spectrophotometer (Peqlab, Erlangen, Germany). To generate single-stranded cDNA, 3 µg of the isolated RNA were reversely transcribed using the cDNA-Synthesis Kit H Minus (Peqlab, Erlangen, Germany) according to the manufacturer's instructions. For quantification of human AT_1R expression (sense: 5′-GGC CAG TGT TTT TCT TTT GAA TTT AGC AC-3′, antisense: 5′-TGA ACA ATA GCC AGG TAT CGA TCA ATG C-3′), real-time RT-PCR was performed using a LightCycler® Instrument (Roche Diagnostics, Rotkreuz, Switzerland) and a LightCycler® 480 SYBR Green I Master (Roche Diagnostics, Rotkreuz, Switzerland). Due to the different tissue origins of both carcinoma cell lines we related the AT_1R expression to the expression of three different housekeeping genes: glyceraldehyde 3-phosphate dehydrogenase GAPDH (sense: 5′-GAA GGT GAA GGT CGG AGT C-3′, antisense: 5′-GAA GAT GGT GAT GGG ATT TC-3′), β-actin (sense: 5'-AGC CTC GCC TTT GCC GA-3', antisense: 5'-CTG GTG CCT GGG GCG-3') and RNA polymerase II (sense: 5'-GCA CCA CGT CCA ATG ACA T-3', antisense: 5'-GTG CGG CTG CTT CCA TAA-3'). Especially RPII has been shown to have a constant expression in different tissues [23], which makes it an ideal reference gene when comparing expression levels between different tissues. Primers were purchased from Eurofins Genomics (Ebersberg, Germany). Real-time PCR was run for 50 cycles with 15 s denaturation at 95 °C, 20 s annealing at 60 °C, and 20 s elongation at 72 °C. The accuracy of the amplicon was

verified by performing a melting-curve analysis after amplification. Data is expressed as mean ± standard deviation (n=3).

2.4 Nanoparticle labeling

EXP3174 (16 nmol) was activated using N-(3-dimethylaminopropyl)-N'-ethylcarbodiimide hydrochloride (EDC, 10 mM) and N-hydroxysulfosuccinimide (sulfo-NHS, 5 mM) in MES-buffered solution. After activation of the carboxylic group of EXP3174 for 1 h, the pH was raised by addition of 50 mM borate buffer at pH 8.5. Qdots® 655 ITK™ amino PEG (160 pmol) were immediately added to the reaction mixture for the labeling reaction. After 16 hours of gentle shaking, EXP3174-modified Qdots were purified by size exclusion chromatography using Sephadex G-25 resin in a PD-10 column (GE Healthcare, Munich, Germany) with DPBS as eluent. Fractions containing EXP3174-coupled Qdots were pooled and further purified by ultrafiltration using a 100 kDa molecular weight cut-off Amicon Ultra-4 filter unit (Millipore, Billerica, MA, USA). Finally, Qdot concentration was determined by fluorescence measurement in a range of 0 to 10 nM using a FluoStar Omega fluorescence microplate reader (BMG Labtech, Ortenberg, Germany) with an excitation and emission wavelength of 450 nm and 650 nm, respectively.

2.5 Confocal laser scanning microscopy

Adrenal gland carcinoma NCI-H295R and HeLa cells were seeded into 8-well µ-slides (Ibidi, Martinsried, Germany) at a density of 10,000 cells per well. After 96 hours (NCI-H295R) or 24 hours (HeLa) of adhering and growing, nanoparticle binding to the cells was analyzed. In a first step, cells were washed with warm DPBS. Pre-warmed nanoparticle test solution in Leibovitz's medium supplemented with 0.5 % bovine serum albumin (BSA) was pipetted onto the cells and incubated for 1 hour at 37 °C. BSA was added to the nanoparticle solutions to block nonspecific nanoparticle binding to the cells. After the incubation period, cells were washed with DPBS, fixed with 2 % paraformaldehyde in DPBS for 10 min at room temperature and washed extensively with DPBS. Analysis of nanoparticle binding to the cells was conducted using a Zeiss Axiovert 200 microscope combined with a LSM 510 laser-scanning device using a 63x Plan-Apochromat (NA 1.4) objective (Zeiss, Jena, Germany). Qdot fluorescence was excited with an argon laser at 488 nm. Qdot emission was recorded after a 650 nm longpass filter. The focal plane was adjusted to 1.1 µm. For image acquisition and processing AIM 4.2

(Zeiss, Jena, Germany) was used. Qdot fluorescence was displayed in false color (green) for better visibility.

2.6 Intracellular calcium mobilization assay

The affinity of the EXP3174-modified Qdots for AT_1R was investigated by the fluorescent fura-2 Ca^{2+} chelator method as originally established by Grynkiewicz *et al.* [24] and as recently described [16]. Confluent HeLa and NCI-H295R cells grown in cell culture flasks were harvested with trypsin, centrifuged (5 min, 200 g, RT) and loaded in suspension with 5 µM fura-2AM (Life Technologies, Carlsbad, CA, USA) and 0.05 % Pluronic F-127 in Leibovitz's L-15 medium (Life Technologies, Carlsbad, CA, USA) for 1 h at room temperature in the dark. After loading of the cells, they were repeatedly washed by centrifugation (3 times, 5 min, 200 g, RT) and resuspended in Leibovitz's medium.

For determination of the agonist stimulation curve, a concentration series of angiotensin II (Bachem, Bubendorf, Switzerland) with each concentration having a volume of 20 µL were pipetted into 96-well plates (Greiner Bio One, Frickenhausen, Germany). Subsequently, 180 µL of the loaded cell suspension ($1*10^6$ cells/mL) were injected into the wells and the fluorescence signal was recorded for 60 s. For the antagonistic efficacy of EXP3174-Qdots, 20 µL were pipetted into 96-well plates and 90 µL of loaded cells with a concentration of $2*10^6$ cells/mL were injected into the wells. After 10 min of antagonist incubation, 90 µL of the EC_{80} of angiotensin II was subsequently injected into each well and the fluorescence signal was immediately recorded with a FluoStar Omega fluorescence microplate reader (BMG Labtech, Ortenberg, Germany) for a time of 30 s. Excitation filters for the ratiometric measurement were 340/20 nm and 380/20 nm and the emission was recorded in a 510/20 nm bandpass filter. The fluorescence signal was calibrated by incubating loaded cells with 0.1 % Triton-X 100 to measure the maximal ratio (Rmax) and 0.1 % Triton-X 100 supplemented with 45 mM ethylene glycol-bis(2-aminoethylether)-N,N,N′,N′-tetraacetic acid (EGTA) to determine the minimal ratio (Rmin). The intracellular calcium concentrations were calculated from the maximal fluorescence ratios based on the equation of Grynkiewicz *et al.* assuming a K_d value of 225 nM for the fura-2-calcium complex [24]. The IC_{50} values (the half maximal inhibitory concentration) and EC_{50} values (the half maximal effective concentration) were calculated using SigmaPlot 12.2 (Systat Software, San Jose, CA, USA) with the help of the sigmoidal dose-response (variable slope) equation.

2.7 Animal experiments

All animal experiments were carried out in accordance with the national and institutional guidelines and were approved by the local authority (Regierung der Oberpfalz, reference number: 54-2532,1-23/11) and the Animal Care and Use Committee (Tierschutz-ausschuss) of the University of Regensburg.

NMRI (nu/nu) mice with an age of at least 12 weeks and weighing around 30 grams were used as model animals. Mice were bred in-house at the University of Regensburg under specified pathogen free (SPF) conditions with food and water *ad libitum*.

2.8 Biodistribution of targeted and non-targeted Qdots

For assessing the overall biodistribution of non-modified and EXP3174-coupled Qdots, 100 µL of a 2 µM Qdot solution (total dose: 200 pmol) of either targeted or non-targeted Qdots were intravenously injected into the jugular vein of mice that were anesthetized by isoflurane inhalation. After one hour of nanoparticle circulation, blood samples of 100 µL were obtained from the vena facialis using heparinized microcapillaries. After the blood was centrifuged the plasma was collected. Subsequently, mice were sacrificed and organs harvested. Eyes were immediately enucleated and fixed in 4 % paraformaldehyde for 1 h. All other organs were fixed overnight. After several washing steps in DPBS, organs were weighed and a representative portion of every organ with a weight of approximately 100 mg was dissolved by microwave-assisted nitric acid digestion using a MARSXpress system (CEM, Matthews, NC, USA). For eyes, only the posterior eye segment with retina, choroid and sclera was used for Qdot quantification. The anterior eye with cornea, lens and vitreous was discarded. Due to their CdSe core, the measured cadmium concentration is linearly related to the nanoparticle amount. With the help of a quadrupole-based inductively coupled plasma mass spectrometer ICP-MS 7700cx system (Agilent Technologies, Boeblingen, Germany) the cadmium-111 concentration in the dissolved tissues was quantified. If the measured cadmium concentration was below the limit of quantification, which was 5 ng g^{-1} tissue (5 ppb), it was set to 0. The total plasma volume was estimated to be 59.4 mL/kg body weight [25]. To assess statistical significance Student's t-test was carried out using SigmaPlot 12.2.

2.9 Localization of Qdots in the retinal vasculature

Prior to nanoparticle administration, mice were anesthetized by intraperitoneal injection of a mixture of ketamine (150 mg/kg) and xylazine (10 mg/kg). After pre-warming the tail

in warm water (approximately 50°C), 200 pmol of either ligand-modified or unmodified nanoparticles were injected into the lateral tail vein. After one hour of nanoparticle circulation in the animals, mice were killed by cervical dislocation and the eyes were enucleated. Eyes were immediately transferred to 4 % paraformaldehyde solution in DPBS and fixed for 4 hours. After a brief washing in DPBS, eyes were cryoprotected using a sucrose gradient in 0.1 M phosphate buffer pH 7.4 at 4 °C, embedded in Tissue Tek® O.C.T.™ Compound (Sakura Finetek, Torrance, CA, USA) and frozen in the gas phase of liquid nitrogen. Specimens were cut into 12 µm thick sections using an HM 500 OM microtome (Microm International, Walldorf, Germany) and transferred onto Superfrost™ plus glass slides (Thermo Scientific, Waltham, MA, USA). Finally, sagittal sections were washed with DPBS and mounted with Mowiol mounting medium. The slides were analyzed using a Zeiss Axiovert 200 microscope combined with an LSM 510 laser-scanning device using a 40x Plan-Neofluar (NA 1.3) objective (Zeiss, Jena, Germany). For localization of Qdot fluorescence in tissue sections, an excitation wavelength of 488 nm was chosen and the emitted light was detected using a Zeiss meta detector (Zeiss, Oberkochen, Germany). The meta detector was set to record the emitted light from 500 to 700 nm in 30 nm intervals (515, 547, 580, 612, 644 and 676 nm). The acquired wavelength stacks were displayed as color-coded pictures. The software used for image acquisition and processing was AIM 4.2 (Zeiss, Oberkochen, Germany).

For retinal flat mounts, eyes were enucleated and fixed in 4 % paraformaldehyde for 1 h. After a thorough washing in DPBS, the cornea and anterior eye segment were removed, retinas were dissected from the eye cups and four radial cuts were made to allow flat-mounting. Specimens were immediately mounted with Mowiol mounting medium. For microscopical analysis, slides were illuminated with a mercury-vapor lamp (Zeiss, Oberkochen, Germany) and Qdot fluorescence was detected using a Qdot 655 filter set (Chroma Technology, Olching, Germany) consisting of an excitation filter with an excitation wavelength maximum of 460 nm and a bandwidth of 50 nm (full width at half maximum, FWHM), a beam splitter at 475 nm and a bandpass emission filter with a center wavelength at 655 nm and a bandwidth of 40 nm (FWHM). The software used for image acquisition and processing of the flat-mounted retinas was AxioVision 4.6 with the MosaiX module (Zeiss, Oberkochen, Germany). For improved visibility, the lookup table "Red Hot" was applied to the microscopic pictures using ImageJ (NIH, Bethesda, MD, USA, http://imagej.nih.gov/ij). The Z-stack was recorded using a confocal Zeiss Axiovert 200 microscope combined with an LSM 510 laser-scanning device using a 40x Plan-

Neofluar (NA 1.3) objective (Zeiss, Jena, Germany). Flat-mounted retinas were excited with an argon laser at 488 nm and scanned using a 650 nm longpass filter with z-stack step size of 6.0 µm.

2.10 Immunohistochemistry

For immunohistochemical staining of CD31, freshly cut cryosections were circled with an ImmEdge Pen (Vector, Burlingame, CA, USA) and blocked for 30 min at room temperature with 10 % horse serum and 1 % BSA in DPBS. After blocking, sections were incubated with polyclonal goat anti-CD31/PECAM-1 IgG 1:40 (#AF3628, R&D systems, Wiesbaden, Germany) formulated in 10 % horse serum and 1 % BSA in DPBS in a moist chamber at 4 °C overnight. As a secondary antibody, donkey anti-goat IgG (1:500) conjugated to Alexa Fluor® 546 (#A11056, Life Technologies, Carlsbad, CA, USA) was used in 1 % BSA in DPBS.

For F-actin staining, eye sections were incubated with phalloidin conjugated to Alexa Fluor® 546 (#A22283, Life Technologies, Carlsbad, CA, USA) in 1 % BSA in DPBS for 60 min. Labeled sections were mounted with Mowiol mounting medium and analyzed using the aforementioned Zeiss meta detector, which was set to record the emitted light from 560 to 700 nm in 30 nm increments (558, 590, 622, 654 and 687 nm). The tissue sections were excited using a 488 nm argon laser. For visual representation the 590 nm channel representing Alexa Fluor® 546 and the 654 nm channel depicting the Qdots were used.

3 Results and discussion

EXP3174-modified nanoparticles were obtained by covalently conjugating the carboxylic acid functional group of EXP3174 to amino-PEG terminated Qdots with the help of EDC/NHS chemistry. Use of a 100-fold molar excess of EXP3174 with respect to the Qdots resulted in approximately 11 ligands per nanoparticle. Following a thorough purification process, no unreacted ligand was present [16]. The inorganic core of the semiconductor nanoparticles had a length of 17.8 ± 2.1 nm and a width of 7.7 ± 1.1 nm [16]. Especially in the context of evaluating multivalent nanoparticle-cell interactions, the use of nanomaterials with narrow dispersity is crucial [26].

3.1 Nanoparticle binding *in vitro*

Two cell lines, used to demonstrate *in vitro* nanoparticle binding behavior, were assayed for AT_1R expression and functionality using quantitative reverse-transcriptase PCR (qRT-

PCR) and intracellular calcium measurements, respectively. At the mRNA level, AT_1R expression was more than 100-fold higher in NCI-H295R cells than in HeLa cells for all tested reference genes (Fig. 1A).

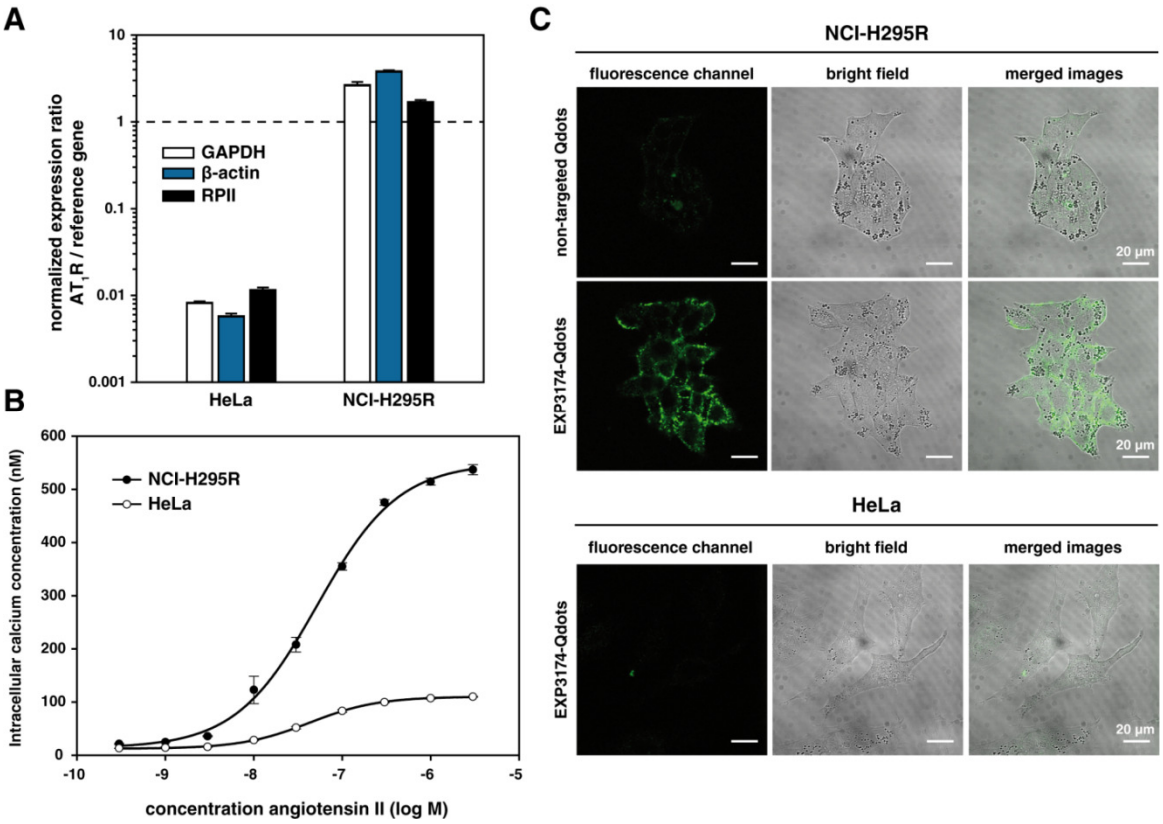

Figure 1: Receptor characterization and nanoparticle binding for NCI-H295R and HeLa cell lines. **(A)** When AT_1R expression was determined by qRT-PCR, NCI-H295R cells showed an over 100-fold greater expression compared to HeLa cells. **(B)** Similarly, using intracellular calcium measurements with fura-2AM, NCI-H295R cells exhibited a vastly increased intracellular calcium mobilization upon angiotensin II agonist binding **(C)** When NCI-H295R cells were incubated with non-targeted and EXP3174-Qdots, only EXP3174-coupled Qdots significantly interacted with AT_1R-high NCI-H295R cells. When EXP3174-Qdots were incubated with HeLa cells, the nanoparticles showed only minor cellular binding. For NCI-295R cells, the fluorescence of EXP3174-Qdots was clearly associated with the cell membrane.

Although small varieties in gene expression oftentimes do not equally transfer to the protein level, this distinct difference in gene expression clearly provided strong evidence for markedly different AT_1R expression levels in the two cell lines. The lack of specific antibodies against AT_1R [27,28], rendered the verification of the AT_1R expression at the protein level impossible. Fortunately, due to their Gq-coupling, AT_1 receptors respond with an increase in cytosolic calcium following agonist binding. Echoing our AT_1R mRNA expression results the cytosolic calcium concentration of NCI-H295R cells upon AT_1R activation with angiotensin II reached calcium concentrations of over 500 nM.

For HeLa cells, on the other hand, the intracellular calcium levels upon agonist stimulation did not exceed calcium concentrations of approximately 100 nM (Fig. 1B). Thus, for nanoparticle binding experiments, NCI-H295R and HeLa cells were used as cell lines with high and low receptor expression, respectively. Although nanoparticle binding to both cell lines was previously investigated, HeLa cells were originally not identified as a cell line with low receptor expression due to the absence of qRT-PCR data and were initially designated receptor negative cells [16].

Binding of non-targeted and EXP3174-targeted Qdots was demonstrated with confocal microscopy and intracellular calcium measurements. We found EXP3174-Qdots to exhibit a high degree of association with AT_1R-high NCI-H295R cells (Fig. 1C). The colloids were primarily located at the cell membrane and showed no significant uptake after one hour, which is typical for nanoparticles bound to a receptor antagonist, as originally observed for the neuropeptide Y receptor Y_1 [29] and the melanocortin type-1 receptor [30]. Since angiotensin receptor blockers bind the receptor but do not initiate receptor internalization [31], antagonist-coupled nanoparticles are not immediately taken up into the cells but instead rest at the surface of the cell membrane. In contrast, PEGylated but non-targeted Qdots showed only weak and non-specific interaction with NCI-H295R cells. When AT_1R-low HeLa cells were incubated with EXP3174-coupled nanoparticles, only minor Qdot fluorescence was observable, lending further support to the multivalent receptor-mediated nature of the nanoparticle binding. For the colloids to establish an affine binding to the cell a certain AT_1 receptor density is undoubtedly needed. That AT_1 receptors on NCI-H295R cells can be targeted in a multivalent fashion was recently demonstrated with agonist-modified nanoparticles [32].

Next, the influence of EXP3174-modified nanoparticles on GPCR activation was investigated using calcium-sensitive ratiometric imaging techniques [24]. In this binding assay, EXP3174-Qdots blocked the angiotensin II-induced calcium influx into the cytosol with an IC_{50} of 3.8 ± 0.9 nM (Fig. 2). Non-targeted Qdots exhibited no influence on the calcium signal, proving that the fluorescence ratio decrease of the calcium chelator fura-2 was indeed due to successful receptor blockade by EXP3174 immobilized on the nanoparticle surface and not due to a quenching of the fluorescent signal by the highly absorbing Qdot core. The affinity of the EXP3174-conjugated nanoparticles for the cells was slightly lower than that of free EXP3174, which had an IC_{50} of 2.0 ± 0.5 nM (Supporting information Fig. S1). This minor decrease in receptor affinity is a result of the ligand's attachment to the hydrophilic PEG corona that protects the colloid from serum

protein adsorption. When attached to the PEG chains, the ligands lose a significant degree of receptor affinity. Due to the low affinity of this monovalent interaction, which is above 500 nM [16], the colloids have to necessarily build up multivalent nanoparticle-cell interactions in order to establish a strong interaction with the target cell. This is in turn is only possible if the receptor density on the target cell surface is sufficiently high. The capacity of multivalent nanomaterials to increase receptor binding affinity has already been demonstrated for other GPCRs such as the adenosine [33] and neuropeptide receptors [29]. Besides increasing cellular affinity, nanoparticle multivalency has also been successfully utilized for cell-specific targeting [34], control of colloidal cytotoxicity [35] and alteration of cell responses by crosslinking membrane receptors [36].

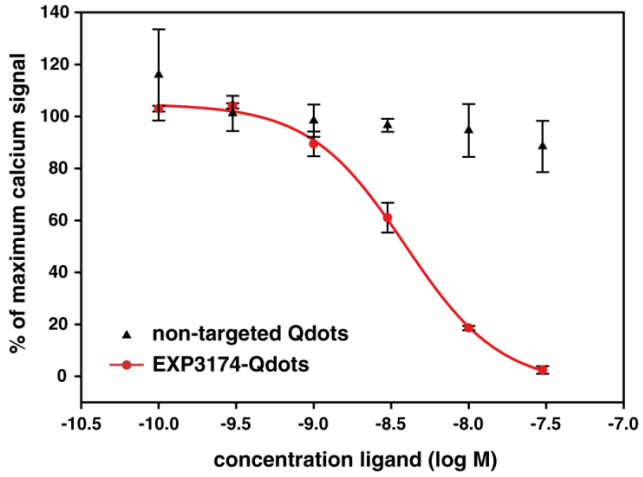

Figure 2: Influence of EXP3174-Qdots on the angiotensin II-induced calcium mobilization on NCI-H295R cells. EXP3174-modified Qdots blocked receptor signaling with an IC_{50} of 3.8 ± 0.9 nM. In contrast, non-targeted Qdots showed no influence on the angiotensin II receptor binding or the fura-2 fluorescence.

3.2 Biodistribution and accumulation in off-target tissue

Since EXP3174-Qdots strongly associated with cells of high receptor expression and exhibited only minor binding to cells of low AT_1R expression *in vitro*, we asked whether the nanoparticles would be able to sufficiently circulate in the blood and if the Qdots would accumulate in AT_1R expressing off-target tissue. For that reason, mature adult mice were intravenously injected with a dose of 200 pmol of either targeted or non-targeted Qdots. The extremely low affinity of the monovalent PEGylated EXP3174 ligand (IC_{50} of 630 nM) [16] is insufficient to appreciably bind AT_1 receptors at the applied equivalent nanoparticle concentration in the blood (~66 nM), which is why PEGylated, non-targeted Qdots were used as a control nanomaterial. After injection the nanoparticles were allowed to circulate for 1 h. This duration was chosen as it allows the nanoparticles in sufficient

time to bind the endothelium and accumulate in the tissue [37–39]. In addition, due to the relatively short blood circulation time of these Qdots [40], a major fraction of unbound and weakly bound nanoparticles will be rapidly cleared from the blood and sequestered within organs with a prominent mononuclear phagocyte system, such as liver and spleen [41]. After the mice were sacrificed, representative portions of major organs were dissolved by microwave-assisted nitric acid digestion and then analyzed for cadmium-111 content by inductively coupled plasma mass spectrometry (ICP-MS). Because the Qdots consist of a CdSe/ZnS core/shell structure, the cadmium concentration is linearly related to the amount of deposited nanoparticles in the tissue. Measuring Cd-111 by ICP-MS is the standard technique for quantitative assessment of the biodistribution pattern of Cd-containing Qdots [42,43], and is more accurate and sensitive than fluorescence imaging techniques [44].

In our experiments, kidneys, lung and heart exhibited comparable nanoparticle uptake for non-targeted and EXP3174-Qdots (Fig. 3A), whereas liver and spleen, the two most prominent organs of the mononuclear phagocyte system, accumulated significantly less EXP3174-Qdots than non-targeted Qdots. This is remarkable, as attachment of targeting ligands usually leads to decreased blood circulation time and an elevated hepatosplenic uptake by liver and spleen-associated macrophages [45,46]. Epifluorescence pictures of spleen and liver confirmed the ICP-MS findings (Supporting information Fig. S2). Although EXP3174 possesses a charged tetrazole ring that could theoretically attract blood plasma proteins, the integrity of the nanoparticle's PEG corona is obviously not compromised. Moreover, organs with high AT_1R expression such as kidney and heart [15] showed no significant accumulation of EXP3174-modified Qdots, which is mostly due to the inaccessibility of the receptors to circulating nanoparticles. Especially in the heart, AT_1R is mainly associated with the conduction system [47] and is not within reach of circulating nanoparticles.

Although elevated for EXP3174-Qdots, the plasma cadmium concentration was not significantly different than that of non-targeted Qdots after 1 hour of circulation. Since the kidneys are an important off-target organ due to their large amount of AT_1 receptors that are easily accessible from the blood stream we investigated the detailed distribution pattern of EXP3174-targeted Qdots. CD31 immunohistochemistry, which stains endothelial cells, was performed on cryosections of kidneys that passively accumulated EXP3174-targeted Qdots during their circulation. The stained peritubular capillaries and glomerular endothelium showed only minute nanoparticle association (Fig. 3B).

However, a significant amount of Qdots accumulated in the glomerular mesangium. This is not surprising, since the kidney mesangium has been shown to be a passive accumulation site for several nanoparticle species [48–50], as well as non-targeted CdSe Qdots of the same size [51]. Similar to observations by Praetner e*t al.* on non-targeted Qdots [52], the nanoparticles were mainly eliminated via hepatobiliary excretion whereas renal elimination was only minute.

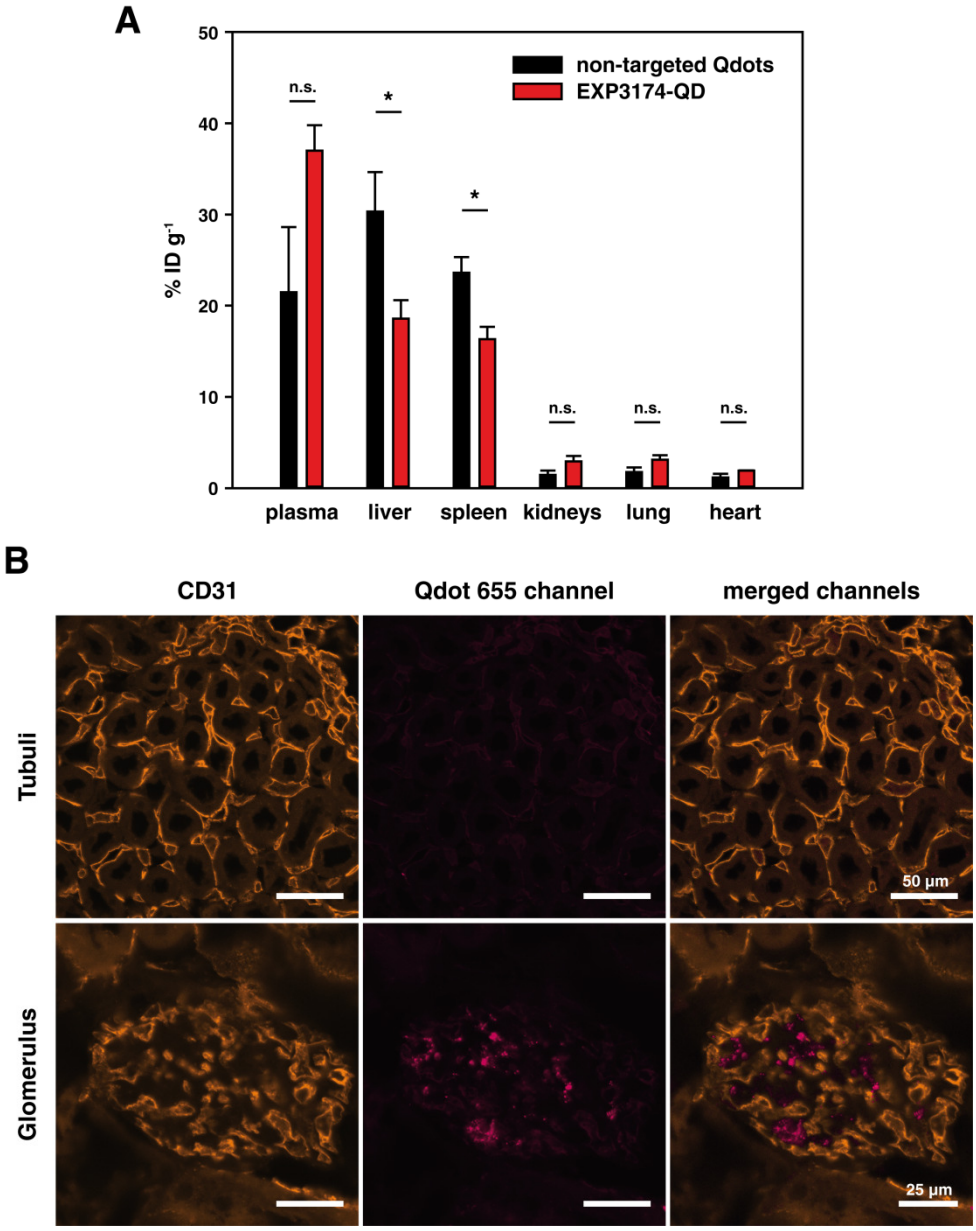

Figure 3: Nanoparticle distribution in off-target tissue. **(A)** Biodistribution of non-targeted and EXP3174-modified nanoparticles after systemic administration and one hour of circulation. Qdot concentration in tissues was analyzed by determining the cadmium concentration with ICP-MS. Data is expressed as mean ± SEM (n=3). Levels of statistical significance are indicated as: (*) $p < 0.05$; (n.s.) $p > 0.05$. **(B)** Distribution pattern of EXP3174-coupled Qdots in the kidney. Qdots are mainly associated with the glomerular mesangium but not with the glomerular or peritubular capillaries.

3.3 EXP3174-Qdots accumulate in the choriocapillaris

After we had experimentally confirmed that EXP3174-Qdot had a sufficient blood circulation time we investigated whether the nanoparticles could actively accumulate in the AT_1R-expressing microvasculature of the posterior eye segment. To this end, mature adult mice were again intravenously injected with a dose of 200 pmol of either targeted or non-targeted Qdots, which were allowed to circulate for 1 h. After the mice had been sacrificed, the eyes were enucleated, sagittal cryosections were obtained and Qdot fluorescence was investigated. To clearly distinguish between nanoparticle fluorescence and bright tissue autofluorescence and to identify the nanoparticles in the highly complex tissue of the posterior eye segment, we used multi-spectral imaging with the help of a Zeiss META detector. Due to the Qdots' large Stokes shift und their narrow emission spectrum this technique allowed to precisely locate the nanoparticles in the complex ocular tissue.

In the posterior eye of mice who received non-targeted Qdots, no specific Qdot 655 fluorescence could be observed. This is in accordance with earlier studies which investigated the distribution of non-functionalized Qdots in the posterior eye [37]. Conversely, in eye sections of mice that received a bolus of EXP3174-Qdots, a substantial accumulation of magenta Qdot 655 fluorescence was clearly visible (Fig. 4A). The EXP3174-conjugated nanoparticles were detected principally in the choroid and its immediate vicinity (Fig. 4A) as well as in the intraretinal blood vessels (Supporting information Fig. S3). Although the bright yellow-green tissue autofluorescence gave good structural hints as to the location of the nanoparticles, F-actin and CD31 counterstaining using fluorescently-labeled phalloidin and a labeled anti-CD31 antibody, respectively, was conducted to pinpoint the nanoparticles' location within the posterior eye (Fig. 4B). EXP3174-Qdots were exclusively associated with the endothelium and were not observed within the RPE or sclera. The choriocapillaris is highly fenestrated towards the RPE [53] with pores of approximately 80 nm [54]. These fenestrae could potentially allow nanoparticle extravasation, similar to the hyperpermeable vasculature of solid tumors [55]. Furthermore, the RPE itself expresses several components of the renin-angiotensin-system [56] including AT_1R [57], to which EXP3174-targeted nanoparticles could bind. However, EXP3174-Qdots showed no observable extravasation. This can be attributed to a fenestral diaphragm that spans the fenestrations and reduces the endothelial cell fenestration size to approximately 20-30 nm [58]. Given that the Qdots' hydrodynamic diameter is approximately 36 nm [52], they were likely unable to transit

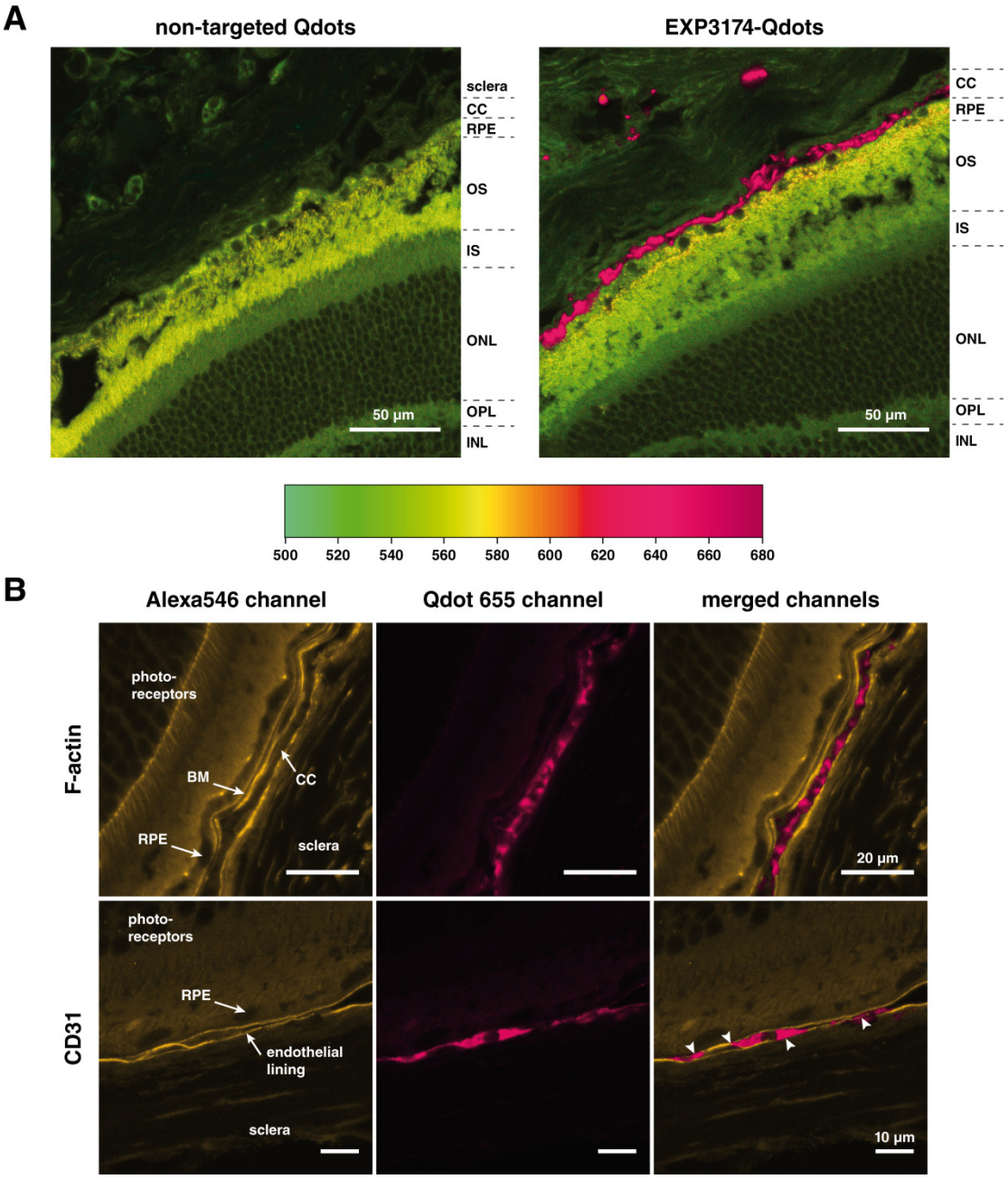

Figure 4: Sagittal eye sections of mice that received 200 pmol either ligand- or non-targeted Qdots. **(A)** Upon systemic administration, EXP3174-modified Qdots accumulated in the choriocapillaris and intraretinal capillaries in the posterior eye. Fluorescence of non-targeted Qdots could not be found in sagittal eye sections. CC-choriocapillaris, RPE-retinal pigment epithelium, OS-outer segment, IS-inner segments, ONL-outer nuclear layer, OPL-outer plexiform layer, INL-inner nuclear layer. **(B)** With the help of F-actin and CD31 counterstaining using fluorescently labeled phalloidin and a labeled anti-CD31 antibody, the precise localization of EXP3174-Qdots in the eye sections could be determined. Qdot fluorescence was limited to the capillaries and showed no distribution within the sclera or RPE. Arrowheads indicate the colocalization of CD31 and nanoparticles. BM-Bruch's membrane.

the endothelial fenestrations. Immunohistochemical staining of CD31 further confirmed association of the nanoparticles with endothelial cells, showing distinct colocalization of EXP3174-Qdot fluorescence with the CD31 endothelial cell marker (Fig. 4B arrowheads).

Similar to AT_1R, CD31 is expressed on the surface of endothelial cells [59]. Since EXP3174-Qdots are not immediately internalized upon receptor binding but rest at the endothelial cell surface, the nanoparticles were not found inside the cell 1 h after intravenous injection as observed by the F-actin staining.

3.4 EXP3174-coupled nanoparticles bind retinal vessels

For a more complete picture of nanoparticle accumulation in the retinal blood vessels, retinas of mice that received either non-targeted or EXP3174-Qdots were flat-mounted and analyzed as a whole. Epifluorescence images of flat-mounted retinas from mice that received an intravenous infusion of non-targeted Qdots showed only a small degree of nanoparticle fluorescence throughout the retinal blood vessels, indicating that most of the Qdots had already exited from circulation. In contrast, retinas of mice that received EXP3174-Qdot displayed a high degree of nanoparticle accumulation in small and larger blood vessels (Fig. 5A). Upon magnification, EXP3174-nanoparticle binding to the retinal microvasculature was clearly evident, whereas non-targeted Qdots only sparsely adhered to the vessel walls. Confocal z-stack imaging analysis of EXP3174-Qdot-filled retinas showed nanoparticle fluorescence in all three layers of the retinal network: the superficial vascular plexus, the intermediate vascular plexus and the deep vascular plexus (Fig. 5B). Considering that in proliferative diabetic retinopathy these intraretinal capillaries begin to proliferate rapidly and sprout into the vitreous [60], this finding is quite promising. For a quantitative comparison of nanoparticle accumulation in the posterior eye, the cadmium concentration in retina and in the RPE/choroid/sclera complex was analyzed using ICP-MS. In mice that received no Qdots at all, the Cd concentration was below the limit of quantitation of 5 ng g^{-1} tissue. Mice that intravenously received non-targeted Qdots had 0.22 μg Cd g^{-1} whereas mice injected with EXP3174-Qdots accumulated a significantly higher dose of 0.40 μg Cd g^{-1} (Fig. 5C).

Although the targeting and receptor binding we present could itself act as a therapeutic, encapsulation of a "second" drug to further potentiate the colloid's therapeutic efficacy is possible. However, for this to occur, the base material for the nanoparticle would have to be altered to allow encapsulation and controlled release; therapeutic nanomaterials such as liposomes, polymeric micelles or poly(lactide-co-glycolide) (PLGA) nanoparticles are all possibilities. These colloids allow for attachment of a targeting moiety and simultaneous incorporation of an active therapeutic, which could be another small

molecule drug, an siRNA (e.g. targeting VEGF, hypoxia-inducible factor 1α [61] or erythropoietin [62]) or a plasmid (e.g. encoding for an anti-VEGF intraceptor [63]).

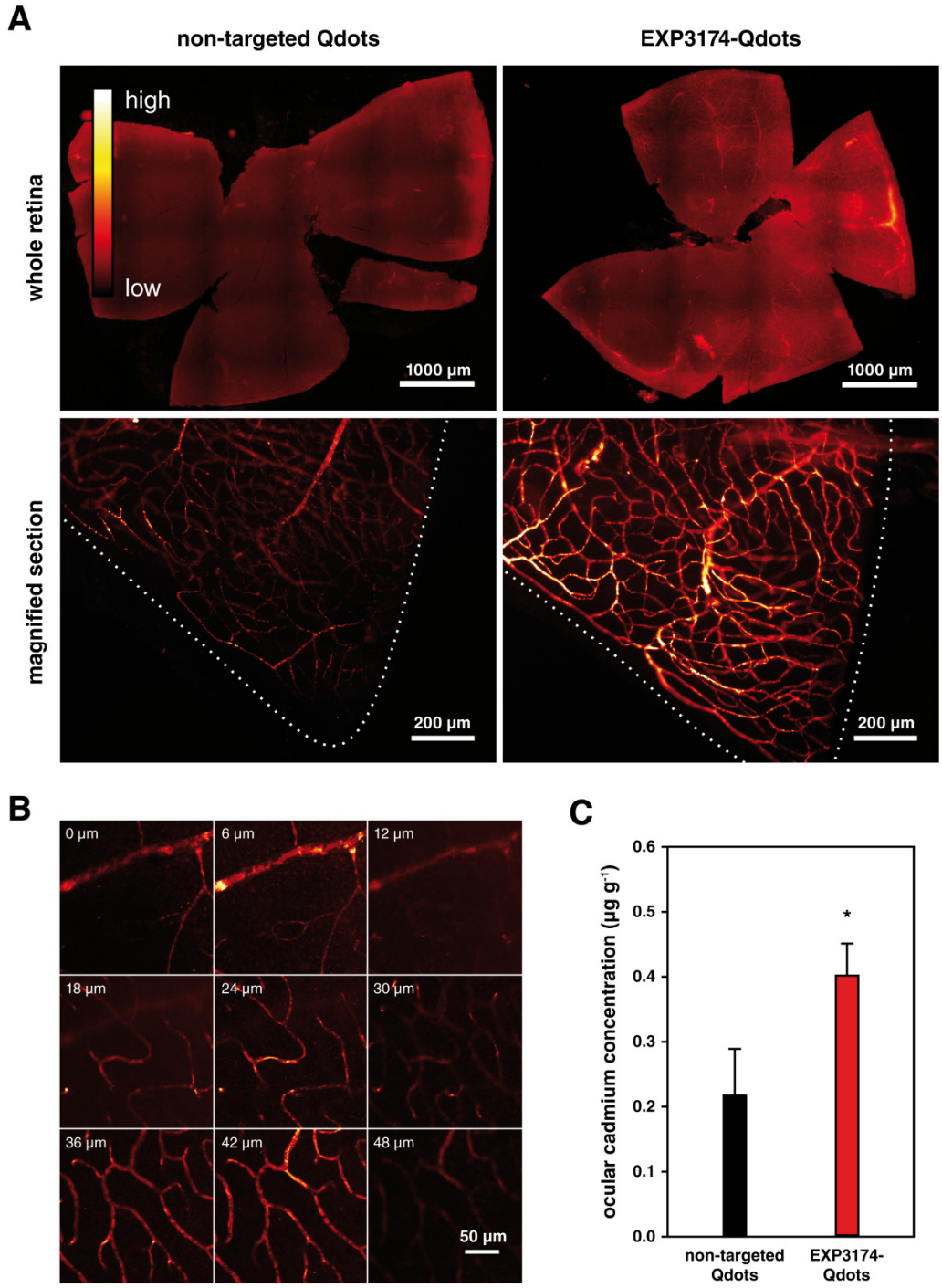

Figure 5: Microscopic analysis of flat-mounted retinas. **(A)** Epifluorescence images of whole retina show a marked increase in nanoparticle accumulation for EXP3174-modified Qdots. At higher magnification, the capillary-associated nanoparticle fluorescence is clearly visible. scale bar: 1000 µm (top), 200 µm (bottom) **(B)** In a confocal z-stack picture, EXP3174-Qdot fluorescence can be clearly seen through all three retinal vascular layers. **(C)** When the nanoparticles are quantified by ICP-MS, a significantly higher concentration of cadmium can be found in mice that received EXP3174- Qdots. Data is expressed as mean ± SEM (n=6). Levels of statistical significance are indicated as: (*) $p < 0.05$

However, due to the different sizes of these colloids compared to the Qdots and the resulting impact on circulation and cellular interactions, a careful evaluation must be made.

Due to multivalent binding of the EXP3174-modified nanoparticles, the colloids exclusively bind cells and tissues with a sufficiently high level of receptor expression at the cell surface. Differential AT_1R expression between the retina (higher) and other organs (lower) is one possible reason targeted nanoparticles bind to the retinal vasculature but not to the endothelium of other organs such as the kidney. Notably, the ICP-MS values represent nanoparticle accumulation in the healthy posterior eye. During the course of choroidal neovascularization, the hallmark of exudative age-related macular degeneration, AT_1R expression is dramatically increased [7], which would further augment the multivalent nanoparticle binding. Likewise, in streptozotocin-induced diabetic retinopathy AT_1R expression is also markedly increased [8]. Although preferential binding of the targeted Qdots to the retinal or choroidal vasculature was not observed, AT_1R up-regulation in the proliferating vessels of one or the other will naturally lead to increased binding of such multivalent nanoparticles to the diseased sites.

In addition, when neovascularizations form in the posterior eye, blood vessels become leaky. This leads to enhanced permeation and retention (EPR) of macromolecular and colloidal structures [17], which is typically known from the angiogenesis of solid tumors. Around these leaky areas the microvascular blood velocity is decreased, which could further enhance the retention of the colloids and thus increase the capability to form a strong multivalent binding. Since AT_1R blockade has beneficial effects on retinal cells [64,65], extravasation of ARB-targeted nanoparticles could further extend their therapeutic potential.

4 Conclusion

We have demonstrated that ARB-conjugated nanoparticles bind cells with high AT_1R expression *in vitro* and retinal and choroidal blood vessels *in vivo*. Using confocal microscopy and intracellular calcium measurements we confirmed the multivalent binding of EXP3174-Qdots to their cognate receptor. Due to their multivalency EXP3174-Qdots specifically accumulated in the intraretinal and choroidal blood vessels of the posterior eye in mice as shown with multi-spectral imaging and ICP-MS measurements. Moreover, the colloids only sparsely accumulate in off-target tissues such as the kidney, as

a prominent and well-perfused organ known to express AT_1R. The multivalent targeting approach presented here opens the door for highly attractive nanoparticle targeting strategies in which nanoparticles are able to multivalently bind a tissue, exhibit a pharmacological effect and deliver a therapeutic payload.

References

[1] M. de Gasparo, K.J. Catt, T. Inagami, J.W. Wright, T. Unger, International union of pharmacology. XXIII. The angiotensin II receptors, Pharmacol. Rev. 52 (2000) 415–472.

[2] P. Dandona, S. Dhindsa, H. Ghanim, A. Chaudhuri, Angiotensin II and inflammation: the effect of angiotensin-converting enzyme inhibition and angiotensin II receptor blockade, J. Hum. Hypertens. 21 (2007) 20–27.

[3] Y. Suzuki, M. Ruiz-Ortega, O. Lorenzo, M. Ruperez, V. Esteban, J. Egido, Inflammation and angiotensin II, Int. J. Biochem. Cell Biol. 35 (2003) 881–900.

[4] A.Y. Khakoo, R.L. Sidman, R. Pasqualini, W. Arap, Does the renin-angiotensin system participate in regulation of human vasculogenesis and angiogenesis?, Cancer Res. 68 (2008) 9112–9115.

[5] C. Bunce, W. Xing, R. Wormald, Causes of blind and partial sight certifications in England and Wales: April 2007-March 2008, Eye (Lond) 24 (2010) 1692–1699.

[6] R.D. Jager, W.F. Mieler, J.W. Miller, Age-related macular degeneration, N. Engl. J. Med. 358 (2008) 2606–2617.

[7] N. Nagai, Y. Oike, K. Izumi-Nagai, T. Urano, Y. Kubota, K. Noda, Y. Ozawa, M. Inoue, K. Tsubota, T. Suda, S. Ishida, Angiotensin II type 1 receptor-mediated inflammation is required for choroidal neovascularization, Arterioscler. Thromb. Vasc. Biol. 26 (2006) 2252–2259.

[8] J.H. Kim, J.H. Kim, Y.S. Yu, C.S. Cho, K.-W. Kim, Blockade of angiotensin II attenuates VEGF-mediated blood-retinal barrier breakdown in diabetic retinopathy, J. Cereb. Blood Flow Metab. 29 (2009) 621–628.

[9] H. Funatsu, H. Yamashita, T. Ikeda, Y. Nakanishi, S. Kitano, S. Hori, Angiotensin II and vascular endothelial growth factor in the vitreous fluid of patients with diabetic macular edema and other retinal disorders, Am. J. Ophthalmol. 133 (2002) 537–543.

[10] N. Chaturvedi, M. Porta, R. Klein, T. Orchard, J. Fuller, H.H. Parving, R. Bilous, A.K. Sjølie, Effect of candesartan on prevention (DIRECT-Prevent 1) and progression (DIRECT-Protect 1) of retinopathy in type 1 diabetes: randomised, placebo-controlled trials, Lancet 372 (2008) 1394–1402.

[11] A.K. Sjølie, R. Klein, M. Porta, T. Orchard, J. Fuller, H.H. Parving, R. Bilous, N. Chaturvedi, Effect of candesartan on progression and regression of retinopathy in type 2 diabetes (DIRECT-Protect 2): a randomised placebo-controlled trial, Lancet 372 (2008) 1385–1393.

[12] M. Mauer, B. Zinman, R. Gardiner, S. Suissa, A. Sinaiko, T. Strand, K. Drummond, S. Donnelly, P. Goodyer, M.C. Gubler, R. Klein, Renal and retinal

effects of enalapril and losartan in type 1 diabetes, N. Engl. J. Med. 361 (2009) 40–51.

[13] Z.H. Israili, Clinical pharmacokinetics of angiotensin II (AT1) receptor blockers in hypertension, J. Hum. Hypertens. 14 Suppl 1 (2000) S73-86.

[14] J. Li, X. Zhu, C. Yang, R. Shi, Characterization of the binding of angiotensin II receptor blockers to human serum albumin using docking and molecular dynamics simulation, J. Mol. Model. 16 (2010) 789–798.

[15] D.T. Dinh, A.G. Frauman, C.I. Johnston, M.E. Fabiani, Angiotensin receptors: distribution, signalling and function, Clin. Sci. 100 (2001) 481–492.

[16] R. Hennig, K. Pollinger, A. Veser, M. Breunig, A. Goepferich, Nanoparticle multivalency counterbalances the ligand affinity loss upon PEGylation, J. Control. Release 194C (2014) 20–27.

[17] R. Hennig, A. Goepferich, Nanoparticles for the treatment of ocular neovascularizations, Eur. J. Pharm. Biopharm. 95 (2015) 294–306.

[18] E. Vaculikova, V. Grunwaldova, V. Kral, J. Dohnal, J. Jampilek, Preparation of candesartan and atorvastatin nanoparticles by solvent evaporation, Molecules 17 (2012) 13221–13234.

[19] A. Geçer, N. Yıldız, A. Çalımlı, B. Turan, Trimethyl chitosan nanoparticles enhances dissolution of the poorly water soluble drug Candesartan-Cilexetil, Macromol. Res. 18 (2010) 986–991.

[20] H. Patel, V. Oza, A. Koli, K. Ranch, D. Shah, Formulation Development and Evaluation of Lipid Based Nanoparticles of Valsartan by Microemulsification, Drug Deliv. Lett. 3 (2013) 200–209.

[21] W.A. Hild, M. Breunig, A. Goepferich, Quantum dots - nano-sized probes for the exploration of cellular and intracellular targeting, Eur. J. Pharm. Biopharm. 68 (2008) 153–168.

[22] R.E. Galian, J.C. Scaiano, Fluorescence quenching of CdSe quantum dots by tertiary amines and their surface binding effect, Photochem. Photobiol. Sci. 8 (2009) 70–74.

[23] A. Radonić, S. Thulke, I.M. Mackay, O. Landt, W. Siegert, A. Nitsche, Guideline to reference gene selection for quantitative real-time PCR, Biochem. Biophys. Res. Commun. 313 (2004) 856–862.

[24] G. Grynkiewicz, M. Poenie, R.Y. Tsien, A new generation of Ca2+ indicators with greatly improved fluorescence properties, J. Biol. Chem. 260 (1985) 3440–3450.

[25] A.C. Riches, J.G. Sharp, D.B. Thomas, S.V. Smith, Blood volume determination in the mouse, J. Physiol. 228 (1973) 279–284.

[26] M.A. van Dongen, J.E. Silpe, C.A. Dougherty, A.K. Kanduluru, S.K. Choi, B.G. Orr, P.S. Low, M.M. Banaszak Holl, Avidity mechanism of dendrimer-folic acid conjugates, Mol. Pharm. 11 (2014) 1696–1706.

[27] M. Herrera, M.A. Sparks, A.R. Alfonso-Pecchio, L.M. Harrison-Bernard, T.M. Coffman, Lack of Specificity of Commercial Antibodies Leads to Misidentification of Angiotensin Type 1 Receptor Protein, Hypertension 61 (2012) 253–258.

[28] K.J. Elliott, K. Kimura, S. Eguchi, Lack of specificity of commercial antibodies leads to misidentification of angiotensin type-1 receptor protein, Hypertension 61 (2013) e31.

[29] W. Hild, K. Pollinger, A. Caporale, C. Cabrele, M. Keller, N. Pluym, A. Buschauer, R. Rachel, J. Tessmar, M. Breunig, A. Goepferich, G protein-coupled receptors function as logic gates for nanoparticle binding and cell uptake, Proc. Natl. Acad. Sci. U.S.A. 107 (2010) 10667–10672.

[30] W. Lu, C. Xiong, R. Zhang, L. Shi, M. Huang, G. Zhang, S. Song, Q. Huang, G.-Y. Liu, C. Li, Receptor-mediated transcytosis: a mechanism for active extravascular transport of nanoparticles in solid tumors, J. Control. Release 161 (2012) 959–966.

[31] F.L. Fierensa, P.M. Vanderheyden, C. Roggeman, J.-P. de Backer, T.J. Thekkumkara, G. Vauquelin, Tight binding of the angiotensin AT1 receptor antagonist [3H]candesartan is independent of receptor internalization, Biochem. Pharmacol. 61 (2001) 1227–1235.

[32] R. Hennig, K. Pollinger, J. Tessmar, A. Goepferich, Multivalent targeting of AT1 receptors with angiotensin II-functionalized nanoparticles, J. Drug Target. 23 (2015) 681–689.

[33] A. Kecskés, D.K. Tosh, Q. Wei, Z.-G. Gao, K.A. Jacobson, GPCR ligand dendrimer (GLiDe) conjugates: adenosine receptor interactions of a series of multivalent xanthine antagonists, Bioconjug. Chem. 22 (2011) 1115–1127.

[34] R. Weissleder, K. Kelly, E.Y. Sun, T. Shtatland, L. Josephson, Cell-specific targeting of nanoparticles by multivalent attachment of small molecules, Nat. Biotechnol. 23 (2005) 1418–1423.

[35] J. Wang, S. Tian, R.A. Petros, M.E. Napier, J.M. DeSimone, The Complex Role of Multivalency in Nanoparticles Targeting the Transferrin Receptor for Cancer Therapies, J. Am. Chem. Soc. 132 (2010) 11306–11313.

[36] W. Jiang, Kim, Betty Y. S., J.T. Rutka, W.C.W. Chan, Nanoparticle-mediated cellular response is size-dependent, Nat. Nanotech. 3 (2008) 145–150.

[37] K. Pollinger, R. Hennig, A. Ohlmann, R. Fuchshofer, R. Wenzel, M. Breunig, J. Tessmar, E.R. Tamm, A. Goepferich, Ligand-functionalized nanoparticles target endothelial cells in retinal capillaries after systemic application, Proc. Natl. Acad. Sci. U.S.A. 110 (2013) 6115–6120.

[38] S.D. Perrault, C. Walkey, T. Jennings, H.C. Fischer, W.C.W. Chan, Mediating tumor targeting efficiency of nanoparticles through design, Nano Lett. 9 (2009) 1909–1915.

[39] W.J.M. Mulder, G.J. Strijkers, J.W. Habets, E.J.W. Bleeker, D.W.J. van der Schaft, G. Storm, G.A. Koning, A.W. Griffioen, K. Nicolay, MR molecular imaging and fluorescence microscopy for identification of activated tumor endothelium using a bimodal lipidic nanoparticle, FASEB J. 19 (2005) 2008–2010.

[40] M.L. Schipper, Z. Cheng, S.-W. Lee, L.A. Bentolila, G. Iyer, J. Rao, X. Chen, A.M. Wu, S. Weiss, S.S. Gambhir, microPET-based biodistribution of quantum dots in living mice, J. Nucl. Med. 48 (2007) 1511–1518.

[41] B.R. Smith, Z. Cheng, A. De, A.L. Koh, R. Sinclair, S.S. Gambhir, Real-time intravital imaging of RGD-quantum dot binding to luminal endothelium in mouse tumor neovasculature, Nano Lett. 8 (2008) 2599–2606.

[42] L. Ye, K.-T. Yong, L. Liu, I. Roy, R. Hu, J. Zhu, H. Cai, W.-C. Law, J. Liu, K. Wang, J. Liu, Y. Liu, Y. Hu, X. Zhang, M.T. Swihart, P.N. Prasad, A pilot study in non-human primates shows no adverse response to intravenous injection of quantum dots, Nat. Nanotech. 7 (2012) 453–458.

[43] N. Liu, Y. Mu, Y. Chen, H. Sun, S. Han, M. Wang, H. Wang, Y. Li, Q. Xu, P. Huang, Z. Sun, Degradation of aqueous synthesized CdTe/ZnS quantum dots in mice: differential blood kinetics and biodistribution of cadmium and tellurium, Part. Fibre Toxicol. 10 (2013) 37.

[44] S.L. Sewell, M.M. Higgins, C.S. Bell, T.D. Giorgio, Quantification of Quantum Dot Concentration Using Inductively Coupled Plasma-Mass Spectrometry (ICP-MS), J. Biomed. Nanotechnol. 7 (2011) 685–690.

[45] J.V. Jokerst, T. Lobovkina, R.N. Zare, S.S. Gambhir, Nanoparticle PEGylation for imaging and therapy, Nanomedicine (Lond.) 6 (2011) 715–728.

[46] M. Wang, M. Thanou, Targeting nanoparticles to cancer, Pharmacol. Res. 62 (2010) 90–99.

[47] E. Kaschina, T. Unger, Angiotensin AT1/AT2 Receptors: Regulation, Signalling and Function, Blood. Press. 12 (2003) 70–88.

[48] C.H.J. Choi, J.E. Zuckerman, P. Webster, M.E. Davis, Targeting kidney mesangium by nanoparticles of defined size, Proc. Natl. Acad. Sci. U.S.A. 108 (2011) 6656–6661.

[49] L. Manil, J.C. Davin, C. Duchenne, C. Kubiak, J. Foidart, P. Couvreur, P. Mahieu, Uptake of nanoparticles by rat glomerular mesangial cells in vivo and in vitro, Pharm. Res. 11 (1994) 1160–1165.

[50] H. Shimizu, Y. Hori, S. Kaname, K. Yamada, N. Nishiyama, S. Matsumoto, K. Miyata, M. Oba, A. Yamada, K. Kataoka, T. Fujita, siRNA-Based Therapy Ameliorates Glomerulonephritis, J. Am. Soc. Nephrol. 21 (2010) 622–633.

[51] K. Pollinger, R. Hennig, S. Bauer, M. Breunig, J. Tessmar, A. Buschauer, R. Witzgall, A. Goepferich, Biodistribution of Quantum Dots in the Kidney After Intravenous Injection, J. Nanosci. Nanotech. 14 (2014) 3313–3319.

[52] M. Praetner, M. Rehberg, P. Bihari, M. Lerchenberger, B. Uhl, M. Holzer, M.E. Eichhorn, R. Fürst, T. Perisic, C.A. Reichel, The contribution of the capillary endothelium to blood clearance and tissue deposition of anionic quantum dots in vivo, Biomaterials 31 (2010) 6692–6700.

[53] Y. Shimomura, A. Hirata, S. Ishikawa, S. Okinami, Changes in choriocapillaris fenestration of rat eyes after intravitreal bevacizumab injection, Graefes Arch. Clin. Exp. Ophthalmol. 247 (2009) 1089–1094.

[54] A. Sugita, M. Hamasaki, R. Higashi, Regional difference in fenestration of choroidal capillaries in Japanese monkey eye, Jpn. J. Ophthalmol. 26 (1982) 47–52.

[55] D. Feng, J.A. Nagy, A.M. Dvorak, H.F. Dvorak, Different pathways of macromolecule extravasation from hyperpermeable tumor vessels, Microvasc. Res. 59 (2000) 24–37.

[56] A.J.R. White, S.C. Cheruvu, M. Sarris, S.S. Liyanage, E. Lumbers, J. Chui, D. Wakefield, P.J. McCluskey, Expression of classical components of the renin-angiotensin system in the human eye, J. Renin Angiotensin Aldosterone Syst. 16 (2014) 59–66.

[57] V.M. Milenkovic, M. Brockmann, C. Meyer, M. Desch, F. Schweda, A. Kurtz, V. Todorov, O. Strauss, Regulation of the renin expression in the retinal pigment epithelium by systemic stimuli, Am. J. Physiol. Renal Physiol. 299 (2010) F396-403.

[58] V.-P. Ranta, E. Mannermaa, K. Lummepuro, A. Subrizi, A. Laukkanen, M. Antopolsky, L. Murtomäki, M. Hornof, A. Urtti, Barrier analysis of periocular drug delivery to the posterior segment, J. Control. Release 148 (2010) 42–48.

[59] S. Quarmby, R.D. Hunter, S. Kumar, Irradiation induced expression of CD31, ICAM-1 and VCAM-1 in human microvascular endothelial cells, Anticancer Res. 20 (2000) 3375–3381.

[60] A.W. Stitt, N. Lois, R.J. Medina, P. Adamson, T.M. Curtis, Advances in our understanding of diabetic retinopathy, Clin. Sci. 125 (2013) 1–17.

[61] J. Jiang, X.-B. Xia, H.-Z. Xu, Y. Xiong, W.-T. Song, S.-Q. Xiong, Y. Li, Inhibition of retinal neovascularization by gene transfer of small interfering RNA targeting HIF-1alpha and VEGF, J. Cell. Physiol. 218 (2009) 66–74.

[62] J. Chen, K.M. Connor, C.M. Aderman, K.L. Willett, O.P. Aspegren, L.E.H. Smith, Suppression of retinal neovascularization by erythropoietin siRNA in a mouse model of proliferative retinopathy, Invest. Ophthalmol. Vis. Sci. 50 (2009) 1329–1335.

[63] N. Singh, S. Amin, E. Richter, S. Rashid, V. Scoglietti, P.D. Jani, J. Wang, R. Kaur, J. Ambati, Z. Dong, B.K. Ambati, Flt-1 intraceptors inhibit hypoxia-induced VEGF expression in vitro and corneal neovascularization in vivo, Invest. Ophthalmol. Vis. Sci. 46 (2005) 1647–1652.

[64] T. Kurihara, Y. Ozawa, K. Shinoda, N. Nagai, M. Inoue, Y. Oike, K. Tsubota, S. Ishida, H. Okano, Neuroprotective effects of angiotensin II type 1 receptor (AT1R) blocker, telmisartan, via modulating AT1R and AT2R signaling in retinal inflammation, Invest. Ophthalmol. Vis. Sci. 47 (2006) 5545–5552.

[65] T. Narimatsu, Y. Ozawa, S. Miyake, N. Nagai, K. Tsubota, Angiotensin II type 1 receptor blockade suppresses light-induced neural damage in the mouse retina, Free Radic. Biol. Med. 71 (2014) 176–185.

Multivalent nanoparticles bind the retinal and choroidal vasculature

1 Intracellular calcium measurements

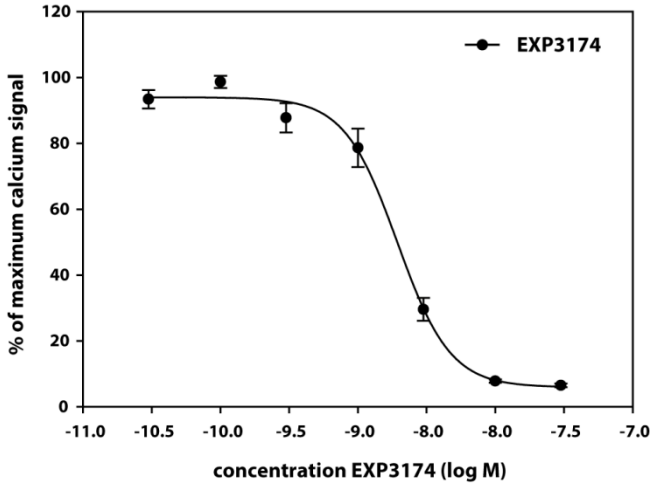

Figure S1: Using calcium mobilization with fura-2AM, EXP3174 blocked the angiotensin II-induced calcium influx into the cytosol of NCI-H295R cells with an IC_{50} of 2.0 ± 0.5 nM.

2 Nanoparticle deposition in liver and spleen

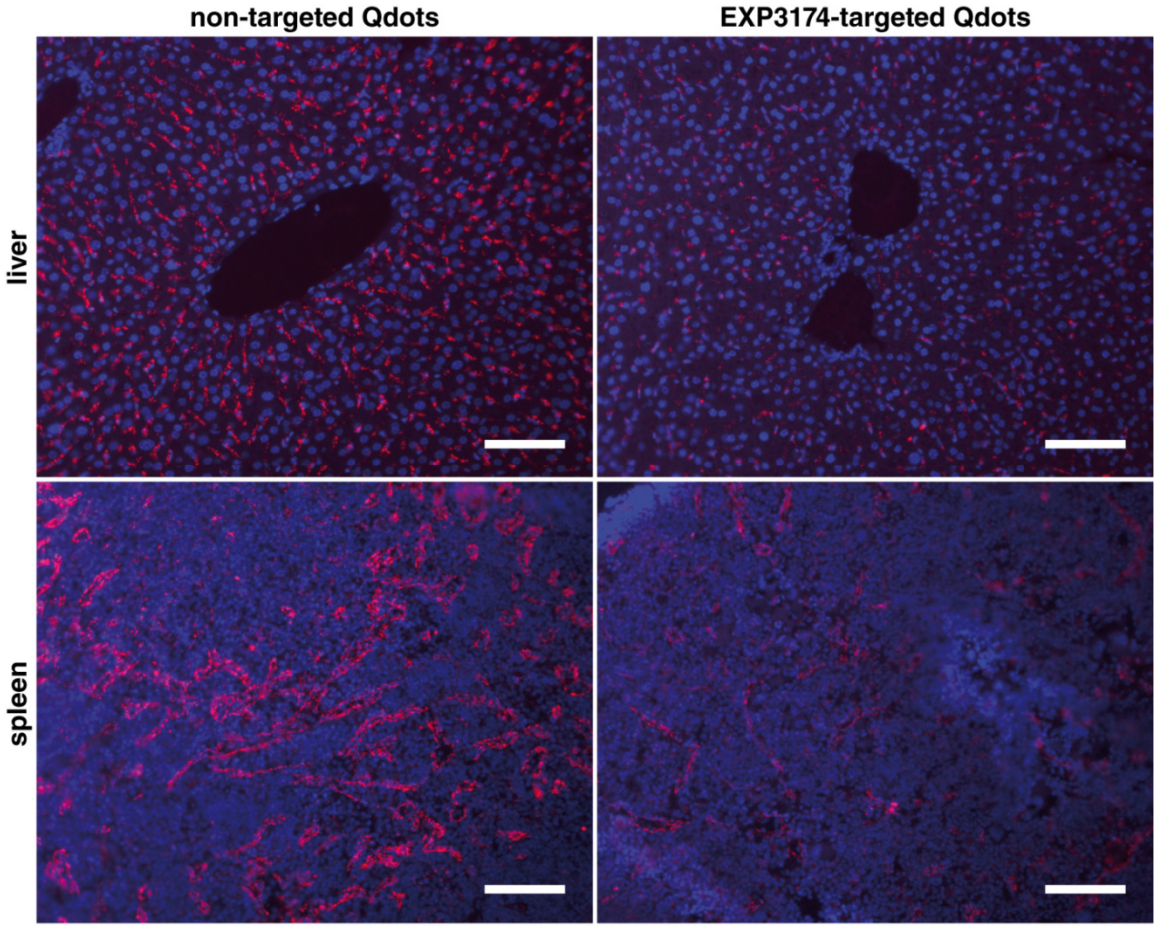

Figure S2: Accumulation of non-targeted and EXP3174-targeted Qdots in cryosections of liver and spleen after 1 h circulation as investigated by epifluorescence microscopy. Blue fluorescence depicts DAPI-stained cell nuclei whereas red fluorescence represents the Qdots. Scale bar: 100 µm.

3 Nanoparticle accumulation in the posterior eye segment

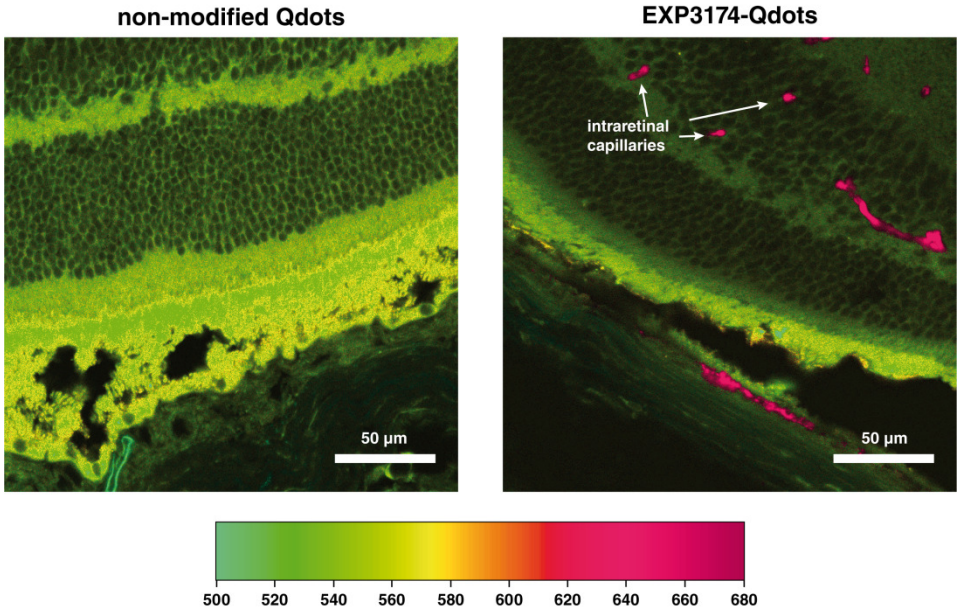

Figure S3: Multispectral-imaging of sagittal eye sections shows EXP3714-Qdot fluorescence in intraretinal blood vessels but no fluorescence of non-modified Qdots

Chapter 5

Branched polymer-drug conjugates for multivalent blockade of angiotensin II receptors

Published in Molecular Pharmaceutics
2015, 12, 3292–3302

This chapter was published as: R. Hennig, A. Veser, S. Kirchhof and A. Goepferich, Molecular Pharmaceutics, 2015, 12, 3292–3302, doi: 10.1021/acs.molpharmaceut.5b00301. Data that was not obtained or analyzed by R. Hennig is highlighted.

Abstract

The use of angiotensin receptor blockers (ARBs) for treatment of ocular diseases associated with neovascularizations, such as proliferative diabetic retinopathy, shows tremendous promise but is presently limited due to short intravitreal half-life. Conjugation of ARB molecules to branched polymers could vastly augment their therapeutic efficacy. EXP3174, a potent non-peptide ARB, was conjugated to branched poly(ethylene glycol) (PEG) and poly(amido amine) (PAMAM) dendrimers: 7.8 ligand molecules were tethered to each 40 kDa PEG molecule whereas 16.7 ligand molecules were linked to each PAMAM generation 5 dendrimer. The multivalent PEG and PAMAM conjugates blocked AT_1R signaling with an IC_{50} of 224 and 36.3 nM, respectively. The 6-fold higher affinity of the multivalent ligand-conjugated PAMAM dendrimers was due to their unique microarchitecture and ability to suppress polymer-drug interactions. Remarkably, both polymer-drug conjugates exhibited no cytotoxicity, in stark contrast to plain PAMAM dendrimers. With sufficiently long vitreous half-lives, both synthesized polymer-ARB conjugates have the potential to pave a new path for the therapy of ocular diseases accompanied by retinal neovascularizations.

1 Introduction

Blockade of the angiotensin II receptor type 1 (AT_1R) has proven highly beneficial for the treatment of retinal neovascularizations [1–3]. Unfortunately, systemic therapy with angiotensin receptor blockers (ARBs) only modestly inhibited disease progression [4]. Due to their high plasma protein binding [5] and the plethora of off-target sites that express the AT_1 receptor [6], systemically administered ARBs lack intravitreal efficacy [7]. One way to overcome this limitation would be to increase intraocular drug bioavailability by directly injecting drugs into the vitreous chamber. In this way, intravitreally administered antibody formulations are able to sustain therapeutic drug concentrations for several weeks [8]. However, since ARBs have a drastically shorter intravitreal half-life, typically only a few hours [9], new techniques which sustain effective angiotensin receptor antagonism in the eye are urgently needed. One method proven to successfully increase the half-lives of intravitreal drugs is polymer conjugation; attachment of a 40 kDa poly(ethylene glycol) (PEG) molecule to pegaptanib (Macugen®), a vascular endothelial growth factor (VEGF)-binding RNA aptamer, significantly decreased its clearance from the eye [10], since the aptamer's mobility in the vitreous humor was markedly slowed [11].

With the present approach, we explored the AT_1R blocking potential of an angiotensin receptor antagonist conjugated to branched, eight-armed poly(ethylene glycol) with a molecular weight of 40 kDa or to poly(amido amine) (PAMAM) generation 5 dendrimers. Specifically, we evaluated the multivalent receptor affinity and cytotoxicity of said constructs; in addition to intravitreal half-life, both AT_1R affinity and cytotoxicity are key performance metrics for intravitreal inhibition of pathologic neovascularizations. PEG was chosen as a candidate polymer backbone due to its excellent biocompatibility [12] and because PEGylation is the most common strategy for half-life extension [13]. In addition, PAMAM dendrimers were used as an alternative polymer material because of their fundamentally different microarchitecture. Furthermore, PAMAM dendrimers selectively accumulate in neuroinflamed retinal cells after intravitreal injection and persist there for several weeks [14,15]. However, although chemical conjugation could potentially increase intravitreal drug half-life, attachment of small molecule ligands to PEG or other hydrophilic polymers can drastically alter their receptor binding capability. PEGylation of EXP3174, a non-peptide ARB which is the active metabolite of losartan, decreased its receptor affinity 580-fold [16]. Therefore, to

obtain highly affine conjugates, multivalent interactions between the cell surface receptors and the polymer-drug conjugate are highly desirable. Due to the small size of ARB molecules (mostly <500 Da), several ligands can be conjugated to one polymer molecule, possibly allowing for formation of multivalent ligand-receptor interactions.

The present work aims to investigate the *in vitro* receptor binding affinity of EXP3174 molecules after conjugation to polymeric scaffolds. Furthermore, since toxicity concerns are relevant for dendrimer-based therapeutics [17], cytotoxicity testing of plain and conjugated polymers was performed. Overall, this is the first study that addresses conjugation, affinity testing and cytotoxicity of multivalent polymer-drug conjugates that block angiotensin receptors.

2 Experimental Section

2.1 Materials

The angiotensin receptor blocker EXP3174 was purchased from Santa Cruz (Heidelberg, Germany). Eight-armed poly(ethylene glycol), molecular weight 40 kDa (hexaglycerol core, 8armPEG40k-NH_2 and eight-armed poly(ethylene glycol), molecular weight 20 kDa (hexaglycerol core, 8armPEG20k-OH) were purchased from JenKem Technology (Allen, TX, USA). Poly(amido amine) generation 5 dendrimers with an ethylene diamine core and 128 amine surface groups were purchased from Sigma Aldrich (Taufkirchen, Germany).

All chemicals were obtained from Sigma Aldrich (Taufkirchen, Germany) in analytical grade unless stated otherwise. Ultrapure water was obtained from a Milli-Q water purification system (Millipore, Billerica, MA, USA). Dulbecco's phosphate buffered saline (DPBS) pH 7.4 consisting of 1.5 mM KH_2PO_4, 8 mM Na_2HPO_4, 2.7 mM KCl and 138 mM NaCl was purchased from Life Technologies (Carlsbad, CA, USA).

2.2 Cell culture

Rat mesangial cells were chosen as a model cell line for assaying receptor affinity due to their stable expression of AT_1R, and were cultured in RPMI 1640 medium containing 10 % fetal calf serum (FCS) (Sigma Aldrich, Taufkirchen, Germany) supplemented with insulin-transferrin-selenium (Life Technologies, Carlsbad, CA, USA), penicillin-streptomycin (Life Technologies, Carlsbad, CA, USA) and 100 nM hydrocortisone. Mouse fibroblast L-929 cells (ATCC No. CCL-1) were cultured in Eagle's Minimum

Essential Medium (EMEM) containing 10 % FCS and were used for cytotoxicity measurements. All cells were cultured in T-75 cell culture flasks (Corning, Corning, NY, USA).

2.3 Conjugation of EXP3174 to branched 8armPEG40k

2.9 µmol EXP3174 were dissolved in 250 µL dimethyl sulfoxide (DMSO). After complete dissolution, 450 µL of 10 mM 2-(N-morpholino)ethanesulfonic acid (MES) buffer at pH 4.8, 200 µL of N-(3-dimethylaminopropyl)-N'-ethylcarbodiimide hydrochloride solution (EDC, 250 mM in MES buffer) and 100 µL of N-hydroxysulfosuccinimide (sulfo-NHS, 100 mM in MES buffer) were added. The solution was stirred for 1 h for complete activation of EXP3174's carboxylic group. Subsequently 0.18 µmol 8armPEG40k-NH_2 in 500 µL borate buffer (50 mM, pH 8.5) were added to the solution and stirred for 18 h at room temperature. After successful conjugation the mixture was diluted with water to a total volume of 4 mL and initially purified by ultrafiltration using a 10 kDa molecular weight cut-off Amicon Ultra-15 filter unit (Millipore, Billerica, MA, USA). The concentrated solution was further purified by size exclusion chromatography using a Sephadex G-25 resin in a PD-10 column (GE Healthcare, Munich, Germany) with DPBS as the eluent. The 8armPEG40k-EXP3174 concentration of each fraction was determined by fluorescence measurements: 50 µL of each fraction were diluted with 50 µL citrate buffer (100 mM, pH 2.5) and analyzed with an LS-55 fluorescence plate reader (Perkin Elmer, Waltham, MA, USA) using an excitation wavelength of 250 nm and an emission wavelength of 370 nm. Fractions containing 8armPEG-EXP3174 were pooled and further purified by 3-fold ultrafiltration as described above.

2.4 Conjugation of EXP3174 to generation 5 PAMAM dendrimers

1.5 µmol EXP3174 were dissolved in 500 µL DMSO and activated with 50 mM EDC and 25 mM sulfo-NHS in 500 µL MES buffer (5 mM, pH 4.8), for a total reaction volume of 1000 µL. After 1 h of activation in a glass reaction microtube, 0.15 µmol PAMAM G5 dendrimer in 500 µL borate buffer (50 mM, pH 8.5) were added to the mix and stirred overnight. Purification of the dendrimer-EXP3174 conjugate was identical to the purification of the branched PEGs. To remove all EXP3174 molecules non-covalently 'encapsulated' in the dendritic box, size exclusion chromatography was performed with DPBS as eluent. As an isotonic solution it will lead to rapid release of encapsulated EXP3174 due to weakening of electrostatic interactions between the cationic dendrimer

and the anionic EXP3174 as shown for other weak acids such as methotrexate [18] and ibuprofen [19].

2.5 Determination of concentration and degree of conjugation

The total concentration and degree of labeling was determined by quantification of unreacted and reacted surface amine groups. Amine groups that had reacted with EXP3174 were quantified by measuring the EXP3174 fluorescence using an excitation wavelength of 250 nm and an emission wavelength of 370 nm. Briefly, conjugate solutions were diluted with citrate buffer (100 mM, pH 2.5), excited on a fluorescence plate reader and analyzed against an EXP3174 standard.

The amount of unreacted amine groups was determined by a fluorescamine assay. Briefly, 80 µL borate buffer (50 mM, pH 8.5), 10 µL fluorescamine solution (0.3 mg/mL in acetone) and 10 µL of test solution were mixed in 1.5 mL reaction tubes. The fluorescence was analyzed with an LS-55 fluorescence plate reader using an excitation wavelength of 360 nm, a 430 nm beam splitter and an emission wavelength of 480 nm. Concentrations of unreacted amine groups were then determined by using a calibration of diluted solutions of respective unreacted polymers. The concentration of the conjugate was calculated using equation 1.

$$c_{conjugate} = \frac{c_{EXP3174} + c_{unreacted\ amines}}{n_{total\ available\ amines}}$$

Equation 1: Calculation of conjugate concentration based on the measured concentrations of EXP3174 and unreacted amines

Due to the long Stokes shifts of EXP3174 and EXP3174-amide[16] and because there is no overlap between the emission and extinction spectrum, non-radiative chromophore-chromophore interactions such as FRET are impossible. Fluorescence self-quenching and thus distortion of ligand quantification measurements as described for fluorescein [20] or coumarin-based dyes [21] can, therefore, be ruled out for the EXP3174-conjugates.

2.6 Reversed-phase high performance liquid chromatography (RP18-HPLC)

The purity of EXP3174-conjugated branched PEGs and dendrimers was analyzed by a reversed phase high performance liquid chromatography (RP18-HPLC) system consisting of a Shimadzu LC-10ATVP pump (Shimadzu, Duisburg, Germany), a Shimadzu SIL-10ADVP autosampler connected to a Shimadzu CTO-10ASVP column oven.

For elution of branched PEGs a Luna® 5 µm C18(2) 100 Å 250 x 4.60 mm LC column (Phenomenex, Aschaffenburg, Germany) was used. The mobile phase consisted of citrate buffer (pH 2.5, 50 mM)-acetonitrile (50:50 v/v) at a flow rate of 1 mL/min. The column temperature was maintained at 30 °C. A Shimadzu RF-10AXL fluorescence detector set to an excitation of 250 nm and an emission wavelength of 370 nm detected the conjugated polymers.

PAMAM G5 dendrimers labeled with EXP3174 were analyzed using a Vydac 218 TP C18 5 µm 300 Å 250 x 4.60 mm LC column (Sigma Aldrich) and eluted by a linear acetonitrile–trifluoroacetic acid (TFA)–water gradient with a flow rate of 1 mL/min. Elution was obtained by using the following gradient of solvents A (0.1 % (v/v) TFA in water) and B (0.1 % (v/v) TFA in acetonitrile): 90:10 (A:B) to 20:80 in 14 min and reequilibration to 90:10 in the following 8 min. The column was operated at 35 °C and the dendrimers were detected using the exact same technique used to detect PEG conjugates, described above.

2.7 Intracellular calcium measurements

The intracellular calcium concentration was measured with a plate reader-based system using the ratiometric fluorescent calcium chelator fura-2AM, as recently described [16]. Briefly, suspensions of rat mesangial cells were incubated with 5 µM fura-2AM (Life Technologies, Carlsbad, CA, USA) and 0.05 % Pluronic F-127 in Leibovitz's L-15 medium (Life Technologies, Carlsbad, CA, USA) for 1 h at room temperature in the dark. After removal of excess fura-2AM, the cells were incubated with a concentration series of EXP3174-conjugated polymers in 96-well plates (Greiner Bio One, Frickenhausen, Germany). After an incubation time of 10 min, a quantity equivalent to the EC_{80} of angiotensin II (300 nM, Bachem, Bubendorf, Switzerland) was added to the cells. The fluorescence signal was immediately recorded with a FluoStar Omega fluorescence microplate reader for 30 s. Excitation filters for the ratiometric measurement were 340/20 nm and 380/20 nm and the emission was recorded using a 510/20 nm bandpass filter. The intracellular calcium concentrations were calculated using the Grynkiewicz equation [22].

2.8 Pyrene assay

25 µL of a 40 mg/mL pyrene solution in acetone was pipetted into HPLC vials, yielding 1 mg pyrene per vial. After evaporation with nitrogen, the vials were dried under vacuum

for 1 h. Subsequently, 200 µL of an 8armPEG40K-EXP3174 or Ceteareth-20 (Kolb, Hedingen, Switzerland) dilution were added to a pyrene aliquot and incubated for 24 h under gentle shaking. Ceteareth-20 is an amphiphilic linear PEG(20) cetyl/stearyl ether and is also known as Sympatens ACS/200 G. In a next step, the solutions were centrifuged at 12,000 g for 10 min to sediment undissolved pyrene. 100 µL of the supernatant was transferred to a 96-well fluorescence plate (Greiner Bio One, Frickenhausen, Germany). Pyrene fluorescence was analyzed with an LS-55 fluorescence plate reader using an excitation wavelength of 339 nm, a 350 nm beam splitter and an emission wavelength of 390 nm.

Emission spectra of pyrene were obtained by dissolving a 10 µg pyrene aliquot in 2 mL of pure water, an aqueous solution of 0.025 % Ceteareth-20 or an aqueous solution of 0.025 % 8armPEG40k-EXP3174. Pyrene fluorescence was excited at 339 nm and recorded from 350 to 450 nm with an LS-55 fluorescence plate reader using a quartz glass cell (Hellma, Müllheim, Germany).

2.9 Labeling and analysis of 8armPEG20k-AngII

8armPEG20k-succinimidyl carbonate (8armPEG20k-SC), the precursor of the labeling reaction, was synthesized as described in the literature [23]. For the preparation of the ligand-polymer conjugate, 4 µmol angiotensin II were mixed with 0.25 µmol 8armPEG20k-SC, yielding a 16-fold excess of ligand over polymer. In a total volume of 1000 µL borate buffer (50 mM, pH 8.5) the solution was stirred for 16 h at room temperature. Purification of the resulting conjugate was achieved with the help of ultrafiltration and size exclusion chromatography. First, unreacted angiotensin II was removed via ultrafiltration using a 10 kDa molecular weight cut-off Amicon Ultra-15 filter unit. Second, the concentrated solution was purified by size exclusion chromatography using a Sephadex G-25 resin in a PD-10 column with DPBS as the eluent. The 8armPEG20k-AngII concentration of each fraction was determined with a bicinchoninic acid (BCA) Assay using the Pierce™ BCA Protein Assay Kit (Life Technologies). Briefly, 25 µL of each fraction were thoroughly mixed with 200 µL of the reagent mix containing 196 µL kit reagent A and 4 µL kit reagent B. After a 30 min incubation at 37 °C the fractions were analyzed on a plate reader at 562 nm. Subsequently, fractions containing 8armPEG20k-AngII were pooled and further purified by ultrafiltration as described above.

The concentration of the conjugate was analyzed with the help of RP18-HPLC and a well-plate PEG determination assay. For the latter, 125 µL 8armPEG20k-SC solutions yielding a final concentration of 2.5 µg/mL to 25 µg/mL 8armPEG20k-SC were mixed with 50 µL of a 5 % $BaCl_2$ solution in 1 M hydrochloric acid and 25 µL of 0.1 N iodine solution (Carl Roth, Karlsruhe, Germany). The 8armPEG20k-AngII solution was prepared similarly. After a 15 min incubation at room temperature the absorbance of the PEG-iodine complex was measured at 535 nm. Ang II concentration and purity were analyzed with a RP18-HPLC system using a Luna® 5 µm C18(2) 100 Å 250 x 4.60 mm LC column. Elution of angiotensin II and its polymer conjugate was obtained by using the following gradient of solvents A (0.1 % (v/v) TFA in water) and B (0.1 % (v/v) TFA in acetonitrile): 85:15 (A:B) to 30:70 in 14 min and reequilibration to 85:15 in the following 8 min.

2.10 Cytotoxicity

To assess the cellular toxicity of the synthesized conjugates, a metabolic assay using the reagent (3-(4,5-Dimethylthiazol-2-yl)-2,5-Diphenyltetrazolium Bromide) (MTT) (PanReac AppliChem, Darmstadt, Germany) according to ISO 10993-5:2009 (Biological evaluation of medical devices — Part 5: Tests for in vitro cytotoxicity) was performed. Briefly, mouse fibroblast L-929 cells were seeded in 96-well plates at a density of 10,000 cells per well. After the cells had adhered overnight, the conjugate test solutions, which were prepared in EMEM medium with 10 % FCS, were pipetted onto the cells and incubated for 4 h in a humidified incubator with a 5 % CO_2 atmosphere. Subsequently, the test solutions were substituted by a 1.5 mM MTT solution in serum-containing medium and similarly incubated for 4 h. After removal of the MTT solution, 80 µL of a 10 % sodium dodecyl sulfate (SDS) solution was added to each well. The plates were incubated at room temperature overnight to completely solubilize the synthesized purple formazan derivative. Finally, the absorbance at 570 nm and 690 nm was measured for each well using a FluoStar Omega fluorescence microplate reader (BMG Labtech, Ortenberg, Germany). The difference (A_{570} - A_{690}) was used to calculate the viability of cells. As a viability control, cells were incubated with serum containing medium alone. In contrast, a 0.1 % SDS solution was used as positive control to ensure complete cell death. Where possible, IC_{50} values were calculated with SigmaPlot 12.2 using sigmoidal dose-response curve fitting with a variable slope. Microscope images were recorded with a Nikon DS-U1 camera (Nikon, Düsseldorf, Germany) connected to a Leica DM IRB microscope (Leica,

Wetzlar, Germany) and processed using ImageJ (NIH, Bethesda, MD, USA, http://imagej.nih.gov/ij).

2.11 Flow cytometric assessment of apoptosis

Mouse fibroblast L929 cells were grown to subconfluency and harvested by trypsinization. Subsequently, 100,000 suspended cells were incubated with 10 µM PAMAM G5-NH_2 or 10 µM PAMAM G5-EXP3174 in Dulbecco's modified Eagle's medium (DMEM) supplemented with 10 % fetal calf serum. Cells were incubated with pure FCS-containing medium as live control. After 4 h of incubation at 37 °C, cells were centrifuged (200 rpm, 5 min) and resuspended in Tyrode's solution (20 mM HEPES, 134 mM NaCl, 2.9 mM KCl, 5 mM glucose, 0.34 mM NaH_2PO_4, 1 mM $MgCl_2$, 12 mM $NaHCO_3$, 1 mM $CaCl_2$ and 0.5 % bovine serum albumin) containing 2.5 µg/mL FITC-lactadherin (Haematologic Technologies, Essex Junction, VT, USA). After further incubation for 30 min at room temperature, propidium iodide (Sigma Aldrich) was added to a final concentration of 1 µg/mL. Finally, cells were analyzed on a FACSCalibur flow cytometer (Becton Dickinson, Franklin Lakes, NJ, USA). FITC-lactadherin and propidium iodide (PI) fluorescence were both elicited by excitation at 488 nm and recorded using a 530/30 nm FL1 bandpass filter and a 670 nm FL3 longpass filter, respectively. The resulting data was evaluated using WinMDI 2.9 (The Scripps Research Institute, San Diego, CA, USA). The population of intact cells was gated and used for fluorescence analysis. All experiments were performed in triplicate.

2.12 Statistics

To assess the statistical significance of cytotoxicity data, Student's t-tests were carried out using SigmaPlot 12.2. Levels of statistical significance were set as indicated.

3 Results and Discussion

3.1 Conjugation procedure and purification

Our two-step synthesis strategy provided us with two branched polymer-EXP3174 conjugates: an 8armPEG40k polymer, (Fig. 1B) with an average of 7.8 conjugated antagonist molecules per polymer molecule and a PAMAM generation 5 dendrimer, (Fig. 1A) to which 16.7 molecules of EXP3174 were bound on average. This left only 0.2 unreacted amine groups for the branched PEG. In contrast, only 13 % of 128 total amine groups on the PAMAM dendrimer surface reacted with EXP3174, leaving the majority of terminal amine groups unreacted.

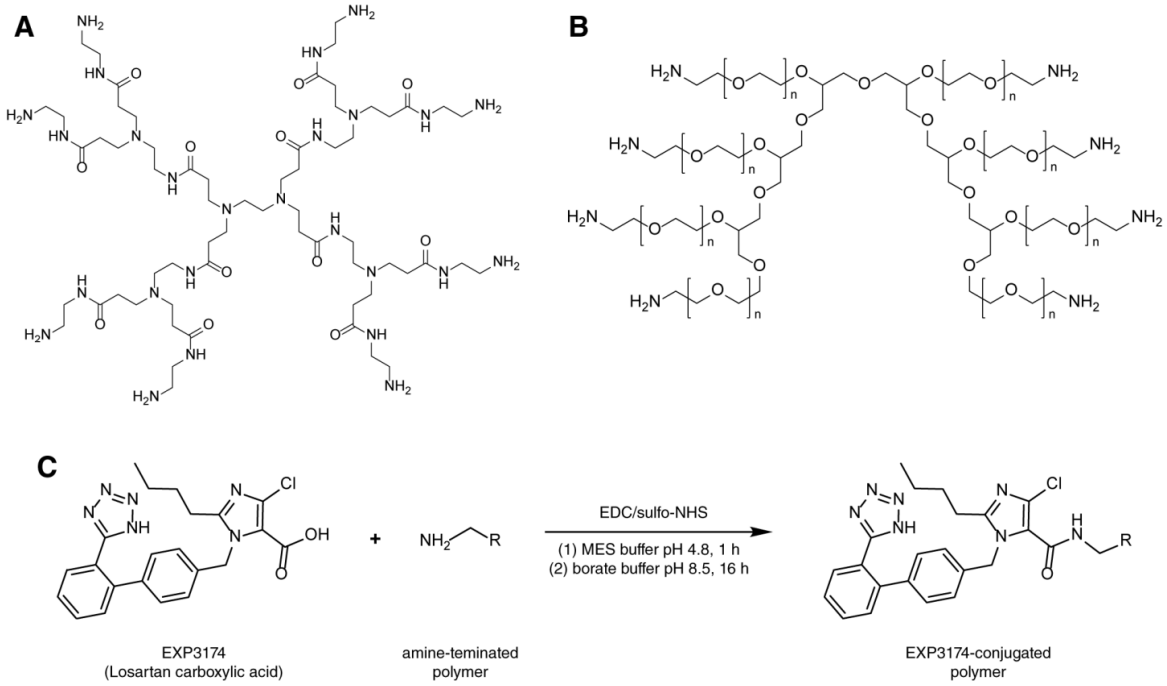

Figure 1: Chemical structure of the polymers used and their conjugation to EXP3174. **(A)** Depiction of a generation 1 PAMAM dendrimer representing the ethylene diamine core and the typical tree-like structure of PAMAM dendrimers. **(B)** Chemical structure of an 8armPEG-NH_2 molecule. Depending on the molecular weight the individual PEG chains differ in their total length **(C)** The conjugation procedure to covalently couple EXP3174 to the terminal amine groups of the polymers using EDC/sulfo-NHS chemistry and a 2-step buffer system.

To ensure that no unreacted EXP3174 was present after the purification, as this would distort affinity measurements, reversed phase high performance liquid chromatography (RP18-HPLC) was conducted. Due to its bright fluorescence, EXP3174 concentrations down to a minimum of 0.5 ng/mL can be quantified by HPLC analysis [24]. Neither the 8armPEG40k-EXP3174 nor the PAMAM G5-EXP3174 dendrimer exhibited free EXP3174 (Fig. 2). In the chromatogram corresponding to the G5-EXP3174 dendrimer, a second peak appeared at a retention time of 13.0 min, clearly distinct from the EXP3174

peak at 13.6 min. This peak most likely represented oligomeric branching defects such as dimers and trimers present in the purchased dendrimer [25,26]. Since the ultrafiltration and size exclusion chromatography purifications only eliminated smaller impurities and trailing generations, it is expected that the slower-eluting oligomeric branching defects reacted with EXP3174 and were retained post-purification. Conjugation of EXP3174 to the polymers led to decreased retention times in the reversed phase HPLC, clearly indicating successful conjugation of the hydrophobic ligand to the hydrophilic polymers.

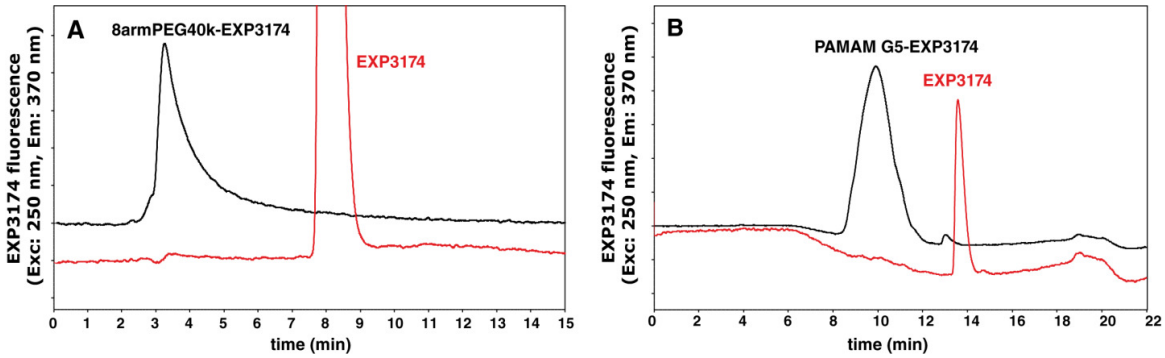

Figure 2: RP18-HPLC chromatograms of the conjugated polymers. **(A)** HPLC Chromatogram of 8arm-PEG40K-EXP3174 and EXP3174 for comparison. Due to the highly hydrophilic polymer, the conjugate has a markedly faster elution. The chromatogram shows the absence of free EXP3174, proving the success of the purification procedure **(B)** HPLC chromatogram of PAMAM G5-EXP3174 and free EXP3174 for comparison. Again, the hydrophilic G5 PAMAM dendrimer is eluted earlier than EXP3174 and shows no unreacted EXP3174. The additional peak in the chromatogram can presumably be attributed to multimeric impurities.

3.2 Conjugate affinity

The affinity of the synthesized EXP3174 conjugates for AT_1R was measured with an intracellular calcium mobilization assay using fura-2AM. Because the AT_1R is a Gq-coupled receptor [27], calcium ions act as a second messenger in the cytosol. Upon angiotensin II receptor binding, the intracellular calcium concentration rapidly increases, resulting in calcium chelation by supplemented fura-2. The binding of calcium ions to fura-2 leads to a distinct change in the dye's excitation spectrum [28], which permits the calculation of calcium ion concentrations, and thus ligand affinities. The 8armPEG40k-EXP3174 polymer-drug conjugate exhibited a receptor binding affinity of 224 ± 34 nM. Although PAMAM G5-EXP3174 showed a 6-fold improved affinity towards AT_1R, with an IC_{50} of 36.3 ± 4.6 nM (Fig. 3A), the conjugate affinity was about 30-fold lower than the native ligand's affinity, which is approximately 1 nM [16]. Interestingly, when normalized on a per-unit-ligand basis, the affinity of the dendrimer-bound EXP3174 was still 3-fold higher (606 nM) than that of the branched 8armPEG-bound EXP3174 (1750 nM). Compared to the affinity of a linear mPEG5k-EXP3174 conjugate, which was

approximately 630 nM [16], the attachment of EXP3174 to the multi-arm PEG polymers decreased its affinity even further. Besides the affinity loss from steric hindrance of the PEG chain, another effect apparently prevents EXP3174 from binding its cognate receptor. The flexible nature of the PEG chains of the multi-arm PEGs could lead to extensive wrapping of the PEG molecule around the ligand, leading to masking of the ligand (Fig. 3B). This shroud formation has been observed with PEGylated proteins such as PEGylated staphylokinase [29] PEGylated trypsin [30] and PEGylated bovine serum albumin [31]. García-Arellano and coworkers proposed that conjugated PEG coils around the protein surface and thus acts as a cage due to interactions between the hydrophobic cluster on the protein surface and the hydrophobic regions of PEGs [32]. In general, the biphenylimidazole class of angiotensin receptor antagonists are also quite hydrophobic, resulting in the potential for a similar interaction with PEG. That EXP3174 has strong hydrophobic character can be observed from its tremendous plasma protein binding of over 99.7 % [33]. In addition, losartan, the precursor of EXP3174, has a poor aqueous solubility of only 71.4 μg/mL [34]. Although EXP3174 possesses an additional carboxylic group, its solubility is not increased. In addition, this extra acidic character is abolished when EXP3174 is present as part of a polymer conjugate, as the carboxylic acid is used to link EXP3174 to the polymers' terminal amines.

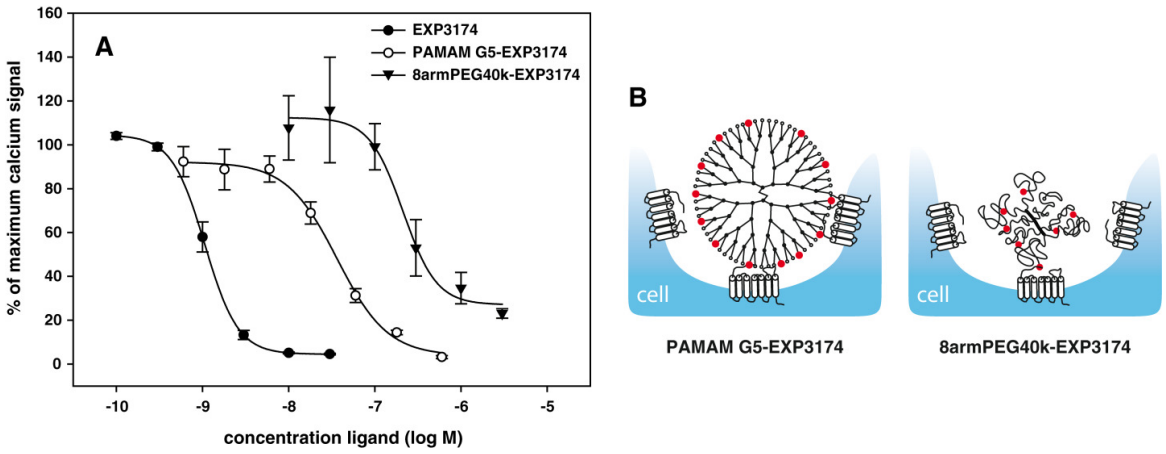

Figure 3: Affinity measurements of polymer-drug conjugates **(A)** Intracellular calcium mobilization diagrams for both EXP3174-conjugated polymers. The PAMAM generation 5 dendrimer showed an IC_{50} of 36.3 ± 4.6 nM. In contrast, the 8armPEG40K branched star polymer inhibited the angiotensin II-induced receptor signaling with an IC_{50} of 224 ± 34 nM. **(B)** Schematic depiction of ligand-conjugated dendrimer and 8armPEG polymer binding to cell surface receptors. The extended structure of the dendrimer allows for easier multivalent binding. For simplicity's sake a generation 4 dendrimer is pictured.

In contrast to the coiling of PEG, poly(amido amine) chains of dendrimers exhibit a greatly different microarchitecture. At neutral pH conditions, at which the receptor

binding experiments were performed, most of the primary amines are charged [35], leading to electrostatic repulsion between neighboring groups [36]. Consequently, dendrimers of generation 4 to 6 show a significant 'stretching-out' effect [37], which results in the presentation of the ligands on the dendrimer surface [38]. Through molecular dynamics simulations Maiti and coworkers revealed that 75 of the 128 terminal amines of the PAMAM G5 dendrimer are located at the periphery under neutral pH conditions resulting in a high sphericity of the dendrimer [39]. Together with fact that the G5 dendrimer is a threshold generation between the sterically crowded and thus more rigid dendrimers ($G \geq 6$) and the more flexible dendrimers ($G \leq 4$) [40], its stretched-out structure could be the reason that the PAMAM G5-EXP3174 dendrimer exhibited a higher multivalency and thus an increased avidity for the receptors compared to the 8armPEG40k-EXP3174 conjugate (Fig. 3). That dendrimers have the capability to enable multivalent binding of cell surface receptors was already demonstrated for concavalin A [41], folic acid receptors [42] and the adenosine A3 receptor [43]. Notably, Banaszak Holl and coworkers showed that due to strong nonspecific interactions between dendrimers and the folate binding protein, a monovalent folic acid-PAMAM dendrimer conjugate exhibited enhanced binding when compared to free folic acid [44]. Bao and coworkers synthesized a chitosan-poly(ethyleneimine)-candesartan conjugate for inhibition of tumor-associated angiogenesis [45]. However, instead of multivalent AT_1R blockade, their complexes were designed to release candesartan in a controlled fashion upon linker cleavage.

Although conjugation to polymer scaffolds markedly decreased the binding affinity of the antagonists (Table 1), a significantly increased intravitreal half-life could readily compensate for the loss of affinity. For example, despite a four-fold reduction in the affinity of pegaptanib towards VEGF following aptamer PEGylation [46], the greatly decreased elimination from the vitreous humor still led to improved therapeutic efficacy [47] and ultimately introduction of the PEGylated form onto the market [48]. Since ARB molecules are rapidly cleared from the vitreous in only few hours [9], an extension of the intravitreal half-life could be even more pronounced for these molecules. In addition, Iezzi and coworkers impressively showed that after intravitreal injection, PAMAM dendrimers were retained in the neuroinflamed retina for more than one month and accumulated in activated microglia [14]. In a similar fashion, hydroxyl-terminated PAMAM dendrimers accumulated for several weeks in an ischemia/reperfusion mouse

eye [15]. Thus, conjugation to polymers could tremendously increase antagonist efficacy although binding affinity is initially decreased.

3.3 Investigation of hydrophobic interactions

To investigate whether the decreased affinity of the 8armPEG40k-EXP3174 conjugate was due to the formation of micellar structures between several ligand molecules or due to polymer-drug interactions, a pyrene assay was conducted. Upon micelle formation, the hydrophobic pyrene exhibits an increased effective aqueous solubility, yielding a measurable increase in fluorescence. Similar to linear PEG, branched PEG can easily form micelles and micelle-like structures when its chain ends are tethered to hydrophobic molecules [49–51]. For 8armPEG40k-EXP3174 at concentrations up to approximately 0.1 % (m/V), which corresponded to the highest tested concentration in the affinity measurements (30 µM), no increase in pyrene fluorescence was observed, indicating that the ligand-PEG conjugate did not form micelle-like structures (Fig. 4A). In contrast, Ceteareth-20, also known as Sympatens ACS/200G, is an amphiphilic linear PEG (20) cetyl/stearyl ether and clearly demonstrated increased pyrene fluorescence and thus formation of micelles over the same range of concentrations (Fig. 4A). Depending on the hydrophobicity of the environment, the emission spectrum of pyrene changes significantly; relative intensities of the five vibronic bands found in the fine structure change noticeably and can be used to probe hydrophobic cavities [52]. The ratio of I_1 (372 nm) to I_3 (383 nm) was 1.7 for pyrene in ultrapure water (Fig. 4B). The vibronic band I_3 is insensitive to the environment whereas I_1 greatly varies upon hydrophobicity changes of the solvent [53]. When pyrene was incubated with an aqueous solution of Ceteareth-20 the I_1/I_3 fluorescence ratio was reduced to 1.0, which clearly indicated changes in the hydrophobicity of the probe environment. However, when pyrene was incubated with an aqueous solution of 8armPEG40k-EXP3174 its emission spectrum was almost identical to the spectrum in water, with a nearly identical I_1/I_3 ratio of 1.7 (Fig. 4B). This demonstrated that pyrene was solely surrounded by water molecules and that polymer-tethered EXP3174 molecules did not form hydrophobic cavities to which pyrene distributed.

To further investigate the influence of ligand hydrophobicity on conjugate affinity for AT_1R, the AT_1R agonist angiotensin II (Ang II) was conjugated to the arms of an 8armPEG20k polymer. As opposed to most ARBs, Ang II is a hydrophilic molecule with good aqueous solubility of about 25 mg/mL. Via reaction with 8armPEG20k-succinimidyl

carbonate, the N-terminal amine group of Ang II was covalently bound to the branched polymer. After conjugation and purification, around 4.6 Ang II molecules were conjugated to each polymer. This 8armPEG20k-Ang II activated the receptor with an EC_{50} of 225 ± 13 nM, which was only 3.2-fold less affine than free Ang II (Fig. 4C). In contrast, 8armPEG40k-EXP3174 had a 200-fold decreased affinity when compared to free EXP3174, which underscores the impact of ligand hydrophobicity on affinity. However, due to different PEG lengths, different receptor binding pockets and different receptor responses upon ligand binding, the comparison of 8armPEG40k-EXP3174 and 8armPEG20k-Ang II must be interpreted with caution.

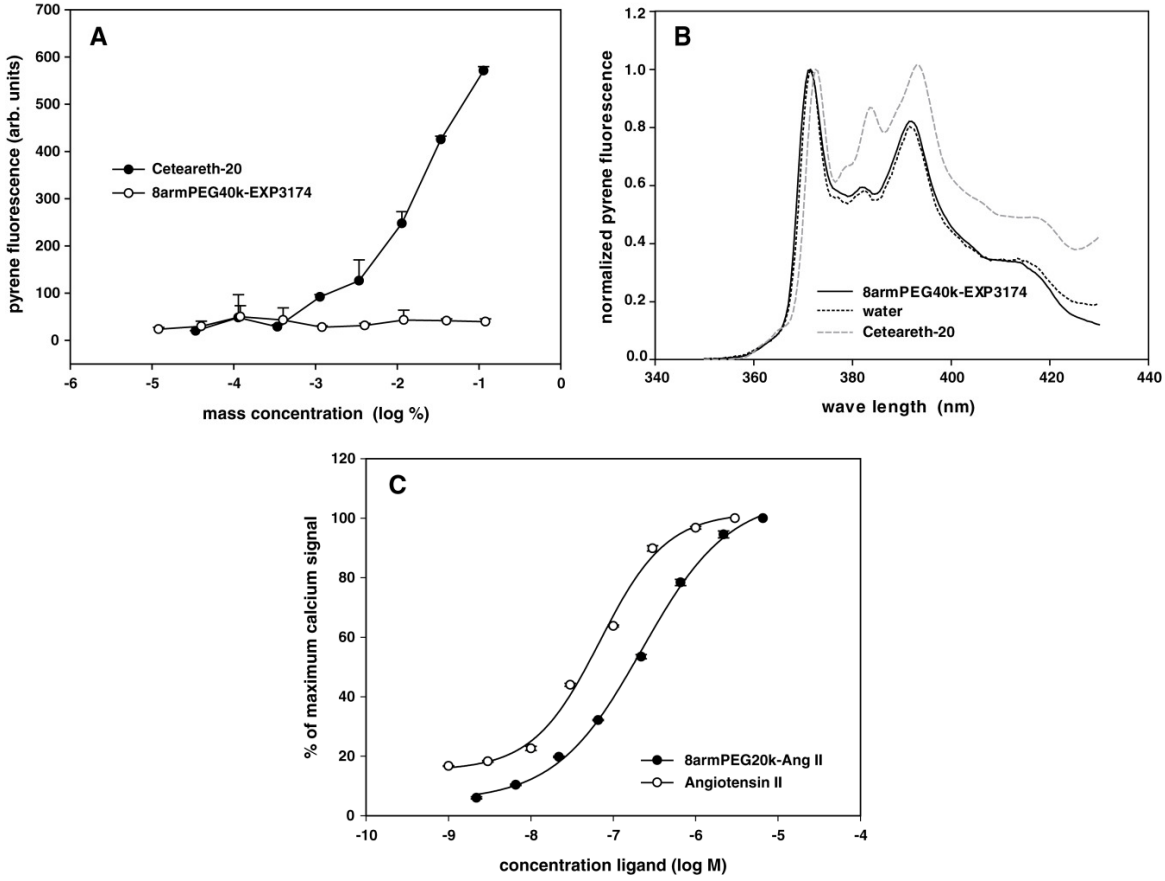

Figure 4: Investigation of the decreased affinity of ligand-conjugated branched PEGs. **(A)** With the help of a pyrene assay the capability of 8armPEG40k-EXP3174 to form micellar structures was investigated. Ceteareth-20, a PEG-containing surfactant, was used as a positive control. **(B)** Pyrene in water and a solution of 8armPEG40k-EXP3174 exhibited similar emission spectra. In a solution of Ceteareth-20 the vibronic bands of pyrene emission clearly changed. **(C)** When the hydrophilic AT_1R ligand angiotensin II was conjugated to an 8armPEG20k polymer its affinity was only decreased by 3.2-fold.

3.4 Conjugate cytotoxicity

Finally, the cytotoxicity of the conjugates and their precursors was assessed using an MTT assay, performed with mouse fibroblast L-929 cells according to ISO 10993-5:2009. First, in 96-well plates, seeded L-929 cells were incubated with PEG polymers or PAMAM

dendrimers for 4 hours. Then, after removal of the test solutions, water-soluble MTT was added to the cells. Viable and active cells reduce MTT to an insoluble purple formazan, whose concentration can be determined after solubilization with sodium dodecyl sulfate.

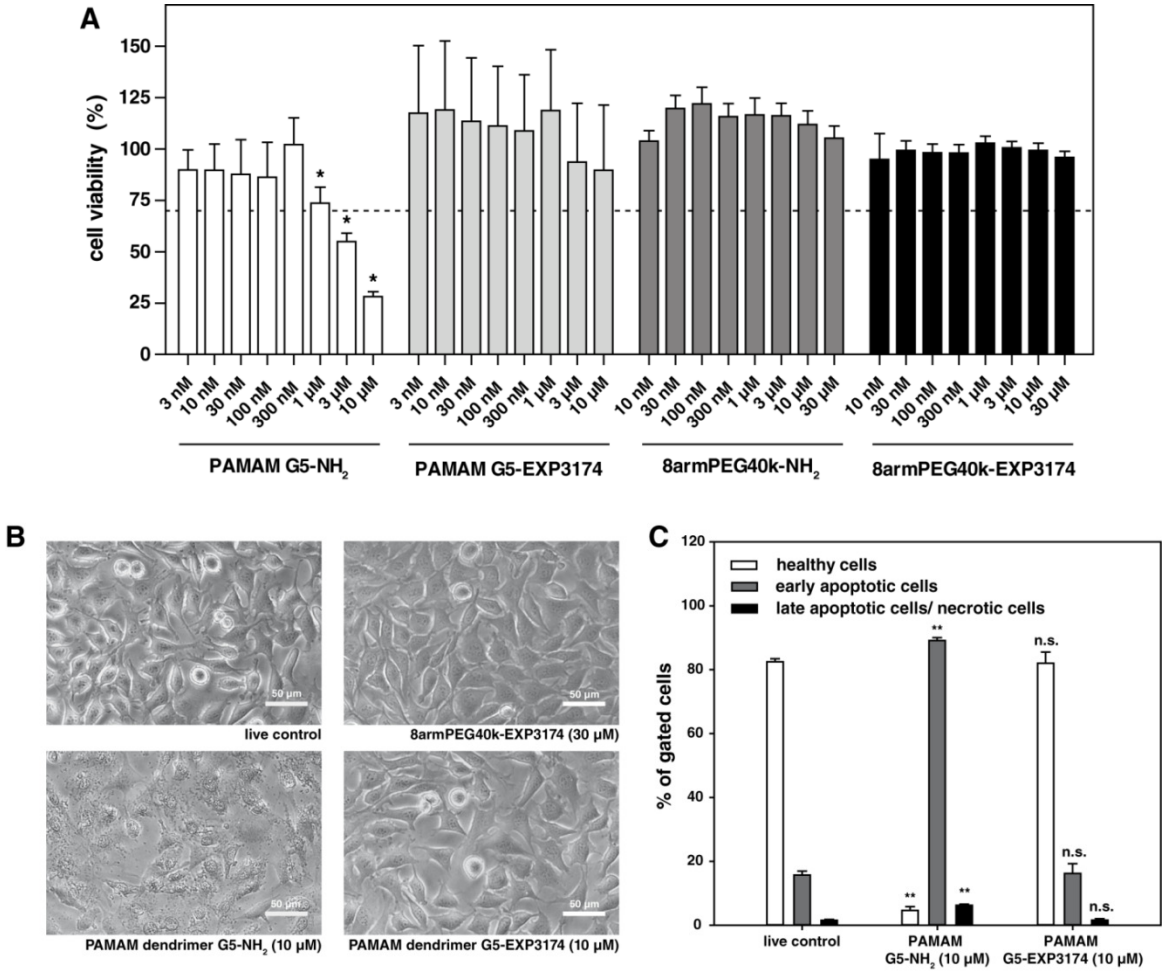

Figure 5: Cytotoxicity of unconjugated and EXP3174-conjugated polymers as tested with an MTT and apoptosis assay. **(A)** Besides the raw PAMAM generation 5 dendrimers, the polymers showed no toxicity in L-929 cells over the range of concentrations within the incubation time of 4 h. The dashed line indicates 70 % cell viability. Levels of statistical significance are indicated as: (*) $p < 0.01$ compared to cell viability of PAMAM G5-EXP3174 at the same concentration **(B)** Microscopic pictures of L-929 cells after 4 h incubation with the respective polymers. Cells incubated with unfunctionalized PAMAM generation 5 dendrimer display severe cellular damage. **(C)** When apoptosis was quantified using phosphatidylserine detection, PAMAM G5-NH_2 but not PAMAM G5-EXP3174 induced apoptosis in L929 cells. Levels of statistical significance are indicated as: (**) $p < 0.01$; (n.s.) $p > 0.05$ compared to live control.

In our tests neither unconjugated 8armPEG40k-NH_2 nor 8armPEG40k-EXP3174 exhibited any cytotoxicity over the tested concentration range, up to 30 µM (Fig. 5A), consistent with the well-known biocompatibility of PEG. In contrast, incubation with unconjugated PAMAM generation 5 dendrimers had a substantial influence on cell viability: after 4 h of incubation the cellular dye-reducing potential decreased to 28 %

compared to the control (Fig. 5A), demonstrating pronounced cell death. The LC_{50} (concentration that leads to 50 % cell death) was 2.7 μM, which agrees well with PAMAM dendrimer cytotoxicity studies by Roberts *et al.* [54]. Due to the high surface density of cationic groups, the dendrimers readily interact with negatively charged cell membranes leading to membrane disruption, pore formation and ultimately, cell death [55]. Microscopic pictures of cells following incubation with plain PAMAM dendrimers further revealed the toxic nature of unconjugated dendrimers (Fig. 5B). A vast amount of cellular debris was visible, which suggested the formation of apoptotic bodies due to the induction of programmed cell death by plain dendrimers. When quantified by a flow cytometry-based apoptosis assay using fluorescently labeled-lactadherin, it was clearly observable that treatment with plain amine-terminated PAMAM dendrimers induced apoptosis in the majority of L929 cells (Fig. 5C). As a result, lactadherin-positive apoptotic bodies were generated upon treatment with plain dendrimers (Supporting information, Fig. S1). This is in line with observations that exposing cells to plain PAMAM dendrimers leads to generation of reactive oxygen species (ROS) [56,57], disruption of the mitochondrial membrane potential [58,59], and ultimately apoptosis. For this reason, several strategies to reduce the inherent toxicity of PAMAM dendrimers have been employed, which include acetylation [60], PEGylation [61] or attachment of small carbohydrates to yield glycodendrimers [62]. Remarkably, PAMAM G5-EXP3174 dendrimers showed no cytotoxicity over the tested range of concentrations, up to 10 μM. None of the concentrations reduced the cell viability below 70 %, which is the threshold of biocompatibility according to ISO 10993-5:2009. Apparently, substitution of approximately 16 of the total 128 surface amine groups significantly altered the toxicity profile for L-929 cells. In contrast to cells that were incubated with unconjugated dendrimers, cells exposed to PAMAM G5-EXP3174 showed neither observable cell toxicity nor alteration of cell morphology (Fig. 5B). Furthermore, PAMAM G5-EXP3174 dendrimers did not induce significant apoptosis (Fig. 5C) or formation of apoptotic bodies (Supporting information, Fig. S1) in L929 cells, which was in stark contrast to amine-terminated PAMAM dendrimers.

However, in scenarios where further derivatization or bioconjugation is intended, the substantial number of surface-facing functional groups per dendrimer molecule can be considered a distinct advantage. Aside from the amino groups used for ligand conjugation, the remaining amines can be utilized to attach fluorescent or radioactive labels, which help track the polymers in cell culture and *in vivo* environments.

Commercially available isothiocyanates or NHS-esters of fluorophores and chelating agents readily react with these amine groups. NHS-esters of anionic chelators show especially high conjugation efficiency when reacted with dendrimers, due to strong electrostatic interactions between the anionic NHS esters and the cationic dendrimer surface [63]. If desired, unnecessary surface amine groups can be acetylated to yield multi-functional drug delivery platforms.

Table 1
Overview of native EXP3174 and the synthesized ligand-coupled polymers

conjugate	# EXP3174 ligands	# unreacted amines	Conjugate affinity (nM)	Affinity per ligand (nM)	Toxicity, IC_{50} (μM)
EXP3174	1	n/a	1.1 ± 0.2 [16]	1.1 ± 0.2	n/a
mPEG5k-EXP3174	1	0	630 ± 130 [16]	630 ± 130	n/a
8armPEG40K-EXP3174	7.8	0.2	224 ± 34	1750	> 30
PAMAM G5-EXP3174	16.7	111.3	36.3 ± 4.6	606	> 30

4 Conclusions

Multivalent polymer-drug conjugates that bind and block AT_1R have been successfully synthesized. Conjugation of EXP3174 to generation 5 PAMAM dendrimers resulted in a higher overall and per-ligand affinity than the branched PEG conjugates, presumably due to hydrophobic ligand-polymer interactions that masked the ligand. EXP3174 conjugation to dendrimers, and the concomitant reduction of surface amine groups, resulted in a significant decrease in the toxicity of the conjugate relative to the original dendrimer. Optimization of ligand density on PAMAM dendrimers could further increase the degree of multivalency, and hence increase the overall affinity. Derivatization of the remaining amine groups with fluorescence or radioactive labels could help track the *in vitro* or *in vivo* fate of these conjugates. This is the first study to report polymer-drug conjugates that effectively block angiotensin receptors.

References

[1] C.J. Moravski, D.J. Kelly, M.E. Cooper, R.E. Gilbert, J.F. Bertram, S. Shahinfar, S.L. Skinner, J.L. Wilkinson-Berka, Retinal neovascularization is prevented by blockade of the renin-angiotensin system, Hypertension 36 (2000) 1099–1104.

[2] N. Nagai, K. Izumi-Nagai, Y. Oike, T. Koto, S. Satofuka, Y. Ozawa, K. Yamashiro, M. Inoue, K. Tsubota, K. Umezawa, S. Ishida, Suppression of diabetes-induced retinal inflammation by blocking the angiotensin II type 1 receptor or its downstream nuclear factor-kappaB pathway, Invest. Ophthalmol. Vis. Sci. 48 (2007) 4342–4350.

[3] S. Nakamura, K. Tsuruma, M. Shimazawa, H. Hara, Candesartan, an angiotensin II type 1 receptor antagonist, inhibits pathological retinal neovascularization by downregulating VEGF receptor-2 expression, Eur. J. Pharmacol. 685 (2012) 8–14.

[4] N. Chaturvedi, M. Porta, R. Klein, T. Orchard, J. Fuller, H.H. Parving, R. Bilous, A.K. Sjølie, Effect of candesartan on prevention (DIRECT-Prevent 1) and progression (DIRECT-Protect 1) of retinopathy in type 1 diabetes: randomised, placebo-controlled trials, Lancet 372 (2008) 1394–1402.

[5] Z.H. Israili, Clinical pharmacokinetics of angiotensin II (AT1) receptor blockers in hypertension, J. Hum. Hypertens. 14 Suppl 1 (2000) S73-86.

[6] D.T. Dinh, A.G. Frauman, C.I. Johnston, M.E. Fabiani, Angiotensin receptors: distribution, signalling and function, Clin. Sci. 100 (2001) 481–492.

[7] I.S. Byon, H.S. Jeon, H.W. Kim, S.J. Lee, J.E. Lee, B.S. Oum, The effect of a systemic angiotensin receptor blocker on vascular endothelial growth factor in the vitreous of patients with proliferative diabetic retinopathy, Curr. Eye Res. 38 (2013) 774–780.

[8] T.U. Krohne, N. Eter, F.G. Holz, C.H. Meyer, Intraocular pharmacokinetics of bevacizumab after a single intravitreal injection in humans, Am. J. Ophthalmol. 146 (2008) 508–512.

[9] J.E. Lee, D.W. Lim, H.J. Park, J.H. Shin, S.M. Lee, B.S. Oum, Intraocular toxicity and pharmacokinetics of candesartan in a rabbit model, Invest. Ophthalmol. Vis. Sci. 52 (2011) 2924–2929.

[10] A.A. Moshfeghi, C.A. Puliafito, Pegaptanib sodium for the treatment of neovascular age-related macular degeneration, Expert Opin. Investig. Drugs 14 (2005) 671–682.

[11] C.S. Fishburn, The pharmacology of PEGylation: balancing PD with PK to generate novel therapeutics, J. Pharm. Sci. 97 (2008) 4167–4183.

[12] N.A. Alcantar, E.S. Aydil, J.N. Israelachvili, Polyethylene glycol-coated biocompatible surfaces, J. Biomed. Mater. Res. 51 (2000) 343–351.

[13] R.E. Kontermann, Strategies for extended serum half-life of protein therapeutics, Curr. Opin. Biotechnol. 22 (2011) 868–876.

[14] R. Iezzi, B.R. Guru, I.V. Glybina, M.K. Mishra, A. Kennedy, R.M. Kannan, Dendrimer-based targeted intravitreal therapy for sustained attenuation of neuroinflammation in retinal degeneration, Biomaterials 33 (2012) 979–988.

[15] S.P. Kambhampati, Clunies-Ross, Alexander J M, I. Bhutto, M.K. Mishra, M. Edwards, D.S. McLeod, R.M. Kannan, G. Lutty, Systemic and Intravitreal Delivery of Dendrimers to Activated Microglia/Macrophage in Ischemia/Reperfusion Mouse Retina, Investigative ophthalmology & visual science 56 (2015) 4413–4424.

[16] R. Hennig, K. Pollinger, A. Veser, M. Breunig, A. Goepferich, Nanoparticle multivalency counterbalances the ligand affinity loss upon PEGylation, J. Control. Release 194C (2014) 20–27.

[17] R. Duncan, L. Izzo, Dendrimer biocompatibility and toxicity, Adv. Drug Deliv. Rev. 57 (2005) 2215–2237.

[18] Y.-Y. Jiang, G.-T. Tang, L.-H. Zhang, S.-Y. Kong, S.-J. Zhu, Y.-Y. Pei, PEGylated PAMAM dendrimers as a potential drug delivery carrier: in vitro and in vivo comparative evaluation of covalently conjugated drug and noncovalent drug inclusion complex, J. Drug Target. 18 (2010) 389–403.

[19] P. Kolhe, E. Misra, R.M. Kannan, S. Kannan, M. Lieh-Lai, Drug complexation, in vitro release and cellular entry of dendrimers and hyperbranched polymers, Int. J. Pharm. 259 (2003) 143–160.

[20] C.A. Dougherty, J.C. Furgal, van Dongen, Mallory A, T. Goodson, Banaszak Holl, Mark M, J. Manono, S. DiMaggio, Isolation and characterization of precise dye/dendrimer ratios, Chemistry 20 (2014) 4638–4645.

[21] C. Wängler, G. Moldenhauer, R. Saffrich, E.-M. Knapp, B. Beijer, M. Schnölzer, B. Wängler, M. Eisenhut, U. Haberkorn, W. Mier, PAMAM structure-based multifunctional fluorescent conjugates for improved fluorescent labelling of biomacromolecules, Chemistry 14 (2008) 8116–8130.

[22] G. Grynkiewicz, M. Poenie, R.Y. Tsien, A new generation of Ca2+ indicators with greatly improved fluorescence properties, J. Biol. Chem. 260 (1985) 3440–3450.

[23] F. Brandl, N. Hammer, T. Blunk, J. Tessmar, A. Goepferich, Biodegradable hydrogels for time-controlled release of tethered peptides or proteins, Biomacromolecules 11 (2010) 496–504.

[24] M.A. Ritter, C.I. Furtek, M.W. Lo, An improved method for the simultaneous determination of losartan and its major metabolite, EXP3174, in human plasma and urine by high-performance liquid chromatography with fluorescence detection, J. Pharm. Biomed. Anal. 15 (1997) 1021–1029.

[25] M.A. van Dongen, A. Desai, B.G. Orr, J.R. Baker, M.M. Banaszak Holl, Quantitative analysis of generation and branch defects in G5 poly(amidoamine) dendrimer, Polymer 54 (2013) 4126–4133.

[26] M.A. van Dongen, B.G. Orr, M.M. Banaszak Holl, Diffusion NMR study of generation-five PAMAM dendrimer materials, J. Phys. Chem. B 118 (2014) 7195–7202.

[27] M. de Gasparo, K.J. Catt, T. Inagami, J.W. Wright, T. Unger, International union of pharmacology. XXIII. The angiotensin II receptors, Pharmacol. Rev. 52 (2000) 415–472.

[28] C. Huang, Q. Ramadan, J.B. Wacker, H.C. Tekin, C. Ruffert, G. Vergères, P. Silacci, Gijs, M. A. M., Microfluidic chip for monitoring Ca 2+ transport through a confluent layer of intestinal cells, RSC Adv 4 (2014) 52887–52891.

[29] Q. Mu, T. Hu, J. Yu, Molecular insight into the steric shielding effect of PEG on the conjugated staphylokinase: biochemical characterization and molecular dynamics simulation, PLoS ONE 8 (2013) e68559.

[30] B. Treetharnmathurot, C. Ovartlarnporn, J. Wungsintaweekul, R. Duncan, R. Wiwattanapatapee, Effect of PEG molecular weight and linking chemistry on the biological activity and thermal stability of PEGylated trypsin, Int. J. Pharm. 357 (2008) 252–259.

[31] C.J. Fee, J.M. Van Alstine, Prediction of the viscosity radius and the size exclusion chromatography behavior of PEGylated proteins, Bioconjug. Chem. 15 (2004) 1304–1313.

[32] H. García-Arellano, B. Valderrama, G. Saab-Rincón, R. Vazquez-Duhalt, High Temperature Biocatalysis by Chemically Modified Cytochrome c, Bioconjug. Chem. 13 (2002) 1336–1344.

[33] D.D. Christ, Human plasma protein binding of the angiotensin II receptor antagonist losartan potassium (DuP 753/MK 954) and its pharmacologically active metabolite EXP3174, J. Clin. Pharmacol. 35 (1995) 515–520.

[34] Y.-D. Yan, H.-K. Kim, K.-H. Seo, W.S. Lee, G.-S. Lee, J.-S. Woo, C.-S. Yong, H.-G. Choi, The Physicochemical Properties, in Vitro Metabolism and Pharmacokinetics of a Novel Ester Prodrug of EXP3174, Mol. Pharm. 7 (2010) 2132–2140.

[35] D. Cakara, J. Kleimann, M. Borkovec, Microscopic Protonation Equilibria of Poly(amidoamine) Dendrimers from Macroscopic Titrations, Macromolecules 36 (2003) 4201–4207.

[36] Y. Niu, L. Sun, R.M. Crooks, Determination of the Intrinsic Proton Binding Constants for Poly(amidoamine) Dendrimers via Potentiometric pH Titration, Macromolecules 36 (2003) 5725–5731.

[37] A. Ramzi, R. Scherrenberg, J. Brackman, J. Joosten, K. Mortensen, Intermolecular Interactions between Dendrimer Molecules in Solution Studied by Small-Angle Neutron Scattering, Macromolecules 31 (1998) 1621–1626.

[38] S. Svenson, D.A. Tomalia, Dendrimers in biomedical applications--reflections on the field, Adv. Drug Deliv. Rev. 57 (2005) 2106–2129.

[39] P.K. Maiti, T. Çağın, S.-T. Lin, W.A. Goddard, Effect of Solvent and pH on the Structure of PAMAM Dendrimers, Macromolecules 38 (2005) 979–991.

[40] G.M. Pavan, L. Albertazzi, A. Danani, Ability to adapt: different generations of PAMAM dendrimers show different behaviors in binding siRNA, J. Phys. Chem. B 114 (2010) 2667–2675.

[41] S.L. Mangold, M.J. Cloninger, Binding of monomeric and dimeric Concanavalin A to mannose-functionalized dendrimers, Org. Biomol. Chem. 4 (2006) 2458–2465.

[42] S. Hong, P.R. Leroueil, I.J. Majoros, B.G. Orr, J.R. Baker, M.M. Banaszak Holl, The binding avidity of a nanoparticle-based multivalent targeted drug delivery platform, Chem. Biol. 14 (2007) 107–115.

[43] D.K. Tosh, L.S. Yoo, M. Chinn, K. Hong, S.M. Kilbey, M.O. Barrett, I.P. Fricks, T.K. Harden, Z.-G. Gao, K.A. Jacobson, Polyamidoamine (PAMAM) dendrimer conjugates of "clickable" agonists of the A3 adenosine receptor and coactivation of the P2Y14 receptor by a tethered nucleotide, Bioconjug. Chem. 21 (2010) 372–384.

[44] M.A. van Dongen, J.E. Silpe, C.A. Dougherty, A.K. Kanduluru, S.K. Choi, B.G. Orr, P.S. Low, Banaszak Holl, Mark M, Avidity mechanism of dendrimer-folic acid conjugates, Mol. Pharm. 11 (2014) 1696–1706.

[45] X. Bao, W. Wang, C. Wang, Y. Wang, J. Zhou, Y. Ding, X. Wang, Y. Jin, A chitosan-graft-PEI-candesartan conjugate for targeted co-delivery of drug and gene in anti-angiogenesis cancer therapy, Biomaterials 35 (2014) 8450–8466.

[46] J. Ruckman, L.S. Green, J. Beeson, S. Waugh, W.L. Gillette, D.D. Henninger, L. Claesson-Welsh, N. Janjić, 2'-Fluoropyrimidine RNA-based aptamers to the 165-amino acid form of vascular endothelial growth factor (VEGF165). Inhibition of receptor binding and VEGF-induced vascular permeability through interactions requiring the exon 7-encoded domain, J. Biol. Chem. 273 (1998) 20556–20567.

[47] D.W. Drolet, J. Nelson, C.E. Tucker, P.M. Zack, K. Nixon, R. Bolin, M.B. Judkins, J.A. Farmer, J.L. Wolf, S.C. Gill, R.A. Bendele, Pharmacokinetics and safety of an anti-vascular endothelial growth factor aptamer (NX1838) following injection into the vitreous humor of rhesus monkeys, Pharm. Res. 17 (2000) 1503–1510.

[48] E.W.M. Ng, D.T. Shima, P. Calias, E.T. Cunningham, D.R. Guyer, A.P. Adamis, Pegaptanib, a targeted anti-VEGF aptamer for ocular vascular disease, Nat. Rev. Drug Discov. 5 (2006) 123–132.

[49] P. Jie, S.S. Venkatraman, F. Min, Freddy, Boey Yin Chiang, G.L. Huat, Micelle-like nanoparticles of star-branched PEO-PLA copolymers as chemotherapeutic carrier, J. Control. Release 110 (2005) 20–33.

[50] H. Ding, K.-T. Yong, I. Roy, R. Hu, F. Wu, L. Zhao, W.-C. Law, W. Zhao, W. Ji, L. Liu, E.J. Bergey, P.N. Prasad, Bioconjugated PLGA-4-arm-PEG branched polymeric nanoparticles as novel tumor targeting carriers, Nanotechnology 22 (2011) 165101.

[51] I. Orienti, G. Zuccari, M. Falconi, G. Teti, N.A. Illingworth, G.J. Veal, Novel micelles based on amphiphilic branched PEG as carriers for fenretinide, Nanomedicine 8 (2012) 880–890.

[52] K. Kalyanasundaram, J.K. Thomas, Environmental effects on vibronic band intensities in pyrene monomer fluorescence and their application in studies of micellar systems, J. Am. Chem. Soc. 99 (1977) 2039–2044.

[53] A. Nakajima, Fluorescence spectra of anthracene and pyrene in water and in aqueous surfactant solution, J. Lumin. 15 (1977) 277–282.

[54] J.C. Roberts, M.K. Bhalgat, R.T. Zera, Preliminary biological evaluation of polyamidoamine (PAMAM) StarburstTM dendrimers, J. Biomed. Mater. Res. 30 (1996) 53–65.

[55] K. Jain, P. Kesharwani, U. Gupta, N.K. Jain, Dendrimer toxicity: Let's meet the challenge, Int. J. Pharm. 394 (2010) 122–142.

[56] W. Wang, W. Xiong, J. Wan, X. Sun, H. Xu, X. Yang, The decrease of PAMAM dendrimer-induced cytotoxicity by PEGylation via attenuation of oxidative stress, Nanotechnology 20 (2009) 105103.

[57] P.C. Naha, M. Davoren, F.M. Lyng, H.J. Byrne, Reactive oxygen species (ROS) induced cytokine production and cytotoxicity of PAMAM dendrimers in J774A.1 cells, Toxicol. Appl. Pharmacol. 246 (2010) 91–99.

[58] M. Labieniec, T. Gabryelak, Preliminary biological evaluation of poli(amidoamine) (PAMAM) dendrimer G3.5 on selected parameters of rat liver mitochondria, Mitochondrion 8 (2008) 305–312.

[59] J.-H. Lee, K.E. Cha, M.S. Kim, H.W. Hong, D.J. Chung, G. Ryu, H. Myung, Nanosized polyamidoamine (PAMAM) dendrimer-induced apoptosis mediated by mitochondrial dysfunction, Toxicol. Lett. 190 (2009) 202–207.

[60] C.L. Waite, S.M. Sparks, K.E. Uhrich, C.M. Roth, Acetylation of PAMAM dendrimers for cellular delivery of siRNA, BMC Biotechnol. 9 (2009) 38.

[61] K. Fant, E.K. Esbjörner, A. Jenkins, M.C. Grossel, P. Lincoln, B. Nordén, Effects of PEGylation and acetylation of PAMAM dendrimers on DNA binding, cytotoxicity and in vitro transfection efficiency, Mol. Pharm. 7 (2010) 1734–1746.

[62] M. Labieniec, C. Watala, PAMAM dendrimers — diverse biomedical applications. Facts and unresolved questions, Cent. Eur. J. Biol. 4 (2009) 434–451.

[63] D. Zhou, S.H. Kim, V.M. Carroll, C.S. Dence, J.A. Katzenellenbogen, Utilizing electrostatic interactions to facilitate F-18 radiolabeling of poly(amido)amine (PAMAM) dendrimers, Org. Biomol. Chem. 12 (2014) 8696–8701.

Branched polymer-drug conjugates for multivalent blockade of angiotensin II receptors

Flow cytometric apoptosis detection

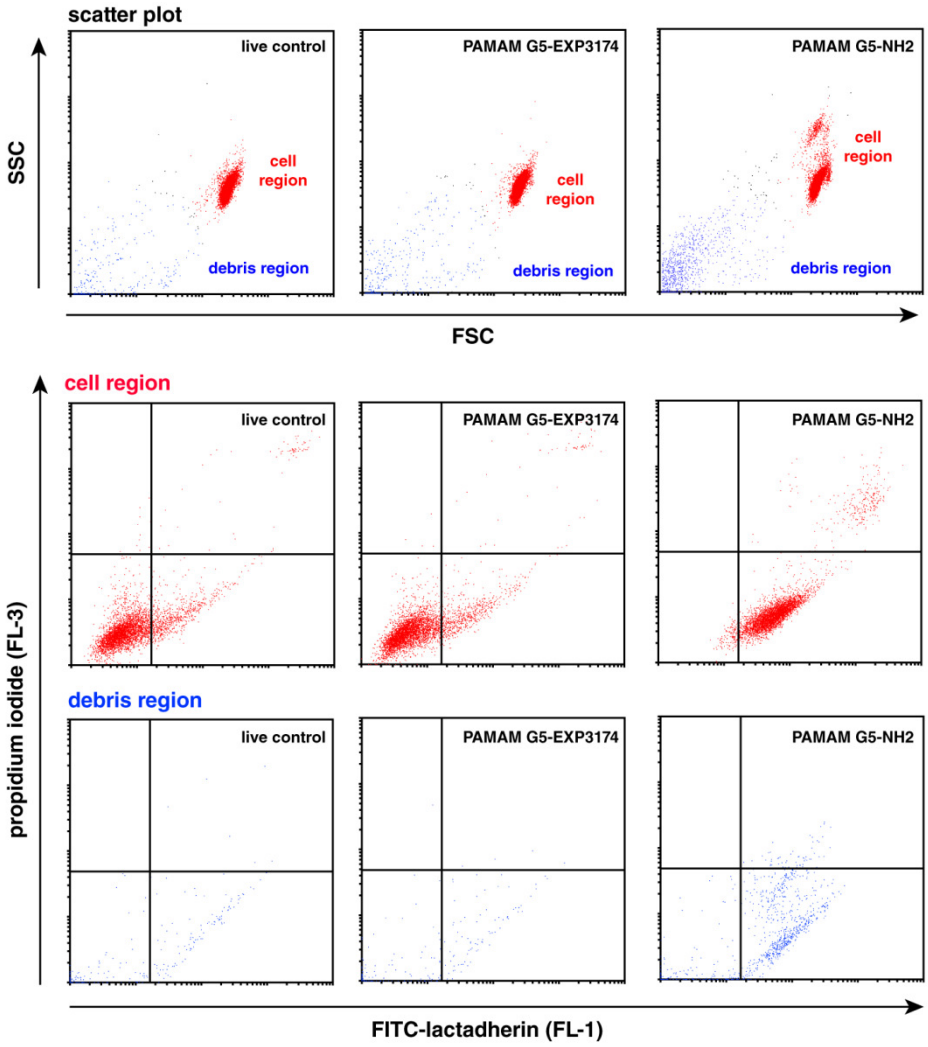

Figure S1: Flow cytometry analysis of apoptosis induced by PAMAM G5 dendrimers. A 4 hour incubation of L929 cells with 10 µM PAMAM G5-NH_2 led to distinct apoptosis in the majority of cells as shown by lactadherin binding to externalized phosphatidylserine. In contrast, 10 µM PAMAM G5-EXP3174 induced no apoptotic events. Upon treatment with PAMAM G5-NH_2, lactadherin-positive apoptotic bodies are formed.

Chapter 6

Multivalent targeting of AT_1 receptors with angiotensin II-functionalized nanoparticles

Published in Journal of Drug Targeting
2015, 23, 681–689

This chapter was published as: R. Hennig, K. Pollinger, J. Tessmar and A. Goepferich, J. Drug Targeting 2015, 23, 681–689, doi: 10.3109/1061186X.2015.1035276. Data that was not obtained nor analyzed by R. Hennig is highlighted.

Abstract

The angiotensin II receptor type 1 (AT_1R) is a G protein-coupled receptor of paramount significance since it is overexpressed in a number of diseased tissues that are highly attractive for nanoparticle targeting. However, it is also expressed at physiological levels in healthy tissue. Multivalent interactions mediated by multiple AT_1R-binding moieties per nanoparticle could promote a high binding avidity to AT_1R overexpressing cells and concomitantly spare off-target tissue. To investigate the feasibility of this approach, angiotensin II was thiolated and conjugated to PEGylated quantum dots. Nanoparticle binding, uptake and affinity to several cell lines was investigated in detail. The colloids were rapidly taken up by clathrin-mediated endocytosis into AT_1R-expressing cells and showed no interaction with receptor negative cells. The EC_{50} of the thiolated angiotensin II was determined to be 261 nM, whereas the ligand-conjugated Qdots activated the receptor with an EC_{50} of 8.9 nM. This 30-fold higher affinity of the nanoparticles compared to the unconjugated peptide clearly demonstrated the presence of multivalent effects when using agonist-targeted nanoparticles. Our study provides compelling evidence that, despite being immediately endocytosed, Ang II-coupled nanoparticles exert potent multivalent ligand-receptor interactions that can be used to establish high affinities to an AT_1R overexpressing cell and tissue.

1 Introduction

The angiotensin II receptor type 1 (AT_1R) is an attractive target for nanoparticle-based drug delivery due to its marked overexpression in severe pathologies such as myocardial infarctions [1,2], cancer [3,4] or choroidal neovascularization [5]. With the present work we demonstrate that nanoparticles to which the physiological ligand angiotensin II (Ang II) is conjugated are able to bind cells expressing the AT_1 receptor in a multivalent nature. Although particles with similar targeting moieties have already been prepared for targeting the infarcted heart [2] and for studying receptor trafficking routes [6,7], the ability of AT_1R-targeted nanoparticles to bind several receptors simultaneously has never been investigated. In situations such as this, where targeting of a receptor present in both healthy and diseased tissue is desirable, multivalency allows for preferential binding of ligand-targeted nanoparticles to cells that overexpress the targeted receptor [8]. Concomitantly, interactions with off-target cells that express the receptor at a lower level can be minimized. In the case of the AT_1R this is of fundamental importance since AT_1 receptors, which are usually known for their role in blood pressure regulation and fluid retention, are not only overexpressed in diseased tissue but also expressed at physiological levels within off-target tissues like the endothelium [9] or the kidney glomerulus [10,11]. Both are exposed to intravenously administered nanoparticles during their circulation in the blood [12] and are prone to off-target nanoparticle binding [13,14].

We recently demonstrated that angiotensin receptor blockers (ARBs), when immobilized on a nanoparticle surface, bind AT_1 receptors by a multi-ligand binding mechanism [15]. However, ARBs do not provoke receptor internalization after binding [16]. This gives the ARB-conjugated particles sufficient time to reach out to further receptors on the cell surface and consequently build up a strong multivalent binding. In contrast to the antagonists, the agonist Ang II immediately induces receptor internalization after binding [17], which we hypothesized could impair the formation of stable multivalent interactions. Furthermore, we were interested if nanoparticles would still be taken up by cells, despite crosslinking several receptors, and thus, exhibiting multivalent attachment to the cell surface. Multivalent interactions between cells and nanoparticles have already been reported for other important receptors such as transferrin receptor [18,19], folate receptor [20,21] or the human epidermal growth factor receptor 2 (HER2) [22,23].

To gain insight into the multivalent nature of Ang II-coupled nanoparticles, the ligand was coupled to highly fluorescent core-shell quantum dots (Qdots). Flow cytometry and

confocal microscopy were utilized to investigate nanoparticle endocytosis, subcellular localization and mechanism of uptake. Changes in intracellular calcium concentrations induced by both the soluble ligands and the ligands conjugated to the nanoparticle surface were measured to quantify the degree of nanoparticle multivalency towards AT_1 receptors.

2 Material and methods

2.1 Materials

Qdots® 655 ITK™ amino PEG (#Q21521MP, Life Technologies, Carlsbad, CA, USA) were used as nanoparticle starting material. Losartan carboxylic acid, also known as EXP3174, was purchased from Santa Cruz (Heidelberg, Germany). All chemicals were obtained from Sigma Aldrich (Taufkirchen, Germany) in analytical grade unless stated otherwise and used without further purification. Ultrapure water was obtained from a Milli-Q water purification system (Millipore, Billerica, MA, USA). Dulbecco's phosphate buffered saline (DPBS) pH 7.40, which was used for nanoparticle purification and cell experiments, consisting of 1.5 mM KH_2PO_4, 8 mM Na_2HPO_4, 2.7 mM KCl and 138 mM NaCl, was purchased from Life Technologies (Carlsbad, CA, USA).

2.2 Cell culture

Rat mesangial cells were a kind gift from Dr. Armin Kurtz (Department of Physiology, University of Regensburg, Germany) and were cultured in RPMI1640 medium containing 10 % fetal bovine serum (Sigma Aldrich, Taufkirchen, Germany) supplemented with insulin-transferrin-selenium (Life Technologies, Carlsbad, CA, USA), penicillin-streptomycin (Life Technologies, Carlsbad, CA, USA) and 100 nM hydrocortisone. Human adrenal gland carcinoma cells NCI-H295R (ATCC No. CRL-2128) were maintained in the same medium. HeLa cells (ATCC No. CCL-2) were cultured in Eagle's Minimum Essential Medium (EMEM) containing 10 % fetal calf serum (FCS) and 1 mM sodium pyruvate. All cells were cultured in T-75 cell culture flasks (Corning, Corning, NY, USA).

2.3 Thiolation of angiotensin II

1.5 µmol angiotensin II (Bachem, Bubendorf, Switzerland) was reacted with 1.875 µmol 2-iminothiolane HCl in borate buffer pH 8.00 (50 mM) for 24 h at room temperature. The resulting N-substituted 2-iminothiolate intermediate was hydrolyzed for 48 hours in

acetate buffer pH 5.00 (100 mM), to which ethylenedinitrilotetraacetic acid disodium salt (Merck, Darmstadt, Germany) in a concentration of 1 mM was added.

To quantify the amount of reactive thiol groups, an Ellman's assay was performed. Briefly, a sample of thiolated peptide was incubated with (5,5'-dithiobis-(2-nitrobenzoic acid) (DTNB) in phosphate buffer pH 8.00 (100 mM) for 15 min and analyzed on a UVIKON 900 double-beam spectrophotometer (Kontron instruments, Milan, Italy) at a wavelength of 412 nm. Using a molar extinction coefficient of 14,150 $M^{-1}cm^{-1}$ the concentration of the thiolated peptide was quantified. Purity and conversion were further analyzed by high-performance liquid chromatography (HPLC) and electrospray ionization mass spectrometry (ESI-MS). The HPLC system consisted of a Shimadzu LC-10ATVP pump (Shimadzu, Duisburg, Germany), a Shimadzu SIL-10ADVP autosampler connected to a Shimadzu SPD-10A UV-Vis detector. A Luna® 5 µm C18(2) 100 Å 250 x 4.60 mm LC column (Phenomenex, Aschaffenburg, Germany) was used as stationary phase. The peptides were analyzed based on a linear acetonitrile–trifluoroacetic acid (TFA)–water gradient with a flow rate of 1 mL/min. Elution was obtained by using the following gradient of solvents A (0.1 % (v/v) TFA in water) and B (0.1 % (v/v) TFA in acetonitrile): 90:10 (A:B) to 30:70 in 15 min and reequilibration to 90:10 in the following 7 min. The column was operated at 35 °C and the peptides were detected at 275 nm, at which angiotensin II has an absorbance maximum. ESI-MS spectra were recorded on a Q-TOF 6540 UHD system (Agilent Technologies, Böblingen, Germany).

2.4 Conjugation of thiolated Ang II to PEGylated Qdots

160 pmol Qdots® 655 ITK™ amino PEG were activated in borate buffer pH 8.50 (50 mM) with 160 nmol sulfosuccinimidyl-4-(N-maleimidomethyl)cyclohexane-1-carboxylate (sulfo-SMCC) (Thermo Fisher, Waltham, MA, USA) at room temperature. After 1 h of gentle shaking the activated Qdots were purified from unreacted sulfo-SMCC by size exclusion chromatography using a Sephadex G-25 resin in a PD-10 column (GE Healthcare, Munich, Germany) with DPBS as eluent. Fractions containing activated Qdots were collected and pooled. Subsequently, 16 nmol of thiolated angiotensin II (100-fold excess) were added to the pooled, purified and maleimide-activated Qdots and reacted for 1 h at room temperature to yield a stable thioether bond. Unreacted maleimide groups on the nanoparticle surface were inactivated with a 100-fold excess of 2-mercaptoethanol for 30 min. The reaction mixture was purified from excess peptide and 2-mercaptoethanol by ultrafiltration using a 100 kDa molecular weight cut-off Amicon

Ultra-4 filter unit (Millipore, Billerica, MA, USA) for 10 min at 1500 g and size exclusion chromatography as described above. Finally the Qdot solution was up-concentrated by ultrafiltration. Qdot concentration was determined by fluorescence measurements using a FluoStar Omega fluorescence microplate reader (BMG Labtech, Ortenberg, Germany) with an excitation and emission wavelength of 450 nm and 650 nm, respectively.

2.5 Flow cytometry

The binding of nanoparticles to receptor positive and receptor negative cell lines was quantified by flow cytometry measurements. NCI-H295R cells, rat mesangial cells and HeLa cells were seeded into 24-well plates (Corning, Corning, NY, USA) at a density of 150,000 cells/well (NCI-H295R) or 100,000 cells/well (HeLa cells, rat mesangial cells). After the cells had been seeded and allowed to grow inside the 24 well-plates for 48 h, they were washed with DPBS. Pre-warmed nanoparticle solutions were then added to the cell monolayer. Qdot solutions of non-targeted and Ang II-targeted Qdots were prepared in Leibovitz's medium (Life Technologies, Carlsbad, CA, USA) at a concentration of 10 nM and supplemented with 0.1 % bovine serum albumin. After a 1 h nanoparticle incubation at 37 °C, the cells were vigorously washed with DPBS and trypsinized. Leibovitz's medium containing 10 % FCS was added to the cells to quench the trypsin activity. After resuspension of the cells, they were centrifuged (5 min, 200 g), resuspended in DPBS, centrifuged again (5 min, 200 g) and finally resuspended in 200 µL DPBS. The cells were analyzed for fluorescence with a FACSCalibur flow cytometer (Becton Dickinson, Franklin Lakes, NJ, USA). Qdot fluorescence was elicited by excitation at 488 nm and the fluorescence was analyzed using a 661/16 nm FL4 bandpass filter. The resulting data was analyzed using WinMDI 2.9 (The Scripps Research Institute, San Diego, CA, USA). Only the population of intact cells was gated and used for the analysis of cellular fluorescence. The geometrical mean, which was used for further analysis and statistics, was determined from the fluorescence histogram.

2.6 Confocal laser scanning microscopy

NCI-H295R cells and rat mesangial cells were seeded into 8-well µ-slides (Ibidi, Martinsried, Germany) at a density of 15,000 cells/well (NCI-H295R) and 10,000 cells/well (rat mesangial cells). After the cells had adhered to the cell culture plastic, nanoparticle binding was assessed. First, cells were washed with warm DPBS. Then, pre-warmed nanoparticle solutions in Leibovitz's medium supplemented with 0.1 % bovine serum albumin (BSA) were pipetted onto the cells and incubated for 1 hour at 37 °C.

After the incubation period, cells were vigorously washed with DPBS. Live cells were analyzed in Leibovitz's medium. Confocal analysis of nanoparticle binding to the cells was performed with a Zeiss Axiovert 200 microscope combined with a LSM 510 laser-scanning device using a 63x Plan-Apochromat (NA 1.4) oil immersion objective (Zeiss, Jena, Germany). Qdot fluorescence was elicited by excitation at 488 nm with an argon laser and recorded after filtering with a 650 nm longpass filter. The confocal pinhole was set to 150 µm, which corresponds to a focal plane of 1.1 µm. For image acquisition AIM 4.2 software (Zeiss, Jena, Germany) was used. Images were processed using ImageJ (NIH, Bethesda, MD, USA, http://imagej.nih.gov/ij).

For colocalization studies NCI-H295R cells and rat mesangial cells were simultaneously incubated with 10 nM Ang II-Qdots and 5 µg/mL Alexa Fluor® 488-labeled transferrin (Life Technologies, Carlsbad, CA, USA) in Leibovitz's medium supplemented with 0.1 % BSA for 30 min. After washing with DPBS the adhering cells were analyzed. The green Alexa Fluor® 488 dye was excited with a 488 nm argon laser and its fluorescence recorded using a 505-530 nm bandpass filter.

2.7 Intracellular calcium measurements

The intracellular calcium concentration was measured via a microscope and plate reader-based system using the ratiometric fluorescent calcium chelator Fura-2. For microscopic analysis, NCI-H295R cells were grown on cell culture dishes (Corning, Corning, NY, USA) and loaded with 5 µM Fura-2AM (Life Technologies, Carlsbad, CA, USA) in the presence of 1X PowerLoad™ permeabilizing reagent (Life Technologies, Carlsbad, CA, USA) in a Ringer type buffer (5 mM HEPES, 138.9 mM NaCl, 3.6 mM KCl, 1 mM $MgCl_2$, 1.3 mM $CaCl_2$, 1.6 mM Na_2HPO_4 and 5.4 mM NaH_2PO_4 at pH 7.40) for 1 h at room temperature. After extensive washing, the cellular fluorescence was measured at 510 nm following excitation at 340 and 380 nm using a Zeiss examiner A1 microscope (Zeiss, Jena, Germany), equipped with a WN-Achroplan 40X objective (Zeiss, Jena, Germany). Images were continuously acquired at 1 image/second using Axiovision 4.8.2.

For determination of EC_{50} values a microplate reader was used. Suspensions of rat mesangial cells were incubated with 5 µM fura-2AM (Life Technologies, Carlsbad, CA, USA) and 0.05 % Pluronic F-127 in Leibovitz's L-15 medium (Life Technologies, Carlsbad, CA, USA) for 1 h at room temperature in the dark. The cells were repeatedly washed by centrifugation (3 x, 5 min, 200 g, RT) and resuspension in Leibovitz's medium. A concentration series of each ligand was pipetted into 96-well plates (Greiner Bio One,

Frickenhausen, Germany) at 20 µL per sample (10X concentration) and 180 µL of loaded cells ($1*10^6$ cells/mL) were injected into the wells. The fluorescence signal was immediately recorded with a FluoStar Omega fluorescence microplate reader (BMG Labtech, Ortenberg, Germany) for 60 s. Excitation filters for the ratiometric measurement were 340/20 nm and 380/20 nm. Emission was recorded using a 510/20 nm bandpass filter. The intracellular calcium concentrations were calculated using the Grynkiewicz equation [24] as recently described [15].

2.8 Statistics

To assess the statistical significance of flow cytometry data, two-way analysis of variances (ANOVA) was carried out with a multiple comparisons test (Tukey's test) by using SigmaPlot 12.2. Levels of statistical significance were set as indicated.

3 Results

3.1 Angiotensin II modification and nanoparticle labeling

To enable conjugation to amine-decorated PEGylated nanoparticles, angiotensin II was covalently modified at the primary amine group of its N-terminal aspartic acid by reaction with 2-iminothiolane (also known as Traut's reagent) in a 2-step reaction (Fig. 1A). Reversed-phase high performance liquid chromatography (RP-HPLC) and Ellman's assay with DTNB confirmed the complete conversion of the native peptide into the thiolated form (Fig. 1B). Electrospray ionization mass spectrometry (ESI-MS) further verified the successful reaction (Fig. 1C). Absence of the $(M+3H)^{3+}$ peak in the mass spectrograph indicated that the conjugation chemically altered a basic group, which clearly suggests reaction at the N-terminal aspartic acid.

The modified Ang II peptide was then coupled to the amine groups of the PEGylated Qdots using the heterobifunctional linker sulfo-SMCC (Fig. 1D). Qdots were activated by reacting their peripheral amine groups with the sulfo-NHS ester of sulfo-SMCC. After purification and removal of unreacted sulfo-SMCC the maleimide-activated nanoparticles were covalently conjugated with the thiolated Ang II in a thiol-ene Michael addition click reaction to form a stable thioether bond. Transmission electron microscopy revealed that the conjugation of the ligand to the Qdot PEG corona did not lead to aggregation. After coupling the Qdots remained monodisperse and evenly distributed (Supporting information Fig. S1).

3.2 Nanoparticle binding and uptake

Nanoparticle binding to selected cell lines was investigated by flow cytometry and confocal laser scanning microscopy. AT_1R-expressing NCI-H295R cells and rat mesangial cells as well as AT_1R-negative HeLa cells were incubated with non-targeted and Ang II-targeted Qdots at a concentration of 10 nM. Although non-targeted Qdots showed some association to the AT_1-expressing cell lines, binding of Ang II-targeted Qdots to NCI-H295R and rat mesangial cells was significantly higher (Fig. 2). Conversely, ligand-coupled Qdots showed no association nor binding to receptor negative HeLa cells, indicating that ligand immobilization on the nanoparticle surface was indeed successful.

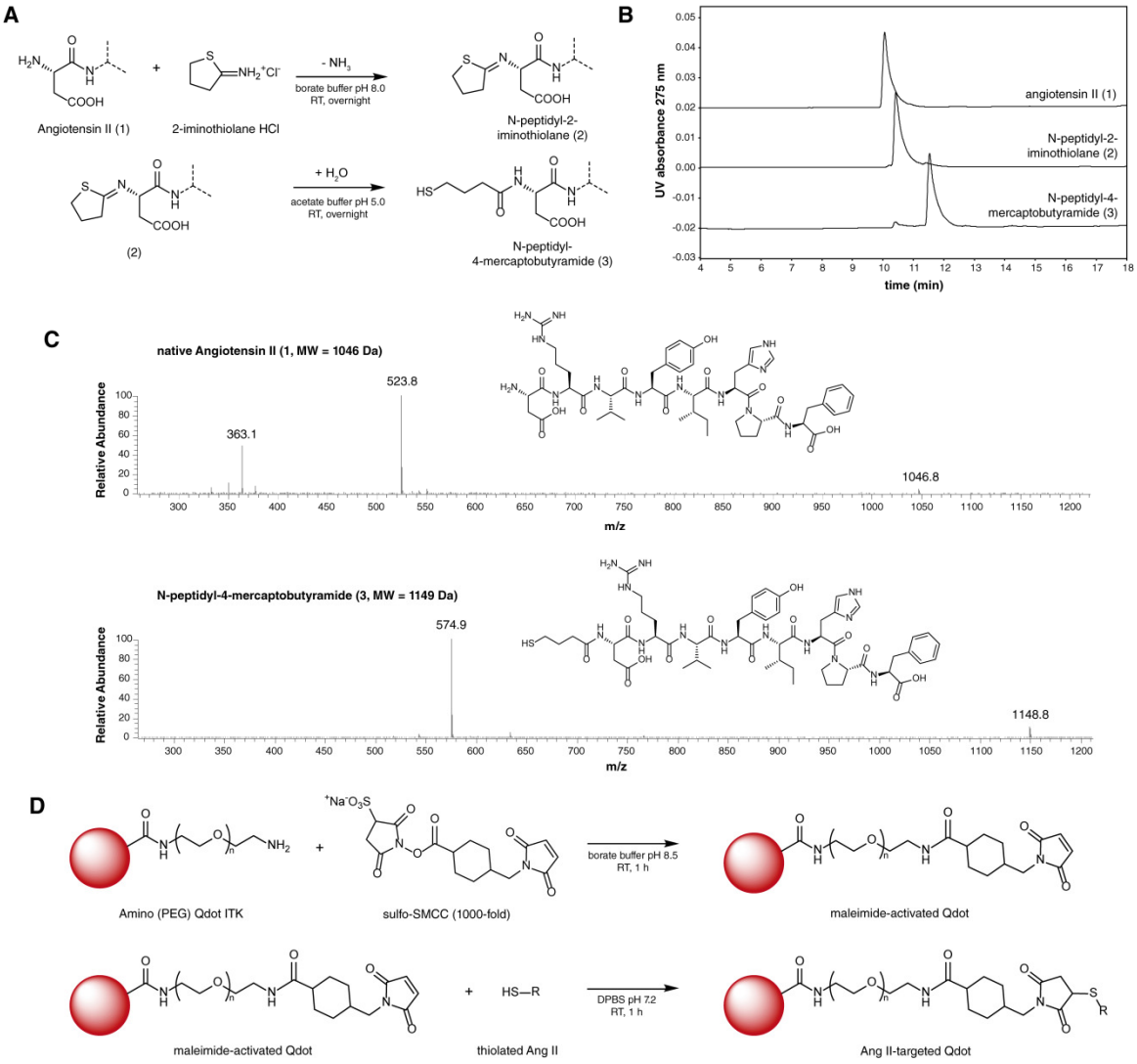

Figure 1: Strategy for angiotensin II conjugation to nanoparticles. **(A)** First, a thiol group was introduced at the N-terminal aspartic acid of angiotensin II using 2-iminothiolane **(B)** Reversed phase HPLC analysis verified the successful two-step reaction **(C)** Electrospray ionization mass spectrometry (ESI-MS) of the native and the modified peptide **(D)** To conjugate the thiolated angiotensin II to nanoparticles, PEGylated amine-terminated Qdots were activated with sulfo-SMCC and subsequently coupled to the ligand. A thorough purification was performed after each step.

By confocal laser scanning microscopy, subcellular localization of the nanoparticles was analyzed in detail. From this data, it is evident that not only did the ligand-targeted Qdots bind to the cell surface, but they were also rapidly taken up into the cells. After just a 30-minute incubation, the cells had begun to exhibit a massive amount of Qdot fluorescence. Nanoparticles were visible in vesicular regions throughout the cytoplasm and seemed to accumulate preferentially in the perinuclear region (Fig. 3), whereas non-targeted Qdots appeared to adhere in a non-specific manner to the cell surface. When the cells were coincubated with Ang II-targeted nanoparticles and losartan carboxylic acid, a specific and potent AT_1R antagonist, most of the intracellular fluorescence was eliminated,

verifying that the nanoparticle uptake was predominantly mediated by the AT_1 receptor. With the help of fluorescently labeled transferrin the predominant uptake route of the nanoparticles was studied in more detail. The distinct endocytic vesicles of Ang II-targeted Qdots clearly colocalized with the Alexa Fluor® 488-transferrin fluorescence (Fig. 4); this was the case for both the NCI-H295R cells and the rat mesangial cells.

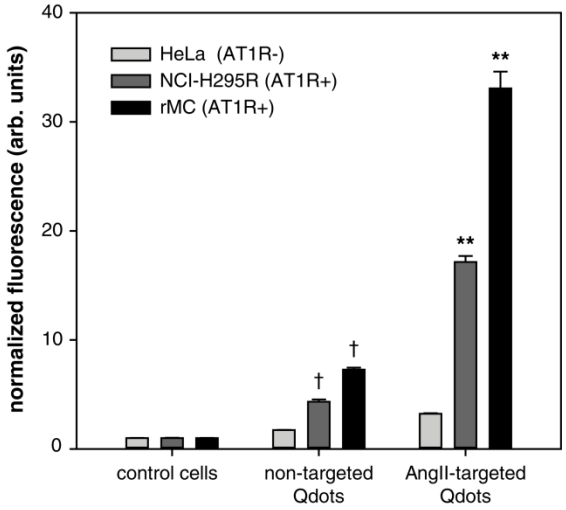

Figure 2: Nanoparticle binding to receptor positive and receptor negative cell lines by flow cytometry after 1 h incubation. Ang II-targeted Qdots strongly associated with AT_1R-expressing rat mesangial cells and NCI-H295R cells, whereas they showed no association with AT_1 negative HeLa cells. Levels of statistical significance are indicated as: (†) $p < 0.01$ compared to fluorescence of untreated control cells; (**) $p < 0.01$ compared to cellular fluorescence of non-targeted Qdots. Data is expressed as mean ± standard deviation (n=3).

3.3 Receptor binding affinity and activation

The cellular binding affinity and thus the multivalency of both the ligand alone and the ligand-conjugated nanoparticles was determined by intracellular calcium measurements with the help of the fluorescent calcium chelator fura-2. First, a microscope-based single cell tracking approach was used to examine the influence of the highly absorbing semiconductor Qdot core on fura-2 emission. When NCI-H295R cells were perfused with 10 nM of non-targeted Qdots the fura-2 emission ratio was unchanged (Fig. 5A, top). However, when the cells were perfused with 10 nM angiotensin II, a sharp increase in the emission signal was observed, indicating a calcium influx into the cytosol. When the cells were perfused with 10 nM Ang II-targeted Qdots, an increase in the fura-2 emission ratio was observed, to an even greater extent than the change elicited by the Ang II peptide alone (Fig. 5A, bottom). In addition, a plate reader-based calcium mobilization approach was used to pinpoint the receptor binding affinities. Again, non-targeted Qdots showed no alteration of the basal calcium signal over a wide range of concentrations (Fig. 5B, top).

In contrast, the native angiotensin II peptide bound and activated the receptor with an EC_{50} of 70.1 ± 1.8 nM. Modification of the N-terminal aspartic acid of Ang II by introducing a thiol moiety decreased the receptor affinity to 261 ± 25 nM. Likewise, introduction of a 5 kDa PEG chain to the N-terminal amino acid lowered the peptide's affinity to 320 ± 42 nM (Supporting information Fig. S2). Ang II-targeted nanoparticles activated the AT_1 receptor with an EC_{50} of 8.9 ± 0.3 nM indicating the multivalent nature of the nanoparticle binding. Qdot concentrations higher than 30 nM could not be tested since the broad and potent Qdot absorbance quenched the Fura-2 emission signal.

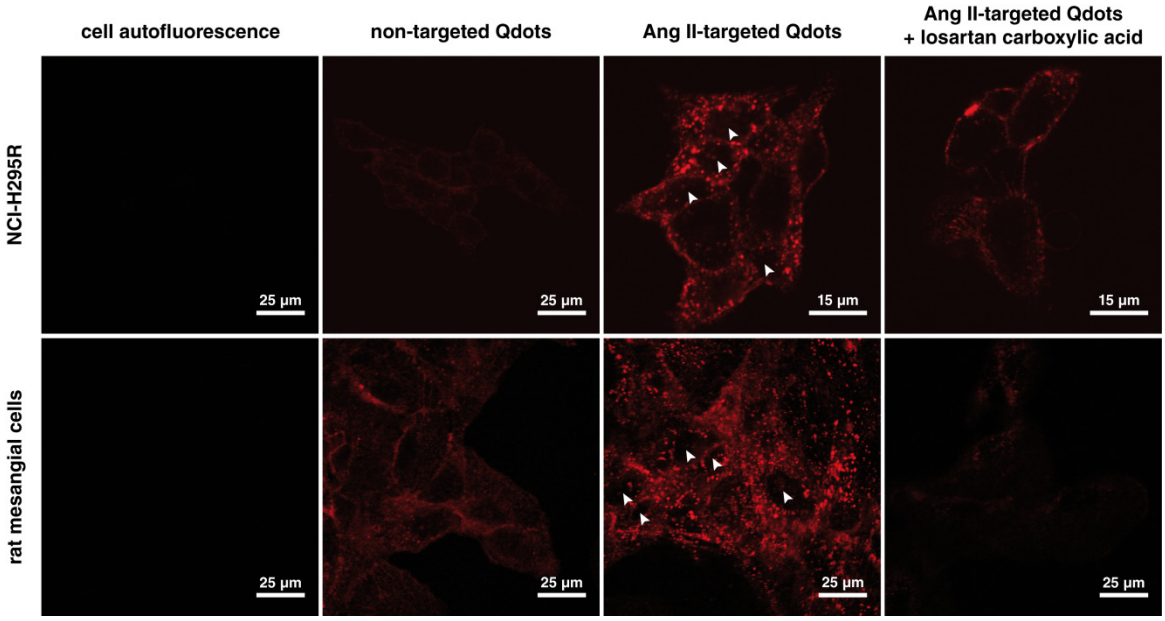

Figure 3: Nanoparticle uptake as investigated with confocal microscopy. Ang II-targeted Qdots are readily endocytosed by rat mesangial and NCI-H295R cells and located in the perinuclear region of cells. Arrowheads mark cell nuclei. The AT_1R antagonist losartan carboxylic acid (10 µM) markedly inhibited the uptake of ligand-modified Qdots. Non-targeted Qdots showed only weak association to cells.

4 Discussion

An N-terminal thiolated angiotensin II derivative was synthesized and covalently coupled to PEGylated quantum dots. The thiol moiety required for coupling to Qdots was introduced at the amino-terminus of the peptide since the negatively charged carboxy terminus is essential for receptor binding and activation [25,26]. Thus, the alternative modifications using an amide or ester formation at the C- terminus would lead to loss of the negative charge and a subsequent loss of the peptide's and conjugate's ability to bind the AT_1 receptor.

However, the reaction of the primary amino group of Asp[1] with 2-iminothiolane (Traut's reagent) was anomalous and did not immediately form the mercapto group. Instead, an N-peptidyl-2-iminothiolane intermediate was generated that had to be hydrolyzed at a reduced pH of 5.0 (Fig. 1A). After acid-catalyzed hydrolysis an N-peptidyl-4-mercaptobutyramide was formed with the intended reactive thiol moiety. This quite uncommon reaction pathway has also been observed for bombensin antagonists [27] and has been systematically investigated using short dipeptides [28]. The success of the subsequent angiotensin II conjugation to the nanoparticle surface was verified by flow cytometry and confocal microscopy. HeLa cells, which do not express functional AT_1 receptors [15], were not observed to associate with the obtained nanoparticles. In contrast, Ang II-targeted Qdots bound extensively to NCI-H295R and rat mesangial cells, both of which are AT_1R positive [29,30].

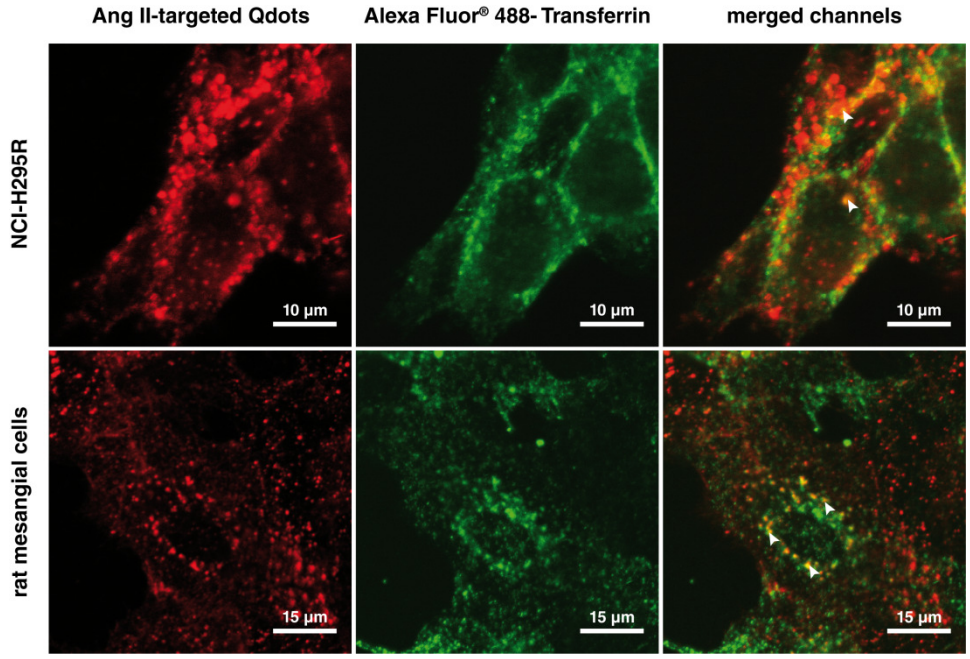

Figure 4: Coincubation of cells with fluorescently labeled transferrin reveals the endocytosis route. Receptor positive cells were incubated with Ang II-targeted Qdots and Alexa Fluor® 488 labeled transferrin and incubated for 30 min. Colocalization of Qdots and Alexa Fluor® 488 indicate that Qdots are taken up by clathrin-mediated endocytosis.

Qdots were mainly taken up into the cells by clathrin-mediated endocytosis, since most of the Qdots were colocalized with fluorescently labeled transferrin, a typical pathway marker for both clathrin-mediated uptake [31,32] and early and recycling endosomes [33]. Similar to many other GPCRs, the AT_1 receptor is mainly internalized by clathrin-mediated endocytosis upon agonist binding, which explains why a potent inhibitor of clathrin-mediated endocytosis greatly hindered angiotensin II inter-

nalization [34]. For targeted drug or gene delivery with nanoparticles, uptake of colloids into the cell is highly valuable. This is especially true for nucleic acid therapeutics like plasmids or siRNA, which have to reach intracellular targets. These molecules usually cannot cross the cell membrane by themselves and need potent carriers to promote their uptake. Since the AT_1 receptor is a G_q-coupled receptor [26], binding of agonist to the receptor leads to a calcium influx into the cytosol. Kobilka and coworkers discovered that, although intracellular signal transduction via inositol 1,4,5-trisphosphate and Ca^{2+} pathways had been completely desensitized, AT_1 receptors were still being rapidly internalized after Ang II binding due to the receptor's immediate recycling [35]. This interesting feature of the AT_1R underscores the receptor's feasibility as a nanoparticle target, since it allows for extensive nanoparticle uptake into the target cells.

Non-targeted Qdots, which were not endocytosed after 1 h of incubation, had no effect on the basal calcium concentration. In contrast, Ang II-targeted nanoparticles induced a calcium influx into the cytosol that was higher compared to the calcium influx that was induced by the same concentration of Ang II. When quantified, the EC_{50} of the native peptide and the thiolated peptide were determined to be 70.1 nM and 261 nM, respectively. A salt bridge between the terminal amino group Asp^1 and the terminal carboxy group of Phe^8 gives Ang II its classical hairpin-like conformation [36], which also stabilizes the binding of the peptide to the receptor [26]. When the terminal Asp^1 amino group is converted to a thiol moiety, this ion pair formation is no longer possible, ultimately leading to nearly 4-fold loss of receptor binding affinity for the N-thiolated peptide (Fig. 5B, bottom). Likewise, introduction of a 5 kDa mPEG chain to the amino group of Asp^1 lowered the receptor affinity by a factor of 4.5 (Supporting information Fig. S2). This is in great contrast to the ARB EXP3174, where PEGylation led to a 580-fold affinity loss [15]. Since the amino acids of the receptor that contribute to the angiotensin II binding are mainly located in the extracellular receptor regions [26], PEGylation only had a minor influence on its affinity. On the other hand, because the receptor residues that are implicated in antagonist binding are located deep in the transmembrane region [37] PEGylation of EXP3174 severely harmed its receptor affinity and led to a profound loss of affinity by a factor of 580 [15]. Qdots on which the thiolated Ang II was immobilized regained affinity with an EC_{50} of 8.9 nM, which was approximately 30-fold more affine than the thiolated ligand alone.

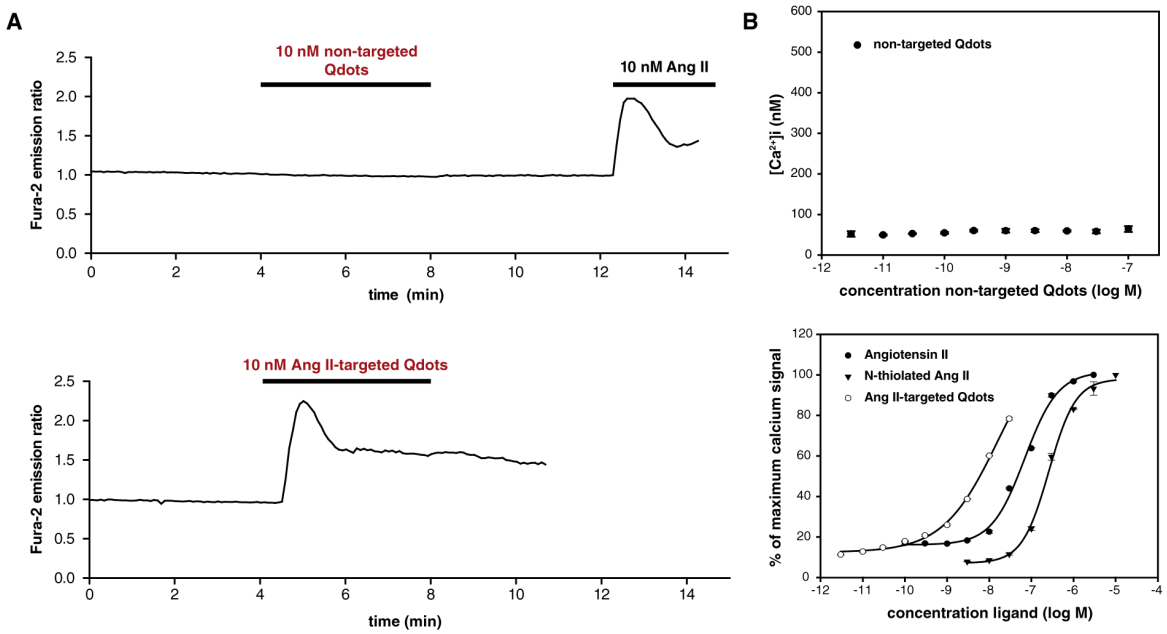

Figure 5: Influence of Ang II-targeted Qdots on cytosolic calcium concentrations. **(A)** Perfusion of NCI-H295R cells with non-targeted Qdots does not alter their intracellular calcium concentration, whereas incubation with 10 nM Ang II-targeted Qdots led to an influx of calcium ions into the cytosol, demonstrating receptor activation. **(B)** When quantified in a plate reader-based approach, non-targeted Qdots again show no influence on the cytosolic calcium (top). angiotensin II and N-modified angiotensin II bind and activate the receptor with an EC_{50} of 70.1 ± 1.8 nM and 261 ± 25 nM, respectively, whereas Ang II-targeted Qdots activate the AT_1 receptor with an EC_{50} of 8.9 ± 0.3 nM, demonstrating a distinct multivalent effect.

Based on the number of available amine groups on the nanoparticle surface and the observed coupling efficiency, we estimate that 5 to 7 ligand molecules were conjugated to each Qdot. The same conjugation procedure using endothelial growth factor (EGF) instead of angiotensin II resulted in 4 EGF molecules per Qdot [38]. Since Ang II is a smaller peptide we believe that a higher ligand number could be conjugated to the nanoparticle surface. As defined by Montet [39], 6 Ang II ligands per Qdot would result in a multivalent enhancement (MVE, β) of 5 compared to the unbound ligand. Compared to the multivalent enhancement of AT_1R antagonist-modified nanoparticles, which was 22.5 [15], the MVE of the Ang II-targeted Qdots was substantially lower. This can be explained by the decreased contact time of the colloids with the cell surface. Due to their rapid internalization into the cell the time available for each nanoparticle to bind to several receptors is limited. However, although this prompt endocytosis weakens the multivalent interactions between particles and cells, the increased uptake could be immensely useful as a method for increasing intracellular concentrations of molecules with otherwise poor membrane permeability. Since cells with a higher receptor expression

can be expected to endocytose a significantly higher amount of bound nanocarriers, such multivalent interactions could lead to selective drug delivery into specific cells and tissues.

5 Conclusions

Ang II-targeted nanoparticles strongly interact with the AT_1 receptor in a highly multivalent fashion and show no association to cells that do not express the receptor. After binding, the colloids are rapidly taken up via clathrin-mediated endocytosis. This constitutes the first experimental evidence that the binding of Ang II-targeted nanoparticles to their cognate type 1 receptors is multivalent in nature, which potentially allows for their use in the targeting of tissue that overexpresses this receptor.

References

[1] T. Higuchi, K. Fukushima, J. Xia, W.B. Mathews, R. Lautamäki, P.E. Bravo, M.S. Javadi, R.F. Dannals, Z. Szabo, F.M. Bengel, Radionuclide imaging of angiotensin II type 1 receptor upregulation after myocardial ischemia-reperfusion injury, J. Nucl. Med. 51 (2010) 1956–1961.

[2] T. Dvir, M. Bauer, A. Schroeder, J.H. Tsui, D.G. Anderson, R. Langer, R. Liao, D.S. Kohane, Nanoparticles targeting the infarcted heart, Nano Lett. 11 (2011) 4411–4414.

[3] B. de Paepe, V.L. Verstraeten, De Potter, C R, L.A. Vakaet, G.R. Bullock, Growth stimulatory angiotensin II type-1 receptor is upregulated in breast hyperplasia and in situ carcinoma but not in invasive carcinoma, Histochem. Cell Biol. 116 (2001) 247–254.

[4] F. Deshayes, C. Nahmias, Angiotensin receptors: a new role in cancer?, Trends Endocrinol. Metab. 16 (2005) 293–299.

[5] N. Nagai, Y. Oike, K. Izumi-Nagai, T. Urano, Y. Kubota, K. Noda, Y. Ozawa, M. Inoue, K. Tsubota, T. Suda, S. Ishida, Angiotensin II type 1 receptor-mediated inflammation is required for choroidal neovascularization, Arterioscler. Thromb. Vasc. Biol. 26 (2006) 2252–2259.

[6] J.N. Mason, H. Farmer, I.D. Tomlinson, J.W. Schwartz, V. Savchenko, L.J. DeFelice, S.J. Rosenthal, R.D. Blakely, Novel fluorescence-based approaches for the study of biogenic amine transporter localization, activity, and regulation, J. Neurosci. Methods 143 (2005) 3–25.

[7] S.H. Young, E. Rozengurt, Qdot nanocrystal conjugates conjugated to bombesin or ANG II label the cognate G protein-coupled receptor in living cells, Am. J. Physiol., Cell Physiol. 290 (2006) C728-32.

[8] J.E. Silpe, M. Sumit, T.P. Thomas, B. Huang, A. Kotlyar, M.A. van Dongen, M.M. Banaszak Holl, B.G. Orr, S.K. Choi, Avidity modulation of folate-targeted multivalent dendrimers for evaluating biophysical models of cancer targeting nanoparticles, ACS Chem. Biol. 8 (2013) 2063–2071.

[9] T. Watanabe, T.A. Barker, B.C. Berk, Angiotensin II and the endothelium: diverse signals and effects, Hypertension 45 (2005) 163–169.

[10] K. Suzuki, G.D. Han, N. Miyauchi, T. Hashimoto, T. Nakatsue, Y. Fujioka, H. Koike, F. Shimizu, H. Kawachi, Angiotensin II type 1 and type 2 receptors play opposite roles in regulating the barrier function of kidney glomerular capillary wall, Am. J. Pathol. 170 (2007) 1841–1853.

[11] R. Ardaillou, Angiotensin II receptors, J. Am. Soc. Nephrol. 10 Suppl 11 (1999) S30-9.

[12] K. Pollinger, R. Hennig, S. Bauer, M. Breunig, J. Tessmar, A. Buschauer, R. Witzgall, A. Goepferich, Biodistribution of Quantum Dots in the Kidney After Intravenous Injection, J. Nanosci. Nanotech. 14 (2014) 3313–3319.

[13] K. Pollinger, R. Hennig, A. Ohlmann, R. Fuchshofer, R. Wenzel, M. Breunig, J. Tessmar, E.R. Tamm, A. Goepferich, Ligand-functionalized nanoparticles target endothelial cells in retinal capillaries after systemic application, Proc. Natl. Acad. Sci. U.S.A. 110 (2013) 6115–6120.

[14] K. Pollinger, R. Hennig, M. Breunig, J. Tessmar, A. Ohlmann, E.R. Tamm, R. Witzgall, A. Goepferich, Kidney podocytes as specific targets for cyclo(RGDfC)-modified nanoparticles, Small 8 (2012) 3368–3375.

[15] R. Hennig, K. Pollinger, A. Veser, M. Breunig, A. Goepferich, Nanoparticle multivalency counterbalances the ligand affinity loss upon PEGylation, J. Control. Release 194C (2014) 20–27.

[16] F.L. Fierensa, P.M. Vanderheyden, C. Roggeman, J.-P. de Backer, T.J. Thekkumkara, G. Vauquelin, Tight binding of the angiotensin AT1 receptor antagonist [3H]candesartan is independent of receptor internalization, Biochem. Pharmacol. 61 (2001) 1227–1235.

[17] G. Bkaily, S. Sleiman, J. Stephan, C. Asselin, S. Choufani, M. Kamal, D. Jacques, Gobeil, Jr, F, P. D'Orléans-Juste, Angiotensin II AT 1 receptor internalization, translocation and de novo synthesis modulate cytosolic and nuclear calcium in human vascular smooth muscle cells, Can. J. Physiol. Pharmacol. 81 (2003) 274–287.

[18] J. Wang, S. Tian, R.A. Petros, M.E. Napier, J.M. DeSimone, The Complex Role of Multivalency in Nanoparticles Targeting the Transferrin Receptor for Cancer Therapies, J. Am. Chem. Soc. 132 (2010) 11306–11313.

[19] D. Banerjee, A.P. Liu, N.R. Voss, S.L. Schmid, M.G. Finn, Multivalent display and receptor-mediated endocytosis of transferrin on virus-like particles, Chembiochem 11 (2010) 1273–1279.

[20] T.P. Thomas, M. Joice, M. Sumit, J.E. Silpe, A. Kotlyar, S. Bharathi, J. Kukowska-Latallo, J.R. Baker, S.K. Choi, Design and in vitro validation of multivalent dendrimer methotrexates as a folate-targeting anticancer therapeutic, Curr. Pharm. Des. 19 (2013) 6594–6605.

[21] Z. Tang, D. Li, H. Sun, X. Guo, Y. Chen, S. Zhou, Quantitative control of active targeting of nanocarriers to tumor cells through optimization of folate ligand density, Biomaterials 35 (2014) 8015–8027.

[22] S. Barua, J.-W. Yoo, P. Kolhar, A. Wakankar, Y.R. Gokarn, S. Mitragotri, Particle shape enhances specificity of antibody-displaying nanoparticles, Proc. Natl. Acad. Sci. U.S.A. 110 (2013) 3270–3275.

[23] B.S. Hendriks, S.G. Klinz, J.G. Reynolds, C.W. Espelin, D.F. Gaddy, T.J. Wickham, Impact of tumor HER2/ERBB2 expression level on HER2-targeted liposomal doxorubicin-mediated drug delivery: multiple low-affinity interactions lead to a threshold effect, Mol. Cancer Ther. 12 (2013) 1816–1828.

[24] G. Grynkiewicz, M. Poenie, R.Y. Tsien, A new generation of Ca2+ indicators with greatly improved fluorescence properties, J. Biol. Chem. 260 (1985) 3440–3450.

[25] L. Hunyady, T. Balla, K.J. Catt, The ligand binding site of the angiotensin AT1 receptor, Trends Pharmacol. Sci. 17 (1996) 135–140.

[26] M. de Gasparo, K.J. Catt, T. Inagami, J.W. Wright, T. Unger, International union of pharmacology. XXIII. The angiotensin II receptors, Pharmacol. Rev. 52 (2000) 415–472.

[27] M. Mokotoff, Y.M. Mocarski, B.L. Gentsch, M. Miller, J.-H. Zhou, J. Chen, E.D. Ball, Caution in the use of 2-iminothiolane (Traut's reagent) as a cross-linking agent for peptides. The formation of N-peptidyl-2-iminothiolanes with bombesin (BN) antagonist (d-Trp6,Leu13-psi[CH2NH]-Phe14)BN6-14 and d-Trp-Gln-Trp-NH2, J. Pept. Res. 57 (2001) 383–389.

[28] R. Singh, L. Kats, W.A. Blättler, J.M. Lambert, Formation of N-substituted 2-iminothiolanes when amino groups in proteins and peptides are modified by 2-iminothiolane, Anal. Biochem. 236 (1996) 114–125.

[29] H. Nishi, H. Arai, T. Momiyama, NCI-H295R, a human adrenal cortex-derived cell line, expresses purinergic receptors linked to Ca^{2+}-mobilization/influx and cortisol secretion, PLoS ONE 8 (2013) e71022.

[30] Q. Huang, Y. Guo, H. Zeng, W. Xie, H. Yan, H. Ding, Visfatin stimulates a cellular renin-angiotensin system in cultured rat mesangial cells, Endocr. Res. 36 (2011) 93–100.

[31] L.J. Mutch, J.D. Howden, Jenner, Emma Poppy Louise, N.S. Poulter, J.Z. Rappoport, Polarised Clathrin-Mediated Endocytosis of EGFR During Chemotactic Invasion, Traffic 15 (2014) 648–664.

[32] A. Motley, N.A. Bright, Seaman, Matthew N J, M.S. Robinson, Clathrin-mediated endocytosis in AP-2-depleted cells, J. Cell Biol. (The Journal of cell biology)h 162 (2003) 909–918.

[33] T.-G. Iversen, T. Skotland, K. Sandvig, Endocytosis and intracellular transport of nanoparticles: Present knowledge and need for future studies, Nano Today 6 (2011) 176–185.

[34] T.A. Morinelli, L.P. Walker, Velez, Juan Carlos Q, M.E. Ullian, Clathrin-dependent internalization of the angiotensin II AT1A receptor links receptor internalization to COX-2 protein expression in rat aortic vascular smooth muscle cells, Eur. J. Pharmacol. 748C (2014) 143–148.

[35] L. Hein, L. Meinel, R.E. Pratt, V.J. Dzau, B.K. Kobilka, Intracellular trafficking of angiotensin II and its AT1 and AT2 receptors: evidence for selective sorting of receptor and ligand, Mol. Endocrinol. 11 (1997) 1266–1277.

[36] K.A. Carpenter, B.C. Wilkes, P.W. Schiller, The octapeptide angiotensin II adopts a well-defined structure in a phospholipid environment, Eur. J. Biochem. 251 (1998) 448–453.

[37] H. Ji, M. Leung, Y. Zhang, K.J. Catt, K. Sandberg, Differential structural requirements for specific binding of nonpeptide and peptide antagonists to the AT1 angiotensin receptor. Identification of amino acid residues that determine binding of the antihypertensive drug losartan, The Journal of biological chemistry 269 (1994) 16533–16536.

[38] P. Diagaradjane, J.M. Orenstein-Cardona, N.E. Colón-Casasnovas, A. Deorukhkar, S. Shentu, N. Kuno, D.L. Schwartz, J.G. Gelovani, S. Krishnan, Imaging epidermal growth factor receptor expression in vivo: pharmacokinetic and biodistribution characterization of a bioconjugated quantum dot nanoprobe, Clin. Cancer Res. 14 (2008) 731–741.

[39] X. Montet, M. Funovics, K. Montet-Abou, R. Weissleder, L. Josephson, Multivalent effects of RGD peptides obtained by nanoparticle display, J. Med. Chem. 49 (2006) 6087–6093.

Multivalent targeting of AT_1 receptors with angiotensin II-functionalized nanoparticles

1 Transmission electron microscopy

3 µL of a 60 nM aqueous solution Qdots was pipetted on a carbon-coated copper grid (Plano, Wetzlar, Germany) and air dried. The sample was analyzed using a Zeiss Libra 120 electron microscope (Zeiss, Oberkochen, Germany). Electron microscopy pictures were acquired with Image SP (Zeiss, Oberkochen, Germany) and analyzed with ImageJ.

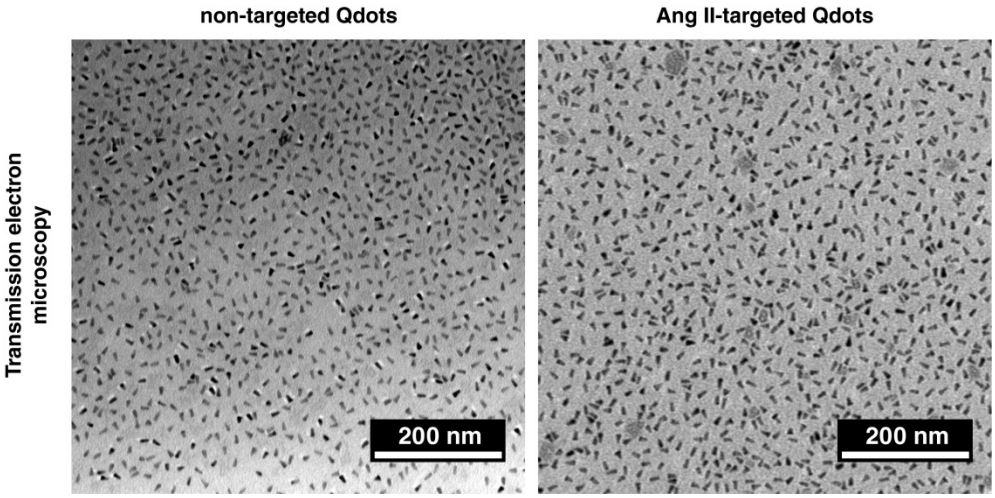

Figure S1: Transmission electron microscopy pictures of Qdots before and after conjugation. The conjugation process did not alter the dispersity and did not lead to Qdot aggregation.

2 PEGylation of angiotensin II

2 µmol angiotensin II was reacted with 4 µmol mPEG5k-succinimidyl carbonate for 16 hours at room temperature in borate buffer (50 mM, pH 8.5). mPEG5k-succinimidyl carbonate was synthesized as described in the literature [1]. The reaction mixture was purified by size exclusion chromatography using a Sephadex G-25 resin in a PD-10 column with DPBS as the eluent. Fractions containing PEGylated Ang II were pooled and further purified by ultrafiltration using a 5 KDa molecular weight cut-off Amicon Ultra-15 filter unit. Final purity and conjugate concentration were determined using RP18-HPLC: The HPLC system consisted of a Shimadzu LC-10ATVP pump (Shimadzu, Duisburg, Germany), a Shimadzu SIL-10ADVP autosampler connected to a Shimadzu SPD-10A UV-Vis detector. A Luna® 5 µm C18(2) 100 Å 250 x 4.60 mm LC column (Phenomenex, Aschaffenburg, Germany) was used as separation column. The peptides were analyzed based on a linear acetonitrile–trifluoroacetic acid (TFA)–water gradient with a flow rate of 1 mL/min. Elution was obtained by using the following gradient of solvents A (0.1 % (v/v) TFA in water) and B (0.1 % (v/v) TFA in acetonitrile): 75:25 (A:B) to 30:70 in 20 min and reequilibration to 90:10 in the following 7 min. The column was

operated at 35 °C. The peptide and its PEG conjugate were detected at 275 nm. The affinity of the conjugate was measured with an intracellular calcium mobilization assay using fura-2AM.

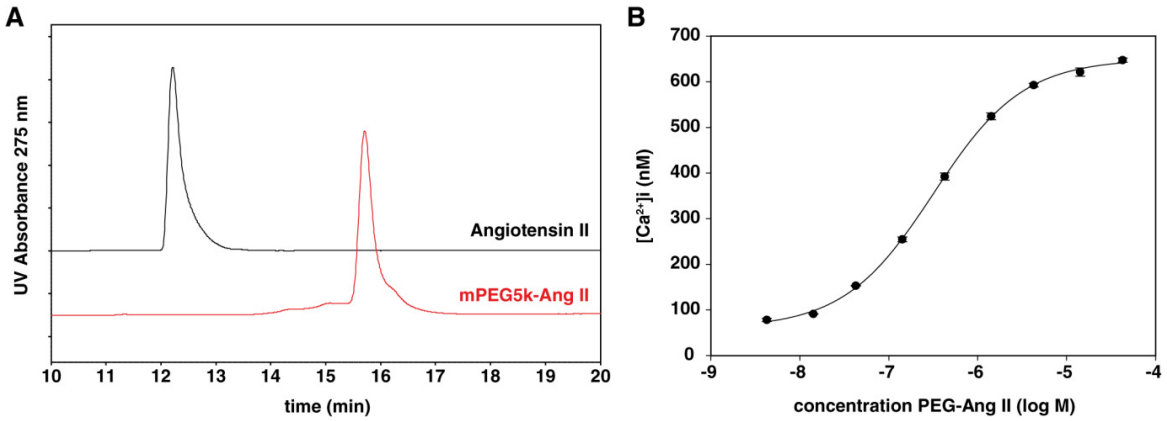

Figure S2: PEGylation of angiotensin II **(A)** RP18-HPLC analysis of Ang II and its PEGylated counterpart showing the absence of unreacted Ang II. **(B)** Upon PEGylation, the peptide's affinity dropped 4.5-fold to 320 ± 42 nM

References

[1] F. Brandl, N. Hammer, T. Blunk, J. Tessmar, A. Goepferich, Biodegradable hydrogels for time-controlled release of tethered peptides or proteins, Biomacromolecules 11 (2010) 496–504.

Chapter 7

Cyclic RGD peptides target trabecular meshwork cells and ameliorate connective tissue growth factor-induced fibrosis

This chapter was published as: R. Hennig, S. Küspert, A. Haunberger, A. Goepferich and Rudolf Fuchshofer, J. Drug Targeting 2016, doi: 10.3109/1061186X.2016.1163709. Data that was not obtained nor analyzed by R. Hennig is highlighted.

Abstract

The major risk factor for primary open-angle glaucoma is increased intraocular pressure stemming from elevated outflow resistance in the trabecular meshwork (TM) region. Integrins play a pivotal role in the TM by influencing its biological properties and growth factor signaling. Pathologic changes in the TM are partially mediated by growth factors like connective tissue growth factor (CTGF). Specific targeting of TM cells could play a critical clinical role by increasing the therapeutic efficacy of nanoparticles, e.g. for nonviral gene delivery. Quantum dots with cyclo(RGDfC) covalently immobilized to their surface effectively targeted cultured TM cells and were rapidly and efficiently endocytosed by binding to $\alpha_v\beta_3$ and $\alpha_v\beta_5$ integrins. Compared to the integrin-overexpressing U87-MG cell line, the association of RGD-modified nanoparticles with the TM cells was significantly higher. Binding and uptake into TM cells was receptor-mediated and suppressible with free peptide. Soluble cyclic RGD peptides effectively attenuated CTGF-mediated effects and inhibited CTGF signaling. Due to their antagonism for $\alpha_v\beta_3$ and $\alpha_v\beta_5$ integrins, these cyclic RGD pentapeptides effectively ameliorated the CTGF-induced effects and strongly promoted specific nanoparticle association. Thus, cyclic RGD peptides are powerful multifunctional ligands for both addressing nanomaterials to the TM and interfering with pathologic CTGF signaling upon arrival.

1 Introduction

Primary open angle glaucoma (POAG) is the second leading cause of blindness in the world [1] and is characterized by the degeneration of optic nerve axons. The main risk factor for POAG is increased intraocular pressure (IOP) due to abnormally high aqueous humor outflow resistance in the trabecular outflow pathways. In the trabecular outflow pathways, such resistance to flow is generated by the juxtacanalicular tissue (JCT) and Schlemm's canal (SC) endothelium. The causative factors for altered outflow resistance appear to be increased contractility of TM cells together with an accumulation of extracellular matrix (ECM) in the JCT region [2]. The molecular signaling pathways that modulate TM contractility and ECM synthesis in the TM are not yet completely understood; however, transforming growth factor (TGF)-β signaling pathways are involved in the pathogenetic changes in POAG [3–6]. Recent studies have indicated that the action of TGF-β2 on TM is dependent on connective tissue growth factor (CTGF) as a downstream mediator [7]. CTGF belongs to the CCN (CYR61/CCN1, CTGF/CCN2, NOV/CCN3) family, which consists of six matricellular regulatory proteins [8,9], and is strongly and constitutively expressed in the TM [10]. Additionally, CTGF expression is markedly upregulated in glaucomatous SC cells compared to the SC cells of healthy donors [11]. A therapeutic approach to prevent further pathologic changes within the TM could be the inhibition of TGF-β/CTGF signaling pathways: CTGF mainly mediates its effects by binding to integrins in various cell types, especially to $\alpha_v\beta_3$ and $\alpha_v\beta_5$ integrins. Therefore, attenuation of CTGF-dependent effects by blocking specific integrins could represent a promising therapeutic approach for POAG patients.

Although several potent IOP-reducing drugs exist on the market [12], they are commonly formulated as eye drop solutions which must be frequently applied [13]. However, due to poor patient adherence and improper application technique, anti-glaucoma eye drops often do not elicit the desired therapeutic effects [14]. For this reason, gene therapy has been intensely researched for glaucoma therapy as a long-term intervention alternative [15,16]. Although initial gene therapy efforts utilizing viral vectors experienced early success [17], nonviral vectors have not gained traction, due to their low transfection efficiency and tissue specificity [18].

One way to at least partially overcome these disadvantages is the attachment of targeting moieties to a nonviral vector's surface [19]. A prominent example involves use of the Arg-Gly-Asp (RGD) motif, which has been successfully deployed in the context of nonviral

vector-based cancer therapy [20]. Notably, RGD peptides antagonize $\alpha_v\beta_3$ and $\alpha_v\beta_5$ integrins, which are readily expressed by cells of the TM [21]. Although linear RGD peptides have been tested for their influence on IOP [22,23] they have not yet been evaluated as targeting moieties for delivering nanoparticles to the TM. We consider RGD peptides to be of high potential in this application for two reasons: first, since RGD peptides have an inherent influence on matrix-cell interactions due to their capability to compete and disrupt cell-matrix contacts [24]. Second, after integrin binding, they have demonstrated the ability to rapidly induce receptor-mediated endocytosis [25]. Both features provide clear incentives for using RGD peptides as targeting ligands.

Here, we investigate the feasibility of targeting TM cells with nanoparticles whose surface is coated with cyclic RGD peptides. Compared to their linear counterparts, cyclic RGD peptides exhibit a 100-fold increased integrin binding affinity [26]. As a model nanoparticle platform, highly fluorescent quantum dots (Qdots) were used to enable precise tracking of nanoparticles in the cellular environment. To the best of our knowledge this is the first *in vitro* study that uses ligand-coupled nanoparticles for active targeting of TM cells, which are among the key actors in the pathogenesis of POAG. Furthermore, due to the intrinsic pharmacological effects of the RGD peptides on integrin receptors, we investigated their influence on connective tissue growth factor (CTGF)-induced fibrosis in TM cells.

2 Materials and Methods

2.1 Materials

Cyclo(-Arg-Gly-Asp-D-Phe-Cys) [cyclo(RGDfC)] was purchased from Bachem (Bubendorf, Switzerland). Prior to use, cyclo(RGDfC) was reduced with tris(2-carboxyethyl)phosphine (TCEP) to cleave any inter-peptide disulfide bonds. 0.4 mg/mL cyclo(RGDfC) was incubated with 6 mg/mL TCEP for 1 h under vigorous shaking. Human recombinant connective tissue growth factor (CTGF) was isolated from transfected HEK293 cells as previously described [7]. Unless stated otherwise all chemicals were obtained from Sigma Aldrich (Taufkirchen, Germany) in analytical grade and used without further purification. Ultrapure water was obtained from a Milli-Q water purification system (Millipore, Billerica, MA, USA).

2.2 Cell culture

Human trabecular meshwork (HTM) cells were isolated from the eyes of four human donors (donors ranged in age from 34 to 76 years) according to previously published protocols [27] and maintained in F10-HAM medium supplemented with 10 % fetal calf serum (FCS). TM cells in the third to fifth passage were seeded in 35 mm Petri dishes at a density of 4.0×10^5 cells/well. Confluent TM cells were deprived of serum for 24 h, and then incubated in fresh serum-free medium containing 50 ng/mL CTGF, 10^{-6} M cyclo(RGDfC) or 50 ng/mL CTGF in combination with 10^{-6} M cyclo(RGDfC). Treated TM cells were then harvested for protein and RNA analyses.

Human glioblastoma U87-MG cells (ATCC No. HTB-14) were a kind gift from Dr. Armin Buschauer (Faculty of Pharmacy and Chemistry, University of Regensburg) and were maintained in minimal essential medium containing Earl's salts (EMEM) and supplemented with 10 % FCS. HTM and U87-MG cells were both grown in a 5 % CO_2 atmosphere at 37 °C. In addition, an immortalized SV40-transformed HTM cell line (HTM-N) was used. This cell line was provided by Iok-Hou Pang and Louis DeSantis (Alcon Research Laboratories, Fort Worth, TX), and was cultured according to previously published protocols [28,29]. Methods for securing human tissues were humane, included proper consent and approval and complied with the Declaration of Helsinki.

2.3 Quantum dot modification with cyclo(RGDfC)

160 pmol Qdots® 655 ITK™ amino PEG (Life Technologies, Carlsbad, CA, USA) were activated with 160 nmol sulfosuccinimidyl-4-(N-maleimidomethyl)cyclohexane-1-carboxylate (sulfo-SMCC) (Thermo Fisher, Waltham, MA, USA) by gentle shaking in borate buffer at pH 8.50 (50 mM) for 1 h at room temperature. The maleimide-activated Qdots were purified from unreacted sulfo-SMCC by size exclusion chromatography using a Sephadex G-25 resin in a PD-10 column (1.45 x 5.0 cm) (GE Healthcare, Munich, Germany). Dulbecco's phosphate buffered saline (DPBS) at pH 7.4, consisting of 1.5 mM KH_2PO_4, 8 mM Na_2HPO_4, 2.7 mM KCl and 138 mM NaCl, was used as eluent. Collected fractions containing thiol-reactive Qdots were pooled. Next, 16 nmol of reduced cyclo(RGDfC) were added to the maleimide-activated Qdots and reacted for 1 h to yield a stable thioether bond. Unreacted maleimides were quenched with a 1000-fold molar excess of 2-mercaptoethanol relative to Qdots for 30 min. By using a 100 kDa molecular weight cut-off Amicon Ultra-4 filter unit (Millipore, Billerica, MA, USA) the reaction mixture was purified to remove a large portion of unreacted cyclo(RGDfC) and 2-mercapoethanol. Qdots were further purified by size exclusion chromatography as described above. Last, a final ultrafiltration step was performed to concentrate the Qdots. The cyclo(RGDfC)-Qdot concentration was calibrated by fluorescence measurements using a FluoStar Omega fluorescence microplate reader (BMG Labtech, Ortenberg, Germany), an excitation wavelength of 450 nm and an emission wavelength of 650 nm.

2.4 Flow Cytometry

HTM and U87-MG cells were seeded into 24-well plates (Corning, Corning, NY, USA) at a density of 100,000 cells/well. After cells had been allowed to grow for 96 h (HTM cells) or 48 h (U87-MG), they were washed with DPBS. Nanoparticle solutions of non-targeted and c(RGDfC)-targeted Qdots were prepared in binding buffer at a concentration of 10 nM. Binding buffer for nanoparticle uptake experiments was composed of 20 mM Tris, 150 mM NaCl, 2 mM $CaCl_2$, 1 mM $MnCl_2$, 1 mM $MgCl_2$ and 0.1 % bovine serum albumin at pH 7.4 [25]. Cells were incubated with the pre-warmed solutions at 37 °C. After 1 h, the nanoparticle solutions were removed and cells were vigorously washed and subsequently trypsinized for 5 min. Then, Leibovitz's medium (Life Technologies, Carlsbad, CA, USA) containing 10 % FCS was added to the cells, which were subsequently centrifuged (5 min, 200 g) and resuspended in DPBS. After a final centrifugation step (5 min, 200 g), cells were resuspended in ice-cold DPBS and analyzed for Qdot fluorescence using a

FACSCalibur flow cytometer (Becton Dickinson, Franklin Lakes, NJ, USA). Qdot fluorescence was elicited by using an argon-ion laser at 488 nm; emission was captured using a 661/16 nm bandpass filter. The resulting data was processed using WinMDI 2.9 (The Scripps Research Institute, San Diego, CA, USA). The fluorescence histogram was used to calculate the geometrical mean, for which only intact cells were gated.

2.5 Confocal microscopy

HTM cells were seeded into 8-well µ-slides (Ibidi, Martinsried, Germany) at a density of 10,000 cells/well. After cells had been allowed to grow for 120 h, nanoparticle binding was assessed. Cells were washed with DPBS and pre-warmed nanoparticle solutions in binding buffer were pipetted onto the cells. After incubation for 1 h at 37 °C, Qdot solutions were removed and cells washed with pre-warmed DPBS. Cells were analyzed in Leibovitz's medium. Nanoparticle binding to HTM cells was analyzed using a 63x Plan-Apochromat (NA 1.4) oil immersion objective with a Zeiss Axiovert 200 microscope equipped with an LSM 510 laser-scanning device (Zeiss, Jena, Germany). Using an argon-ion laser, Qdots were excited at 488 nm and fluorescence emission was recorded after filtering with a 650 nm longpass filter. The focal plane was adjusted to 1.1 µm. For image acquisition AIM 4.2 software (Zeiss, Jena, Germany) was used. Images were processed using ImageJ (NIH, Bethesda, MD, USA, http://imagej.nih.gov/ij).

2.6 RNA analysis

Total RNA was isolated from 35 mm Petri dishes using TriFast™ (Peqlab, Erlangen, Germany) as described by Chomczynski and Sacchi [30] and according to the manufacturer's recommendations. cDNA was prepared from total RNA using the qScript™cDNA Synthesis Kit (Quanta Biosciencies, Gaithersburg, USA) according to the manufacturer's instructions. Real-time reverse transcribed (RT)-PCR was performed using the Bio-Rad iQ5 Real-time PCR Detection System (Bio-Rad, München, Germany). PCR was run for 40 cycles with 10 s melting at 95 °C and 40 s of annealing and extension at 60 °C. Primer pairs (table 1) for CTGF, fibronectin, GNB2L and α-smooth muscle actin were purchased from Life Technologies (Darmstadt, Germany) and extended over exon-intron boundaries. RNA that was not reverse transcribed served as negative control for real-time RT-PCR. The accuracy of the amplicons was verified by performing a melting-curve analysis after amplification. For relative quantification of the experiments, GNB2L was used as a housekeeping gene. Quantification was performed using Bio-Rad iQ5 Standard Edition (Version no. 2.0.148.60623, Bio-Rad).

Table 1
Primer pairs used for real-time RT-PCR

Type	Sequence	Position	Temperature (°C)
Human CTGF	5'-CTCCTGCAGGCTAGAGAGC-3' 5'-GATGCACTTTTTGCCCTTCTT-3'	884-977	59 60
Human GNB2L	5'-GCTACTACCCCGCAGTTCC-3' 5'-CAGTTTCCACATGATGATGGTC-3'	170-241	59 60
Fibronectin	5'-CCCTGATTGGAAGGAAAAAGA-3' 5'-ATGAAGATTGGGGTGTGGAA-3'	6217-6284	60 60
Human α-smooth muscle actin (α-SM-actin)	5'-CTGAAGTACCCGATAGAACATGG-3' 5'-TTGTAGAAAGAGTGGTGCCAGAT-3'	252-328	59 60

2.7 Western blot analysis

Protein extracts were obtained by directly lysing cells in RIPA lysis buffer containing 150 mM NaCl, 1 % NP-40, 0.5 % deoxycholic acid and 0.1 % SDS in a 50 mM Tris buffer at pH 8. Isolated protein content was measured via the bicinchoninic acid (BCA) kit (Interchim, Montluçon Cedex, France). After an electrophoretic separation via SDS-PAGE, proteins were transferred to polyvinylidene fluoride membranes (Roche, Mannheim, Germany). Western blots were probed using rabbit anti-fibronectin (1:1000, Dako, Hamburg, Germany) and rabbit anti-(p-)extracellular signal-regulated kinase-1 (1:1000, Cell Signaling Technology, Danvers, MA, USA) primary antibodies, followed by horseradish peroxidase-coupled donkey anti-rabbit (1:2000; Santa Cruz, Heidelberg, Germany). Chemiluminescence was detected on an LAS 3000 imaging workstation (Raytest, Straubenhardt, Germany) with Luminata™ Forte Western HRP chemiluminescent substrate (Millipore, Billerica, MA. USA). The intensity of the bands detected by Western blot analysis was determined using appropriate software (AIDA Image analyzer software, Raytest). Obtained signals were normalized by detection and quantification of α-tubulin.

2.8 Statistics

To assess the statistical significance of cell culture data, Student's t-tests were carried out. FACS data was analyzed by two-way ANOVA using SigmaPlot 12.2 (Systat Software, San Jose, CA, USA). Levels of statistical significance were set as indicated.

3 Results

3.1 Cyclo(RGDfC)-coated nanoparticles bind primary HTM cells

To target nanoparticles to HTM cells, amine-bearing quantum dots were functionalized with the $\alpha_v\beta_3$ specific ligand cyclo(Arg-Gly-Asp-d-Phe-Cys) (cyclo[RGDfC]) in a two-step reaction (Fig. 1). As recently shown with transmission electron microscopy imaging [25,31], this conjugation strategy neither alters the size distribution nor the nanoparticle dispersity. The successful conjugation of cyclic RGD peptides to nanoparticles was demonstrated by investigating Qdot binding to glioblastoma U87-MG cells, using flow cytometry for detection. PEGylated but non-targeted nanoparticles exhibited weak association with U87-MG cells whereas binding of cyclo(RGDfC)-modified particles was 10-fold higher (Fig. 2). When cells were incubated with integrin-targeted Qdots and a surplus of free cyclic RGD peptide, the mean fluorescence was significantly decreased, proving the receptor-mediated nature of the nanoparticle binding. Similarly, primary HTM cells were incubated with PEGylated and RGD-targeted nanoparticles and analyzed for their fluorescence. When normalized relative to cell autofluorescence, HTM cells accumulated a significantly higher amount of nanoparticle fluorescence than U87-MG cells; this effect was also reversed in the presence of excess cyclic RGD peptide (Fig. 2). Notably, cyclo(RGDfC)-targeted Qdots did not interact with immortalized HTM cells (HTM-N), in stark contrast to the impressive binding we observed with primary HTM cells.

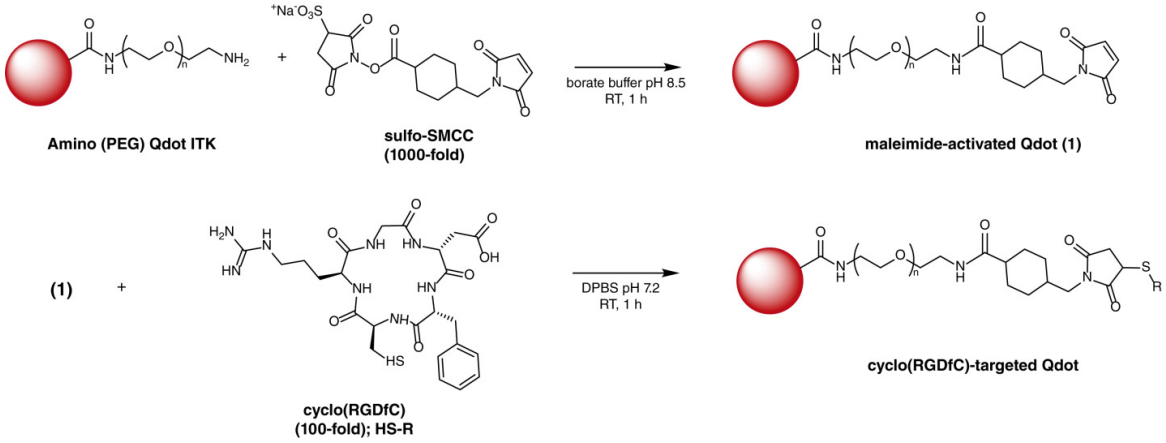

Figure 1: Scheme for immobilization of cyclo(RGDfC) peptides on PEGylated quantum dots. After introduction of thiol-reactive maleimide groups onto the Qdot surface, the thiol moiety of cyclo(RGDfC) is reacted with the activated Qdots in a Michael-type addition reaction. Unreacted maleimide groups are quenched with 2-mercaptoethanol.

3.2 HTM cells rapidly endocytose cyclo(RGDfC)-Qdots

Since cyclo(RGDfC)-modified nanoparticles showed a strong association with primary HTM cells, we asked whether the colloids were taken up into the cells after integrin binding. To investigate this, HTM cells were incubated with non-targeted or cyclo(RGDfC)-Qdots for 1 h. After removal of non-bound Qdots and thorough washing, nanoparticle internalization was visualized by confocal laser scanning microscopy. This data clearly illustrates that ligand-modified Qdots were efficiently endocytosed into HTM cells (Fig. 3). The cyclo(RGDfC)-Qdot fluorescence was visible in vesicle-like structures throughout the cytoplasm, whereas only cell nuclei seemed to be free of nanoparticle fluorescence. Co-incubation of cells with cyclo(RGDfC)-Qdots and a surplus of cyclo(RGDfC) peptide completely abolished intracellular fluorescence, underscoring the $\alpha_v\beta_3$ integrin-mediated nature of nanoparticle entry into the cell. Conversely, non-targeted Qdots adhered only sparsely to the cell surface, exhibiting weak nonspecific binding.

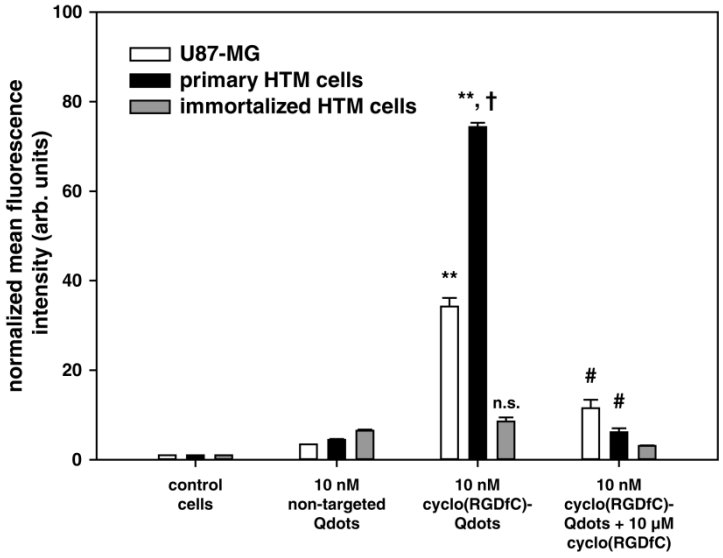

Figure 2: Flow cytometry data for HTM and U87-MG cells incubated with non-targeted and cyclo(RGD)-targeted nanoparticles. Non-targeted Qdots show only minor association to the tested cell lines, whereas targeted Qdots effectively bind primary HTM and U87-MG cells but not immortalized HTM cells. With a surplus of free cyclo(RGD) peptide, the nanoparticle binding can be displaced. Levels of statistical significance are indicated as: (**) $p < 0.01$ compared to non-targeted Qdots; (†) $p < 0.01$ compared to cyclo(RGDfC)-Qdots on U87-MG cells; (#) $p < 0.01$ vs. cyclo(RGDfC)-Qdots. Data is expressed as mean ± standard deviation (n=3).

3.3 Cyclic RGD peptides ameliorate CTGF-induced fibrosis

After we verified that cyclo(RGDfC)-targeted nanoparticles bind $\alpha_v\beta_3$ integrins on HTM cells and are rapidly endocytosed, we investigated whether or not the targeting moiety, the soluble cyclo(RGDfC) peptide, has intrinsic pharmacological effects on the cells of the TM. With the help of qRT-PCR and Western blots, regulation of extracellular matrix proteins like fibronectin and important cell signaling proteins on HTM cells was determined at the level of both mRNA and protein. Upon treatment with 50 ng/mL CTGF, mRNA levels of fibronectin (1.63 ± 0.23 fold, $p < 0.05$) and α-smooth muscle actin (α-SM-actin, 1.81 ± 0.53 fold, $p < 0.05$) were significantly upregulated (Fig. 4). CTGF expression was also significantly increased (1.38 ± 0.28 fold, $p < 0.01$) upon treatment with exogenous CTGF.

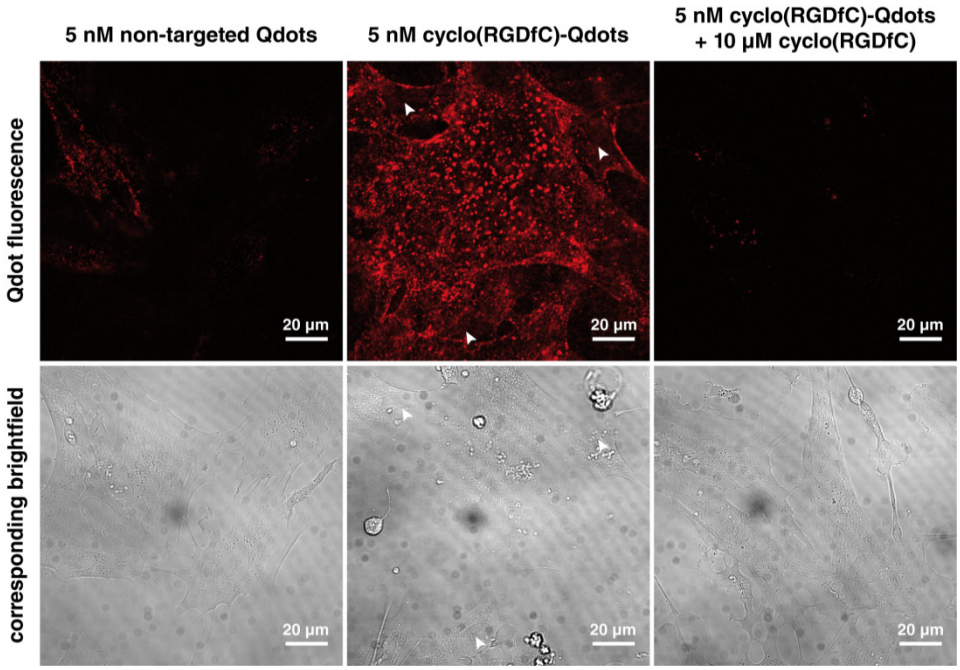

Figure 3: Confocal microscopy pictures of primary HTM cells incubated with targeted or non-targeted Qdots. Non-targeted Qdots show only weak cellular association. In contrast, cyclo(RGDfC)-Qdots are readily taken up by the cells and trafficked into vesicle-like structures. With a surplus of free cyclo(RGDfC) peptide, nanoparticle uptake is tremendously decreased, clearly underscoring the receptor-mediated nature of this endocytosis. Arrowheads depict cell nuclei, which were free of Qdot fluorescence.

To investigate the influence of the RGD peptide alone, HTM cells were treated with the cyclo(RGDfC) peptide at a concentration of 10^{-6} M. Expression of CTGF (1.24 ± 0.44 fold, $p > 0.05$) and fibronectin (1.27 ± 0.42 fold, $p > 0.05$) mRNA were slightly elevated compared to the control, but not in a statistically discernible manner (Fig. 4), whereas α-SM-actin mRNA was significantly elevated (1.47 ± 0.47 fold, $p < 0.05$). However, when cells were co-treated with 50 ng/mL CTGF and 10^{-6} M cyclo(RGDfC), mRNA expression

of CTGF (1.02 ± 0.42 fold), fibronectin (0.98 ± 0.40 fold) and α-SM-actin (1.11 ± 0.21 fold) was significantly lowered compared to the CTGF treatment alone and ultimately 'reset' to the level of the untreated control cells (Fig. 4).

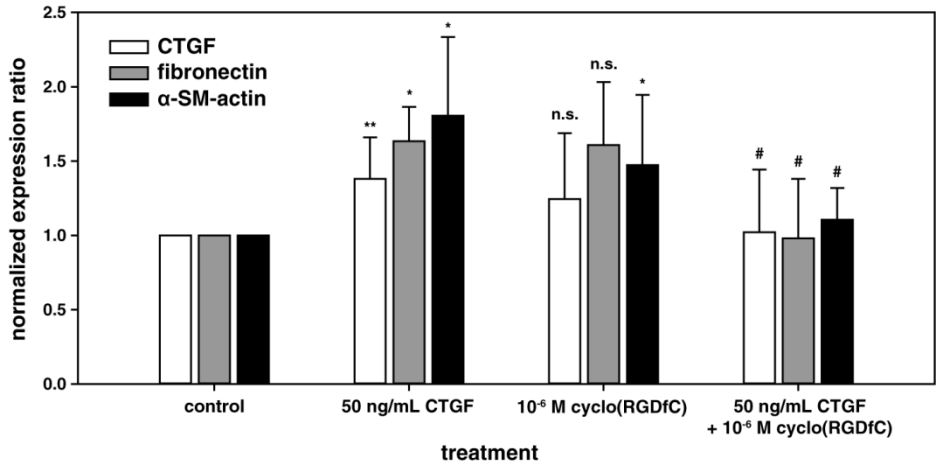

Figure 4: qRT-PCR data for CTGF, fibronectin and α-SM-actin from HTM cells after incubation with CTGF, cyclo(RGDfC) or both. Levels of statistical significance are indicated as: (*) $p < 0.05$ compared to control; (**) $p < 0.01$ compared to control; (#) $p < 0.05$ compared to CTGF treatment; (n.s.) $p > 0.05$ compared to control. Data is expressed as mean ± standard deviation.[1]

In a next step we investigated the influence of CTGF and cyclo(RGDfC) on phosphorylation of the extracellular regulated kinase 1/2 (ERK1/2) and on fibronectin expression in HTM cells via Western blotting. Similar to the results obtained by qRT-PCR, CTGF treatment significantly increased phosphorylation of ERK1/2 (1.78 ± 0.43 fold, $p < 0.05$) and synthesis of fibronectin (2.36 ± 0.30 fold, $p < 0.01$). Cyclo(RGDfC) treatment alone did not result in a significant increase of either pERK1/2 (0.81 ± 0.15 fold, $p > 0.05$) nor fibronectin (1.48 ± 0.62 fold, $p > 0.05$). When HTM cells were simultaneously incubated with CTGF and cyclo(RGDfC), the effects induced by CTGF were effectively inhibited by cyclo(RGDfC). ERK1/2 phosphorylation and fibronectin synthesis were both significantly lowered to 0.74 ± 0.13 and 0.98 ± 0.45 compared to the expression levels of CTGF-treated HTM cells.

4 Discussion

Conjugation of $\alpha_v\beta_3$-specific ligand cyclo(RGDfC) to fluorescent Qdots enabled the nanoparticles to efficiently associate with HTM cells. As demonstrated by flow cytometry, binding of cyclo(RGDfC)-targeted Qdots to HTM cells was significantly higher than Qdot

[1] qRT-PCR data for CTGF, fibronectin and α-SM-actin from HTM cells was obtained and analyzed at the Department for Human Anatomy and Embryology (University of Regensburg) by Rudolf Fuchshofer & colleagues.

binding to U87-MG glioblastoma cells. This is remarkable since U87-MG is a cancer cell line that has one of the highest cellular $\alpha_v\beta_3$ integrin expression levels, with over 100,000 receptors per cell [32]; for this reason, they are regularly used as a benchmark for RGD-targeted nanomaterials [33,34]. This pronounced binding of cyclo(RGDfC)-targeted Qdots to primary HTM cells signifies the importance of $\alpha_v\beta_3$ and $\alpha_v\beta_5$ integrins for the TM. Nanoparticle binding to an immortalized, SV40-transformed HTM cell line (HTM-N) was in stark contrast to the primary HTM cells; cyclo(RGDfC)-Qdots did not show higher binding than the non-targeted Qdot control. Similar observations have been made by Gagen et al. using immunofluorescence measurements. In their experiments, an immortalized TM cell line had no measurable $\alpha_v\beta_3$ expression, in contrast to cultured but non-immortalized cells [21]. Presumably due to immortalization, continued cultivation and absence of the physiological environment, $\alpha_v\beta_3$ integrin expression is drastically downregulated in these cells. This also shows that cyclo(RGDfC)-targeted Qdots exclusively bind cells expressing $\alpha_v\beta_3$ integrins. As recently demonstrated, the association to $\alpha_v\beta_3$ negative cells is negligible [25,35]. This is of paramount importance, since the off-target neural retinal cells show neither $\alpha_v\beta_3$ nor $\alpha_v\beta_5$ integrin expression in a healthy state [36,37] and would, therefore, be unlikely to exhibit unwanted binding and internalization of RGD-functionalized nanoparticles. However, the retinal pigment epithelium (RPE), the cell layer that constitutes the outer blood-retinal barrier and that is responsible for maintenance of the photoreceptors does show $\alpha_v\beta_5$ expression on its apical side [38] and thus may be an off-target accumulation site if the RGD-functionalized nanoparticles are able to cross the inner limiting membrane. Furthermore, it has been shown that glial cells can express integrin $\alpha_v\beta_3$ following injury [36], which would result in an off-target site for RGD-targeted nanomaterials in an injured state.

Confocal microscopy experiments revealed that not only did targeted Qdots bind TM cells, but they were also rapidly and efficiently endocytosed. Efficient uptake into target cells is known to be a critical determinant of overall efficacy for nonviral vectors [39]. Commonly, this uptake is promoted by polycationic carrier polymers such as polyethyleneimine, poly-L-lysine or poly(amido amine) dendrimers [40]. At physiological pH, their amines are protonated and carry a cationic charge that electrostatically interacts with the negatively charged cell membrane, inducing cell uptake [41]. However, the polycationic nature of these polymers and lipids also pose inherent toxicity problems; these multiple positive charges have the potential to induce apoptosis in a wide range of cells [42]. Although cell penetrating peptides such as TAT peptides have been investigated

for TM cell targeting [43], their mode of action is much more nonspecific than that of RGD-mediated receptor binding [44,45]. As a result, cells without integrin expression would also endocytose nanoparticles, ultimately reducing the colloid's TM availability and increasing the risk of undesirable off-target effects. Recently, viral vectors have been recombinantly modified to display RGD units on their surface with the aim of increasing their tropism at the anterior eye. For adenoviral carriers the RGD motif was incorporated into the fiber knob [46] whereas for adenovirus-associated viruses the RGD peptide was incorporated into the capsid protein [47]. However, because the non-RGD-modified viral vectors were already capable of entry into the TM, RGD modification yielded no significant advantage. Besides gene delivery, the nanoparticle-mediated uptake into the cell we demonstrate here could also immensely increase the intracellular concentration of conventional drug molecules with otherwise poor membrane permeability. Therefore, efficient endocytosis into TM cells with low toxic side effects could be one main advantage of both RGD-targeted nonviral nucleic acid vectors and nanoparticles loaded with drug molecules.

In a next step, we analyzed functional aspects of the cyclic RGD peptide. As integrin $\alpha_v\beta_3$ has been shown to be a potential receptor for CTGF in different cell types [48,49] we investigated the influence of the cyclic peptide on CTGF signaling in TM cells. CTGF is of interest in POAG as it acts as a critical downstream mediator of TGF-β2 in HTM cells [7] – it is found in high concentrations in the aqueous humor of POAG patients [3–6] – and because of its increased expression levels in glaucomatous Schlemm's canal endothelial cells [11]. CTGF is suggested to play a pivotal role in the formation of increased outflow resistance by inducing expression of extracellular matrix proteins like fibronectin and by enhancing the contractile properties of TM cells [50]. Wallace and colleagues showed that *in vitro* treatment with a humanized monoclonal anti-CTGF antibody attenuated the ECM expression in TM cells after incubation with aqueous humor of POAG patients [51]. In our experiments, CTGF-induced effects were significantly halted and reset to control expression levels when TM cells were co-incubated with cyclic RGD peptides and CTGF. Previously, we were able to show that CTGF activates MAPK signaling pathway by increasing the phosphorylation state of ERK1/2 [50]. Elevated pERK1/2 levels lead to increased extracellular matrix synthesis in HTM cells [52]. Notably, co-treatment of HTM cells with cyclic RGD peptide and CTGF significantly halted pERK1/2 up-regulation. This is in agreement with studies by Tan et al., in which a cyclic RGD peptide inhibited CTGF-induced ERK phosphorylation in chondrosarcoma cells [53]. The reduced pERK1/2 levels

were associated with significantly reduced fibronectin synthesis in comparison to CTGF-treated HTM cells. The potent anti-fibrotic effects of RGD peptides have also previously been demonstrated for choroidal neovascularization [54] and liver fibrosis [55,56]. Notably, minuscule concentrations of cyclic RGD peptides are known to be potentially agonistic for the $\alpha_v\beta_3$ integrin [57], which could hinder CTGF inhibition if RGD-nanoparticles are highly diluted at the anterior eye.

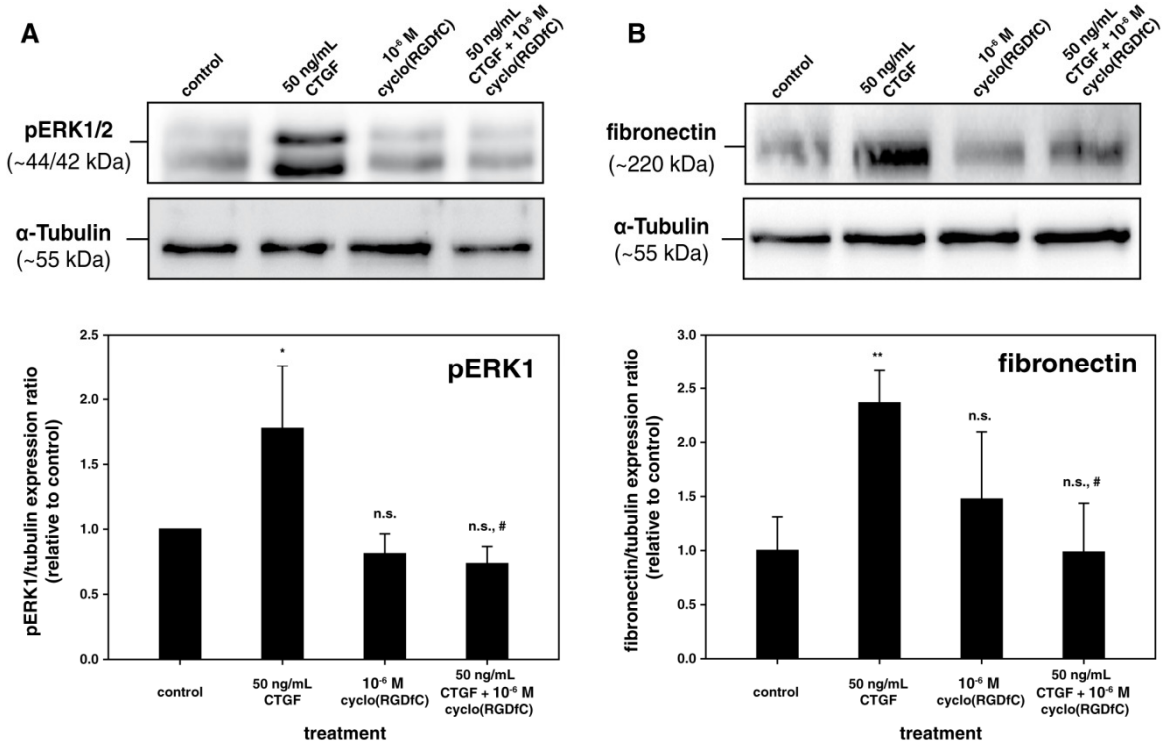

Figure 5: Western blot data for pERK1/2 and fibronectin. **(A)** Treatment with 50 ng/mL CTGF significantly increased pERK1 protein after a 3 h incubation period. When co-incubated with 1 µM cyclo(RGDfC), pERK1/2 expression was reduced to basal levels. Incubation with cyclo(RGDfC) and without CTGF did not influence pERK1/2 expression. **(B)** Similarly, fibronectin expression was dependent on CTGF stimulation. Again, co-treatment with cyclo(RGDfC) inhibited CTGF-induced protein expression. Levels of statistical significance are indicated as: (*) $p < 0.05$ compared to control; (**) $p < 0.01$ compared to control; (#) $p < 0.05$ compared to CTGF treatment; (n.s.) $p > 0.05$ compared to control. Data is expressed as mean ± standard deviation. Equal loading was ensured by detection of α-tubulin.[2]

CTGF comprises four structural modules: an amino-terminal insulin-like growth-factor (IGF) binding domain, a Willebrand type c (VWC) domain followed by a thrombospondin-1 (TSP-1) domain, and a carboxy-terminal cysteine knot (CT) domain [58]. Although no specific receptors for CTGF have been identified so far [59], several studies have shown that CTGF mediates effects such as adhesion, migration and most importantly extracellular matrix protein deposition through activation of integrins [60].

[2] Western blot data for pERK1/2 and fibronectin was obtained and analyzed at the Department for Human Anatomy and Embryology (University of Regensburg) by Rudolf Fuchshofer & colleagues.

Due to the lack of RGD motifs in the CCN family of matricellular proteins, to which CTGF belongs, binding to integrins is thought to be non-RGD-dependent [61]. Furthermore, the specific integrin(s) that interact with CTGF are dependent upon cell type [62]. Although non RGD-dependent, CTGF's activation of integrin $\alpha_v\beta_3$ takes place via its fourth module and can be inhibited by linear RGD-containing peptides, as shown in hepatic stellate cells [63]. Besides RGD peptides, an $\alpha_v\beta_3$ integrin-neutralizing antibody has also been shown to modulate the effects of CTGF, markedly attenuating CTGF-induced motility of breast cancer cells [48]. Due to their antagonism for $\alpha_v\beta_3$ and $\alpha_v\beta_5$ integrins, cyclic RGD pentapeptides effectively ameliorate the CTGF-induced fibrotic effects *in vitro* and can be utilized to precisely address nanoparticles to the TM.

5 Conclusions

With our present work we provide compelling *in vitro* evidence for the potential of cyclic RGD peptides as powerful targeting moieties for addressing nanoparticles to TM cells. Nanoparticles coated with cyclo(RGDfC) peptides showed strong and specific receptor-mediated uptake into TM cells, whereas cyclic RGD peptides ameliorated CTGF-mediated matrix production and stress fiber formation. Thus, cyclic RGD peptides attached to nonviral vectors could not only increase transfection specificity but also effectively attenuate fibrotic events.

References

[1] H.A. Quigley, A.T. Broman, The number of people with glaucoma worldwide in 2010 and 2020, Br. J. Ophthalmol. 90 (2006) 262–267.

[2] B.M. Braunger, R. Fuchshofer, E.R. Tamm, The aqueous humor outflow pathways in glaucoma: A unifying concept of disease mechanisms and causative treatment, Eur. J. Pharm. Biopharm. 95 (2015) 173–181.

[3] M. Inatani, H. Tanihara, H. Katsuta, M. Honjo, N. Kido, Y. Honda, Transforming growth factor-beta 2 levels in aqueous humor of glaucomatous eyes, Graefes Arch. Clin. Exp. Ophthalmol. 239 (2001) 109–113.

[4] Y. Ochiai, H. Ochiai, Higher concentration of transforming growth factor-beta in aqueous humor of glaucomatous eyes and diabetic eyes, Jpn. J. Ophthalmol. 46 (2002) 249–253.

[5] G. Picht, U. Welge-Luessen, F. Grehn, E. Lütjen-Drecoll, Transforming growth factor beta 2 levels in the aqueous humor in different types of glaucoma and the relation to filtering bleb development, Graefes Arch. Clin. Exp. Ophthalmol. 239 (2001) 199–207.

[6] R.C. Tripathi, J. Li, W.A. Chan, B.J. Tripathi, Aqueous Humor in Glaucomatous Eyes Contains an Increased Level of TGF-β2, Exp. Eye Res. 59 (1994) 723–728.

[7] B. Junglas, Yu, Alice H L, U. Welge-Lüssen, E.R. Tamm, R. Fuchshofer, Connective tissue growth factor induces extracellular matrix deposition in human trabecular meshwork cells, Exp. Eye Res. 88 (2009) 1065–1075.

[8] H. Ihn, The role of TGF-beta signaling in the pathogenesis of fibrosis in scleroderma, Arch. Immunol. Ther. Exp. 50 (2002) 325–331.

[9] M.K. Phanish, S.K. Winn, Dockrell, M E C, Connective tissue growth factor-(CTGF, CCN2)--a marker, mediator and therapeutic target for renal fibrosis, Nephron Exp. Nephrol. 114 (2010) e83-92.

[10] S.I. Tomarev, G. Wistow, V. Raymond, S. Dubois, I. Malyukova, Gene Expression Profile of the Human Trabecular Meshwork: NEIBank Sequence Tag Analysis, Invest. Ophthalmol. Vis. Sci. 44 (2003) 2588.

[11] D.R. Overby, E.H. Zhou, R. Vargas-Pinto, R.M. Pedrigi, R. Fuchshofer, S.T. Braakman, R. Gupta, K.M. Perkumas, J.M. Sherwood, A. Vahabikashi, Q. Dang, J.H. Kim, C.R. Ethier, W.D. Stamer, J.J. Fredberg, M. Johnson, Altered mechanobiology of Schlemm's canal endothelial cells in glaucoma, Proc. Natl. Acad. Sci. U.S.A. 111 (2014) 13876–13881.

[12] J.-W. Cheng, S.-W. Cheng, L.-D. Gao, G.-C. Lu, R.-L. Wei, Intraocular pressure-lowering effects of commonly used fixed-combination drugs with timolol: a systematic review and meta-analysis, PLoS ONE 7 (2012) e45079.

[13] R. van der Valk, C.A.B. Webers, J.S.A.G. Schouten, M.P. Zeegers, F. Hendrikse, M.H. Prins, Intraocular pressure-lowering effects of all commonly used glaucoma drugs: a meta-analysis of randomized clinical trials, Ophthalmology 112 (2005) 1177–1185.

[14] R. Kholdebarin, R.J. Campbell, Y.-P. Jin, Y.M. Buys, Multicenter study of compliance and drop administration in glaucoma, Can. J. Ophthalmol. 43 (2008) 454–461.

[15] T. Borrás, Advances in glaucoma treatment and management: gene therapy, Invest. Ophthalmol. Vis. Sci. 53 (2012) 2506–2510.

[16] F.I. Al-Saikhan, The gene therapy revolution in ophthalmology, Saudi J. Ophthalmol. 27 (2013) 107–111.

[17] C.A. Rasmussen, P.L. Kaufman, Exciting directions in glaucoma, Can. J. Ophthalmol. 49 (2014) 534–543.

[18] D.W. Pita-Thomas, J.L. Goldberg, Nanotechnology and glaucoma: little particles for a big disease, Curr. Opin. Ophthalmol. 24 (2013) 130–135.

[19] T. Wang, J.R. Upponi, V.P. Torchilin, Design of multifunctional non-viral gene vectors to overcome physiological barriers: dilemmas and strategies, Int. J. Pharm. 427 (2012) 3–20.

[20] J. Park, K. Singha, S. Son, J. Kim, R. Namgung, C.-O. Yun, W.J. Kim, A review of RGD-functionalized nonviral gene delivery vectors for cancer therapy, Cancer Gene Ther. 19 (2012) 741–748.

[21] D. Gagen, M.S. Filla, R. Clark, P. Liton, D.M. Peters, Activated αvβ3 integrin regulates αvβ5 integrin-mediated phagocytosis in trabecular meshwork cells, Invest. Ophthalmol. Vis. Sci. 54 (2013) 5000–5011.

[22] D. Overby, H. Gong, G. Qiu, T.F. Freddo, M. Johnson, The mechanism of increasing outflow facility during washout in the bovine eye, Invest. Ophthalmol. Vis. Sci. 43 (2002) 3455–3464.

[23] C.K. Bahler, C.R. Hann, M.P. Fautsch, D.H. Johnson, Pharmacologic disruption of Schlemm's canal cells and outflow facility in anterior segments of human eyes, Invest. Ophthalmol. Vis. Sci. 45 (2004) 2246–2254.

[24] D. Telci, Z. Wang, X. Li, Verderio, Elisabetta A M, M.J. Humphries, M. Baccarini, H. Basaga, M. Griffin, Fibronectin-tissue transglutaminase matrix rescues RGD-impaired cell adhesion through syndecan-4 and beta1 integrin co-signaling, J. Biol. Chem. 283 (2008) 20937–20947.

[25] K. Pollinger, R. Hennig, M. Breunig, J. Tessmar, A. Ohlmann, E.R. Tamm, R. Witzgall, A. Goepferich, Kidney podocytes as specific targets for cyclo(RGDfC)-modified nanoparticles, Small 8 (2012) 3368–3375.

[26] C. Mas-Moruno, F. Rechenmacher, H. Kessler, Cilengitide: the first anti-angiogenic small molecule drug candidate design, synthesis and clinical evaluation, Anticancer Agents Med. Chem. 10 (2010) 753–768.

[27] R. Fuchshofer, Yu, Alice H L, U. Welge-Lüssen, E.R. Tamm, Bone morphogenetic protein-7 is an antagonist of transforming growth factor-beta2 in human trabecular meshwork cells, Invest. Ophthalmol. Vis. Sci. 48 (2007) 715–726.

[28] I.-H. Pang, D.L. Shade, A.F. Clark, H.T. Steely, L. DeSantis, Preliminary characterization of a transformed cell strain derived from human trabecular meshwork, Curr. Eye Res. 13 (1994) 51–63.

[29] E.R. Tamm, P. Russell, D.H. Johnson, J. Piatigorsky, Human and monkey trabecular meshwork accumulate alpha B-crystallin in response to heat shock and oxidative stress, Invest. Ophthalmol. Vis. Sci. 37 (1996) 2402–2413.

[30] P. Chomczynski, N. Sacchi, Single-step method of RNA isolation by acid guanidinium thiocyanate-phenol-chloroform extraction, Anal. Biochem. 162 (1987) 156–159.

[31] R. Hennig, K. Pollinger, J. Tessmar, A. Goepferich, Multivalent targeting of AT1 receptors with angiotensin II-functionalized nanoparticles, J. Drug Target. 23 (2015) 681–689.

[32] X. Zhang, Z. Xiong, Y. Wu, W. Cai, J.R. Tseng, S.S. Gambhir, X. Chen, Quantitative PET imaging of tumor integrin alphavbeta3 expression with 18F-FRGD2, J. Nucl. Med. 47 (2006) 113–121.

[33] G. Hong, S.M. Tabakman, K. Welsher, Z. Chen, J.T. Robinson, H. Wang, B. Zhang, H. Dai, Near-infrared-fluorescence-enhanced molecular imaging of live cells on gold substrates, Angew. Chem. Int. Ed. 50 (2011) 4644–4648.

[34] E.C. Cho, Y. Zhang, X. Cai, C.M. Moran, L.V. Wang, Y. Xia, Quantitative Analysis of the Fate of Gold Nanocages In Vitro and In Vivo after Uptake by U87-MG Tumor Cells, Angew. Chem. 125 (2013) 1190–1193.

[35] K. Pollinger, R. Hennig, A. Ohlmann, R. Fuchshofer, R. Wenzel, M. Breunig, J. Tessmar, E.R. Tamm, A. Goepferich, Ligand-functionalized nanoparticles target endothelial cells in retinal capillaries after systemic application, Proc. Natl. Acad. Sci. U.S.A. 110 (2013) 6115–6120.

[36] A.-G. Wang, M.-Y. Yen, W.-M. Hsu, M.-J. Fann, Induction of vitronectin and integrin alphav in the retina after optic nerve injury, Mol. Vis. 12 (2006) 76–84.

[37] J.W. Pearce, K.S. Janardhan, S. Caldwell, B. Singh, Angiostatin and integrin alphavbeta3 in the feline, bovine, canine, equine, porcine and murine retina and cornea, Vet. Ophthalmol. 10 (2007) 313–319.

[38] S.C. Finnemann, V.L. Bonilha, A.D. Marmorstein, E. Rodriguez-Boulan, Phagocytosis of rod outer segments by retinal pigment epithelial cells requires

alpha(v)beta5 integrin for binding but not for internalization, Proceedings of the National Academy of Sciences of the United States of America 94 (1997) 12932–12937.

[39] M.A. Mintzer, E.E. Simanek, Nonviral vectors for gene delivery, Chem. Rev. 109 (2009) 259–302.

[40] H. Yin, R.L. Kanasty, A.A. Eltoukhy, A.J. Vegas, J.R. Dorkin, D.G. Anderson, Non-viral vectors for gene-based therapy, Nat. Rev. Genet. 15 (2014) 541–555.

[41] S. Dinçer, M. Türk, E. Pişkin, Intelligent polymers as nonviral vectors, Gene Ther. 12 Suppl 1 (2005) S139-45.

[42] A.C. Hunter, Molecular hurdles in polyfectin design and mechanistic background to polycation induced cytotoxicity, Adv. Drug Deliv. Rev. 58 (2006) 1523–1531.

[43] H. Sakai, B.-C. Park, X. Shen, Yue, Beatrice Y J T, Transduction of TAT fusion proteins into the human and bovine trabecular meshwork, Invest. Ophthalmol. Vis. Sci. 47 (2006) 4427–4434.

[44] J.S. Suk, J. Suh, K. Choy, S.K. Lai, J. Fu, J. Hanes, Gene delivery to differentiated neurotypic cells with RGD and HIV Tat peptide functionalized polymeric nanoparticles, Biomaterials 27 (2006) 5143–5150.

[45] A. Subrizi, E. Tuominen, A. Bunker, T. Róg, M. Antopolsky, A. Urtti, Tat(48-60) peptide amino acid sequence is not unique in its cell penetrating properties and cell-surface glycosaminoglycans inhibit its cellular uptake, J. Control. Release 158 (2012) 277–285.

[46] K. Ueyama, K. Mori, T. Shoji, H. Omata, P.L. Gehlbach, D.E. Brough, L.L. Wei, S. Yoneya, Ocular localization and transduction by adenoviral vectors are serotype-dependent and can be modified by inclusion of RGD fiber modifications, PLoS ONE 9 (2014) e108071.

[47] L.K. Buie, C.A. Rasmussen, E.C. Porterfield, V.S. Ramgolam, V.W. Choi, S. Markovic-Plese, R.J. Samulski, P.L. Kaufman, T. Borrás, Self-complementary AAV virus (scAAV) safe and long-term gene transfer in the trabecular meshwork of living rats and monkeys, Invest. Ophthalmol. Vis. Sci. 51 (2010) 236–248.

[48] P.-S. Chen, M.-Y. Wang, S.-N. Wu, J.-L. Su, C.-C. Hong, S.-E. Chuang, M.-W. Chen, K.-T. Hua, Y.-L. Wu, S.-T. Cha, M.S. Babu, C.-N. Chen, P.-H. Lee, K.-J. Chang, M.-L. Kuo, CTGF enhances the motility of breast cancer cells via an integrin-alphavbeta3-ERK1/2-dependent S100A4-upregulated pathway, J. Cell. Sci. 120 (2007) 2053–2065.

[49] S.-C. Liu, C.-J. Hsu, H.-T. Chen, H.-K. Tsou, S.-M. Chuang, C.-H. Tang, CTGF increases IL-6 expression in human synovial fibroblasts through integrin-dependent signaling pathway, PLoS ONE 7 (2012) e51097.

[50] B. Junglas, S. Kuespert, A.A. Seleem, T. Struller, S. Ullmann, M. Bösl, A. Bosserhoff, J. Köstler, R. Wagner, E.R. Tamm, R. Fuchshofer, Connective tissue growth factor causes glaucoma by modifying the actin cytoskeleton of the trabecular meshwork, Am. J. Pathol. 180 (2012) 2386–2403.

[51] D.M. Wallace, A.F. Clark, K.E. Lipson, D. Andrews, J.K. Crean, C.J. O'Brien, Anti-connective tissue growth factor antibody treatment reduces extracellular matrix production in trabecular meshwork and lamina cribrosa cells, Invest. Ophthalmol. Vis. Sci. 54 (2013) 7836–7848.

[52] P.P. Pattabiraman, P.V. Rao, Mechanistic basis of Rho GTPase-induced extracellular matrix synthesis in trabecular meshwork cells, Am. J. Physiol., Cell Physiol. 298 (2010) C749-63.

[53] T.-W. Tan, C.-H. Lai, C.-Y. Huang, W.-H. Yang, H.-T. Chen, H.-C. Hsu, Y.-C. Fong, C.-H. Tang, CTGF enhances migration and MMP-13 up-regulation via alphavbeta3 integrin, FAK, ERK, and NF-kappaB-dependent pathway in human chondrosarcoma cells, J. Cell. Biochem. 107 (2009) 345–356.

[54] L. Luo, X. Zhang, Y. Hirano, P. Tyagi, P. Barabás, H. Uehara, T.R. Miya, N. Singh, B. Archer, Y. Qazi, K. Jackman, S.K. Das, T. Olsen, S.R. Chennamaneni, B.C. Stagg, F. Ahmed, L. Emerson, K. Zygmunt, R. Whitaker, C. Mamalis, W. Huang, G. Gao, S.P. Srinivas, D. Krizaj, J. Baffi, J. Ambati, U.B. Kompella, B.K. Ambati, Targeted intraceptor nanoparticle therapy reduces angiogenesis and fibrosis in primate and murine macular degeneration, ACS Nano 7 (2013) 3264–3275.

[55] K. Kotoh, M. Nakamuta, M. Kohjima, M. Fukushima, S. Morizono, N. Kobayashi, M. Enjoji, H. Nawata, Arg-Gly-Asp (RGD) peptide ameliorates carbon tetrachloride-induced liver fibrosis via inhibition of collagen production and acceleration of collagenase activity, Int. J. Mol. Med. 14 (2004) 1049–1053.

[56] L.-S. Wang, Y.-W. Chen, D.-G. Li, H.-M. Lu, Arg-gly-asp-mannose-6-phosphate inhibits activation and proliferation of hepatic stellate cells in vitro, World J. Gastroenterol. 12 (2006) 1303–1307.

[57] D.F. Legler, G. Wiedle, F.P. Ross, B.A. Imhof, Superactivation of integrin alphavbeta3 by low antagonist concentrations, Journal of cell science 114 (2001) 1545–1553.

[58] B. Perbal, CCN proteins: multifunctional signalling regulators, Lancet 363 (2004) 62–64.

[59] H. Hendesi, M.F. Barbe, F.F. Safadi, M.A. Monroy, S.N. Popoff, Integrin mediated adhesion of osteoblasts to connective tissue growth factor (CTGF/CCN2) induces cytoskeleton reorganization and cell differentiation, PLoS ONE 10 (2015) e0115325.

[60] D. Brigstock, The CCN family: a new stimulus package, J. Endocrinol. 178 (2003) 169–175.

[61] L.F. Lau, S.C. Lam, The CCN family of angiogenic regulators: the integrin connection, Exp. Cell Res. 248 (1999) 44–57.

[62] J.A. Arnott, A.G. Lambi, C. Mundy, H. Hendesi, R.A. Pixley, T.A. Owen, F.F. Safadi, S.N. Popoff, The role of connective tissue growth factor (CTGF/CCN2) in skeletogenesis, Crit. Rev. Eukaryot. Gene Expr. 21 (2011) 43–69.

[63] R. Gao, D.R. Brigstock, Connective tissue growth factor (CCN2) induces adhesion of rat activated hepatic stellate cells by binding of its C-terminal domain to integrin alpha(v)beta(3) and heparan sulfate proteoglycan, J. Biol. Chem. 279 (2004) 8848–8855.

Chapter 8

Summary and Conclusions

Summary

It was more than 100 years ago when Paul Ehrlich coined the idea of the 'Magic Bullet', a personalized and tailored drug that precisely targets diseased cells in the human body and leaves healthy cells untouched [1]. Among many examples that resemble this concept, targeted delivery of nanoparticles to specific tissues is often designated as the most promising one [2]. Active targeting, which is addressing nanoparticles to individual tissues, is usually achieved by conjugating ligand molecules to the colloidal surface. Moreover, since multiple ligand molecules can be attached to the particle corona, highly sophisticated multivalent material-cell interactions are imaginable. Although they add another layer of complexity to the system, they may ultimately determine a particle's fate.

A prominent example in which nanoparticle formulations have gained much interest recently is the treatment of pathologic neovascularizations in the posterior eye segment. Their outstanding features, which include the encapsulation of drugs, the accumulation in areas of increased vascular permeability or the controlled release of active ingredients, has prompted immense research efforts for the intravitreal but also systemic application. In addition, certain nanomaterials exhibit unique anti-proliferative and anti-oxidative effects that could impressively expand and improve the current therapeutic arsenal **(Chapter 1)**.

However, although there are tremendous efforts going into the design and development of nanoparticle formulations, the actual amount of novel formulations entering clinical trials or being approved is very limited [3]. A potential pitfall that could reduce nanoparticle applicability is the loss of nanoparticle targeting efficacy due to ligand affinity decrease, which can be a consequence of ligand attachment to the nanoparticle polymer corona. EXP3174, a non-peptide angiotensin receptor blocker, underwent a 580-fold decreased receptor binding affinity after conjugation to a PEG chain. When multivalently presented on a nanoparticle surface, initially lost affinity was rapidly regained, which was a consequence of the nanoparticle's capability to bind several receptors simultaneously (**Chapter 3**). However, for this to happen, a sufficiently high receptor density is required. Owing to the weak affinity of a monovalent nanoparticle-cell interaction compared to the multivalent interaction, the colloids gained the ability to differently target cells depending on their receptor expression levels. For this reason,

EXP3174-targeted Qdots strongly associated with NCI-295R cells that showed a high AT_1R expression, but not with HeLa cells with a low receptor expression. The receptor's physiological ligand angiotensin II is a potent growth factor and of critical importance for neovascularizations in the posterior eye segment. Hence, the type-1 receptor in the ocular vasculature is a logical target for nanoparticles that are capable of blocking the receptor over an extended period of time. EXP3174-Qdots specifically accumulated in the retinal and choroidal vessels but not in off-target tissue such as the kidney, which was attributed to the multivalent ligand display. Remarkably, the nanoparticle's blood circulation time did not suffer from ligand attachment but, in contrast, was improved **(Chapter 4)**.

Since the semiconductor Qdots were mainly used as reporter particles in the preceding studies due to their outstanding fluorescence properties, the multivalent binding and blocking of AT_1 receptors was transferred to drug-polymer-conjugates as potential therapeutic agents. EXP3174-modified multi-arm PEGs and generation 5 PAMAM dendrimers both blocked AT_1R receptors with nanomolar affinity. Due to their unique microarchitecture PAMAM dendrimers retained a 6-fold higher receptor binding affinity than the branched PEGs, whose lowered affinity was presumably due to hydrophobic interactions between EXP3174 and the polymer. Both conjugates showed no measurable *in vitro* cytotoxicity, which was impressively in stark contrast to the unmodified PAMAM dendrimers (**Chapter 5**).

Compared with antagonist-modified nanoparticles which are not immediately taken up but rest at the cell membrane, agonist-modified colloids are promptly endocytosed into the cell after receptor activation. However, as tested with calcium mobilization experiments the instant cell uptake did not impede the formation of multivalent nanoparticle-cell interactions for angiotensin II-targeted Qdots, as the agonist-targeted colloids exhibited a 30-fold higher affinity than the free ligand. In a cell binding model the ligand-modified Qdots exclusively interacted with receptor expressing cells. The resulting receptor-mediated endocytosis occurred via clathrin-coated pits and was inhibitable with receptor antagonists. Interestingly, although the immediate uptake did not suppress multivalent binding formation, the multivalency was lower than observed for antagonist-modified nanoparticles (**Chapter 6**).

The trabecular meshwork, a sponge-like tissue in the iridocorneal angle of the eye is responsible for aqueous humor drainage and thus pivotal key player in the pathogenesis of primary open-angle glaucoma. Nanoparticles coated with cyclic RGD peptides and

targeted towards integrin receptors were rapidly and massively endocytosed into human trabecular meshwork cells. The association to the cultured trabecular meshwork cells was significantly higher than the association to the prominent $\alpha_v\beta_3$ integrin-overexpressing glioblastoma cell line U87-MG. As demonstrated by real-time PCR and western blotting, the cyclic RGD peptide mitigated connective tissue growth factor-induced fibrotic events such as matrix deposition and stress fiber formation. The experimental data convincingly illustrated why cyclic RGD peptides are powerful targeting moieties when the aim is to address nanoparticles, e.g. for gene delivery, specifically to the trabecular meshwork (**Chapter 7**).

Conclusion

The present work unveiled the immense potential of multivalent nanoparticle-cell interactions and promising applications thereof. Not only can nanoparticle multivalency be utilized to differentially target organs, tissue and cells based on divergent receptor expression levels, but it can also be used to amplify cell-specific targeting. The difference in multivalent behavior between antagonistic and agonistic nanoparticles targeting the AT_1 receptor was clearly evident and a result of different receptor responses upon ligand binding. In this regard, especially the binding of antagonistic nanoparticles to angiotensin receptors of retinal and choroidal blood vessels and thus blockade of these receptors holds great potential for tissue-specific attenuation of pathologic neovascularizations. In a similar fashion, blockade of integrin receptors by cyclo(RGDfC)-coated nanoparticles and cell-specific delivery of therapeutic agents to the trabecular meshwork is a promising strategy to enhance glaucoma treatment options that currently appear on the horizon.

Taken together, the newly gained understanding of nanoparticles and their multivalent interactions with cells has significant potential to carve out new paths for treating severe diseases of the anterior and posterior eye segment.

References

[1] K. Strebhardt, A. Ullrich, Paul Ehrlich's magic bullet concept: 100 years of progress, Nat. Rev. Cancer 8 (2008) 473–480.

[2] T.M. Fahmy, P.M. Fong, A. Goyal, W.M. Saltzman, Targeted for drug delivery, Mater. Today 8 (2005) 18–26.

[3] Z. Cheng, A. Al Zaki, J.Z. Hui, V.R. Muzykantov, A. Tsourkas, Multifunctional nanoparticles: cost versus benefit of adding targeting and imaging capabilities, Science 338 (2012) 903–910.

Appendix

Abbreviations

AGEs	advanced glycosylation end products
AMD	age-related macular degeneration
Ang II	angiotensin II
ARB	angiotensin receptor blocker
α-SM-actin	α-smooth muscle actin
AT_1R	angiotensin II receptor type 1
ATCC	American Type Culture Collection
AuNP	gold nanoparticles
BAB	blood-aqueous barrier
bFGF	basic fibroblast growth factor
BM	Bruch's membrane
BRB	blood-retinal barrier
BSA	bovine serum albumin
CC	choriocapillaris
cDNA	complementary DNA
CLSM	confocal laser scanning microscopy
CNV	choroidal neovascularization
CTGF	connective tissue growth factor
DABCO	1,4-diazabicyclo[2.2.2]octane
DHA	docosahexaenoic acid
DMEM	Dulbecco's modified Eagle's medium
DMSO	dimethyl sulfoxide
DPBS	Dulbecco's phosphate buffered saline

DR	diabetic retinopathy
DXR	doxorubicin
EC_{50}	half maximal effective concentration
EDC	N-(3-dimethylaminopropyl)-N'-ethylcarbodiimide hydrochloride
EGF	endothelial growth factor
EGTA	ethylene glycol-bis(2-aminoethylether)-N,N,N′,N′-tetraacetic acid
EMEM	Eagle's minimal essential medium
EPR	enhanced permeation and retention
ER	endoplasmic reticulum
ERK	extracellar-signal regulated kinase
FA	fluorescein angiography
FCS	fetal calf serum
FDA	US Food and Drug Administration
FITC	fluorescein isothiocyanate
FGF	fibroblast growth factor
FWHM	full width at half maximum
G	generation
GAPDH	glyceraldehyde 3-phosphate dehydrogenase
GNB2L	guanine nucleotide binding protein beta polypeptide 2-like 1
GPCR	G protein-coupled receptor
HEPES	(4-(2-hydroxyethyl)-1-piperazineethanesulfonic acid)
HIF-1α	hypoxia-inducible factor 1α
HPLC	high performance liquid chromatography
HTM	human trabecular meshwork
HUVEC	human umbilical vein endothelial cells
IC_{50}	half maximal inhibitory concentration
ICAM-1	intracellular adhesion molecule-1
ICP-MS	inductively coupled plasma mass spectrometry
ID	initial dose
IFP	interstitial fluid pressure
IGF	insulin-like growth factor
IgG	immunoglobulin G
IOP	intraocular pressure
INL	inner nuclear layer

IS	inner segments
IV	intravenous
IVT	intravitreal
JCT	juxtacanalicular tissue
LDL	low density lipoproteins
MES	2-(N-morpholino)ethanesulfonic acid
MPS	mononuclear phagocyte system
mRNA	messenger RNA
MTT	(3-(4,5-dimethylthiazol-2-yl)-2,5-diphenyltetrazolium bromide)
MVE	multivalent enhancement
MW	molecular weight
NMRI	Naval Medical Research Institute
NP	nanoparticle
OIR	oxygen-induced retinopathy
OPL	outer plexiform layer
ONL	outer nuclear layer
OS	outer segments
PAMAM	poly(amido amine)
PDGF	platelet-derived growth factor
pDNA	plasmid DNA
PDR	proliferative diabetic retinopathy
PDT	photodynamic therapy
PECAM	platelet endothelial cell adhesion molecule
PEDF	pigment epithelium-derived factor
PEG	poly(ethylene glycol)
PI	propidium iodide
PLA	poly(lactic acid)
PLGA	poly(lactid-*co*-glycolide)
PO	peroral
POAG	primary open angle glaucoma
ppb	parts per billion
PRP	panretinal photocoagulation
Qdots	quantum dots
RGD	arginine-glycine-aspartate peptide

RPII	RNA polymerase II
RNV	retinal neovascularization
ROP	retinopathy of prematurity
ROS	reactive oxygen species
RPE	retinal pigment epithelium
RP-HPLC	reverse phase high performance liquid chromatograpy
RT	room temperature
SC	Schlemm's canal
SDS	sodium dodecyl sulfate
SEC	size exclusion chromatography
sulfo-NHS	N-hydroxysulfosuccinimide
shRNA	small hairpin RNA
siRNA	small interfering RNA
SPR	surface plasmon resonance
TEM	transmission electron microscopy
TFA	trifluoroacetic acid
TGF	transforming growth factor
TM	trabecular meshwork
VEGF	vascular endothelial growth factor

Curriculum Vitae

Name:	Robert Stephan Hennig
Date of birth:	22nd of February, 1986
Place of birth	Halle (Saale)
Nationality	German

Scientific education

Since 09/2015	Research Scientist, Chemical & Pharmaceutical Development, Merck Biopharma Merck KGaA, Darmstadt
04/2011 – 07/2015	PhD candidate, Department of Pharmaceutical Technology, University of Regensburg
02/2011	Licensure as Pharmacist
06/2010 – 11/2010	Practical training, Schiller-Apotheke Leipzig
11/2009 – 05/2009	Diploma thesis, Department of Pharmaceutical Technology, University of Leipzig, Prof. Dr. Michaela Schulz-Siegmund und Michael Hacker "*Synthesis and characterization of maleic anhydride-based copolymers*"

10/2005 – 10/2009	Study of Pharmacy, University of Leipzig

School education

08/2004 – 05/2005	Community service in the Kreiskrankenhaus Stollberg
06/2004	General qualification for university entrance
09/1996 – 06/2004	Grammar school, Drei-Tannen-Gymnasium Thalheim
08/1992 – 05/1996	Primary school, Grundschule Thalheim

Peer-reviewed publications

Hennig, Robert; Goepferich, Achim: *Nanoparticles for the treatment of ocular neovascularizations*. In: European Journal of Pharmaceutics and Biopharmaceutics 2015, 95b, 294–306 **(Chapter 1)**

Hennig, Robert; Pollinger, Klaus; Veser, Anika; Breunig, Miriam; Goepferich, Achim: *Nanoparticle multivalency counterbalances the ligand affinity loss upon PEGylation*. In: Journal of Controlled Release 2014, 194C, 20–27 **(Chapter 3)**

Hennig, Robert; Ohlmann, Andreas; Staffel, Janina; Pollinger, Klaus; Haunberger, Alexandra; Breunig, Miriam; Schweda, Frank; Tamm, Ernst; Goepferich, Achim: *Multivalent nanoparticles bind the retinal and choroidal vasculature.* In: Journal of Controlled Release 2015, Vol, Pages **(Chapter 4)**

Hennig, Robert; Veser, Anika; Kirchhof, Susanne; Goepferich, Achim: *Branched polymer-drug conjugates for multivalent blockade of angiotensin II receptors.* In: Molecular Pharmaceutics 2015, 12 (9), 3292–3302 **(Chapter 5)**

Hennig, Robert; Pollinger, Klaus; Tessmar, Joerg; Goepferich, Achim: *Multivalent targeting of AT1 receptors with angiotensin II-functionalized nanoparticles.* In: Journal of Drug Targeting 2015, 23 (7–8), 681–689 **(Chapter 6)**

Herrnberger, Leonie; Hennig, Robert, Kremer, Werner; Hellerbrand, Claus; Goepferich, Achim; Kalbitzer, Hans Robert; Tamm, Ernst: *Formation of fenestrae in murine liver*

sinusoids depends on plasmalemma vesicle-associated protein and is required for lipoprotein passage. In: PLoS ONE 2014, 9, e115005

Pollinger, Klaus; Hennig, Robert; Bauer, Stefanie; Breunig, Miriam; Tessmar, Joerg; Buschauer Armin; Witzgall, Ralph; Goepferich, Achim: *Biodistribution of Quantum Dots in the Kidney After Intravenous Injection.* In: Journal of Nanoscience and Nanotechnology 2014, 14 (5), 3313–3319

Loth, Tina; Hennig, Robert; Kascholke, Christian; Hötzel, Rudi; Hacker, Michael: *Reactive and stimuli-responsive maleic anhydride containing macromers–multi-functional cross-linkers and building blocks for hydrogel fabrication*. In: Reactive and Functional Polymers 2013, 73 (11), 1480–1492.

Pollinger, Klaus; Hennig, Robert; Ohlmann, Andreas; Fuchshofer, Rudolf; Wenzel, Rebecca; Breunig, Miriam; Teßmar, Joerg; Tamm, Ernst; Goepferich, Achim*: Ligand-functionalized nanoparticles target endothelial cells in retinal capillaries after systemic application*. In: Proc. Natl. Acad. Sci. U.S.A. 2013, 110 (15), 6115–6120.

Pollinger, Klaus; Hennig, Robert; Breunig, Miriam; Teßmar, Joerg; Ohlmann, Andreas; Tamm, Ernst; Witzgall, Ralph; Goepferich, Achim*: Kidney podocytes as specific targets for cyclo(RGDfC)-modified nanoparticles*. In: Small 2012, 8 (21), 3368–3375.

Oral presentations

Hennig, Robert: *Influence of the nanoparticle PEG corona on the affinity of targeting ligands.* European Conference for Clinical Nanomedicine & Targeted Medicine. In: Basel, Switzerland, June 24th, 2014

Hennig, Robert: *Nanoparticles for the cellular recognition.* 1st Research symposium of Experimental Orthopaedics. In: Bad Abbach, Germany, April 19th, 2013

Conference abstracts

Hennig, Robert; Pollinger, Klaus; Veser, Anika; Breunig, Miriam; Goepferich, Achim (2014): *Influence of the nanoparticle PEG corona on the affinity of targeting ligands*. 248th ACS National Meeting, San Francisco, CA, USA, 2014.

Hennig, Robert; Pollinger, Klaus; Veser, Anika; Breunig, Miriam; Goepferich, Achim (2014): *Influence of the nanoparticle PEG corona on the affinity of targeting ligands*.

European Conference on Clinical Nanomedicine & Targeted Medicine, Basel, Switzerland, 2014.

Hennig, Robert; Pollinger, Klaus; Veser, Anika; Breunig, Miriam; Goepferich, Achim (2014): *Multivalent ligand-receptor interactions of nanoparticles*. 9th World Meeting on Pharmaceutics, Biopharmaceutics and Pharmaceutical Technology, Lisbon, Portugal, 2014.

Hennig, Robert; Pollinger, Klaus; Veser, Anika; Breunig, Miriam; Goepferich, Achim (2013): *Multivalent nanoparticle-receptor interactions*. 2013 AAPS Annual Meeting and Exposition, San Antonio, TX, USA, 2013.

Hennig, Robert; Pollinger, Klaus; Breunig, Miriam; Tessmar, Joerg; Goepferich, Achim (2013): *Targeting of mesangial cells with ligand-conjugated quantum dots*. 246th ACS National Meeting, Indianapolis, IN, USA, 2013.

Hennig, Robert; Pollinger, Klaus; Breunig, Miriam; Tessmar, Joerg; Goepferich, Achim (2013): *Angiotensin II-functionalized Quantum Dot Interactions with Cells*. Society for Biomaterials, World Meeting. Boston, MA, USA, 2013.

Hennig, Robert; Pollinger, Klaus; Breunig, Miriam; Tessmar, Joerg; Goepferich, Achim (2013): *Targeting of mesangial cells with ligand-conjugated quantum dots*. Conference for Clinical Nanomedicine & Targeted Medicine. Basel, Switzerland, 2013.

Hennig, Robert; Pollinger, Klaus; Wenzel, Rebecca; Breunig, Miriam; Tessmar, Joerg; Goepferich, Achim (2012): *Sartan-modified quantum dots targeting the Angiotensin II receptor type 1*. DPhG Jahrestagung. Greifswald, Germany, 2012.

Hennig, Robert; Pollinger, Klaus; Wenzel, Rebecca; Breunig, Miriam; Tessmar, Joerg; Goepferich, Achim (2012): *Targeting the Angiotensin II Receptor Type 1 with Agonist-Modified Quantum Dots*. Summer school "Medicinal Chemistry". Universität Regensburg. Regensburg, Germany, 2012.

Acknowledgements

First and foremost I would like to express my sincerest gratitude to Prof. Dr. Achim Göpferich for giving me the opportunity to be part of his research group and for committing this engaging project to me. The joy he has for his research was both contagious and motivational to me. I appreciate all his contributions of time and ideas to make my PhD experience productive and stimulating. In this regard I am deeply thankful for his continued enthusiasm throughout the years, his invaluable intellectual contributions, the many inspiring discussions we had and for providing me with the opportunity to attend several national and international meetings.

I also thank Dr. Jörg Teßmar, PD Dr. Miriam Breunig and Dr. Ferdinand Brandl for their excellent scientific advices throughout the last 4 years. They always had an open ear for my questions and provided fruitful scientific input for my work.

I want to express my gratitude to Prof. Dr. Ernst Tamm for the good cooperation on working at the nanoparticle delivery to the posterior eye. My sincere thanks are due to PD Dr. Andreas Ohlmann, PD Dr. Rudolf Fuchshofer and PD Dr. Dr. Barbara Braunger for their continuous scientific contributions and for always having an answer on my many eye-related questions.

My thanks go to Dr. Thilo Spruß and Janina Staffel for their vital support with the animal experiments.

Furthermore I express my gratitude to Kelsey Knewtson and Paul Bisso for their critical revision of my manuscripts. Especially Paul, who proofread most of my manuscripts,

provided an invaluable contribution to the success of our manuscripts and my dissertation.

I express my deep gratitude to all my former and present colleagues in the research group of the Department of Pharmaceutical Technology. They created an atmosphere of companionship and made the past few years a highly memorable time. In this regard, a special 'thank you' goes out to the following colleagues:

Dr. Klaus Pollinger for his scientific guidance during my first two years at the work group. I thank him for showing me all of his methods revolving nanoparticles, his genuine interest in our work and for the emerged friendship.

My lab mates Rebecca Wenzel & Alexandra Haunberger for a very harmonious, friendly but also open and constructive atmosphere in our lab.

Dr. Susanne Kirchhof for insightful discussions and time-consuming trouble-shooting with PEGs and other polymers.

Michael Backofen for our good connection and for always being incredibly helpful when the HPLC suffered from a breakdown.

Sabine Hofmeister for her great assistance during her time as research intern and for her friendship.

Manuel Gregoritza for intriguing scientific discussions and for being a great gym buddy during the last months.

Further thanks are due to Eva Wrobel for her outstanding organizational skills.

Moreover I thank Renate Liebl, Angelika Berie, Edith Schindler and Stefan Kolb for their excellent technical assistance and for many delightful morning coffee sessions. In this sense, a big thank-you also goes to Andrea Blaimer for her great work done in the background. I further thank Margit Schimmel and Elke Stauber for their assistance with the electron microscopy and the cryosections.

I thank the German Research Foundation (DFG) for their grants during my time as PhD candidate and for financially supporting the travelling to meetings. I also thank the 'Freunde der Universität Regensburg e.V.' for providing me with financial assistance for travels abroad.

I am grateful towards Thomas Stübner for his priceless help with designing graphical abstracts. In addition, I thank him and all my other friends for their ongoing support for my time in Regensburg.

Finally, I want to thank my family for all their love and supprt. I want to especially thank my parents, who raised me with a love towards science. They encouraged me to follow my path, supported me in every possible way and most importantly, believed in me.

Statement in Lieu of an Oath

I hereby confirm that I have written this thesis on my own and that I have not used any other media or materials than the ones referred to in this thesis.

Regensburg, ……..……. …….

(Robert Hennig)